Journal of ASTM International
Selected Technical Papers

STP 1535

Static and Dynamic Spinal Implants: Are We Evaluating Them Appropriately?

JAI Guest Editors:
Laura M. Jensen
David B. Spenciner
Jove Graham
Paul A. Anderson

Journal of ASTM International
Selected Technical Papers STP1535
Static and Dynamic Spinal Implants: Are We Evaluating Them Appropriately?

JAI Guest Editors:
Laura M. Jensen
David B. Spenciner
Jove Graham
Paul A. Anderson

ASTM International
100 Barr Harbor Drive
PO Box C700
West Conshohocken, PA 19428-2959

Printed in the U.S.A.

ASTM Stock #: STP1535

Library of Congress Cataloging-in-Publication Data
Static and dynamic spinal implants: are we evaluating them appropriately? / guest editors, Laura M. Jensen et al.
p. cm. -- (JAI; STP 1535)
Includes bibliographical references and indexes.
ISBN 978-0-8031-7521-1 (alk. paper)
I. Jensen, Laura M., 1974- II. ASTM International. III. Series: Journal of ASTM International. Selected technical papers; STP 1535. [DNLM: 1. Spine--surgery. 2. Device Approval. 3. Implants, Experimental. 4. Prosthesis Design. WE 725]
617.4'710592--dc23 2012013744

Journal of ASTM International (JAI) Scope

The JAI is a multi-disciplinary forum to serve the international scientific and engineering community through the timely publication of the results of original research and critical review articles in the physical and life sciences and engineering technologies. These peer-reviewed papers cover diverse topics relevant to the science and research that establish the foundation for standards development within ASTM International.

Photocopy Rights

Peer Review Policy

Each paper published in this volume was evaluated by two peer reviewers and at least one editor. The authors addressed all of the reviewers' comments to the satisfaction of both the technical editor(s) and the ASTM International Committee on Publications.

The quality of the papers in this publication reflects not only the obvious efforts of the authors and the technical editor(s), but also the work of the peer reviewers. In keeping with long-standing publication practices, ASTM International maintains the anonymity of the peer reviewers. The ASTM International Committee on Publications acknowledges with appreciation their dedication and contribution of time and effort on behalf of ASTM International.

Citation of Papers

When citing papers from this publication, the appropriate citation includes the paper authors, "paper title", J. ASTM Intl., volume and number, Paper doi, ASTM International, West Conshohocken, PA, Paper, year listed in the footnote of the paper. A citation is provided as a footnote on page one of each paper.

Printed in Baltimore, MD
May, 2012

Foreword

THIS COMPILATION OF THE JOURNAL OF ASTM INTERNATIONAL (JAI), STP1535 *Static and Dynamic Spinal Implants: Are We Evaluating Them Appropriately?* contains papers that were presented at a symposium in San Antonio, TX, on November 16, 2010 and sponsored by ASTM Committees F04 on Medical and Surgical Materials and Devices and F04.25 on Spinal Devices.

The Symposium Chairs and JAI Guest Editors are Laura M. Jensen, MS, Zimmer Spine, Minneapolis, MN, David Spenciner, PE, ScM, MBA, DePuy Mitek (Johnson & Johnson), Raynham, MA, Jove Graham, PhD, Geisinger Center for Health Research, Danville, PA, and Paul Anderson, MD, University of Wisconsin-Madison, Madison, WI.

Contents

Longitudinal Systems

Overview

Background

> "The field of spinal implants continues to be a dynamic one. New designs of modular constructs and components used in spinal fusions and the development of spinal implants intended to allow or maintain motion are major areas of change [I]."

These words described the state of affairs for ASTM Subcommittee F04.25 on Spinal Devices in 2001, when a symposium was held on the subject of "Spinal Implants: Are We Evaluating Them Appropriately?" This description still holds true ten years later, even after having revised nearly a dozen standards and created several more. Clinicians are able to implant a bewildering array of spinal devices, some meant to maintain certain physiological motions while others focus on achieving a solid fusion mass. At the same time that much of the growth in the spinal device market is being driven by the development of new, dynamic implants, the business environment in the spine world is quite a bit different now than it was a decade ago. The atmosphere is harsher, including such well-documented factors as increased price pressure, lowered prospects for industry growth, greater difficulty securing reimbursement for emerging technologies, device failures, and a more difficult fundraising environment. However, even with these challenges, we still see reasons for optimism. The members of ASTM F04.25, including manufacturers, clinicians, academics, and regulatory bodies, are working together to develop more sophisticated methods for the evaluation of spinal devices, Improved test methods help us better understand technologies and quantify improvements. With better measurements, we can design better spinal devices which benefit the ultimate customers–the patients.

On November 16, 2010, the ASTM International Committee F04 on Medical and Surgical Materials and Devices and F04.25 sponsored a symposium titled, "Static and Dynamic Spinal Implants: Are We Evaluating Them Appropriately?" The primary goal of the symposium was to invite discussion among the 113 attendees regarding how spinal devices are evaluated worldwide. There were 25 presentations and ten posters (of nearly 50 submitted) from researchers representing the USA and five other countries. All presenters were encouraged to submit manuscripts for inclusion in this publication. From these efforts, the 20 manuscripts which make up this STP emerged. The peer review process was stringent and we hope that you find this compilation to be a useful resource in the years ahead. The symposium papers published with the current STP can be loosely grouped into four subjects:

interbody fusion devices, disc and nucleus devices, *in vitro* testing methods, and longitudinal systems.

lnterbody Fusion Devices

The goal of this session was to examine several test parameters used in the evaluation of interbody spacers and other fusion devices (ASTM F2077). This represents a maturation of the field in that at the first symposium, this session mainly dealt with the clinical relevance of the test methods. Papers covering variations in the fixture design, bone analog material, and mode of testing are presented.

Disc and Nucleus Devices

At the first symposium, testing of artificial discs was in its infancy, but the breadth of the current papers show an evolving sophistication to the test engineer's knowledge. Topics include the frequency dependence of polymeric core discs, sensitivity of wear and impingement tests to input parameters, and a ground-breaking comparison of human *in vivo* ranges of motion to the parameters outlined in ASTM F2423, "Standard Guide for Functional, Kinematic, and Wear Assessment of Total Disc Prostheses. [2]"

In vitro Testing Methods

This session represented a departure from the previous symposium. Despite that fact that *in vitro* kinematic testing of spines has been performed for decades, no current effort exists within ASTM for an *in vitro* testing standard (ISO is currently developing N438, "Flexibility Testing of Spinal Segments"). Several papers are presented that either mechanically test spinal devices using human spinal segments as the test medium or develop a more physiological loading protocol.

Longitudinal Systems

This topic was expanded to two sessions in the symposium due to the greater number of submissions and higher level of interest. This likely indicates the overarching importance of ASTM F1717 "Standard Test Method for Spinal Constructs in a Vertebrectomy Model" and its related standards to this subcommittee in particular and the spinal industry as a whole. Several papers address various aspects of the standard including suggested improvements. Other papers describe innovative uses for the standard in evaluating new types of rods technologies.

Significance and Future Work

The 2010 symposium, with its Question & Answer sessions and subsequent discussion at the regularly scheduled subcommittee meeting, revealed many areas in which Subcommittee F04.2's standards could be improved. This process of cleaning up inconsistencies has already begun in earnest. As was noted following the 2001 symposium, none of these changes are major, but rather they appear to be a matter of improving clarity and consistency of interpretation.

One sure sign of a maturing testing technology is the community exerting effort to increase the accuracy and repeatability of the measurements. Interestingly, ASTM F04.25's recent interlaboratory study to establish the precision and bias of the methods described in F1717 [3] is currently being repeated with a different design of fusion devices. We look forward to the continued improvement of spinal device testing methods so that users of F04.25's standards can continue to effectively evaluate spinal implants. Relatively mature standards, such as F1717 and F2077 are actively being supplemented by additional standards concerning a wide variety of innovative spine solutions. Current standards activities within F04.25 include impingement of motion preserving technologies, subsidence of interbody fusion devices, evaluation of annular repair, and combination cagelscrew devices.

Laura M. Jensen
David B. Spenciner
Jove Graham
Paul A. Anderson

References

1. Melkerson, M. N., Kirkpatrick, J. S., Griffith, S. L. Eds. Overview in STP1431 *Spinal Implants: Are We Evaluating Them Appropriately?*, ASTM International, West Conshohocken PA, 2003.
2. Cobian, D., Heiderscheit, B., Daehn, N. and Anderson, P. A., "Comparison of Daily Motion of the Cervical and Lumbar Spine to ASTM F2423-11 and IS0 18192-1.2011 Standard Testing." *J. ASTM Intl.*, Vol. 9, No. 1. doi: 10.1520/JA1103522.
3. Spenciner, D. B. Interlaboratory Study to Establish Precision Statements for ASTM F1717, Spinal Constructs in a Vertebrectomy Model, ASTM International Research Report. 2009.

Acknowledgments

Thank you to the ASTM F04 committee for their financial backing and technical support. Thank you also to the ASTM F04.25 subcommittee for their enthusiasm and commitment to making this project happen.

Before this book could even begin, we had some wonderful help in coordinating the symposium. From the ASTM staff, Dan Schultz, Dorothy Fitzpatrick, Mary Mikolajewski, and Hannah Sparks put in considerable work making sure that we had the space, the announcements, the communication, and the coordination that we needed in order to have a successful meeting and venue. Thank you also to Don Marlowe and John Kirkpatrick, members of the F04 committee, for their work on the student competition.

After the symposium, many people helped us make the book a reality. The staff at JAI international was especially important to translate the work from the symposium into the finished papers that you see in this book. We would especially like to thank Linda Boniello, Susan Reilly, and J. Graham Rankin whom we worked with directly on many occasions. Linda, your efforts in finding the lost and redirecting the confused were invaluable; your cheerful attitude made it look easy. Susan, when something needed communicating, you were right there to make sure it happened; thank you for keeping us on task and moving forward. Graham, your quiet presence kept things calm, rational, and moving forward. Thank you also to the rest of the JAI staff who kept things running smoothly even without introduction.

All along the way, many people helped us improve our technical content. Thank you to the following for their help reviewing abstracts and papers. Many of you were doing double or triple duty, and you generated some good discussions. We believe the papers are improved because of your efforts. Thank you to our reviewers in no particular order: Andrew Dooris, Stephen Summy, Marta Villarraga, Ryan Siskey, Lisa Ferrara, Bradley Estes, Dawn Lissy, Dennis Buchanan, Harry McKellop, Steven M. Kurtz, Vaneet Singh, Neil Crawford, Michael Bushelow, Michael C. Anderson, C. Brian Murrell, Bradley Estes, Sophia Sangiorgio, Boyle Cheng, Steve Jwanouskos, Heidi-Lynn Ploeg, Markus Froelich, Neil Crawford, Floyd Larson, Chris Lissy, Michael Adams, Stephen Ferguson, Sasidhar Vadapalli, Jeff Rouleau, Regina Konz, Elisa Bass, Donald Marlowe, Rebecca Blice, Michael Dahl, Anthony Tsantrizos, Dave Paller, Rick Greenwald, Dave Rosler.

Last, but not least, thank you to our families and colleagues who helped us find the time and encouragement we needed to see this project through completion. We're sorry we missed seeing you at the dinner table during busy parts of the project, but we're looking forward to breaking bread with you again next week!

Laura, Dave, Jove, and Paul

INTERBODY FUSION DEVICES

Reprinted from JAI, Vol. 9, No. 2
doi:10.1520/JAI103496
Available online at www.astm.org/JAI

Thomas Hansen[1]

Kinematic Stability Evaluation of Spinal Fusion Devices by Synthetic FSU Model

ABSTRACT: The purpose of the paper is to open discussion for an alternative methodology for stability testing of spinal fusion devices that does not require cadaveric tissue. A simulated single level functional spinal unit (FSU) model was used to evaluate spinal fusion devices as an alternative to using cadaveric human tissue models. Initially, this study was proposed as a feasibility investigation prior to investing in a cadaveric study, but was then developed into an alternative, stand-alone method that eliminates variabilities associated with cadaveric tissue testing for providing comparison testing between spinal devices. The objective of this paper is to present the development of the synthetic FSU model and the apparatus for providing kinematic stability testing on lumbar interbody spinal devices. The synthetic model geometry was based on morphological parameters for the lumbar spine using rigid foam per ASTM F1839. A universal servo-controlled test frame provided the pure moment loading through a system of cables and pulleys for the application of flexion-extension, lateral bending, and axial rotation. Comparable testing was performed using short cyclical, fully reversing runs up to 50 cycles where the last ten cycles were evaluated.

KEYWORDS: biomechanics, spine, lumbar fusion device, FSU model, range of motion, stability testing

Introduction

In vitro studies of isolated or multiple functional spinal units FSUs are often used to measure the biomechanical properties of the spine and any influence the devices may have on the spine's kinematic stability during functional motions. Various spinal fusion systems are used across the disc region between

Manuscript received October 15, 2010; accepted for publication October 31, 2011; published online November 2011.

[1]Biomechanics R&D, LLC, 1375 North Miller Rd., Tempe, Arizona 85281, e-mail: thansen@biomechrd.com

Cite as: Hansen, T., "Kinematic Stability Evaluation of Spinal Fusion Devices by Synthetic FSU Model," *J. ASTM Intl.*, Vol. 9, No. 2. doi:10.1520/JAI103496.

vertebral bodies to prevent collapse of the disc space and to help stabilize the segment until the fusion mass heals across the repaired disc. A spinal fusion system may include a stand-alone component or an assembly of different components. Surgical approaches and techniques for placing the system in the disc affect both the spine section during functional motions and the healing process during fusion across the disc. To provide comparison between systems or a combination of systems across different functional motions, the matrix of test cases for studies are increasing, which ultimately requires additional cadaveric donors. The availability of donors and non-controllable differences between donors can limit the study matrix or influence testing to some degree.

The objective of the paper is to open discussion for an alternative methodology for stability testing of spinal fusion devices that does not require cadaveric tissue. Synthetic models have always been encouraged for medical device testing to help minimize differences between specimens. However, synthetic models will always have some characteristics dissimiliar to fresh ligamentous spine tissues that are not desirable. The question for this discussion is to assess the benefits and deficiencies of a synthetic spine model for kinematic stability evaluations comparing different spinal fusion devices. Would it be appropriate to provide an ASTM standard for kinematic stability testing of spinal devices using a synthetic model similar to the ASTM Standard F1223, "Standard Test Method for Determination of Total Knee Replacement Constraint?"

Background Content

A literature review of lumbar biomechanical/kinematic studies involving fusion studies was conducted. The studies include flexion-extension, lateral bending, and axial rotation motions across the lumbar spine with and without fusion devices. The goal of the review was to provide a brief history on the techniques used for providing stability testing and outline the parameters for stability testing without discussing individual devices tested.

Panjabi's work [1] introduced the technique for the application of pure-moments across the spinal segment as opposed to offset vector loading. Panjabi pointed out that offset vector loading is dependent on geometrical relationships between the points of applied loading and constraint location, where the induced moment is different along the length of the model. The pure-moment loading would have the moment equally distributed along the spinal segment length without being altered by the geometrical relationship between the location of the applied moment and point of constraint. For a single level FSU model, Panjabi would place a coupled moment superior to the FSU segment of interest while constraining the model below. The coupled moment would involve equal but opposite vector forces about a central axis point on the FSU. The pure-moment was introduced quasi-statically through an apparatus consisting of pulleys and sandbags. A small pure-moment force was applied to the apparatus followed by a period of rest for gaining equilibrium in the FSU model prior to making measurements. Physical measurements from reference datum planes were made to provide delta changes in the positions of the spinal

segments induced by the moment. The process would be repeated using small incremental steps, until the moment across the FSU reaches a set functional moment across the spine.

Panjabi's conceptual pure-moment technique has become a standard for providing kinematic studies involving the spine. The technique has had multiple evolutional changes over the years in how the apparatus applies pure-moments and how the resultant motions induced by the moment are measured while still maintaining its core fundamental principles with pure-moment loading across the spinal column.

Cappuccino's study [2] provided a comprehensive review of lumbar fusion constructs which outline the current approaches for kinematic stability studies that have used cadaveric lumbar spinal models. Cappuccino's study addressed nine different investigators which provided similar studies on different lumbar fusion devices.

The apparatuses use in these reported studies involved custom-built systems for providing pure-moments across spinal sections of the spine. Systems ranged from pulleys and cables similar to Panjabi's initial work, up to state-of-the-art systems involving computer controlled servomotors for inducing pure-moments about the spine model. Pure-moment loadings were applied to the superior end of the specimen allowing complete 6 degree-of-freedom movements to the spinal model and were simultaneously constrained at the inferior end. The spinal models tested ranged from single level FSU segments to complete lumbar spines (L1-L5) as the test specimens for evaluating the fusion device. The set functional moment level to which the spine models were subjected ranged from ± 5 to ± 7.5 Nm. Each study used the same level of applied moment for all test cases (flexion-extension, lateral bending, or axial rotation). Cappuccino did not go into the details involving the applied rates for testing between the studies or the order of applied load cases between flexion cases. The application of a compressive normal force across the spinal section in addition to the pure moment loading was addressed to some degree. The compressive normal forces reported ranged from 0 (none) to 100 N for the representation of supporting upper body mass. The use of pre-conditioning cycles of pure-moment loading prior to measuring motions was mentioned, however, it was not discussed in detail other than varying from 3 cycles to upwards of 30 cycles of preconditioning prior to evaluating the motion between investigators.

The monitoring of a spinal section's motion has greatly improved since the Panjabi study, including the use of C-arms with radiographic evaluations during motion, optical or inferred LED markers with various motion measurement systems utilized for tracking the 3D motion of each vertebral body along the spinal section, and the fusion device's motion during testing. Most studies address comparative evaluations between the motions of the intact spinal model followed by the dissected and the various stages of implantation with different devices to the same spinal model. Cappuccino concluded that differences in test methodologies make it difficult to draw exact comparisons among biomechanical studies. A summarization of the trend outcomes between different devices could only be drawn between studies.

Materials and Methods

Test Setup

The apparatus we used for providing kinematic stability testing utilized a servo-controlled hydraulic test frame for the application of pure-moment loading through a pulley and cable system. The pure-moment was produced by an upper linkage arm attached to the actuator through a load cell as diagrammed in Fig. 1. The moment was transferred to the FSU model through cables and pulleys providing pure-moment motion to the superior aspect of the FSU. Uniform tension for transferring the moment through the pulley cables was maintained by attaching the ends of the cables to a free hanging deadweight (~5 kg). The deadweight was free to move vertically as demanded by the pulley and cable system.

The flexion motion across the superior aspect of the FSU model was measured using a two-axis (X, Y) inclination sensor, (ASM, Positilt, Model: PTAM20S-2-3-U6S-CW-T1.0-A300) with a $\pm 30^{\circ}$ range for each direction. This sensor measured the tilt angle with respect to a gravitationally level horizontal plane. The position outputs from the inclinometer were attached to the test frame's controller as auxiliary data channels.

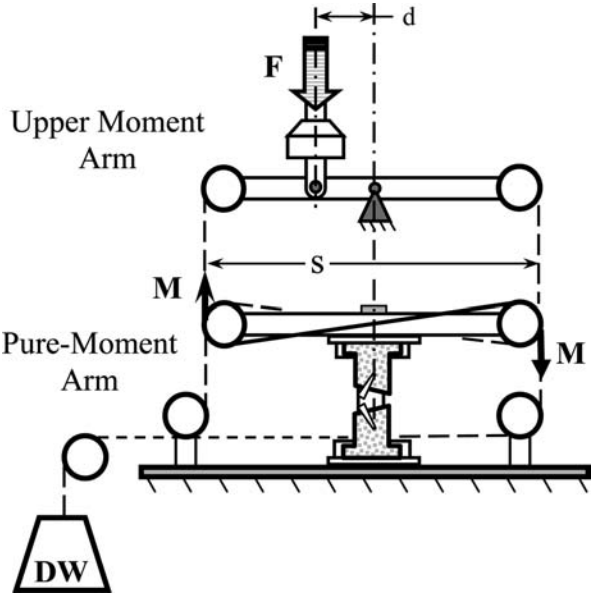

FIG. 1—*Schematic of pure-moment apparatus is presented. The applied force F from the test frame is offset d distance from a fulcrum point for generation of the moment, ($M = F \times d$). The coupled moment is attached through pulleys and cables with the pure-moment arm attached to the superior aspect of the FSU model, where equal but opposite directional forces spread s distance apart, providing the pure-moment about the FSU.*

For each flexion test (flexion-extension, lateral bending, and axial rotation) the pure-moment loading was performed using a fully reversing short cycle between alternating directions of motions. The peak magnitude of the pure-moment taken as the set functional moment across the spine, axial normal force against the FSU, and the rate of applied loading used during testing was developed during the course of feasibility testing based on what the synthetic FSU model could endure. The flexion testing included up to 50 cycles. During testing, elapsed time, load, stroke of the actuator's linear variable differential transformer, and the two angles from the inclination sensor were collected at 40 Hz. The elapsed time was used to determine the period within the cyclic count during testing. The load was converted to the applied moment by multiplication of the offset (L) distance between the load cell and fulcrum on the supported loading arm above the FSU. The test frame actuator's stroke measurement was useful in referencing the apparatus orientation position during testing, however, was not included for evaluations.

The motion of the superior aspect of the FSU model was evaluated through the collected data by the relationship of the flexion motion in the plane of the applied moment with respect to the magnitude of the moment applied. Hysteresis profile curves between the 40th and 45th cycle were used to chart this relationship for each specimen. The range of motion (ROM), neutral zone (NZ), elastic zone (EZ), and mean tangential stiffnesses (TS) within the EZ zone for each direction of motion were calculated as presented in Fig. 2. The TS was determined using a linear regression fit over the most

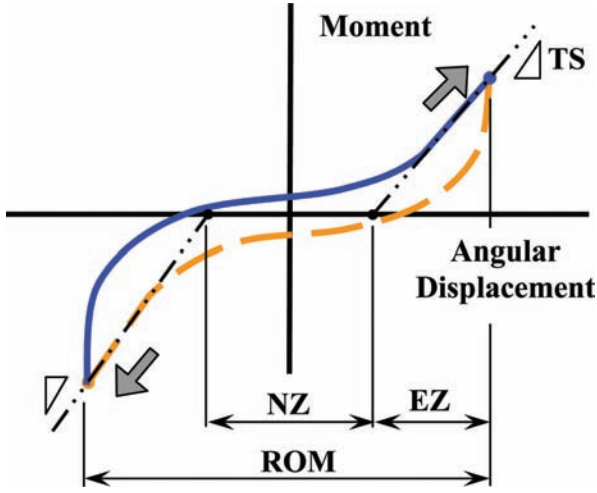

FIG. 2—*The range of motion (ROM), neutral zone (NZ), elastic zone (EZ), and mean tangential stiffnesses (TS) within the EZ zone for each direction of motion were calculated from the attained moment versus angular displacement hysteresis profile curves. The shaded arrows represent the direction of travel during cyclic testing.*

linear aspect of the EZ just prior to the set functional moment. The range for the linear regression fit included only the direction of motion where the magnitude of the moment was still increasing in value towards the set functional moment. The mean slope of the regressional equations over these five cycles was taken as the mean TS. The angular motion between the two x-intercepts from the regressional lines representing mean TS was used to calculate the NZ by using the mean y-intercepts and mean slopes from the five cycles. The ROM was also calculated from the mean regressional equations by using the nominal set functional moments for determining the delta peak-to-peak motion between the peak moments.

Synthetic FSU Model

The preparation of the synthetic FSU model mimics the rationale used for cadaveric spinal testing. Since it is preferable to use high quality bone and ligamentous integrity with fresh cadaveric donor specimens, the quality of the structural materials used for our synthetic model should be based on anatomical structural properties. The synthetic vertebral bodies were made from rigid polyurethane foam block material attained from Sawbones, Pacific Research Laboratories, Inc. Various densities, including 15-pcf (Part #15522-02), 20-pcf (Part #1522-03), and 30-pcf (Part #1522-04) foam blocks were evaluated. The size of the vertebral bodies conformed to unified lumbar L3 level within specified ranges from morphological measurements taken on both middle-aged male and middle-aged female adults as reported by Scoles [3].

For our stability evaluation, two anterior lumbar interbody fusion (ALIF) devices from different manufacturers were compared. Both ALIF devices used for testing contained a 12° lordotic angle, which was incorporated into the synthetic vertebral model. In addition, both an anatomically concaved endplate and flat surface endplate were evaluated, which conformed to the devices.

The synthetic foam vertebral body used during testing is presented in Fig. 3. The foam bodies included a base ledge around the exterior of the foam for mounting to the apparatus during testing. The distance above this mounting ledge was considered to be the height of the vertebral body.

The assembly of the synthetic FSU model was based on surgical procedures, as recommended by the manufacturer, using two bone screws for attaching the fusion device to the FSU. A machinist's vise was used to secure the FSU model while the system was assembled as presented in Fig. 4. The anterior surface of the device was aligned to the anterior edge along the FSU. Pilot holes were drilled through the ALIF for mounting bone screws to about half the screws lengths. The bone screws were fully seated into the ALIF device, except insertion torques were reduced from clinical values to prevent shearing of the foam during tightening. The locking mechanisms for holding the screw against the ALIF device were fully torqued to manufacturer values. Posterior coil tension springs were added across the FSU model to provide some resistance with the ALIF system attachment. The springs represented the posterior aspect of the FSU and joint capsule not included on the FSU model.

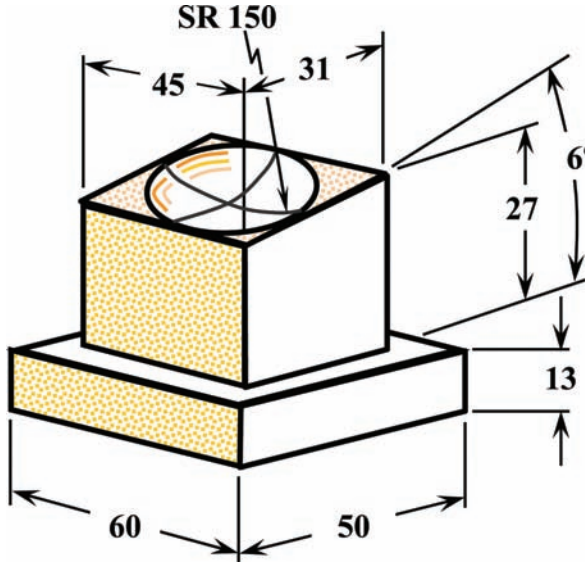

FIG. 3—*Diagram of FSU foam block representing a lumbar vertebral body and clamping base. All dimensions are in millimeters (mm).*

Procedure

The placement of the FSU model within the apparatus determined the flexion angle being tested with the alignment of the applied moment across the model, as shown in Fig. 5. The FSU was mounted against the base of the apparatus for flexion-extension and lateral bending, while the superior aspect was subjected to the pure moment loading. For torsion testing, the FSU was mounted against a vertical side plate with the posterior aspect of the FSU facing upwards. A guide post through the superior fixture assembly was utilized to offset gravity against the specimen.

The following steps were involved for testing the FSU model:

1. The FSU model was assembled on the workbench, including placing the device between the synthetic FSU bone model.
2. The FSU model was mounted to the apparatus in the desired orientation for the flexure motion test case.
3. The apparatus was preset with the actuator in stroke–control, with the fulcrum's lever arm at a level pre-determined horizontal position, allowing for assembly of the cables around the pulleys while aligning the superior aspect of the FSU horizontal.
4. The cable ends were attachment to the 8 kg deadweight to stabilize the system while the deadweights provided tension to the cables.
5. Once the system was stable, with the frame still in stroke-control, the load cell output was tared to a zero load state with no moments across the model.

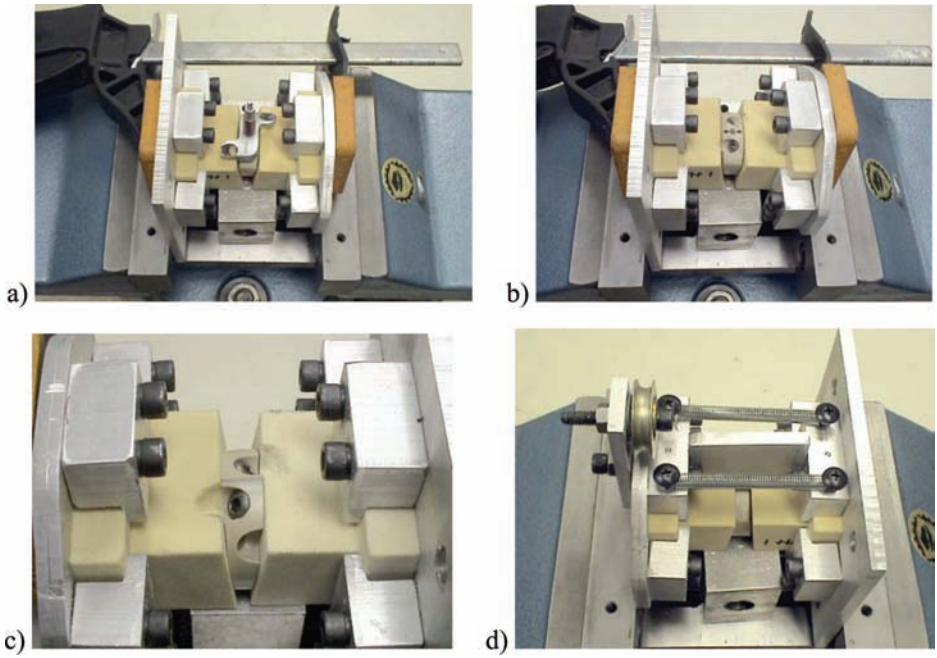

FIG. 4—*Typical assembly of the FSU specimen with the ALIF system is presented. (a) The placement of the device against the anterior surface profile of the FSU. (b) and (c) The final assembled devices within the FSU model used for this feasibility testing, and (d) shows the attachment of the coil springs representing the posterior aspect of the FSU. Posterior coil springs representing the posterior structure on the FSU model were attached along with the ALIF device while on the workbench.*

6. The frame was transferred to load-control for running the test case.
7. The function generator on the controller was engaged to run the short-term cyclic test while collecting output test data.
8. At completion of the testing, the test frame was transferred back to stroke-control to allow removal of the deadweights from the cables and disassembly of the FSU model from the apparatus.
9. The FSU model was visually evaluated while removing the device.
10. Fresh foam blocks were used for each test case, while the fusion devices were re-used between test cases.

Results and Discussion

This feasibility study is a conceptual attempt for providing an alternative methodology for stability testing of spinal fusion devices that does not require cadaveric tissue. The synthetic FSU model was not well established or validated with any known loading parameters along with the test setup used for providing

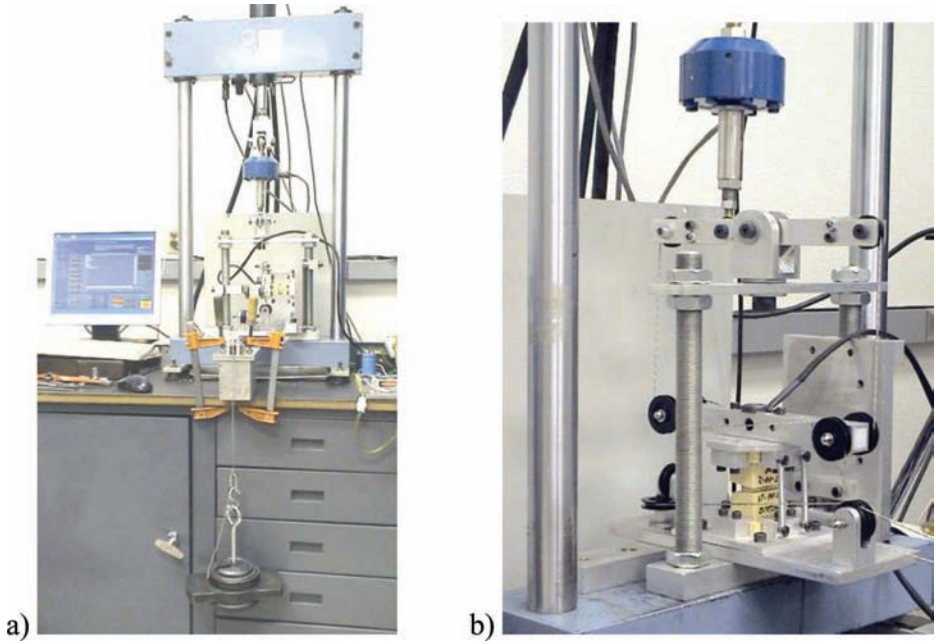

FIG. 5—*Typical assembly of the pure moment apparatus is presented. (a) The overall view showing hanging deadweights for maintaining cable tension during testing. (b) View of the upper moment arm for the application of the pure-moment during flexion-extension testing.*

stability testing being not well established or used prior with cadaveric tissues. The parameters used for testing all interacted with one another to some degree. The following is a brief discussion of our findings for each parameter.

Set Functional Moment

Feasibility testing was initiated by using ±2 Nm using a 0.25 Hz triangular wave profile. The 0.25 Hz rate required 200 s for completing the 50 cycles of testing, which appeared to be a reasonable time frame for evaluating the test. The apparatus was very stable, which allowed us to increase the moment to upwards of ±4 Nm at 0.25 Hz while still maintaining a stable profile over the 50 cycles of testing. Upon increasing the moment to ±5 Nm and above, the stability of the apparatus became an issue. The hysteresis profile would not fully stabilize with the ROMs increasing over each cycle. It was desirable for the apparatus to allow higher pure-moments upwards to the ±7.5 Nm magnitude to be more consistent with literature values. The factors restricting our apparatus were believed to be related to the following: the lack of posterior structure holding the FSU together, the holding strength of the foam model with the attachment of the device, the use of an axial normal force, and/or the size of our coupled forces generating the moment being too small.

Compressive Normal Forces

The two small coil springs which provided some posterior resistance across the FSU model induced approximately 40 N of tensional force across the FSU located 50 mm posterior to the center of the devices. Without the springs, the posterior aspect of the model was unconstrained making the model unstable during testing. With higher applied moments, the unstable flexion motion during testing was related to the device wanting to lift upwards as the moment translated over the model as diagrammed in Fig. 6. Intuitively, an added compressive pre-load across the model during testing will resist the unstable motion allowing for higher moments. The compressive load could be addressed as representing the upper body mass being supported above the spine, since it aids the stability of the model.

We addressed this issue by placing four coil springs across the four sides of the model similar to the smaller springs. In total, the four springs applied approximately 170 N of force across the model. The additional springs did allow a ±5 Nm moment loading, however, it was questionable as a viable solution for the application of the compressive normal force. A deadweight platform above

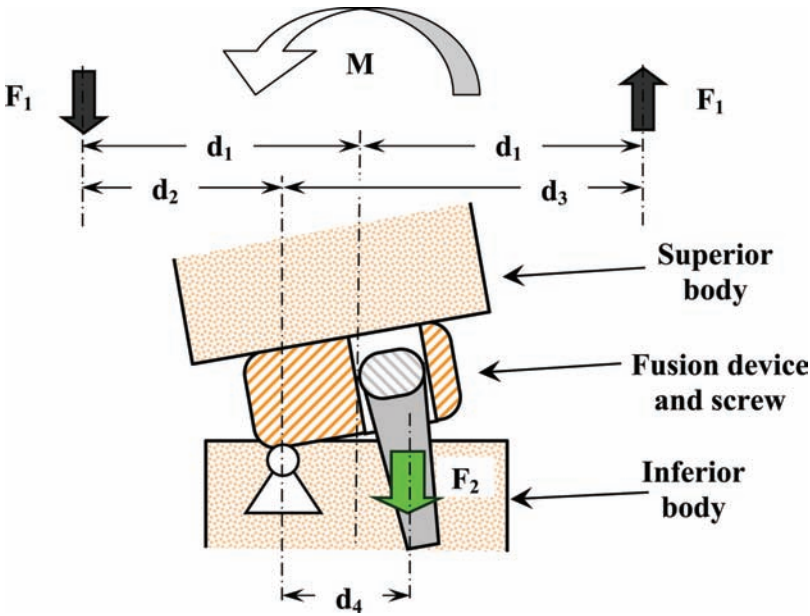

FIG. 6—*Simplified lever scenario with transferring load across the fusion device. The coupled moment M is applied by bi-directional forces F_1. The applied moment M causes the device to lift with the superior vertebral bone as shown during cyclic loading. This introduces an offset fulcrum point on the device that leads to loosening (pullout) of the screw. Equilibrium is regained across this offset fulcrum point as the offset motion balances between the summation of the moments; $(-F_1 \times d_2) + (+F_1 \times d_3) = (-F_2 \times d_4)$.*

the FSU was considered a better alternative for the application of this normal force for future revisions.

Synthetic FSU Model

The rigid polyurethane foam blocks representing the vertebral bodies provided a platform which was well suited for mounting the ALIF fusion device with screw fixation. The density of the model was a factor during testing, similar to how the bone quality between cadaveric donors can affect evaluations. Lower density foams, such as 15-pcf foam, attained a greater degree of motion as compared to higher densities, (20-pcf and 30-pcf), although the device would firmly seat into the foam model. Increasing the foam density provided increased pull-out strength for holding the screws and device within the model. With higher densities such as 30-pcf, the textured surfaces along the devices would not fully subside or seat into the foam, providing less surface contact, leading to device migrating or slide during testing. Post-test evaluation of the device imprint into the foam was a vital mechanism for comparison between devices.

With the FSU not containing a structural disc, it was required that the fusion device provide structural fixation to the model. No intact or dissected spine FSU model could be evaluated for providing baselines for comparison. Testing without placement of the bone screws also did not provide structurally stable testing, with the superior aspect of the FSU having a tendency to migrate during testing. The design of the devices provided placement of the bone screws towards the anterior aspect of the FSU. The posterior aspect was still unconstrained and would lift by induced moments providing a tensile force across the posterior aspect of the device. In future development of the synthetic FSU model, a polyurethane or other elastomeric material representing the disc will improve the model. However, without the disc, the model is allowing the direct visualization of the relative motions of the fusion device between the foam vertebral bodies.

Conclusions

The objective of this study was to open discussion for an alternative methodology for the stability testing of spinal fusion devices that do not require cadaveric tissue. The study provided a synthetic single level FSU model which demonstrated stability testing for flexion-extension, lateral bending, and axial rotation for a lumbar fusion device. Although the model was conceptual in design, it has the potential for advancing testing methodology for the evaluation of spinal fusion devices. Further development of the synthetic FSU models could lead to side-by-side comparisons of various spinal systems using a more controllable medium other than cadaveric tissues.

References

[1] Panjabi, M. M., "Biomechanical Evaluation of Spinal Fixation Devices: I. A Conceptual Framework," *Spine*, Vol. 13(10), 1988, pp. 1129–1134.

[2] Panjabi, M., Abumi, K., Duranceau, J., and Oxland, T., "Spinal Stability and Intersegmental Muscle Forces a Biomechanical Model," *Spine*, Vol. 14(2), 1989, pp. 194–200.

[3] Scoles, P. V., Linton, A. E., Latimer, B., Levy, M. E., and Digiovanni, B. F., "Vertebral Body and Posterior Element Morphology: The Normal Spine in Middle Life," *Spine*, Vol. 13(10), 1988, pp. 1082–1086.

Reprinted from JAI, Vol. 9, No. 1
doi:10.1520/JAI103498
Available online at www.astm.org/JAI

Ameet K. Aiyangar,[1] *Anthony G. Au,*[2] *Paul A. Anderson,*[3] *and Heidi-Lynn Ploeg*[4]

Comparison of Two Bone Surrogates for Interbody Device Subsidence Testing

ABSTRACT: Bone surrogates are proposed alternatives to human cadaveric vertebrae for assessing interbody device subsidence. Polyurethane foam blocks are an accepted surrogate for cancellous bone but do not share their heterogeneous bone density distribution. Synthetic vertebrae have been recently developed as an alternative bone surrogate with representations of cortices, endplates, and cancellous bone. The efficacy of each surrogate was evaluated by uniaxially indenting it with an interbody device. The force-displacement curve profiles, failure forces, and depth of implant subsidence were compared for devices seated centrally and peripherally on the surrogates. The synthetic endplate mimicked human endplates through a gradually increasing endplate thickness toward the periphery. This enabled the synthetic vertebrae to provide additional subsidence resistance to implants seated at the periphery. By contrast, the foam block was insensitive to implant placement. Absence of failure in synthetic vertebrae from peripheral implant indentation suggests the synthetic endplate is stronger than human endplates but further study with human cadaveric vertebrae is needed.

Manuscript received October 15, 2010; accepted for publication August 5, 2011; published online September 2011.

[1]Depart. of Mechanical Engineering, Univ. of Wisconsin-Madison, 3046 Mechanical Engineering Building, 1513 Univ. Ave., Madison, WI-53706, e-mail: aiyangar@cae.wisc.edu

[2]Depart. of Mechanical Engineering, Univ. of Wisconsin-Madison, 3046 Mechanical Engineering Building, 1513 Univ. Ave., Madison, WI, 53706, e-mail: agau@ualberta.ca

[3]Depart. of Orthopedics and Rehabilitation and Dept. of Biomedical Engineering, Univ. of Wisconsin-Madison, 6136, UW Medical Foundation Centennial Building, 1685 Highland Ave, Madison, WI 53705, e-mail: anderson@ortho.wisc.edu

[4]Depart. of Mechanical Engineering and Dept. of Biomedical Engineering, Univ. of Wisconsin-Madison, 3043, Mechanical Engineering Building, 1513 Univ. Ave., Madison, WI, 53706. e-mail: ploeg@engr.wisc.edu

Cite as: Aiyangar, A. K., Au, A. G., Anderson, P. A. and Ploeg, H.-L., "Comparison of Two Bone Surrogates for Interbody Device Subsidence Testing," *J. ASTM Intl.*, Vol. 9, No. 1. doi:10.1520/JAI103498.

KEYWORDS: biomechanics, subsidence, lumbar vertebra, interbody device, polyurethane foam, synthetic vertebra, surrogate

Introduction

Subsidence is one of the complications arising from the use of interbody cage devices for fusion surgeries, described as the sinking of the device into one, or both, of the adjacent vertebrae [1]. Subsidence can potentially affect outcomes adversely in several ways. It can instigate an array of complications, such as the progressive development of spinal deformity, foraminal stenosis, pseudoarthrosis or non-union, and, in the worst case, failure of the device itself [2]. When fusion surgery is performed the device-body construct is held tightly in place by the tension introduced in the ligaments by distracting the vertebrae, known as ligamentotaxis. The reduction in this disc space from subsidence could reduce the ligamentotaxis, which could reduce the structural support provided by the ligaments, which could lead to dislodging of the device and graft. In short, subsidence can potentially cause an unraveling of the putative benefits of fusion surgeries.

The importance of subsidence as a cause of surgical failure has been recognized through an American Society for Testing and Materials (ASTM) standard for characterizing subsidence of fusion cage products (F2267-04) [3]. The biggest advantage of the current standard is the simplicity of the test design and implementation protocol. The standard evaluates devices under a straightforward axial compressive force, which is the most dominant loading condition for anterior interbody devices. It recommends a readily available polyurethane foam block as a surrogate for human vertebrae, obviating the need to account for large variances in the properties of human vertebrae. The foam block models the mechanical behavior of the vertebral trabecular core reasonably well but the human vertebra has two, additional, important structural components: a thin shell of compact bone surrounding the trabecular core and bony endplates located on the superior and inferior surfaces. The polyurethane foam block fails to account for any contributions from the shell and the bony endplates.

Developing a surrogate that accurately represents the structural complexity of the human vertebra can improve the current ASTM standard and make it more relevant in clinical settings. A new lumbar vertebra surrogate has been developed recently (Sawbones, Vashon Island, WA) that captures the geometry of human vertebra, and includes a fiberglass-epoxy shell enclosing a closed-cell polyurethane foam core. The fiberglass-epoxy shell attempts to mimic the outer cylindrical cortical shell and the bony endplates of the vertebra.

In vitro subsidence studies employing human vertebrae have revealed two key findings: (a) placing cages along the stronger, peripheral regions of the lumbar vertebra instead of the weaker central portion reduces the risk of subsidence [2,4] and (b) absence of an endplate lowers the compression and indentation strength of vertebrae [5–7].

The current study investigated the sensitivity of the synthetic vertebra and polyurethane foam block to interbody device placement with regard to subsidence and failure force. It was hypothesized that the presence of an endplate

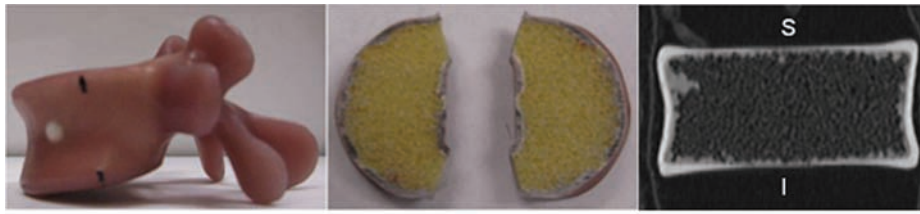

FIG. 1—*(a) Side view of the synthetic vertebra. (b) A transverse section through the anterior vertebral body reveals a polyurethane foam core enclosed by a thin layer of fiberglass-reinforced epoxy. (c) The superior (S) and inferior (I) layers of the epoxy shell increase in thickness as they approach the periphery of the vertebra, as shown by a CT image of the mid-coronal section.*

would generate significant differences in subsidence behavior between synthetic vertebrae and foam blocks.

Methods

Twelve 4 cm × 4 cm × 4 cm polyurethane foam specimens (PU), cut from a single foam block of density 200 mg/cm^3 and six L5 synthetic lumbar vertebrae (SV) (Sawbones, Vashon Island, WA) were used for the study. The synthetic vertebrae were composed of a cellular, rigid polyurethane foam core enclosed in a short-glass-fiber-reinforced (SGFR) epoxy shell (Fig. 1). The foam core was of the same type as the polyurethane (PU) foam blocks, i.e., 200 mg/cm^3 density polyurethane foam from Sawbones, which is a 95 % closed cell rigid foam. The mechanical properties of the foam and epoxy are listed in Table 1. The posterior elements of the synthetic vertebrae were removed and the anterior bodies were transversely sectioned into superior and inferior halves using a stationary band saw, resulting in twelve specimens. The synthetic vertebrae were cast into a polyester resin (Bondo, 3M, St. Paul, MN) within a steel bracket to fix the bottom surfaces, with the endplates facing up. The endplates were adjusted to be horizontal using a bubble level before the resin hardened. Two hollow, aluminum cylindrical "indenters" of different outer and innerdiameters, but similar cross-sectional areas—the difference between the cross-sectional areas was 3.1 %—were used as generic interbody cage implant devices to study the effect of placement on the subsidence characteristics in each of the two surrogate

TABLE 1—*Synthetic vertebra mechanical properties.*

Material	Tensile Modulus	Tensile Strength	Compressive Modulus	Compressive Strength	Flexural Modulus	Flexural Strength
SGFR epoxy (SV)	16 GPa	106 MPa	16.7 GPa	157 MPa	13.7 GPa	133 MPa
Polyurethane foam (PU)	…	…	48 MPa	4 MPa	…	…

TABLE 2—*Inner and outer diameters of the two indenters. Contact area did not include the area from the rounded edges.*

Indenter Size	Inner Diameter (mm)	Outer Diameter (mm)	Contact area (mm^2)
Small	12.7	25.4	238.7
Large	21.2	31.3	246.1

groups (PU and SV). The dimensional details of the cylindrical indenters have been delineated in Table 2.

Specimens in the centrally seated implant group (six PU, six SV) were indented with the "small" implant seated on the central region of the endplate supported solely by the foam core, while specimens in the peripherally seated implant group (six PU, six SV) were indented with the "large" implant to ensure that the indented endplate was supported by both cortical and cancellous bone.

The specimen-implant combination was loaded in compression in a servohydraulic material testing machine (858 Bionix, MTS, Eden Prairie, MN) under a displacement control protocol at a quasi-static displacement rate of 2.5 mm/min up to a total crosshead displacement of 5 mm. The chosen displacement rate was higher than the rate of 1mm/min recommended by the ASTM standard [3]. The higher displacement rate was chosen mainly due to inherent constraints in the data acquisition system of the testing unit used. However, it was deemed to be acceptable for the current study as the loading rate was slow enough to be considered "quasi-static." Moreover, both the surrogates were tested under the same conditions, and the principle aim was to compare the performance of the two vertebral surrogates rather than obtain absolute measures. A preload of approximately 100 N was applied in order to ensure all components were contacting and stable before commencing the test. Axial compressive force, crosshead displacement, and extensometer displacements were recorded for each test. All tests were conducted at room temperature. Figure 2 shows a schematic of the test set up.

Subsidence was measured using four extensometers and reported as the average of the four extensometer readings after unloading. Each extensometer was calibrated with a sliding stage with a resolution of 5 μm (UMR 12.40, Newport, Irvine, CA) to ensure accuracy. The extensometer probes were secured to each platen of the stage and compressed at two ranges: 0.0–1.2 mm and 5.0–6.2 mm. Calibration equations were determined from linear regression curves fit to the displacement data, which had coefficients of determination (r^2) ranging from 0.993 to 1.000. Failure force in synthetic vertebrae was defined as the peak force before the force decreased for the first time. A peak force could not be measured from the foam block curves; therefore failure force was defined as the point of intersection between the force-displacement curve and a line drawn parallel to the slope of the linear region with a displacement offset of 0.2% initial foam block height [8]. In addition, the measured failure force was normalized to the cross-sectional area of the indenters—effectively an ultimate stress measure—in order to account for any potentially confounding effects of the small difference

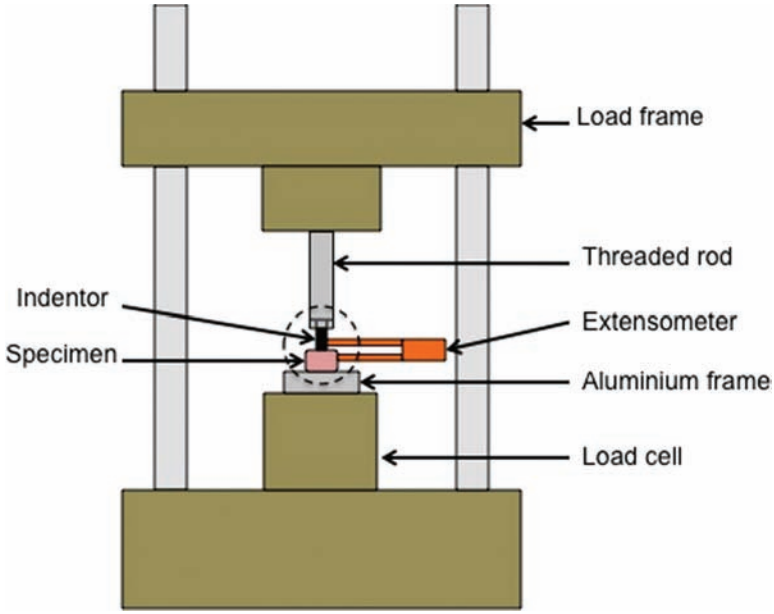

FIG. 2—*Schematic of test setup for implant indentation into synthetic vertebra and polyurethane foam block. Subsidence was measured using four, custom-made extensometers attached between implant and surrogate using needles (front, rear and two side locations). Note: schematic only shows one extensometer.*

in measured cross-sectional areas of the two indenters. One-way factorial analysis of variance was used to determine significant differences in failure force and subsidence between implant seating position (i.e., central or peripheral) within each specimen type. A post hoc Tukey–Kramer test was used to determine which of the means were significantly different from one another within the groups. A 95 % significance level ($\alpha = 0.05$) was used for all tests.

Results and Discussion

Table 3 summarizes the measured failure force and subsidence for the four subgroups: PU, central, and peripheral placement and SV, central, and peripheral placement. Figure 3 illustrates typical force-displacement curves for the two surrogate groups. The failure force for the foam block (central: 1161 ± 89N, peripheral: 1384 ± 131 N) falls within the range of results from studies with implants indenting human cadaveric vertebrae (504 – 818 N [9], 1473 ± 172 N [10], and 510 – 1335 N [11]). However, the synthetic vertebrae were much stronger. The mean failure force for specimens with centrally placed indenters (4497 ± 296 N) was more than three times the failure force for the foam blocks observed in the current study, as well as the failure force for human cadaveric vertebrae, as evidenced by studies conducted on human vertebrae [9–11]. Peripheral placement of the indenters did not result in catastrophic failure of

TABLE 3—*Failure force and subsidence levels for the two surrogate groups under central and peripheral implant placement (mean ± SD).*

Sample	Implant Location	Failure Force (N)	Failure Force/ C.S. Area (N/mm^2)	Subsidence (mm)
Synthetic Vertebra	Central	4497 ± 296^a	18.8 ± 1.2^a	1.01 ± 0.33^a
	Peripheral*	N/A*	N/A*	0.40 ± 0.30^b
Polyurethane Foam	Central	1161 ± 89^b	4.9 ± 0.4^b	2.72 ± 0.04^c
	Peripheral	1384 ± 131^b	5.6 ± 0.5^b	2.66 ± 0.04^c

Note: * = Synthetic vertebrae did not fail under peripheral implant placement. Within each column, differing superscripts (a, b, c) represent significant differences.

the synthetic vertebrae when tested up to 5 mm of crosshead displacement. However, the maximum compressive force at this point (4345 ± 201) was similar to the centrally placed counterparts.

The force-displacement curves reveal some important differences in the response between the PU and SV groups, indicating different modes of failure and damage propagation within the surrogates. The curve for synthetic vertebra, taken from a specimen with centrally placed indenter, shows a peak failure force followed by a drop in the force with further indentation. The force drop coincided with failure of the endplate, whereby subsequent resistance to implant subsidence was provided largely by the foam core. The polyurethane foam, however, displays no such characteristic; rather the force-deformation curve increases linearly up to a yield point upon which the curve becomes much

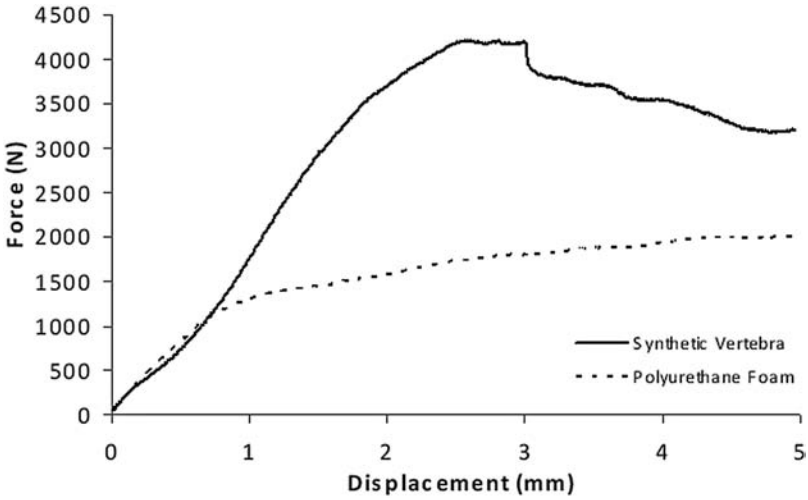

FIG. 3—*Typical force-displacement curves for synthetic vertebrae and polyurethane foam blocks indented with a centrally placed implant.*

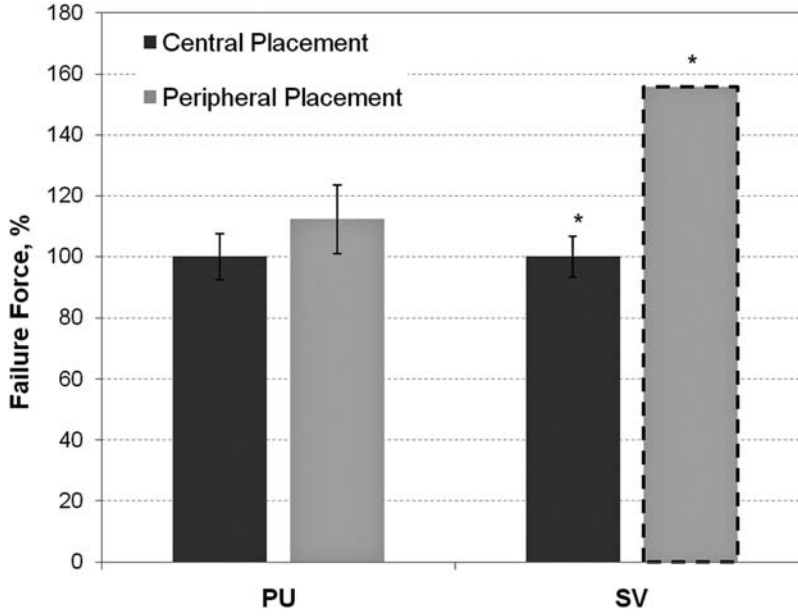

FIG. 4—*Failure forces for the synthetic vertebrae (SV) and polyurethane foam (PU) groups. Data are normalized to the centrally placed failure force for each group. Y-axis values are percentages. An asterisk indicates significant difference between mean values ($\alpha = 0.05$). SV did not fail within the 5 mm crosshead displacement range for the peripherally placed implants hence the bar graph is shown with a dotted outline.*

less sloped, indicating continuous subsidence of the implant into the foam with little additional force required.

The effect of placement within each group reveals an additional difference between the two surrogates. Figures 4 and 5 compare the effect of cage placement on failure force and subsidence within the PU and SV groups; the data were normalized with respect to the value obtained for the centrally placed implant to better portray the contrast within each group. The synthetic vertebrae showed a significantly greater resistance to subsidence (denoted by an asterisk in the figures) under peripheral implant placement. The resistance to peripheral indentation was underscored by the fact that the synthetic vertebrae did not fracture under the 5 mm crosshead displacement range. Thus, the synthetic vertebrae had a greater resistance to failure under peripheral implant placement. The results for the polyurethane foam specimens; however, were statistically indistinguishable based on the implant placement position, mainly due to its homogeneous composition. Since the synthetic vertebra's core is identical to the polyurethane foam, this difference must necessarily be attributed to the outer SGFR-epoxy shell component, which aims to simulate the cortical shell and the endplate. The addition of the (SGFR) epoxy shell to the foam core provided a significantly greater resistance to failure and subsidence compared to the foam block (Table 3). The thickness of the endplate increased progressively as it

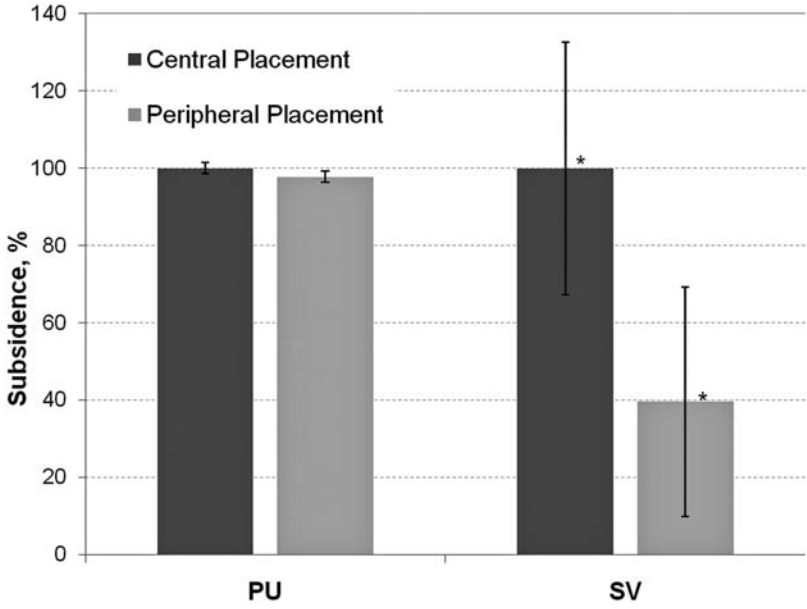

FIG. 5—*Subsidence levels for the synthetic vertebrae (SV) and polyurethane foam (PU) groups. Data are normalized to the centrally placed failure force for each group. Y-axis values are percentages. An asterisk indicates significant difference between mean values* ($\alpha = 0.05$).

approached the periphery, which was particularly influential in the vertebra's ability to resist subsidence from implants seated on the outer endplate.

The synthetic vertebra can be considered to be a composite material with a non-rigid skin (the endplate) fixed to a flexible foundation (the polyurethane foam core) surrounded by a stiff shell. The mechanical response of such a structure to vertical, indentation loads transmitted via the implant is analogous to the behavior of an elastic beam attached to an elasto-plastic foundation, as described for indentation of composite sandwich structures by Shuaeib and Soden [12], based on earlier work by Zingone [13]. The failure modes observed by Shuaeib and Soden [12] were similar to those seen in the current study: the force-deflection curve for synthetic vertebrae (Fig. 3) was initially linear after the toe region, and became non-linear after some audible, cracking noises, culminating in a large cracking sound as the endplate fractured and the force dropped noticeably.

Using their analysis of a concentrated load at the midpoint of a beam on an elasto-plastic foundation, some qualitative insights can be obtained. Briefly reproducing their theoretical analysis, they found that the load at which the core begins yielding is given by the following equation:

$$P_y = 2\sigma_c b \times \left(\frac{4cE_f I_f}{E_c b}\right)^{1/4} \times \frac{\sinh(\lambda L) + \sin(\lambda L)}{\cosh(\lambda L) + \cos(\lambda L) + 2} \tag{1a}$$

If $\lambda L \gg 1$, then

$$P_y = 2\sigma_c b \times \left(\frac{4cE_fI_f}{E_cb}\right)^{1/4} \quad (1b)$$

where P_y = load at core yielding, σ_c = core yield strength, b = beam width, c = foundation thickness, E_f = beam bending modulus, I_f = beam second area moment of inertia, E_c = foundation compression modulus, L = beam length, $\lambda = (E_cb/4cE_fI_f)^{1/4}$.

Equation 1 reveals the load required to cause yielding in the underlying core is proportional to the ratio of the moduli of the beam and the foundation (E_f/E_c), which in the case of synthetic vertebrae, would be the ratio of elastic moduli of the endplate and the foam core. A stiffer endplate compared to the core—the case for both synthetic and human vertebrae—would increase the load required to cause yielding in the core, explaining the higher failure force of the synthetic vertebra compared to the foam block.

Conclusion

The synthetic vertebrae developed by Sawbones (Vashon Island, WA) were more anatomically representative of human vertebrae than polyurethane foam blocks, being comprised of two materials, including an endplate that was thicker and stronger at the periphery. The synthetic vertebrae qualitatively captured a key characteristic of implant subsidence seen in human vertebrae: peripheral placement resulted in better subsidence resistance compared to central placement. This behavior was not observed with polyurethane foam blocks on account of its homogeneous density.

The synthetic vertebrae show promise as a better surrogate for use in the ASTM standard; nevertheless the extent to which the synthetic vertebrae mimic the performance of the human vertebrae can only be quantified by comparing them to experimental results from in vitro tests on human vertebrae. The compressive forces required for failure of the synthetic vertebrae with centrally placed indenters were significantly higher (> 3 times) than previously reported failure forces for human cadaveric vertebra. This observation coupled with the lack of failure of the specimens with peripherally placed indenters within the 5 mm crosshead displacement indicates that the outer shell, including the endplate for the synthetic vertebrae are potentially much stronger than required and its mechanical properties might need to be optimized to better replicate the range of human vertebral strength.

Acknowledgments

The writers would like to thank Ms. Amy Johnson, Dr. Hirohito Kobayashi, and Mr. Ronald McPhee for their technical assistance. The writers are also grateful to the assistance provided by Ms. Yvonne Schumacher and Mr. Geoffrey Piller during testing. This work was supported by the Natural Science and

Engineering Research Council of Canada (NSERC) and the University of Wisconsin Graduate School. The synthetic vertebrae prototypes were provided by Sawbones, Vashon Island, WA, developed as part of an NIH SBIR grant (No. 5R44 AR054289-03).

References

[1] Williams, A. L., Gornet, M. F., and Burkus, J. K., "CT Evaluation of Lumbar Interbody Fusion: Current Concepts," *AJNR Am. J. Neuroradiol.*, Vol. 26(8), 2005, pp. 2057–2066.

[2] Lowe, T. G., Hashim, S., Wilson, L. A., O'Brien, M. F., Smith, D. A. B., Diekmann, M. J., and Trommeter, J., "A Biomechanical Study of Regional Endplate Strength and Cage Morphology as it Relates to Structural Interbody Support, *Spine*, Vol. 29(21), 2004, pp. 2389–2394.

[3] ASTM-F2267-04, 2004, "Standard Test Method for Measuring Load Induced Subsidence of Intervertebral Body Fusion Device Under Static Axial Compression", ASTM International, West Conshohocken, PA.

[4] Grant, J. P., Oxland, T. R., and Dvorak, M. F., "Mapping the Structural Properties of the Lumbosacral Vertebral Endplates," *Spine*, Vol. 26(8), 2001, pp. 889–896.

[5] McBroom, R., Hayes, W. C., Edwards, W. T., Goldberg, R. P., and White, A. A., "Prediction of Vertebral Body Compressive Fracture using Quantitative Computed Tomography," *J. Bone Joint Surg. Am.*, Vol. 67(8), 1985, pp. 1206–1214.

[6] Rockoff, S. D., Sweet, E., and Bleustein, J., "The Relative Contribution of Trabecular and Cortical Bone to the Strength of Human Lumbar Vertebrae," *Calc. Tissue Int.*, Vol. 3(1), 1969, pp. 163–175.

[7] Oxland, T. R., Grant, J. P., Dvorak, M. F., and Fisher, C. G., "Effects of Endplate Removal on the Structural Properties of the Lower Lumbar Vertebral Bodies," *Spine*, Vol. 28(8), 2003, pp. 771–777.

[8] Steffen, T., Tsantrizos, A., and Aebi, M., "Effect of Implant Design and Endplate Preparation on the Compressive Strength of Interbody Fusion Constructs," *Spine*, Vol. 25(9), 2000, pp. 1077–1084.

[9] Tan, J.-S., Bailey, C. S., Dvorak, M. F., Fisher, C. G., and Oxland, T. R., "Interbody Device Shape and Size Are Important to Strengthen the Vertebra-Implant Interface," *Spine*, Vol. 30(6), 2005, pp. 638–644.

[10] Hollowell, J. P., Vollmer, D. G., Wilson, C. R., Pintar, F. A., and Yoganandan, N., "Biomechanical Analysis of Thoracolumbar Interbody Constructs: How Important Is the Endplate?," *Spine*, Vol. 21(9), 1996, pp. 1032–1036.

[11] Hasegawa, K., Abe, M., Washio, T., and Hara, T., "An Experimental Study on the Interface Strength Between Titanium Mesh Cage and Vertebra in Reference to Vertebral Bone Mineral Density," *Spine*, Vol. 26(8), 2001, pp. 957–963.

[12] Shuaeib, F. M. and Soden, P. D., "Indentation Failure of Composite Sandwich Beams," *Compos. Sci. Technol.*, Vol. 57, 1997, pp. 1249–1259.

[13] Zingone, G., "Limit Analysis of a Beam in Bending Immersed in an Elastoplastic Medium," *Meccanica*, 1968, pp. 48–56.

Reprinted from JAI, Vol. 8, No. 7
doi:10.1520/JAI103501
Available online at www.astm.org/JAI

C. Wayne Metheny[1]

Symposium on Static and Dynamic Spinal Implants: Are We Evaluating Them Appropriately?

ABSTRACT: Although the standard characterizes intervertebral fusion devices with simple symmetric shapes, modern devices may contain more complex geometries that may require a pocket to fully characterize their strength. Test fixture design has proven to significantly affect the static shear result and failure mode of intervertebral fusion devices with a bullet-nose (rounded) design. An initial test using fixtures without pockets was unsuccessful in determining the shear strength of the fusion device bodies. Revised fixtures with a pocket to force shear loading through the center of the device were designed to create a functional failure. For this study, testing was performed using the ASTM recommended 45° Z axis with a spherically attached actuator pushrod in 37 degrees C phosphate buffered saline. The initial stainless steel fixtures featured mating tooth geometry and no pocket, which forced failures to the device teeth only, resulting in expulsion of the device from the testing fixtures. The revised stainless steel fixtures featured the mating tooth geometry and incorporated a larger anterior/posterior contact surface; thus creating a pocket to constrain the bullet-nose device that prevented the device from expelling. The fusion devices tested with the revised fixture design produced a compression-shear failure of permanent plastic deformation of the body of the device resulted in a 90.2 % increase in the mean yield strength as compared to the fusion devices tested with the initial no-pocket design fixture that produced failures of only the device teeth. The results of this study revealed how the static shear result and failure mode can change significantly with minor changes in fixture design.

KEYWORDS: ASTM F2077-03, compression-shear, fixture, pocket, static

Manuscript received October 15, 2010; accepted for publication May 8, 2011; published online July 2011.

[1] Medtronic Spinal and Biologics, Memphis, TN 38132.

Cite as: Metheny, C. W., "Symposium on Static and Dynamic Spinal Implants: Are We Evaluating Them Appropriately?," *J. ASTM Intl.*, Vol. 8, No. 7. doi:10.1520/JAI103501.

Introduction

As stated in ASTM F2077, intervertebral body fusion devices are designed to promote arthrodesis at a given spinal motion segment [1]. The interbody fusion devices differ with regard to size, shape, and attachment method based on surgical technique and anatomical conditions [1]. While the test methods of the standard allow for evaluation and comparison of these devices, the components used in the test methods may produce different results due to the need to accommodate for these variations. Although the standard does not address expulsion testing, the need to prevent expulsion during static compression-shear testing may be required due to the combined effects of the test angle and geometry of the device [1]. The current study will serve as an example of how to compensate for the these effects while adhering to the standard when performing static compression-shear testing.

Static compression-shear testing was performed on a 16 mm × 36 mm (height × length) polyetheretherketone (PEEK) intervertebral fusion device. The device has a convex shape with a bullet-tip design and a tooth-like surface to reduce the likelihood of expulsion. The objective of this study was to determine the implant's compressive-shear strength while under a worst-case testing condition. The size was selected as it is the tallest and longest size offered in the spinal system.

White and Panjabi report a compressive load for more common activities, such as a 20° forward flexion motion, to be around 1200 N at lumbar discs [2]. Also, a load of 1200 N is generally used for various studies to evaluate biomechanical properties of lumbar (L1-S1) [3,4]. Clinically, shear loads will be imparted on the device during flexion/extension or lateral bending motions. According to White and Panjabi, the maximum angle between L5-S1 vertebra is 17 degrees in flexion/extension [5].

Considering the biomechanical condition with a compressive load of 1200 N and 17° tilt as the most severe condition in lumbar, the 45° tilt which ASTM F2077-03 [1] specifies as the axial compressive load in compression-shear testing theoretically results in 242 % (sin 45/sin 17 = 2.42) higher shear load than the most severe condition in vivo, under the same compressive load. Therefore, the compression shear testing stated in ASTM F2077-03 [1] simulated a severe shear force condition than reported in vivo, thus creating a worst-case testing condition.

Testing with revised test fixtures was performed after initial testing was unsuccessful in producing a functional failure. It was hypothesized that alternate test fixtures designed in accordance to the standard which incorporated a more robust anterior/posterior contact surface would prevent the device from expelling; thus permitting for a functional failure.

Methods

The study was conducted in the Biomechanical Testing Lab at Medtronic Spinal and Biologics, Memphis, TN. A sample size of six was chosen per Guidance for Industry and FDA Staff [6].

The intradiscal height (H) prior to testing initiation (refer to ASTM F2077-03 Fig. 1) for both fixture designs was 16 mm; therefore, within the standard's specified 4 mm and 18 mm range [1]. Stainless steel test fixtures of the initial test were designed with mating tooth geometry to the device while maintaining minimal influence to the device. Figure 1 is a diagram depicting the fusion device mated to the test fixtures.

Stainless steel test fixtures of the additional test retained the mating tooth geometry of the initial design while incorporating a larger (8 mm) anterior/posterior contact surface; thus creating a pocket to constrain the bullet-nose device and prevent the device from expelling. The contact surface extended from the inferior test fixture to the center of the fusion device. The design was intended to induce a permanent plastic deformation of the body of the device. Figure 2 is a diagram depicting the fusion device mated to the test fixtures.

Testing was conducted in an environmental chamber using 1X phosphate buffered saline (PBS) at 37 ± 3°C. Devices were soaked for a minimum of 24 h in PBS at test temperature prior to testing. Inclined plane (45°) stainless steel test stands compliant to ASTM F2077-03 were utilized for this study [1]. The superior stand was attached via an actuator pushrod suspended by a spherical joint. The inferior stand was attached to an environmental chamber which was fastened to the base of an MTS (Eden Prairie, MN) electro-mechanical load frame with a 50 kN load cell and TestWorks 4 software.

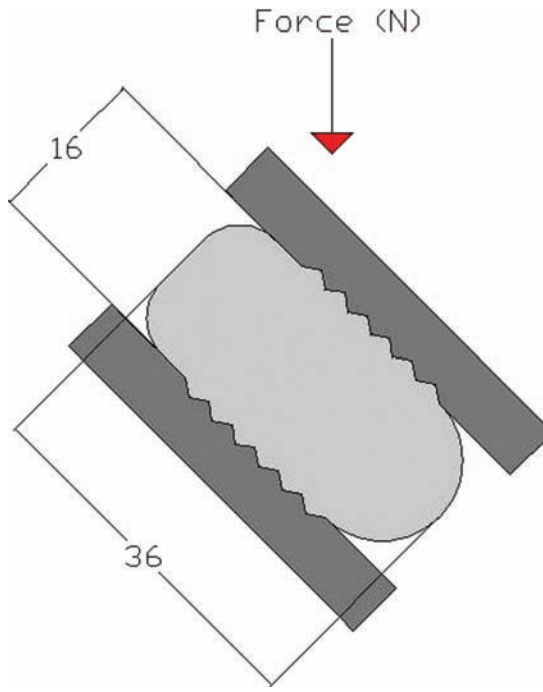

FIG. 1—*Fusion device with initial design test fixture.*

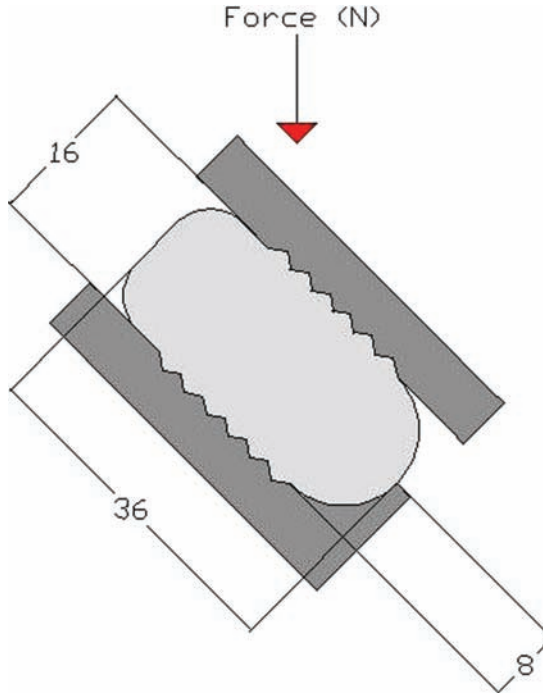

FIG. 2—*Fusion device with revised design test fixture.*

Test fixtures were attached to the inclined plane test stands. The fusion device was placed between the test fixtures. Once alignment of the fusion device to the test fixtures was established, an axial compressive load was applied in stroke control at a rate equal to 6 mm/min until functional or mechanical failure of the device was observed or the limitation of the test machine was reached. The yield load results for each test were normalized to the mean of the initial test group and standard deviations were calculated within each normalized dataset. A Student's *t* test was used to compare each test at a 95 % confidence interval.

Results

Initial testing resulted in a normalized mean yield load of 100 ± 36. Individual results are located in Table 1. The failure mode of the initial testing was mechanical failure of the tooth mating surface which allowed the devices to expel from the testing fixtures prior to a functional device failure occurring. Figure 3 is a graph containing the normalized force versus displacement curves of all initial testing specimens.

Additional testing with the revised test fixtures resulted in a normalized mean yield load of 1024 ± 1.87. Individual results are located in Table 2. Due to a test system malfunction, data was not obtained for what would have been the

TABLE 1—*Initial static compression-shear normalized test results.*

Specimen	Normalized Yield Load
1	136
2	104
3	119
4	32
5	108
6	100
Mean	**100**
St. Dev.	**36**

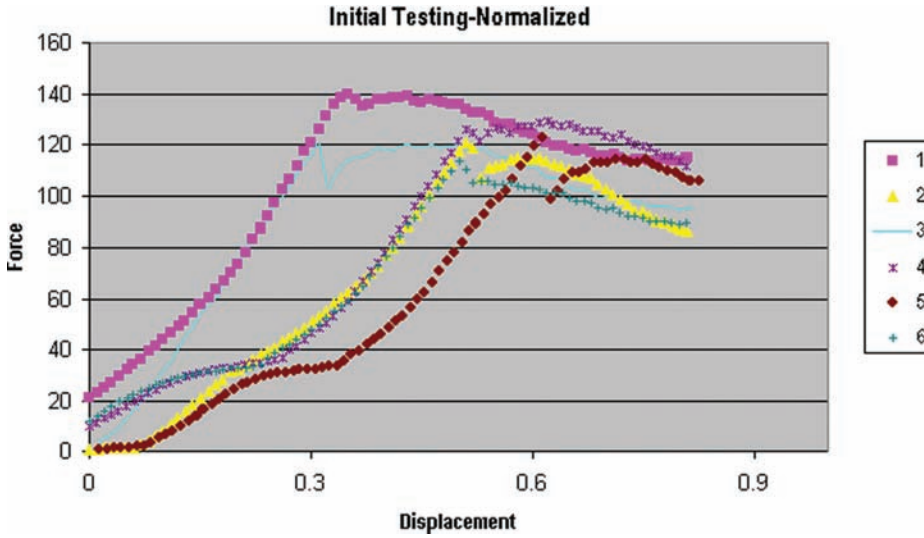

FIG. 3—*Initial testing normalized results graph.*

TABLE 2—*Revised static compression-shear normalized test results.*

Specimen	Normalized Yield Load
1	1166
2	922
3	896
4	857
5	1278
Mean	**1024**
St. Dev.	**187**

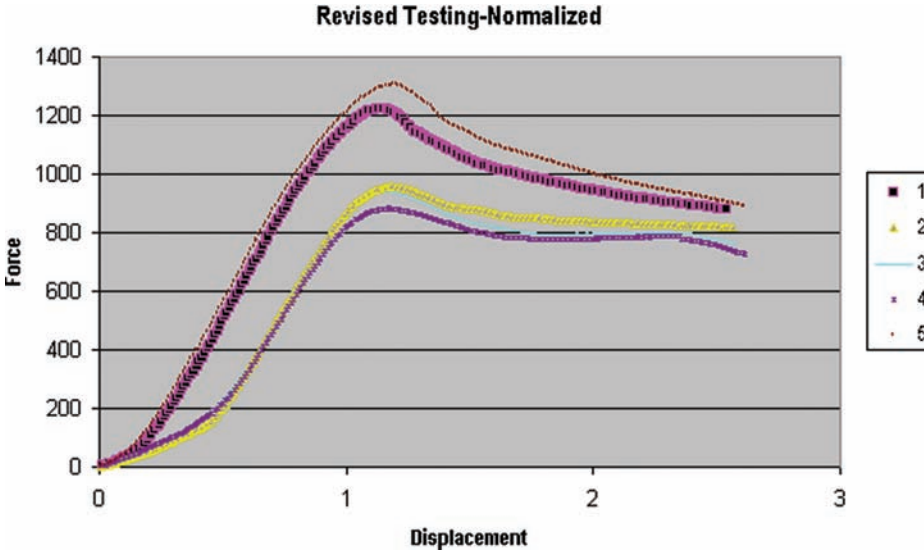

FIG. 4—*Revised testing normalized results graph.*

first specimen. The connection was restored and testing was conducted without further incident. The revised fixture design provided a compression-shear failure of permanent plastic deformation of the body of the device creating a buckling effect about each end of the implant near the teeth interface. Figure 4 is a graph containing the normalized force versus displacement curves of all revised fixture testing specimens.

The normalized mean yield load of the revised testing was significantly greater than the normalized mean yield load of the initial testing ($p = 0.0004$). This represents a 90.2 % increase in mean yield load. Figure 5 is a graphical representation of the normalized mean yield results. Figure 6 is the formula used to calculate the percentage increase.

Discussion

The revised test fixtures provided the resistance necessary to achieve a functional failure of the fusion device. However, in doing so, the pocket created an unrealistic failure mode not likely to occur in vivo. The center of the device was chosen as the point of constraint. The location of the device with respect to the test fixture prevented expulsion and could be adapted to accommodate shorter devices; thus maintaining a compliant intradiscal height. Consideration was given to the design of test fixtures with deeper, but equal superior/inferior pocket depths. Although the considered design would allow for the device utilized in the current study to maintain an acceptable intradiscal height, the considered design may not be applicable to shorter devices in the spinal system and still maintain a compliant intradiscal height.

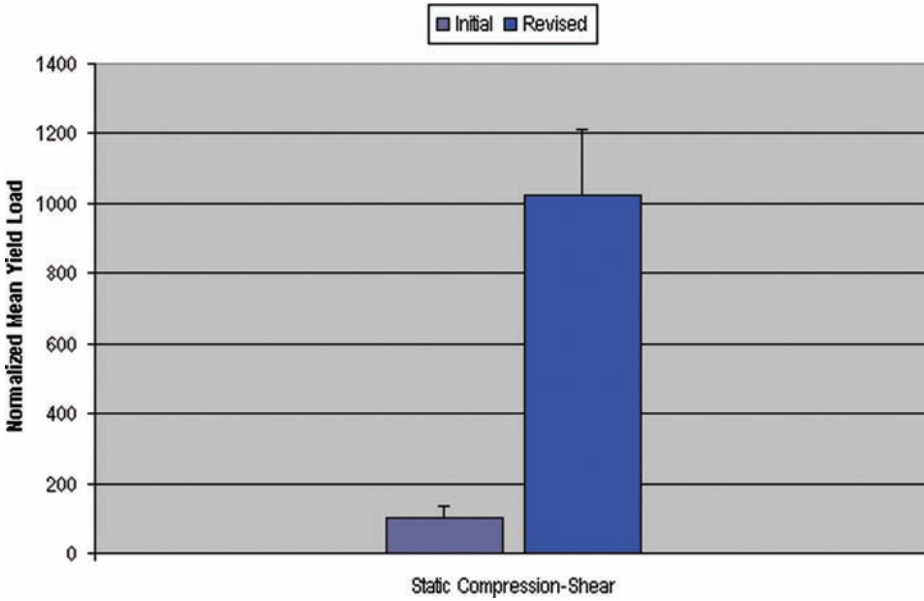

FIG. 5—*Bar graph depicting normalized mean yield load.*

A potential future compression-shear study at the maximum angle between vertebra of 17° [5] could be performed to determine if the ASTM F2077-03 compliant 45° angle [1] contributed to the eventual expulsion of the fusion device prior to functional failure. The reduced angle may provide a more evenly distributed force across the whole mating surface as opposed to the force concentration on the nose of the surface.

Conclusion

The initial testing did not provide a functional failure of the device, but rather a non-physiological failure of the mating tooth component of the device. The revised fixtures provided a functional failure of the device although the failure was attained utilizing an atypical design.

The results of this study demonstrate that changes in fixture design can have a considerable effect on performance and outcome. Both failure mode and yield load were dramatically different between the two tests, even though both

$$\left(\frac{y_2 - y_1}{y_1}\right) \times 100 = x \qquad \left(\frac{100 - 1024}{1024}\right) \times 100 = 90.2\%$$

FIG. 6—*Percentage increase calculation.*

designs maintained the same intradiscal height as defined by the standard [1]. The revised fixture design of this study is not a recommendation for future testing of intervertebral fusion devices with complex geometries but rather to demonstrate the need for a more standardized compression-shear fixture.

References

[1] ASTM F2077-03 "Test Methods for Intervertebral Body Fusion Devices," *Annual Book of ASTM Standards*, ASTM International, West Conshohocken, PA.

[2] White, A. A., III and Panjabi, M. M., *Clinical Biomechanics of the Spine*, 2nd ed., Lippincott, Philadelphia, 1990, p. 461.

[3] Renner, S., et al., "Novel Model to Analyze the Effect of a Large Compressive Follower Preload on Range of Motions in a Lumbar Spine," *J. Biomech.*, Vol. 40, 2007, pp. 1326–1332.

[4] Patwardhan, A., et al., "A Follower Load Increases the Load-Carrying Capacity of the Lumbar Spine in Compression," *Spine*, 24, Vol. 10, 1999, pp. 1003–1009.

[5] White, A. A., III and Panjabi, M. M., *Clinical Biomechanics of the Spine*, 2nd ed., Lippincott, Philadelphia, 1990, pp. 106–109.

[6] Guidance for Industry and FDA Staff – Class II Special Controls Guidance Document: Intervertebral Body Fusion Devices June 12, 2007.

Erratum for JAI103501, Symposium on Static and Dynamic Spinal Implants: Are We Evaluating Them Appropriately?, C. Wayne Metheny, published in the Journal of ASTM International (JAI), July, 2011, Volume 8, Issue 7, and included in STP 1535, Static and Dynamic Spinal Implants: Are We Evaluating Them Appropriately?

The correct title of the article: ASTM F2077-03 Static Compression-Shear Fixture Variations.

DISC AND NUCLEUS DEVICES

Reprinted from JAI, Vol. 9, No. 1
doi:10.1520/JAI103522
Available online at www.astm.org/JAI

Daniel Cobian,[1] *Bryan Heiderscheit,*[2] *Nicole Daehn,*[3] *and Paul A. Anderson*[4]

Comparison of Daily Motion of the Cervical and Lumbar Spine to ASTM F2423-11 and ISO 18192-1.2011 Standard Testing

ABSTRACT: *Background*–The purpose of this investigation is to measure the normal neck and trunk motion of daily living and to compare this to annualized movements as defined by the ASTM F2423-11 and ISO 18192-1:2011 standards. *Methods*–Ten volunteers wore a custom sensor system that monitored their upper and lower spine motion. The system allows continuous measurement of the frequency and magnitude of spinal motion about all three axes. The angular motion can then be determined for the upper and lower spinal segments. The results were extrapolated to yield the yearly frequency and magnitudes of movements. The data were compared to ASTM and International Organization for Standardization (ISO) standards. *Results*–The median magnitude of neck motion was 14.3°, 13.8°, and 21.6°, and the mean annual frequency of cervical motion was 10.6×10^6, 8.5×10^6, and 5.6×10^6 movements in flexion-extension, lateral bending, and axial rotation, respectively. The observed-to-standard (ASTM) ratio of annual cervical excursion was 1.22, 1.09, and 0.69, and for ISO the ratios were 1.22, 1.09, and 1.04 in flexion-extension, lateral bending, and axial rotation, respectively. The median range of motion for the thorax relative to the iliac crest (lumbar)

Manuscript received October 22, 2010; accepted for publication August 16, 2011; published online November 2011.

[1] D.P.T., Dept. of Orthopedics and Rehabilitation, Univ. of Wisconsin-Madison, Madison, WI53705.
[2] Ph.D., Dept. of Orthopedics and Rehabilitation, Univ. of Wisconsin-Madison, Madison, WI53705.
[3] B.S., Dept. of Orthopedics and Rehabilitation, Univ. of Wisconsin-Madison, Madison, WI53705.
[4] M.D., Dept. of Orthopedics and Rehabilitation, Univ. of Wisconsin-Madison, WI53705 (Corresponding author), e-mail: anderson@ortho.wisc.edu

Cite as: Cobian, D., Heiderscheit, B., Daehn, N. and Anderson, P. A., "Comparison of Daily Motion of the Cervical and Lumbar Spine to ASTM F2423-11 and ISO 18192-1.2011 Standard Testing," *J. ASTM Intl.*, Vol. 9, No. 1. doi:10.1520/JAI103522.

was 11.2°, 10.3°, and 12.5°, and the estimated number of annual movements was 6.8×10^6, 5.2×10^6, and 3.8×10^6 in flexion-extension, lateral bending, and rotation. The observed-to-standard ratios from ASTM were 0.63, 0.56 and 1.6, and for ISO they were 1.5, 1.68, and 1.59, in flexion-extension, lateral bending, and rotation respectively. *Discussion*–Neck and lumbar movements in healthy young adults aremore frequent that 1×10^6 times per annum. The amplitude is smaller than specified in current standards. Overall, the total annual angular excursions specified by ASTM correlated well with results, whereas the ISO specified smaller ranges of motion for the lumbar spine, and therefore the observed angular motions were greater than specified. New testing standards should consider using more physiologic movement patterns.

KEYWORDS: daily living motion, spinal kinematics, disc arthroplasty, ASTM, ISO, prosthetic wear testing

Introduction

One of the essential functions of the spinal column is to allow movement that facilitates essential human functions including locomotion, social interaction, recreation, spirituality, and work. In vivo spinal motion can be assessed by measuring the movement of the entire spinal column, movement in a particular segment, or movement at a single interspace. The latter has been defined as the functional spinal unit (FSU), which includes the two adjoining vertebrae, their articulations (the paired zygoapophyseal joints and an intervertebral disc), and associated ligaments. Spinal motions are complex, having translations and angulations along all three axes, which makes them difficult to measure. Further, spinal movements almost always have coupled angular motions about more than one axis and are combined with translations along the axis.

Many investigations have studied global and isolated FSU motions using a variety of techniques such as goniometric, radiographic, fluoroscopic, and optical. These movements have been correlated to requirements for specific tasks, usually those involving activities of daily living or specific ergonomic jobs. However, the in vivo measurements are limited because they might lack complete movements in all six degrees of freedom, are often performed in an artificial laboratory environment, and do not measure movements of individual FSUs. Although an in vivo FSU can be assessed with cineradiography, the results usually consist of a single arc of movement and are often limited to an exaggerated degree of motion (full flexion-extension) that rarely occurs during normal living. These analyses do not assess the regular movements that occur during normal living. The measurement of in vivo daily motion has been attempted for other joints and provides an essential understanding of the requirements for the design and testing of prosthetic devices, especially those having bearing surfaces [1]. Such data are not available for spinal devices.

The cervical and lumbar spine segments have the greatest degrees of mobility and are associated with the highest incidence of derangements, making

them candidates for surgical treatment. Recently, artificial disc replacement has been developed to replace fusion as a treatment for some degenerative conditions of the cervical and lumbar spine. Knowledge of the direction, magnitudes, and number of movements occurring over a unit of time is essential for the proper design of the bearing surfaces of these devices. In general, the design of these spinal devices has been based on kinematic data used to determine FSU movements and on total motion data from the experience of the hip and knee. The total movements of the hip and knee are easy to determine by measuring stride length and counting steps using pedometers. In the spine, this is more difficult, as movements are far more complex and include greater magnitudes of coupled movements, varying magnitudes of each motion, and movements occurring even at rest.

Testing standards to assess the in vitro wear of the bearing surfaces for spinal prosthetic devices have been developed by ASTM and the International Organization for Standardization (ISO) [2,3]. These specify sinusoidal motions along all three axes and recommend the simultaneous coupling of two or three of the axes. Further movements can occur both in phase and out of phase, such as left side bending with left or right axial rotation. The motions proscribed are regular sinusoids having large amplitudes relative to the total FSU movement. The standards recommend regular assessments of the bearing surfaces and debris material at the million cycle period and continued testing for up to 10×10^6 cycles, although longer test periods can be employed. It is generally believed that 1×10^6 cycles is conservatively equivalent to a year of in vivo wear [4]. The validity of this assumption has never been tested, and this could be an important limitation of current testing standards.

We have previously reported the design and validation of an in vivo device that can continuously measure angular movements along all three axes for prolonged periods [5–7]. Using this device, we measured the total head movement relative to the thorax over a five-day period in ten young healthy subjects. We also estimated the total number of motions that occur during a variety of activities of daily living. We estimated that subjects move their cervical spine up to 9×10^6 times per year and that the median neck motion in flexion-extension was only 18°, and for the C5-C6 FSU it was only 2° to 3°.

Hypothesis and Study Aims

We hypothesize that the in vivo daily living motion of the spine is significantly different from that specified in testing standards, in that more movements of shorter amplitudes occur during daily living. The differences between standards and daily living motion when applied to wear simulation testing might affect the wear results. In order to test this hypothesis, our specific aim in this study was to determine the in vivo daily living patterns of spinal movements in the cervical and lumbar spine in healthy subjects. We compared these results to the total motions specified in the ASTM F2423-11 and ISO 18192-1.2011 standards. The daily living motion patterns described can then be used to formulate physiologic motion patterns that can be used to design alternative wear simulation models.

Methods

Subjects

The study had approval from the University of Wisconsin Institutional Review Board. Ten healthy subjects were recruited. Each subject signed a voluntary consent, and all completed the study. The average age of subjects was (22.8 ± 1.9) years, and half were female. None of the subjects had any spinal symptoms or known spinal diseases.

Wisconsin Analysis of Spine Motion Performance (WASP) System

Continuous motions of the upper and lower spine were measured using the Wisconsin Analysis of Spine Motion Performance (WASP) system [5,6]. This consists of three sensors, a data logger, and custom software. Each sensor contains two inclinometers that measure angular displacement in the sagittal (flexion-extension) and coronal (lateral bending) planes and a gyroscope to measure angular velocity in the axial plane. Data are recorded (32 Hz) using the data logger and downsampled to 8 Hz prior to analysis. The data are later downloaded to a computer. The battery life enables continuous measurement for up to 24 h.

The sensors were worn continuously over a three-day period (two weekdays and one day on a weekend) during all activities except bathing and swimming and at night. Based on prior investigations, sleeping was associated with few movements. The sensors were applied to the mastoid, the thorax (under the axilla at about the seventh rib), and the iliac crest using medical adhesive (Medical Spirit Gum 2100, Kryolan, Berlin, Germany) (Fig. 1). The data logger was placed on a belt or in a pocket. The subjects were instructed in the proper placement and orientation of the sensors and operation of the data logger. Each subject met daily with a researcher in order to ensure proper use of the system, to download data, and to replace the batteries. Prior to use of the system, the subjects wore the sensors and underwent calibration against an optical motion capture system in order to ensure reliability and accuracy.

The continuous data were reduced using custom software (Matlab v. 7.2, Mathworks, Natick, MA). For axial rotation, the angular velocity was transformed into angular displacement by integration. Independently for each axis, a motion peak was identified by determining when the slope of the line changed sign and when the magnitude between peaks exceeded 5° (Fig. 2). The movement amplitude was the difference in magnitude between two successive peaks. The frequency of movements in 5° increments was reported. Data were recorded for each axis and normalized for daily and estimated yearly motion patterns.

The excursion occurring at a single cervical functional spine unit (C5-C6) was estimated using previously determined in vivo proportional values of 0.18 for flexion-extension, 0.17 for lateral bending, and 0.10 for axial rotation [8]. The excursion occurring at a single lumbar functional spine unit (L4-L5) was estimated using previously determined in vivo proportional values of 0.195, 0.198, and 0.20 for flexion-extension, lateral bending, and axial rotation, respectively [9].

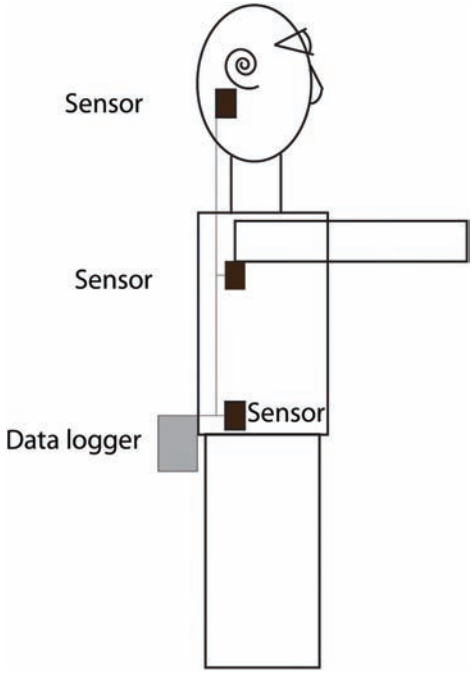

FIG. 1—*Schematic drawing of the location of the sensors (black squares), which are placed over the mastoid, along the chest wall below the axilla, and over the iliac crest. The sensors are connected to a data logger (gray box).*

Validation of WASP

The WASP was validated against a standard material testing system (MTS) [5]. Briefly, known pure moments were applied and measurements of the WASP were compared to displacements observed from the MTS. Correlations for the range of motion were very strong for all three axes (r^2 values = 0.99). The correlation for the detection of movement frequency was exact. Further validation was performed with an optical motion capture system that is accurate to 0.5°. Ten subjects were placed in the system wearing the WASP, and they performed various movements, including single plane and complex movements. The root mean square deviation (RMSD) between the WASP device and the optical motion capture system was obtained and divided by the median deviation to obtain a percentage. For both cervical and lumbar motions, all RMSD values were less than 20 %, except for lateral bending in complex coupled motions. The correlation for the detection of movement frequency was exact.

ASTM and ISO Standards

Similar to hip and knee standards, the annual frequency of motion was assumed to be 1×10^6 cycles. Thetotal excursion based on 1×10^6 cycles for each axis was calculated using the amplitudes shown in Table 1. Assuming an

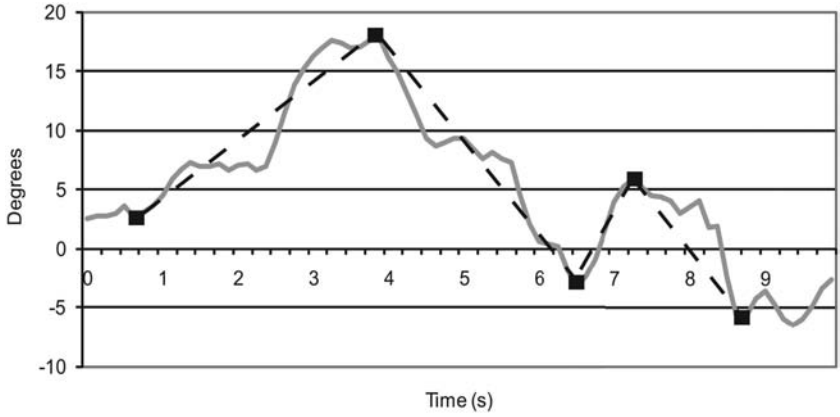

FIG. 2—*Example of data taken from the WASP. The solid gray line represents the observed motion. The squares are at the calculated peaks. The dashed line is the reduction of the continuous data to a linear function. The distance between peaks is the magnitude of motion.*

equivalency of 1×10^6 cycles to a year, the annual total excursion in degrees is calculated as

$$\text{Total excursion}(^\circ) = 4 * 1000000 * \text{ROM}$$

where ROM is the amplitude specified by the standard. These results were compared to the total excursion observed in our subjects.

TABLE 1—*Range of motion and total excursion after 1 000 000 cycles.*

		Flexion-Extension, deg	Lateral Bending, deg	Axial Rotation, deg
ASTM F2423-11				
Cervical	ROM	± 7.5	± 6.0	± 6.0
	Annual excursion	30 000 000	24 000 000	24 000 000
Lumbar	ROM	± 7.5	± 6.0	± 3.0
	Annual excursion	30 000 000	24 000 000	12 000 000
ISO 18192-1.2011				
Cervical	ROM	± 7.5	± 6.0	± 4.0
	Annual excursion	30 000 000	24 000 000	16 000 000
Lumbar	ROM	± 4.5	± 2.0	± 2.0
	Annual excursion	18 000 000	8 000 000	8 000 000

Note: Range of motion (ROM) is the amplitude of the sinusoidal pattern describing the arc of motion.

Results

ASTM F2423-11 and ISO 18192-1:2011 Standards

Cervical Total Disc Replacement—Both ISO and ASTM standards specify ±7.5° and ±6.0° amplitudes in flexion-extension and lateral bending, respectively (Table 1). Axial rotation amplitudes are ±6° and ±4° in ASTM and ISO. Although not specified in either standard, most users assume that the expected annual frequency of motion is similar to that in hip and knee simulations, i.e., 1×10^6 cycles. Using this estimation, the total simulated annual excursions for both standards are 30×10^6 and 24×10^6 degrees in flexion-extension and lateral bending, respectively. The total annual excursion in axial rotation is 24×10^6 and 16×10^6 degrees for the ASTM and ISO standards, respectively.

Lumbar Total Disc Replacement—ASTM specifies ±7.5°, ±6.0°, and ±3.0° amplitudes for flexion-extension, lateral bending, and axial rotation, and the total annual excursion is 30×10^6, 24×10^6, and 12×10^6 degrees (Table 1). For ISO, the amplitude is ±6.0°, ±2.0°, and ±2.0°, and the total annual excursion is 24×10^6, 8×10^6, and 8×10^6 degrees.

Cervical Spine

Motion Magnitude—The distribution of the range of motion is skewed, and therefore we report the median values (Fig. 3). The median range of motion for

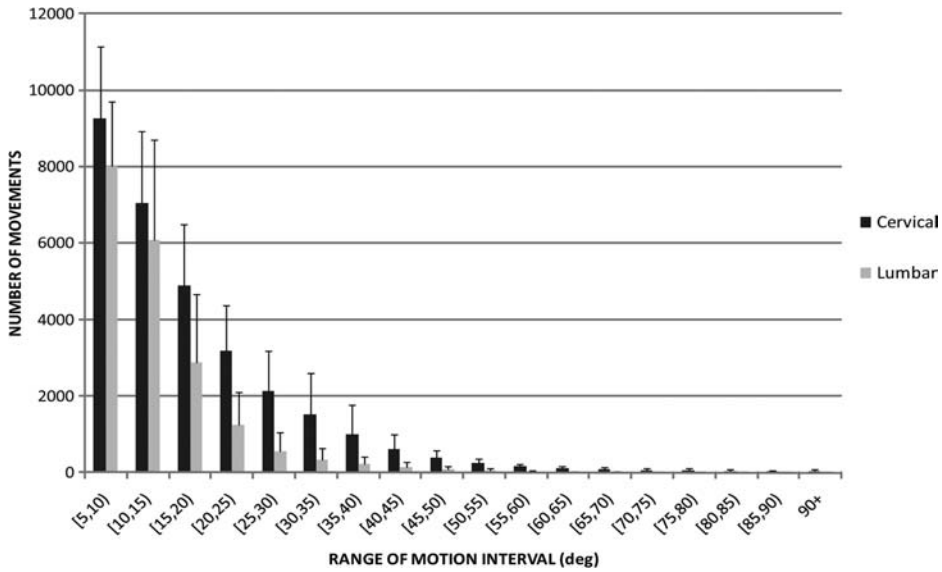

FIG. 3—*The frequency distribution of daily movements in flexion-extension in 5° increments.*

the head relative to the thorax (cervical) was 14.3°, 13.8°, and 21.6° for flexion-extension, lateral bending, and rotation, respectively (Table 2). The majority of movements in all three planes were between 5° and 15°. Less than 3 % of movements exceeded 50° in flexion-extension and lateral bending, whereas less than 15 % were less than 50° in axial rotation. At C5-C6, the median range of motion was 2.6°, 2.3°, and 2.2° for flexion-extension, lateral bending, and axial rotation, respectively.

Motion Frequency—The mean daily number of movements was 29 200, 23 300, and 15 200 for flexion-extension, lateral bending, and rotation, respectively (Table 3). In one year, the estimated number of movements was 10.6×10^6, 8.5×10^6, and 5.6×10^6 in flexion-extension, lateral bending, and rotation, respectively.

Total Motion Excursion—The total annual excursion was calculated by multiplying the median range of motion at C5-C6 and L4-L5 by the number of annual movements. The total annual excursion of the cervical spine is estimated to be 151.6×10^6, 117.3×10^6, and 121×10^6 degrees in flexion-extension, lateral bending, and rotation, respectively. We used the median range of motion at C5-C6 and L4-L5, which results in lower ranges of motion by between 0.25° and 0.5° compared to results obtained using means. The total annual excursion in degrees at C5-C6 is estimated to be 27.3×10^6, 19.9×10^6, and 12.1×10^6 degrees in flexion-extension, lateral bending, and rotation, respectively (Table 4).

TABLE 2—*Median range of motion compared to ASTM and ISO standards.*

	Observed			
	Median Overall Range of Motion, deg	Functional Spinal Unit, deg	ASTM F2423-11, deg	ISO 18192-1.2011, deg
		C5-C6[a]		
FE	14.3	2.6	15	15
LB	13.8	2.3	12	12
AR	21.6	2.2	12	8
Lumbar		L4-L5[b]		
FE	11.2	2.2	15	9
LB	10.3	2.0	12	4
AR	12.5	2.5	6	4

Notes: FE, flexion-extension; LB, lateral bending; AR, axial rotation. The magnitude of the standards combines positive and negative excursions and is therefore doubled and allows comparison to observed movements.

[a]The excursion at C5-C6 is assumed to be 0.18, 0.17, and 0.10 of the observed total excursion of the head and neck.

[b]The excursion at L4-L5 is assumed to be 0.195, 0.198, and 0.20 of the observed total excursion of the trunk.

TABLE 3—*Daily and annual movements and total excursion.*

		Daily Movements ($\times 10^3$)	Daily "Cycles" ($\times 10^3$)	Total Daily Excursion ($\times 10^6$ deg)	Yearly Movements ($\times 10^6$)	Yearly "Cycles" ($\times 10^6$)	Total Yearly Excursion ($\times 10^6$ deg)
Cervical	FE	29.2 (7.3)	14.6	0.556 (0.209)	10.6 (2.7)	5.3	203.1 (76.37)
	LB	23.3 (7.4)	11.6	0.421 (0.200)	8.5 (2.7)	4.3	153.7 (73.13)
	AR	15.2 (4.6)	7.6	0.454 (0.169)	5.6 (1.7)	2.8	165.7 (61.57)
Lumbar	FE	18.6 (5.8)	9.4	0.267 (0.118)	6.8 (2.1)	3.4	97.36 (43.11)
	LB	14.3 (4.4)	7.2	0.186 (0.072)	5.2 (1.6)	2.6	67.97 (26.45)
	AR	10.4 (4.7)	5.2	0.174 (0.091)	3.8 (1.7)	1.9	63.58 (33.34)

Notes: FE, flexion-extension; LB, lateral bending; AR, axial rotation. Movements are reported as a single angular displacement greater than 5°. Two movements combined constitute one cycle. Standard deviation is given in parentheses.

Lumbar Spine

Motion Magnitude—The median range of motion for the thorax relative to the iliac crest (lumbar) was 11.2°, 10.3°, and 12.5° for flexion-extension, lateral bending, and rotation, respectively (Table 2). The majority of movements in all three planes were between 5° and 15°. Less than 3 % of movements exceeded 50° for all three axes. At L4-L5, the median range of motion was 2.2°, 2.0°, and 2.5° for flexion-extension, lateral bending, and axial rotation, respectively.

Motion Frequency—The mean daily number of movements was 18 600, 14 300, and 10 400 for flexion-extension, lateral bending, and rotation, respectively (Table 3). In one year, the estimated number of movements was 6.8×10^6,

TABLE 4—*Comparison between observed and ASTM and ISO total annual excursion.*

		Observed Yearly Excursion at FSU ($\times 10^6$ deg)	ASTM F2423-11 Ratio of Observed to Standard	ISO 18192-1.2011 Ratio of Observed to Standard
Cervical C5-C6[a]	FE	36.6	1.22	1.22
	LB	26.1	1.09	1.09
	AR	16.6	0.69	1.04
Lumbar L4-L5[b]	FE	19.0	0.63	1.05
	LB	13.5	0.56	1.68
	AR	12.7	1.06	1.59

Notes: FE, flexion-extension; LB, lateral bending; AR, axial rotation.
[a]The excursion at C5-C6 is assumed to be 0.18, 0.17, and 0.10 of the observed total annual excursion of the head and neck.
[b]The excursion at L4-L5 is assumed to be 0.195, 0.198, and 0.20 of the observed total excursion of the trunk.

5.2×10^6, and 3.8×10^6 in flexion-extension, lateral bending, and rotation, respectively.

Total Motion Excursion—The total annual excursion of the lumbar spine is estimated to be 76.2×10^6, 53.6×10^6, and 47.5×10^6 degrees in flexion-extension, lateral bending, and rotation, respectively. For the L4-L5 FSU, the annual total excursion is 14.9×10^6, 10.6×10^6, and 9.5×10^6 degrees.

Comparison to ASTM and ISO

Cervical—In vivo cyclical movements were three to five times more frequent than specified in testing standards assuming 1×10^6 cycles per year. However, the total angular excursion was surprisingly similar to that in the ASTM 2423-05 standards, with observed-to-standard ratios of 1.22, 1.09, and 0.69 in flexion-extension, lateral bending, and axial rotation, respectively. For ISO 18192-1.2011, the observed-to-standard ratios were 1.22, 1.09, and 1.04.

Lumbar—Lumbar in vivo movements were two to three times more frequent than specified in testing standards assuming 1×10^6 cycles per year. The total excursions were, in general, greater than specified by the two standards. This was especially true for the ISO standard, which specified small values for axial rotation and lateral bending (only $\pm 2^\circ$). The observed-to-standard ratios for total annual excursion by ASTM 2423-05 were 0.63, 0.56, and 1.6 in flexion-extension, lateral bending, and rotation, respectively. For ISO/CD 18192-1.3, the observed-to-standard ratios were 1.5, 1.68, and 1.59.

Discussion

Restatement of Study Aims

This study was undertaken in order to measure the normal daily living motion of the cervical and lumbar spine. These data could be used to improve the design and testing of prosthetic devices. Additionally, the results could be used to study the etiology of diseases, assess functional effects of interventions, aid in the study of ergonomics, and assess disability impairment. Ultimately, we plan to describe physiologic motion patterns that could be used in spine simulators to test for prosthetic wear. Given the widely variant patterns between the standards and daily living physiology, we would expect to see different wear rates than currently predicted.

Summary of Results

We found that young healthy subjects made measurable movements of their cervical and lumbar spine much more frequently than previously believed. The head and neck annually move cyclically over 3×10^6 to 5×10^6 times in each axis, and the trunk moves approximately 2×10^6 to 3×10^6 times. It is not surprising that the highest frequencies were seen in flexion-extension in the sagittal

plane for both the cervical and lumbar spine. Movements in these planes have the greatest range of motion for both spinal regions and are of the most importance for human activities of daily living [10]. In reality, it was rare for a motion to be in only one plane, and almost all were coupled to other planes of movement.

These movements are of a relatively short arc, with the majority between 5° and 15° and less than 3 % being greater than 50°. For a single FSU, the mean movement is between 2° and 3° along any of the axes. These amplitudes are significantly lower than the relatively large amplitudes specified in the testing standards. We studied healthy young adults and would expect symptomatic patients or older subjects to have fewer movements of shorter amplitudes.

One of the most important findings validates the current ASTM testing protocol in regard to the total angular excursion. We found that the total annual excursion was closely approximated by the excursion of 1×10^6 cycles at the amplitudes specified by the ASTM. This implies that a million cycles with large amplitudes in spine simulators accurately model a year of in vivo spinal motion. The ISO had similarly satisfactory results for the cervical spine but was underpowered in all axes for the lumbar spine. The ranges of motion are different between the two standards, with the ISO standard having lower movements in lateral bending and axial rotation, which accounts for the observed differences. Given that the frequencies are far greater than 1×10^6 cycles per year, increasing the axial rotation and lateral bending in the ISO standard might be prudent.

Review of Relevant Literature

Measuring the total numbers of movements of the spine is problematic. Attempts have been made using observers at the workplace, using videotapes, electromagnetically, and by electromyography. These investigations have usually involved specific tasks or have taken place at specific locations. Other studies have evaluated the spine motions required in order to perform activities of daily living or that occur in patients having back symptoms [10]. These investigations do not provide the information needed in order to properly define testing protocols, such as the number and magnitude of movements per day. The measurement of general physical activity over long time periods has been performed using methods similar to ours. Dinger et al. used a single array of accelerometers mounted on a waist belt and accurately monitored general trunk movement [11]. Their instrument reported only the number of trunk movements and did not provide amplitude data. They found that students moved, on average, 40 000 times per day, which is very close to our observed number of movements of the neck in flexion-extension of 30 000 per day.

Prosthetic wear has been characterized by the Archard relationship, according to which volumetric wear is proportional to the normal force (load), a constant, and the total excursion [12]. This would imply that the total angular excursion is one of the most important parameters to consider when designing simulation tests. In this regard, the current standards do appear to adequately cover the observed motions in our subjects. However, the patterns of wear might also influence the testing results. A higher frequency (more total

movements) with smaller amplitudes might have different wear behavior than that predicted by the current standards. Further, testing with varying motion amplitudes might have an unknown effect.

Wear testing standards are essential for verifying an adequate level of performance of intervertebral disc prostheses. The ranges of motion specified in the current standards are at or near the limits of full motions determined from kinematic, dynamic fluoroscopic, and cadaveric studies. The coupling of angular motions in two or three axes differs between the two standards, and the patterns chosen (sinusoidal) are largely arbitrary. Further, although not specified in the standards, the number of cycles per year is assumed to be 1 000 000, similar to what is used in hip and knee simulations [4]. However, the current standards have little clinical basis or explant analysis to justify their testing parameters. An analysis comparing explants to wear simulation testing done before adoption of the current ASTM and ISO standards demonstrated similar wear patterns and showed that the wear rate appeared to be much lower than that predicted by simulation testing, thus implying that the testing standards were conservative [4].

Prior Investigations

We have previously reported the daily living range of motion of the cervical spine of ten volunteer subjects. In the current study, we modified the WASP system so that we could evaluate both cervical and lumbar movements simultaneously. Our cervical spine results were similar between the two studies, except for lower observed periods of motion in lateral bending and higher angular displacements in axial rotation. Possible explanations for these discrepancies are the abolishment of nighttime monitoring in the present study, poorer accuracy in lateral bending during complex motion, and the time of year when this study was done (i.e., during the school year, whereas the prior was done in the summer).

Study Limitations

The study limitations relate to the accuracy of the WASP system. In single plane motion, we found the accuracy to be high, but with coupled motion the ability to detect accurately the angular displacements decreased. This was especially true for lateral bending coupled with rotation, for which correlations approximate only 50 %. In an attempt to improve the accuracy, we calibrated the sensors before use with a motion capture system, and we were able to show minimal drift and good reliability in the application of the sensors and their use by the subjects.

We utilized normal young adult volunteers who were active and who exercised regularly. It is likely that generalizing to a diseased population (such as those requiring spinal surgery for degenerative conditions) would overestimate motion. Kinematic studies show that the mean range of motion of a normal C5-C6 FSU is 10° to 15°, whereas in the reports of randomized trials of disc arthroplasty devices, the range of motion preoperatively, postoperative after

disc replacement, and at adjacent levels is 7° to 8°. Thus, the reported values in this study are likely an overestimation of the motions of symptomatic or older patients who would be candidates for disc arthroplasty. Further, the analysis assumes that all cervical movement occurs between the occiput and C7 and that lumbar movements are between L1 and S1, thus ignoring contributions of the cervicothoracic and lumbothoracic junctions and the thoracic spine. Therefore, the contributions of in vivo movement credited to C5-C6 and L4-L5 are inflated and overrepresent true values. Although we could have used kinematic data to more accurately model our estimation of the FSU motions, we felt justified in our method, as that would provide a conservative estimate (overrepresenting) the results when comparing simulation testing.

The sensitivity of the device was set at 5°, which could have resulted in missed movements below that threshold. We selected that threshold based on extensive validations previously reported. Most important is that humans are unable to perform neck movements of less than 5°, justifying this threshold.

Clinical Relevance

The clinical relevance of this study is that the patterns of in vivo daily spinal motions are different than specified in testing standards. The overall total angular motions based on 1×10^6 cycles per year are surprisingly close to those specified in the ASTM, but they are less similar to the lumbar ISO standards. The important differences are that movements are more frequent and are of far less amplitude. Further, the in vivo movements have a wide range of amplitudes. The effect of these differences, if applied to in vitro wear simulation, is unknown. Further investigations using these physiologic motion patterns in in vitro wear simulators should be performed.

In designing new testing protocols, the following should be considered: (1) The number of movements is greater than previously considered, and the movements are correspondingly of much lower amplitudes. (2) Designs should consider the total cervical and lumbar amplitudes that vary over a wide distribution from 5° to 50° increments. Up to 2 % might be of large amplitudes past the neutral zone of the FSU or, in the case of prosthesis, where edge impingement might occur. (3) To assume a year of wear, the number of cycles should be 3×10^6 to 5×10^6 times per year for cervical and 2×10^6 to 3×10^6 times per year for lumbar.

Summary and Conclusion

A comparison of testing standards to daily living motion revealed that in vivo movements are three to five times more frequent in the cervical spine and two to three times more frequent in the lumbar spine than specified in standards based on 1×10^6 cycles per year. The majority of spinal segment (cervical and lumbar) movements are between 5° and 15°, and when ascribed to a single FSU they are between 2° and 3°. The annual total excursion correlates well to current ASTM standards, but more motion, especially in the lumbar spine, occurs than tested using ISO standards.

Acknowledgments

The writers want to thank Ron McCabe, M.S., and Ray Vanderby, Ph.D., for their help in performing validation experiments. This study was funded by a grant from Medtronic. Dr. Anderson is a paid consultant for Medtronic.

References

[1] Luinge, H. J., and Veltink, P. H., "Measuring Orientation of the Human Body Segments Using Miniature Gyroscopes and Accelerometers," *Med. Biol. Eng. Comput.*, Vol. 43, 2005, pp. 272–282.

[2] ASTM F2423-11, 2011, "Standard Guide for Functional, Kinematic, and Wear Assessment of Total Disc Prostheses," *Annual Book of ASTM Standards*, Vol. 13.01, ASTM International, West Conshohocken, PA, pp. 1–9.

[3] ISO 18192-1.2011, 2011, "Implants for Surgery—Wear of Total Intervertebral Spinal Disc Prostheses—Part 1: Loading and Displacement Parameters for Wear Testing and Corresponding Environmental Conditions for Tests," *The International Organization for Standardization*, Geneva, Switzerland.

[4] Anderson, P. A., Rouleau, J. P., Toth, J. M., and Riew, K. D., "A Comparison of Simulator-Tested and Retrieved Cervical Disc Prostheses. Invited Submission from the Joint Section Meeting on Disorders of the Spine and Peripheral Nerves, March 2004," *Journal of Neurosurgery: Spine*, Vol. 1, 2004, pp. 202–210.

[5] Syed, F. I., Oza, A. L., Vanderby, R., Heiderscheit, B., and Anderson, P. A., "A Method to Measure Cervical Spine Motion over Extended Periods of Time," *Spine*, Vol. 32, 2007, pp. 2092–2098.

[6] Sterling, A. C., Cobian, D. G., Anderson, P. A., and Heiderscheit, B., "Annual Frequency and Magnitude of Neck Motion in Healthy Individuals," *Spine*, Vol. 33, 2008, pp. 1882–1888.

[7] Cobian, D. G., Sterling, A. C., Anderson, P. A., and Heiderscheit, B., "Task-Specific Frequencies of Neck Motion Measured in Healthy Young Adults over a Five-Day Period," *Spine*, Vol. 34, 2009, pp. E202–E207.

[8] Panjabi, M. M., Crisco, J. J, Vasavada, A., Oda, T., Cholewick, J., and Nibu, K., "Mechanical Properties of the Human Cervical Spine as Shown by Three-Dimensional Load-Displacement Curves," *Spine*, Vol. 26, 2001, pp. 2692–2700.

[9] Yamamoto, I., Panjabi, M. M., Crisco, T., and Oxland, T., "Three-Dimensional Movements of the Whole Lumbar Spine and Lumbosacral Joint," *Spine*, Vol. 14, 1989, pp. 1256–1260.

[10] Bennett, S. E., Schenk, R. J., and Simmons, E. D., "Active Range of Motion Utilized in the Cervical Spine to Perform Daily Functional Tasks," *Journal of Spinal Disorders and Techniques*, Vol. 15, 2002, pp. 307–311.

[11] Dinger, M. K. and Behrens, T. K., "Accelerometer-Determined Physical Activity of Free-Living College Students," *Med. Sci. Sports Exercise*, Vol. 38, 2006, pp. 774–779.

[12] Jacobs, J. J., Hallab, N. J., Urban, R. M., and Wimmer, M. A., "Wear Particles," *J. Bone Jt. Surg., Am. Vol.*, Vol. 88, 2006, pp. 99–102.

Reprinted from JAI, Vol. 9, No. 2
doi:10.1520/JAI103497
Available online at www.astm.org/JAI

Philip Hyde,[1] *Rachel Vicars,*[1] *John Fisher,*[1] *and Richard Hall*[1]

Wear Simulation of Total Disc Arthroplasties: Sensitivity to Device Design and Test Parameters

ABSTRACT: The challenges of measuring in vivo total disc replacement (TDR) kinematics are well recognized, meaning that it is difficult to establish appropriate input conditions for wear simulation. Therefore it is desirable to ascertain the sensitivity of implant wear in vitro to perturbations of the kinematics and other testing parameters. It has previously been demonstrated in other metal-on-polyethylene joint replacements that cross-shear strongly influences wear rate. This study investigates this phenomenon by altering the phasing of the inputs by making the lag in the flexion-extension and lateral bend displacements zero. Further, the effect of an additional anterior-posterior shear, which has been reported in vivo, was investigated for two different TDR designs using an extra load or displacement input in addition to those prescribed by the standard ISO 18192-1. Altering the standard ISO 18192-1 waveform phasing significantly reduced the mean wear rate of the constrained polyethylene disc. The addition of an anterior-posterior input showed no significant change in the rate of wear for the constrained TDR but was increased for the unconstrained device. These results data demonstrate the strong dependency of the wear in these types of joints to the input conditions as well as the device design parameters. Hence, these factors should be given prime consideration when designing both the device itself and the assessment regime in which the construct is to be tested.

KEYWORDS: TDR, total, disc, replacement, wear, Prodisc, Charite, tribology

Manuscript received October 16, 2010; accepted for publication September 2, 2011; published online November 2011.

[1]Institute of Medical and Biological Engineering, School of Mechanical Engineering, Univ. of Leeds, Leeds LS2 9JT, United Kingdom.

Cite as: Hyde, P., Vicars, R., Fisher, J., and Hall, R., "Wear Simulation of Total Disc Arthroplasties: Sensitivity to Device Design and Test Parameters," *J. ASTM Intl.*, Vol. 9, No. 2. doi:10.1520/JAI103497.

Introduction

First generation TDRs rely heavily on current hip and knee replacement technology, in particular the use of metal on ultra high molecular weight polyethylene (UHMWPE) bearings. Functionally, total hip replacements (THR) have proved to be one of the most successful orthopedic operations [1]. Typically an UHMWPE acetabular cup component articulates against a metal femoral head, which has had widespread use since Charnley and Cupic [2] reported excellent 9 and 10 year results of the then new low friction arthroplasty. Although articulating bearings provide excellent functionality, they are subject to wear that produces debris in the form of sub-micron UHMWPE particles. Longer-term follow-up of total joint replacements (TJR) has highlighted the role of wear particles in the failure process [3,4]. Here, UHMWPE debris trigger a biological cascade resulting in macrophage activation that instigates an inflammatory response and osteolysis within the surrounding bone [5]. Recently, osteolysis has been reported in TDR revision surgery [6–8] that suggests that it is even more prudent to quantify both the volume and size of debris that may be released from these articulating bearing prostheses. Given this potential for long-term failure in TDRs, the arguments for the use of simulators for the preclinical assessment of the osteolytic potential in TDRs is highly persuasive.

In vitro wear simulations have been previously conducted using the ISO 18192-1 standard [9] or the ASTM F2423-05 guidance document [10]. These studies have shown a wide variation in wear rates, in the range of 2–20 mg/MC for ISO-based inputs [11–15] and approximately 0.1 mg/million cycles (MC) when ASTM guidelines were utilized [12,16]. Whereas the ISO input motions run concurrently, those in the ASTM guide have usually been input sequentially. In the latter, the test conditions produce very low cross-shear motion [17] at the bearing surfaces resulting in rates of wear that are typically two orders of magnitude lower than those observed in ISO defined tests. Currently, the effect of the input motions have not been fully characterized in terms of their impact on TDR wear [18], and the sensitivity to perturbations in these parameters is unknown. The ISO and ASTM cycles do not include an anterior-posterior (AP) shear load or motion input, although the former has been observed in vivo [19] and the latter confirmed using in vitro cadaveric studies [20,21]. Further, there are nominally two general types of articulating total disc replacement; those that are deemed to be constrained, which allow only rotations around a fixed center, and those that have lesser constraints that are capable of a degree of translation [22].

The aim of this study was to assess the wear rate of metal-on-UHMWPE TDRs under varying kinematic input conditions based upon ISO 18192-1. Modifications to the input parameters included altering the lateral bend (LB) to flexion-extension (FE) motion phasing and incorporating a fifth active degree of freedom AP shear input. Two different design philosophies were assessed.

Methodology

Comparative wear simulations were performed on two different designs of TDR using ISO-based motions on two identical spine simulators. The Prodisc-L TDR

is a constrained TDR utilizing a ball-in-socket design with an inferior UHMWPE disc articulating against a superior cobalt-chromium-molybdenum (CoCrMo) cup (Fig. 1). The UHMWPE disc is attached to a CoCrMo baseplate by means of a snap-lock mechanism. Theoretically, this design provides a fixed center of rotation (COR) that is unlike a natural functional spinal unit in which a mobile instantaneous axis of rotation (IAR) is present [23]. The Charité TDR (Fig. 1) is an unconstrained design utilizing an UHMWPE core that facilitates translation of the CoCrMo endplates relative to each other in the horizontal plane. Prodisc and Charité TDRs were chosen to represent constrained and unconstrained types of bearing design. Wear simulations were performed using two identical seven station spine simulators, denoted A and B (Simulation Solutions, Manchester, UK). The simulators allow 6 df with 5 df actively controlled. All inputs are electromechanically controlled and capable of operating within ISO 18292-1 demand profile limits. Under ISO 18192-1 conditions, the AP and lateral shear are allowed to freely translate; however, within these simulators the AP input can be actively controlled in either a force or displacement mode.

The simulations were split into a number of experimental studies (Table 1) of several million cycles. A summary of the standard and modified input cycles is shown in Table 2. The Prodisc and Charité devices underwent testing under ISO 18192-1 (standard ISO) conditions to establish baseline data (Fig. 2). The second investigation used a modified standard ISO cycle with the phase of the LB changed to give 0° difference between LB and FE (Fig. 3). It was reasoned that this would produce a low cross-shear motion path that would be easily repeatable and allow comparison with the baseline test. A further study applied the standard ISO cycle in addition to either an AP displacement or applied force, depending on whether the device was a Charité or Prodisc, respectively. The rationale for this was that an unconstrained device subject to an AP load may be at risk of dislodging its mobile articulating core due to the minimal resistance to a shear force. The Prodisc design, if subject to an AP displacement, may be at risk of being overloaded due to the limited amount of translation allowed by its design. The AP waveform was idealized as a sinusoid with the

FIG. 1—*Prodisc-L (right, shown with superior endplate mounted in cement) and Charité (left, shown unmounted).*

TABLE 1—*Experimental studies: 3 input cycles applied to Prodisc; 2 input cycles applied to Charité.*

	ISO	ISO + AP	ISO Low Cross-Shear
Prodisc	Standard ISO 18192-1 (baseline)	ISO + additional AP shear *load*	FE and LB motions placed in-phase to create a low cross-shear motion
Charité	Standard ISO 18192-1 (baseline)	ISO + additional AP shear *displacement*	

TABLE 2—*ISO 18192-1 (standard ISO) input cycle parameters—alterations to the standard ISO cycle are highlighted.*

Input	Study	Input Parameter	Input Magnitude	Freq (Hz)	Phase wrt FE (°)
Standard ISO	Baseline	AF	600-2000 N	2	N/A
		AR	+2°/−2°	1	+90
		FE	+6°/−3°	1	0
		LB	+2°/−2°	1	−90
ISO + AP	Effect of AP shear (Prodisc)	AP load	**+175 N/−145 N**	**2**	N/A
	Effect of AP shear (Charité)	AP displacement	**+2 mm/−1.5 mm**	**2**	N/A
ISO low cross-shear	Effect of cross-shear	LB	+2°/−2°	1	**0**

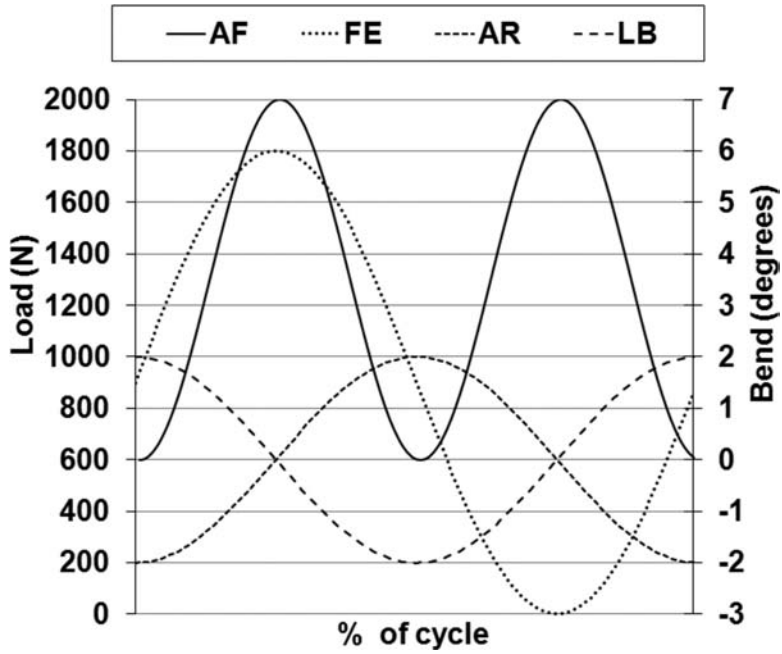

FIG. 2—*ISO 18192-1 lumbar TDR wear testing standard ISO input motions and loads.*

positive load peaks coincident with the FE maximum amplitudes and in-phase with the axial force (AF) input.

Identical experiments were run on both simulators to assess the inter-simulator and observer variability using identical components and inputs (Prodisc TDR, standard ISO cycle). Mean wear rates were calculated from the total mass loss. Verification that the simulator meets ISO 18192-1 tolerances for both phasing and input magnitudes has been confirmed previously [24]. Statistical analysis software (SPSS for Windows, SPSS Inc., Chicago, IL, USA) was used to test for significance between experimental wear rate data using analysis of variance (ANOVA) with $\alpha = 0.05$. Lavene's test for homogeneity of variance was used to determine homogeneity and then followed by Scheffe's post hoc tests assuming equal variance.

General Simulation Method

Before commencement of testing, the UHMWPE components were soaked in distilled water for 14 days to stabilize fluid uptake. This was followed by drying with lint free tissue and removal to a temperature and humidity controlled metrology laboratory for 48 h prior to mass measurement. The same period of stabilization (48 h) was used at each wear measurement point within each test variation. Their mass was determined gravimetrically using a digital balance with a resolution of 0.01 mg (Mettler-Toledo Inc., Columbus, OH). After mass measurement, the polyethylene components were assembled together with the

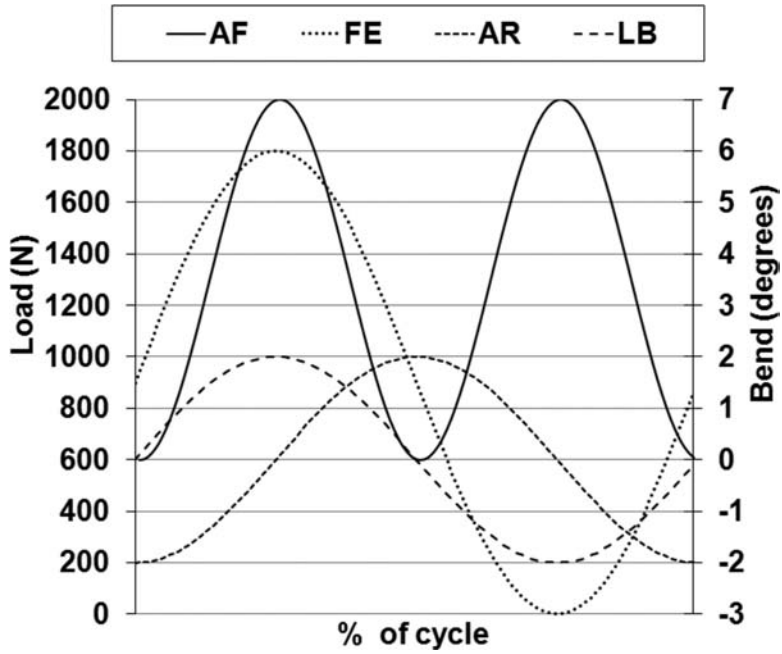

FIG. 3—*ISO 18192-1 lumber TDR wear testing standard with flexion-extension and lateral bend in-phase to give low cross-shear wear path.*

endplates into test cell holders. The TDR fixtures consisted of seven pairs of Prodisc and Charité endplates each of which were mounted in lower and upper holders using PMMA bone cement. To reproduce the exact positioning of the endplates, special jigs were manufactured to enable precise setting in the PMMA cement mantel so that the COR of each device matched that of the simulator. The Charité device has a variable COR, and therefore an arbitrarily fixed point was chosen to be at the center of the polyethylene core when fully assembled. Prodisc polyethylene discs were inserted into their inferior endplate (by a snap-lock mechanism) and holder, then assembled together with the superior endplate and holder. Charité polyethylene cores were placed between inferior and superior endplates. All polyethylene components were numbered, and the test station cells were always replaced in the same positions after measurement. The test cell assemblies were then enclosed in a silicone gaiter to enable complete immersion in lubricant. FE and LB were applied to the upper holders of the simulator and hence to the superior components of the TDRs. Axial rotation (AR) was applied to the lower holders and hence to the inferior TDR components. The axial loading was vertically applied to the lower holders and hence to the inferior side of the TDRs.

The test cells were mounted in one of the two spine simulators, and the holders were attached with screws to each station. A flexible pipe connected to the lower holder of each test cell allowed filling with lubricant: newborn calf

serum, diluted to 15 g/l protein concentration with 0.03 % (wt/vol) sodium azide added to limit bacterial growth between serum changes. In addition, a pipe connected to the upper holder was used to improve the serum draining and refilling process by allowing air intake. During testing the pipes were connected, effectively sealing the test cell from airborne contamination. The serum protein concentration of 15 g/l was less than that stipulated by ISO 18192-1 and ASTM F2423-05 (30 g/l); however, the value of 15 g/l is in the central region of a range of concentrations that have been shown to produce clinically relevant wear data in TJR [25]. The lubricating fluid was replaced every 1/3 MC and subsequently stored at −20°C for future debris analysis. At this time point, each cell was flushed with cleansing agent, soaked in disinfectant solution for 20 min, rinsed with tap water, and then rinsed with distilled water before refilling with lubricant.

The measurement time point was chosen to be 1 MC at which point the test station cells were dismantled for a more thorough cleaning to remove potential bacterial contamination. The polyethylene components were removed and cleaned before being left for 48 h in a metrology lab prior to measurement. The Prodisc polyethylene inlay was removed from the inferior endplate by use of a thin metal spatula inserted between the metallic endplate and the PE disc inlay at the anterior end of the TDR. A small leverage applied to the spatula was sufficient to unlock the snap-lock mechanism and allow the inlay to be slid out for measurement without damage; the Charité polyethylene core is unconstrained. To assist in non-abrasive cleaning of the components, they were submerged in an ultrasonic bath containing isopropanal for 10 min followed by drying with lint-free tissue. After the appropriate stabilizing time was met, the mass was recorded (×6 measurements per disc). The ISO14242-2 standard was followed to calculate mass loss due to wear only. The six articulating discs were measured for gross mass loss, but to limit the effect of fluid absorption, the seventh soak control disc was used to subtract changes in mass due to soak effects only and therefore show net wear mass loss. The soak control disc was cyclically loaded to ensure that absorption was similar to the other articulating ones.

Results

A baseline standard ISO test using Prodisc samples performed on simulator B was followed by a low cross-shear test. The baseline test produced a wear rate of 16.1 ± 1.4 mg/MC (mean ± standard deviation) with the following reduced cross-shear test producing a wear rate of 6.0 ± 1.3 mg/MC. The reduction in mean wear rate for the low cross-shear motion path using the Prodisc device was significant ($P < 0.01$) showing a drop to 37 % of baseline (Fig. 4). A second baseline standard ISO test performed on simulator A for the Prodisc (Fig. 5) produced a mean wear rate of 12.7 ± 2.1 mg/MC. This second baseline test resulted in a significant ($P = 0.02$) reduction in wear rate to 79 % of baseline when compared to simulator B. A following test, on simulator A, with the addition of AP shear loading, produced a mean wear rate of 11.6 ± 1.2 mg/MC. The addition of AP shear force did not significantly ($P = 0.89$) alter the wear rate in the Prodisc device when compared to baseline (Table 3). The baseline standard

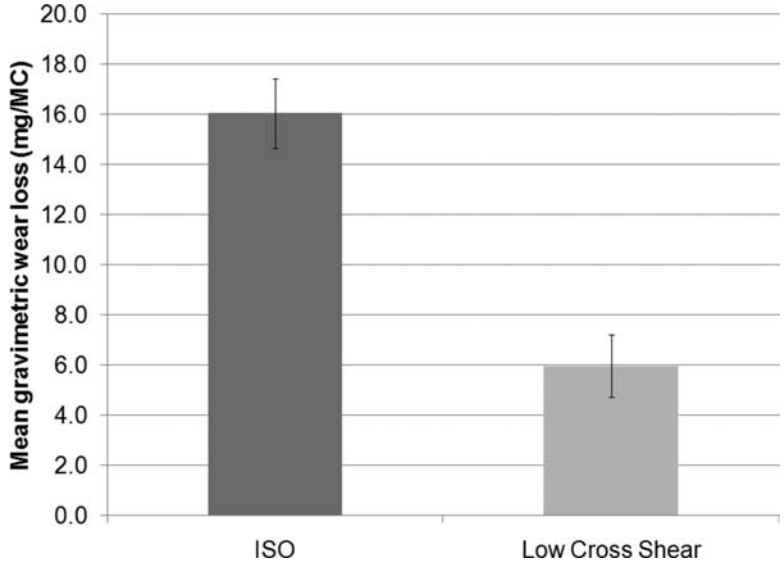

FIG. 4—*Prodisc TDR wear rate showing standard ISO and modified low cross-shear result (mean ± 95 standard deviation).*

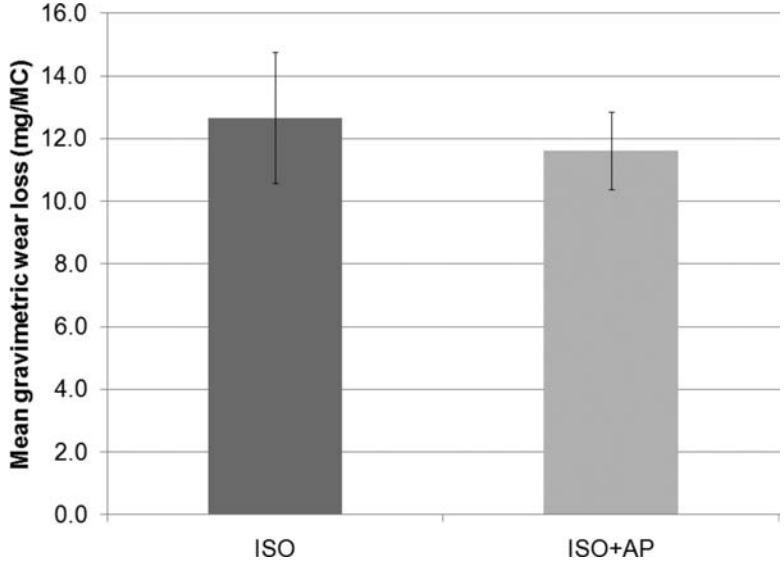

FIG. 5—*Prodisc TDR wear rate showing standard ISO and modified AP shear force input result (mean ± 95 standard deviation).*

TABLE 3—*Significant difference* (**P** *values) between mean wear rate values for each test using one way ANOVA, Scheffe's post hoc test (equal variance assumed).*

	IPA	APA	ICA	ACA	IPB	XPB
IPA		0.89	1.00	<0.01	0.02	<0.01
APA			0.99	<0.01	<0.01	<0.01
ICA				<0.01	<0.01	<0.01
ACA					<0.01	<0.01
IPB						<0.01

IPA, **I**SO input, **P**rodisc device, simulator **A**; APA, ISO plus **A**P input, **P**rodisc device, simulator **A**; ICA, **I**SO input, **C**harité device, simulator **A**; ACA, ISO plus **A**P input, **C**harité device, simulator **A**; IPB, **I**SO input, **P**rodisc device, simulator **B**; XPB, ISO with low **cross**-shear input **P**rodisc device, simulator **B**.

ISO test for the Charité (Fig. 6) performed on simulator A produced a wear rate of 12.2 ± 1.0 mg/MC. The following test, with the addition of AP shear displacement, produced a substantial increase in wear rate to 22.3 ± 1.3 mg/MC; 183% of baseline. The addition of AP shear displacement did significantly ($P < 0.01$) affect the wear rate of the Charité device when compared to baseline. There was a significant difference ($P < 0.01$) in mean wear rate between the low cross-shear input for Prodisc and all other input/disc combinations. Wear scars for all tests showed a large area of wear almost covering the entire dome of the UHMWPE components indicative of full contact between the bearing components. The worn surfaces had a polished appearance that was more pronounced

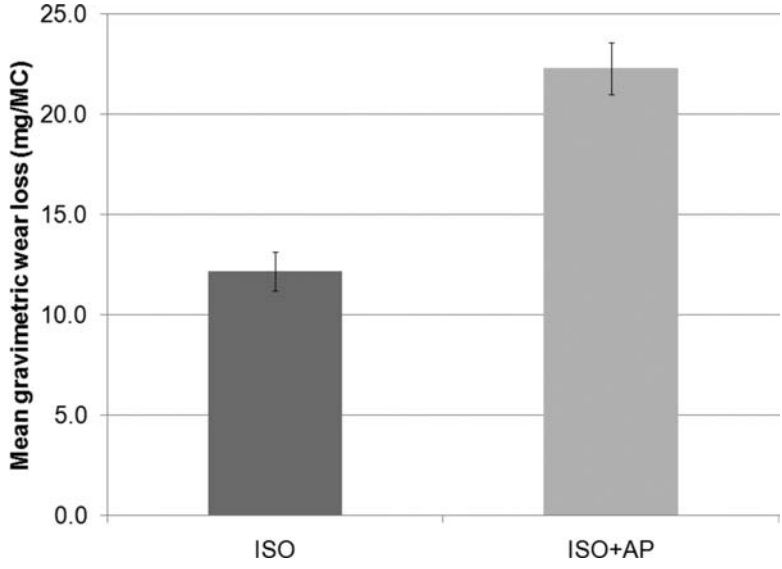

FIG. 6—*Charité TDR wear rate showing standard ISO and modified AP shear displacement input result (mean ± 95 standard deviation).*

FIG. 7—*Typical worn surface topography of a Prodisc polyethylene component showing polished circumferential wear area (each square = 2 mm).*

toward the circumference of the worn area of the Prodisc UHMWPE components (Fig. 7).

Discussion

This study has compared the wear rates of two TDR devices representing two different design rationales, one constrained and the other unconstrained. Standard ISO baseline tests and derivations of these inputs were used to observe the effect of AP shear inputs and low cross-shear scenarios.

Effect of FE-LB phasing

Placing the FE and LB motions in-phase, which created a low cross-shear input cycle, significantly affected the wear rate within the Prodisc device. The low cross-shear cycle produced a decrease in wear rate to 37 % of the baseline ISO test. Similarly, Nechtow et al. experimented with high and low cross-shear input

cycles; however, they used a perturbed version of the ISO standard to represent a "cross-shear" cycle followed by an ASTM-based cycle to represent a "curvilinear" test. The purely curvilinear motion produced zero cross-shear as opposed to the low cross-shear cycle used in the present work. Hence, Nechtow et al. reported a large fall in wear rate to 0.4 % [12] for their Prodisc test. Correspondingly, Grupp et al. [13] compared wear rates for the Activ-L lumbar TDR using a modified version of the input cycles outlined in ISO 18192-1 and the ASTM guide. The mean wear rate for the ISO input cycle (with slightly lower peak loading than the present standard) was low compared to contemporary results reported elsewhere at 2.7 ± 0.3 mg/MC. For the ASTM-based test a rate of 0.14 ± 0.06 mg/MC was recorded. This is a drop in wear rate to 5 % from the relatively high cross-shear ISO test to the curvilinear ASTM test. The small amount of cross-shear introduced by the AR input in the present study may account for the difference in wear rate reductions among Nechtow et al., Grupp et al. and this study. Regardless of testing nuances, the effect of high and low cross-shear input cycles remains broadly similar and there is good agreement between ISO-based Prodisc results from Nechtow et al. (16.59 ± 0.96 mg/MC) and standard ISO results presented here.

Effect of AP Shear

Effect of AP shear input was dependent on device design. Wear rate of the Prodisc design was not influenced by AP loading; however, the wear rate of the Charité device was significantly affected by addition of AP displacement (Table 3). The constrained nature of the Prodisc inhibits transfer of AP loads to increased translation at the bearing surfaces. Also, the consequence of the AP load on the resultant load applied at the bearing surface is minimal when compared to the dominant AF load. This minimal effect on total load combined with constrained translation resulted in a statistically insignificant effect on wear rate. Under AP displacement input conditions, the Charité device showed a substantial increase in wear compared to the standard ISO test. It is postulated that the increase in wear rate of the Charité is due to the mobility of the central articulating core resulting in increased translation between the bearing faces of theUHMWPE core and the metal counterface; hence producing more wear as predicted by the Archard law [26].

Interobserver and Simulator Differences

There was a small but significant difference in wear rate for the two baseline standard ISO Prodisc studies performed on the nominally identical simulators, A and B. There are a number of possible contributors to this observation. These include: (a) the test specimens used on each simulator were taken from different batches, (b) there may be slight variations in the mounting of the discs within the simulator leading to a systematic bias in wear rates, and (c) batch quality or viscosity of bovine serum might have changed and altered the tribological environment. Interoperator differences will also be present, but a standard operating procedure was observed to minimize the effects of

operator or observer error. It must be recognized that wear is not a material property, but an output from a complex tribological engineering system, within which a number of variables can influence the wear process, only some of which are assignable.

Surface Wear Morphology

The circumferential wear pattern present on the Prodisc UHMWPE components was coincident with the contact area of the fillet radii of the metallic cup rim against which it articulates (Fig. 8). Because the standard ISO waveform has a 2 Hz axial load and 1 Hz FE motion, the axial loading peaks occur at the extremes of the FE cycle, with the minimum loading at the midpoint. Perhaps the high loading at the ends of the FE cycle contribute to this deformation. The metal-UHMWPE TDR design also has a bearing couple combination that is the reverse of that for a hip, in that the cup is metallic and the core is UHMWPE. A reversal of this combination may lead to a reduction in edge loading around the circumference of the UHMWPE bearing and hence reduced wear.

General

Testing using low cross-shear motion paths where the inputs are wholly or partially in phase produces a low mean wear rate for UHMWE bearing components in a constrained TDR [12,13,16]. Abnormally low wear rate results gained in this way are not representative of "worst case" scenarios that would be prudent

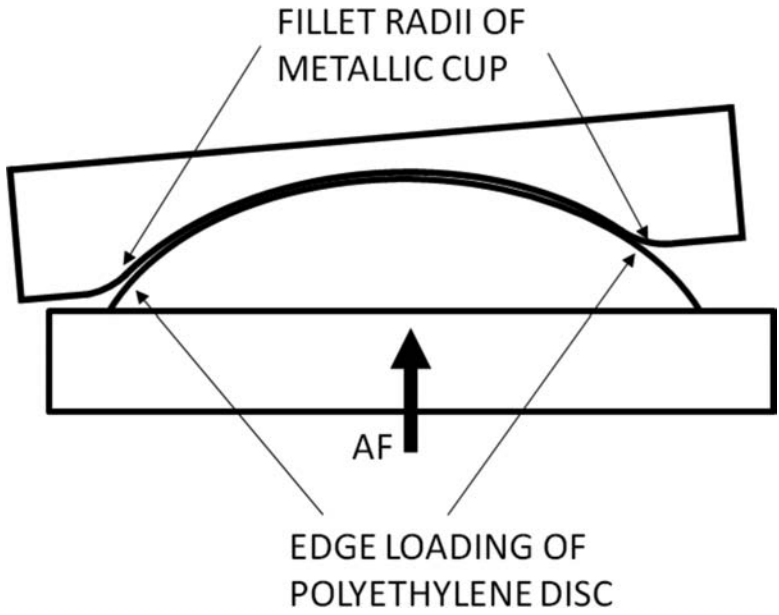

FIG. 8—*Schematic showing fillet radii and the potential for edge loading when the axial load (AF) is applied at the extremes of the rotation angles.*

to represent when testing in vitro. Further, completing tests that alternate among FE, LB, and AR produce zero cross-shear motion paths that could underestimate the mean wear rate in vivo. The lubricating medium and protein content used for TDR testing has followed protocols developed for THR and TKR studies. There is no evidence to suggest that this is relevant to the spine; however, in the absence of this knowledge, it seems reasonable to continue to use the serum concentrations described. It is also noted that the intervertebral disc is not a synovial joint and that after replacement with an articulating device the medium within the joint space is unlikely to be a full synovial fluid; however, a pseudo-synovial fluid of low protein concentration may exist resulting from the fibrous capsule formation that is a consequence of implantation [27]. The constrained bearing Prodisc TDR tested was sensitive to phasing of the motion inputs but was not affected by AP loading. The unconstrained Charité TDR was sensitive to additional AP loading and should be further investigated for sensitivity to phasing of input kinematics and cross-shear. Input cycles that allow in-phase or closely phased motions or that permit sequential testing on separate inputs will probably produce much lower wear rates and will possibly not give a true prediction of wear in vivo. Validation of wear rates between in vitro and ex vivo TDRs of all types and under varied loading and kinematic considerations is needed before concrete conclusions can be drawn [28].

Acknowledgments

This work was supported by the National Institutes of Health Grant No. R01-AR052653 as part of a collaboration between the University of Leeds, University of Iowa, and Spine Centre Munich. Arthritis Research UK was a co-funder (grant number 17911). Professor Fisher, Professor Ingham, and Professor Hall receive support from the NHIR Leeds Musculoskeletal Biomedical Research Unit. The Prodisc implants were provided by Synthes, Inc., PA. The Charité implants were provided by DePuy Spine, Inc., MA.

References

[1] Learmonth, I. D., Young, C., Rorabeck, C. "The Operation of the Century: Total Hip Replacement," *The Lancet*, Vol. 370, No. 9597, 2007, pp. 1508–1519.

[2] Charnley, J., and Cupic, Z., "The Nine and Ten Year Results of the Low-Friction Arthroplasty of the Hip," *Clin. Orthop. Relat. Res.*, Vol. 95, 1973, pp. 9–25.

[3] Green, T. R., Fisher, J., Stone, M., Wroblewski, B. M., and Ingham, E., "Polyethylene Particles of a 'Critical Size' Are Necessary for the Induction of Cytokines by Macrophages In Vitro," *Biomaterials*, Vol. 19, No. 24, 1998, pp. 2297–2302.

[4] Ingham, E., and Fisher, J. "Biological Reactions to Wear Debris in Total Joint Replacement," *Proc. Inst. Mech. Eng., Part H: J. Eng. Med.*, Vol. 214, No. 1, 2000, pp. 21–37.

[5] Schmalzried, T. P., Jasty, M., and Harris, W. H., "Periprosthetic Bone Loss in Total Hip Arthroplasty. Polyethylene Wear Debris and the Concept of the Effective Joint Space," *J. Bone Jt. Surg., Am. Vol.*, Vol. 74, No. 6, 1992, pp. 849–863.

[6] Devin, C. J., Myers, T. G., and Kang, J. D., "Chronic Failure of a Lumbar Total Disc Replacement With Osteolysis Report of a Case With Nineteen-Year Follow-Up," *J. Bone Jt. Surg., Am. Vol.*, Vol. 90, No. 10, 2008, pp. 2230–2234.

[7] Punt, I. M., Cleutjens, J. P. M., de Bruin, T., Willems, P. C., Kurtz, S. M., van Rhijn, L. W., Schurink, G. W. H., and van Ooij, A., "Periprosthetic Tissue Reactions Observed at Revision of Total Intervertebral Disc Arthroplasty," *Biomaterials*, Vol. 30, No. 11, 2009, pp. 2079–2084.

[8] van Ooij, A., Kurtz, S. M., Stessels, F., Noten, H., van Rhijn, L., van Ooij, A., Kurtz, S. M., Stessels, F., Noten, H., and van Rhijn, L., "Polyethylene Wear Debris and Long-Term Clinical Failure of the Charite Disc Prosthesis: A Study of 4 Patients," *Spine*, Vol. 32, No. 2, 2007, pp. 223–229 [erratum appears in *Spine*, Vol. 32, 9, 2007, p. 1052].

[9] ISO-18192, 2008, "Implants for Surgery—Wear of Total Intervertebral Spinal Disc Prostheses. Part 1. Loading and Displacement Parameters for Wear Testing and Corresponding Environmental Conditions for Test," D. C. Kaddick, Ed., International Organization for Standardization, 2008-01-29.

[10] ASTM F 2423-05, 2005, ASTM, "Standard Guide for Functional, Kinematic, and Wear Assessment of Total Disc Prostheses," *Annual Book of ASTM Standards*, ASTM International, West Conshohocken, PA, pp. 1435–1444.

[11] Vicars, R., Hyde, P. J., Brown, T. D., Tipper, J., Ingham, E., Fisher, J., and Hall, R. M., "The Effect of Anterior–Posterior Shear Load on the Wear of ProDisc-L TDR," *Eur. Spine J.*, Vol. 19, No. 8, 2010, pp. 1356–1362.

[12] Nechtow, W., Hintner, M., Bushelow, M., and Kaddick, C., "IVD Replacement Mechanical Performance Depends Strongly on Input Parameters," *Transactions of the 52nd Annual Meeting of the Orthopeadic Research Society*, Chicago, IL, 2006.

[13] Grupp, T. M., Yue, J. J., Garcia, R., Jr., Basson, J., Schwiesau, J., Fritz, B., and Blomer, W., "Biotribological Evaluation of Artificial Disc Arthroplasty Devices: Influence of Loading and Kinematic Patterns During In Vitro Wear Simulation," *Eur. Spine J.*, Vol. 18, No. 1, 2009, pp. 98–108.

[14] Goreham-Voss, C. M., Hyde, P. J., Hall, R. M., Fisher, J., and Brown, T. D., "Cross-Shear Implementation in Sliding-Distance-Coupled Finite Element Analysis of Wear in Metal-on-Polyethylene Total Joint Arthroplasty: Intervertebral Total Disc Replacement as an Illustrative Application," *J. Biomechan.*, Vol. 43, No. 9, 2010, pp. 1674–1681, 2010.

[15] Bushelow, M., Walker, J., Coppes, J., Hinter, M., Nechtow, W., and Kaddick, C., "P32. Comparison of Wear Rates: Metal/UHMWPE and Metal-on-Metal Total Disc Arthroplasty," *Spine J.*, Vol. 7, No. 5, Suppl. 1, 2008, pp. 97S–98S.

[16] Serhan, H. A., Dooris, A. P., Parsons, M. L., Ares, P. J., and Gabriel, S. M., "In Vitro Wear Assessment of the Charite Artificial Disc According to ASTM Recommendations," *Spine*, Vol. 31, No. 17, 2006, pp. 1900–2010.

[17] Wang, A., "A Unified Theory of Wear for Ultra-High Molecular Weight Polyethylene in Multi-Directional Sliding," *Wear*, Vol. 248, No. 1-2, 2001, pp. 38–47.

[18] Hall, R. M., "Introduction to Lumbar Total Disc Replacement: Factors That Affect Tribological Performance," *Proc. Inst. Mech. Eng., Part J: J. Eng. Tribol.*, Vol. 220, No. J8, 2006, pp. 775–786.

[19] Callaghan, J. P., Patla, A. E., and McGill, S. M., "Low Back Three-Dimensional Joint Forces, Kinematics, and Kinetics During Walking," *Clin. Biomechan.*, Vol. 14, No. 3, 1999, pp. 203–216.

[20] Rousseau, M.-A., "Disc Arthroplasty Design Influences Intervertebral Kinematics and Facet Forces," *Spine J.*, Vol. 6, No. 3, 2006, pp. 258–266.

[21] Cunningham, B. W., "Biomechanical Evaluation of Total Disc Arthroplasty: An In-Vitro Human Cadaveric Model," *Spine J.*, Vol. 2, No. 5, Suppl. 1, 2002, p. 104.

[22] Cunningham, B. W., "Basic Scientific Considerations in Total Disc Arthroplasty," *Spine J.*, Vol. 4, No. 6, Suppl. 1, 2004, pp. S219–S230.

[23] Bogduk, N., *Clinical Anatomy of the Lumbar Spine and Sacrum*. Elsevier, New York, 2008.
[24] Vicars, R., "Verification of a Novel Spine Wear Simulator," *British Orthopaedic Research Society Annual Conference*, Manchester, UK 2007.
[25] Wang, A., "The Impact of Lubricant Protein Concentrationon the Outcome of Hip Joint Simulator Testing," *45th Annual Meeting of the Orthopaedic Research Society*, Anaheim, CA, 1999.
[26] Archard, J. F., "Contact and Rubbing of Flat Surfaces," *J. Appl. Phys.*, Vol. 24, No. 8, 1953, pp. 981–988.
[27] Bullough, P. G., "Pathologic Studies of Total Joint Replacement," *Orthoped. Clin. N. Am.*, Vol. 19, No. 3, 1988, pp. 611–625.
[28] Vicars, R. K. S., MacDonald, D., Brown, T., Tipper, J., Fisher, J., Ingham, E., Hall, R., "Height Loss Comparison Between Ex-Vivo and In-Vitro TDR," *ORS*, 2010, New Orleans, LA.

Reprinted from JAI, Vol. 8, No. 6
doi:10.1520/JAI103494
Available online at www.astm.org/JAI

R. L. Blice,[1] *K. B. Zimmers,*[1] *and R. Linovitz*[2]

How Frequency Affects Fatigue Testing of an Artificial Disc With a Viscoelastic Polymer Core

ABSTRACT: The purpose of this study was to determine the highest appropriate test frequency for a viscoelastic total disc replacement (VTDR). Natural intervertebral discs display viscoelastic behavior. Viscoelasticity is the time-dependent property of a material to show sensitivity to the rate of loading or deformation, having stress and strain reactions that are out of phase. If frequency is too high during mechanical testing of a viscoelastic polymer or medical device, the specimen is unable to recover fully before the next load application. Polymers absorb energy with each cycle. Since work (or energy utilized) is defined as the area under the force–displacement curve [Giordano, N. J., *College Physics: Reasoning and Relationships*, Brooks/Cole Publishing, Pacific Grove, CA, 2010], a frequency increase which decreases displacement will by definition also decrease the energy the polymer is using to achieve that decreased displacement. By reducing both total displacement and energy, a high test frequency would "protect" a viscoelastic device. A frequency of 2 Hz was used to determine the expected response of the VTDR during axial compression testing between 400 and 4000N. The response was defined as mean peak-to-peak displacement of five test cycles after 1000 cycles of preconditioning. Comparative data was collected at test frequencies of 3, 6, and 10 Hz. Displacement and energy utilized decreased with increasing test frequency. There were no significant differences between the viscoelastic responses in tests at 2 and 3 Hz. However, there were

Manuscript received October 15, 2010; accepted for publication April 15, 2011; published online July 2011.
[1] AxioMed Spine Corporation, 5350 Transportation Blvd., Suite 18, Garfield Heights, OH 44125.
[2] CORE Orthopaedics, 332 Santa Fe Dr., Suite 110, Encinitas, CA 92024.
Symposium on Static and Dynamic Spinal Implants: Are We Evaluating Them Appropriately? on 16 November 2010 in San Antonio, TX.

Cite as: Blice, R. L., Zimmers, K. B. and Linovitz, R., "How Frequency Affects Fatigue Testing of an Artificial Disc With a Viscoelastic Polymer Core," *J. ASTM Intl.*, Vol. 8, No. 6. doi:10.1520/JAI103494.

significant decreases in displacement and energy utilized at 6 and 10 Hz compared to 2 Hz. Over a 10×10^6 million cycle fatigue test, for this device, the total displacement would be 548 000mm less at 6 Hz and 988 000mm less at 10 Hz compared to 2 Hz. By decreasing the displacement, by definition it decreases the amount of overall work the disc has done when tested at these high frequencies [Giordano, N. J., *College Physics: Reasoning and Relationships*, Brooks/Cole Publishing, Pacific Grove, CA, 2010]. Viscoelastic devices should not be tested at high frequencies which "protect" the device by reducing the energy the device has to use overall by decreasing the total displacement it sees. To accurately evaluate *in vivo* behavior, fatigue testing should utilize test frequencies which do not significantly change the device's viscoelastic response from that experienced at a physiologic loading frequency.

KEYWORDS: viscoelastic, frequency, artificial lumbar disc, total disc replacement

Introduction

The term viscoelastic refers to a material's ability to deform elastically and viscously when stressed, including resistance to deformation, damping, and relaxation [1,2]. A viscoelastic material has stress and strain reactions that are out of phase, meaning that the response of one to the other is delayed. In completely viscous materials, the response delay is 90 degrees, while in perfectly elastic materials; there is no delay in response [3].

A natural disc is viscoelastic [4], in that the degree of stiffness varies with the frequency of any load, and is compliant under loading (shock absorber). To restore the disc function to a degenerated segment, an artificial disc should mimic the properties of the natural disc as closely as possible, including viscoelasticity.

Frequency is an important variable when mechanically testing viscoelastic polymers or devices. Higher testing frequency reduces testing time, and generally cost; the duration of a 10×10^6 cycle continuous fatigue test is 116 days at 1 Hz, 58 days at 2 Hz, 39 days at 3 Hz, 20 days at 6 Hz, and 12 days at 10 Hz. A device may respond in the elastic range at physiologic frequencies. However, if a chosen testing frequency is too high, then the viscoelastic polymer exhibits a lag between applied stress and resulting strain [5] and is not able to respond (displace) fully before application of the next loading cycle. In addition, because the polymer absorbs energy with each cycle, an increase in frequency, if it leads to a decrease in displacement, would in turn decrease the material's absorption of energy.

An abnormally high, non-physiologic test frequency will protect a viscoelastic device by reducing the displacement and energy absorption during the test. That energy loss is then replaced by an increase in the polymer's temperature [6]. An increase in internal temperature can lead to increased polymer compliance and with that an increase in displacement. This rise in temperature may be partially mitigated by testing in a temperature controlled environmental tank.

Materials and Methods

The viscoelastic total disc replacement (VTDR) tested was the Freedom® Lumbar Disc[3] (Fig. 1). The device is composed of titanium alloy plates that are molded and bonded to a core of silicone polycarbonate urethane copolymer.

The dynamic axial compression tests were conducted at AxioMed Spine Corporation (Garfield Heights, OH) using an MTS Mini-Bionix 383 Axial Table Top Servohydraulic Dynamic Testing System (MTS, Eden Prairie, MN) with a 25 kN axial load cell. All tests were conducted using an environmental chamber containing phosphate buffered saline (PBS) at 37°C ± 3°C for the duration of the testing. Stainless steel fixtures were used to maximize fixture stiffness and ensure that all loads were transferred to the test specimen. The test set-up is shown in Fig. 2. All specimens were pre-conditioned in PBS for a minimum of four days at 37°C ± 3°C prior to the commencement of testing.

Compression testing was conducted to elicit solely the polymer response to frequency and eliminate any contribution of the manufactured assembly to the test results. The load applied was 4000 N, chosen as a conservatively high physiologic load [7] and to ensure adequate displacements for comparisons between test groups. Each disc was tested at the following frequencies: 2, 3, 6, and 10 Hz. There was a minimum recovery period between tests of ten times the testing duration. In addition, each device was started at a different frequency and then run through the rest of the test frequencies to minimize the potential effects of test order. After approximately 1000 cycles, load and displacement data were captured for five cycles at a data collection rate of 100 Hz. The area under the force–displacement curve for one cycle at each frequency was calculated to show the capacity of the test specimen to absorb energy at that frequency.

FIG. 1—*The Freedom® Lumbar Disc.*

[3]Caution-Investigational Device. Limited by Federal (or United States) law to investigational use.

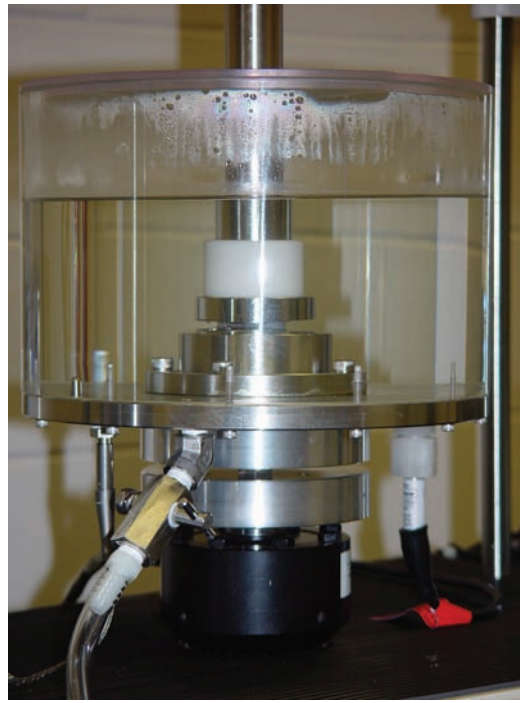

FIG. 2—*Axial compression frequency test set-up.*

Statistical analyses were performed on both displacement and energy data. A single factor analysis of variances (ANOVA) was used to analyze any significant differences ($p < 0.05$) in data between tests at 2 Hz and 3, 6, and 10 Hz. The null hypothesis was that there were no differences in resultant displacements or energy absorption between tests at each frequency.

Results and Discussion

Both resultant displacements and energy absorption (Fig. 3) decreased with increasing test frequency (Table 1 and Fig. 3). The statistical results for significance are shown in Table 2. 2 Hz was considered a baseline for comparison because it is the standard test frequency specified in ASTM testing standards for total disc replacements. In general, utilization of a test frequency greater than 2 Hz requires a rationale when testing polymeric devices.

As shown in Table 2, 3 Hz may be used when testing this VTDR without significant effects to resultant displacement and energy absorption. However, increasing test frequency to 6 or 10 Hz significantly decreased both displacement and energy absorption.

When dynamically testing a viscoelastic medical device, test frequency significantly affects the device's ability to respond to the load applied. Increasing

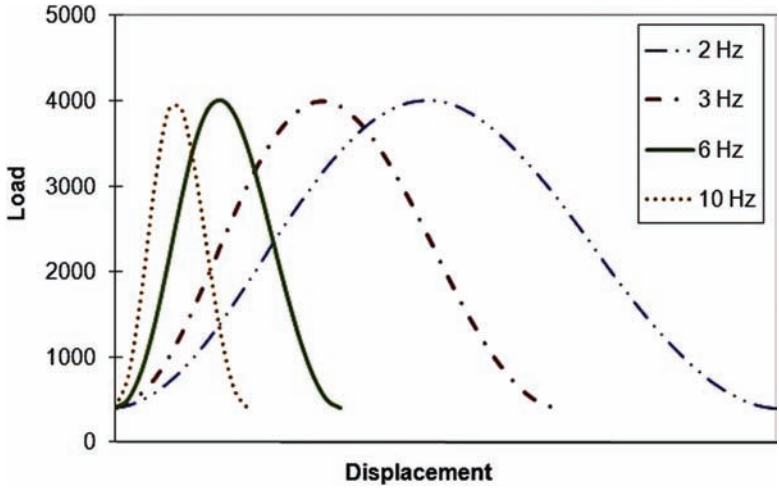

FIG. 3—*Decreasing displacement and energy absorption (area under the curve) with increasing frequency.*

frequency results in decreased displacement response and energy absorption, thereby "shielding" the device. While the displacement and energy differences at different testing frequencies may seem small, they are statistically significant and become more so during a 10×10^6 cycle fatigue test.

Most TDR fatigue testing is conducted to an endurance limit of 10×10^6 cycles. For this reason, the displacement and energy results were multiplied to reflect the distance travelled and energy lost over a 10×10^6 cycle test. Small differences in displacement and energy loss between the tests at different frequencies become more substantial when considering the full length of the test. For the device tested here, the total displacement would be 548 000 mm less and the total energy absorption would be 400 000 J less when tested at 6 Hz than those for a device tested at 2 Hz. The numbers jump to 988 000 mm less and 840 000 J less if the device is tested at 10 Hz. This would certainly lead to less wear and tear on a test sample if it was tested at these high frequencies. The results from this study demonstrate that viscoelastic devices should not be tested at high frequencies which protect the device by reducing the stress and strain experienced.

The human intervertebral disc has been shown to behave differently under different loading rates and frequencies [4,8], demonstrating higher stiffness

TABLE 1—*Displacement and energy differences as a percentage of 2 Hz baseline values.*

(Hz)	Displacement	Energy
2	100	100
3	98	99
6	96	97
10	93	94

TABLE 2—*Results matrix showing statistically significant differences* ($p < 0.05$).

	Displacement	Energy
2 Hz versus 3 Hz	Not significant	Not significant
2 Hz versus 6 Hz	Significant	Significant
2 Hz versus 10 Hz	Significant	Significant

with higher loading rate or frequency. Higher stiffness is represented by a greater slope of the load versus displacement curve; a higher stiffness corresponds to a lower displacement per unit of load and therefore a lower area under the curve (energy absorption). This finding confirms that the human disc, like the VTDR evaluated here, will experience decreasing displacements and energy absorption with increased loading frequency.

While physiologic loading frequencies for the human disc range from 0.001 to 6 Hz, higher frequencies such as 6 Hz are considered to be representative of vibrations experienced when driving trucks, buses, tractors, etc. [9]. Like the human disc, a viscoelastic TDR will respond differently at frequencies representing sitting activities (0.001–0.01 [4]), walking (1–2 Hz [4,10]) and vibration frequencies (6 Hz [9]). Because the human disc and a VTDR demonstrate different responses to loading at different frequencies, a mechanical test which is intended to represent walking or significant bending of a viscoelastic TDR should be conducted at walking or bending frequencies unless it can be shown that higher frequencies do not significantly change the response of the device.

One limitation of this study is lack of data at frequencies other than 2, 3, 6, and 10. Since it was determined that 3 Hz can be used for the VTDR without significant affect, but 6 Hz cannot, it would be interesting to evaluate 4 and 5 Hz to determine if these frequencies could be used for testing this VTDR without significant affect. Additionally, axial compression of the VTDR likely induces lower displacements than those experienced during flexion/extension or rotation testing; the differences in viscoelastic polymer response would then be greater when tested in those modes. Studies should be conducted to address this possible "shielding" in other physiologic loading modes, as these loading modes are commonly used in TDR fatigue tests.

The amount and composition of polymer in a device will affect its reaction at different frequencies, so while it has been concluded that the VTDR tested here should not be tested at frequencies of 6 or 10 Hz, this determination should be made on a case by case basis for other devices.

While the long-term effects of temperature were not of primary consideration in this study, it is recognized that increasing test frequency causes an increase in the internal temperature of polymeric devices. Obtaining temperature data inside the polymer portion of a TDR during a high load fatigue test is technically challenging. In a separate study using this VTDR, the authors found increases of up to 6°C from 1 to 5 Hz in axial compression fatigue testing. However, further studies of the temperatures resulting from fatigue tests at different frequencies are recommended and would be appropriate for TDRs on a case by case basis.

Conclusions

Since natural discs demonstrate viscoelasticity, it seems obvious that an ideal TDR should be viscoelastic as well in order to restore natural function to the spine segment. Test frequency is an important variable in the mechanical testing of viscoelastic medical devices or materials. Increasing the frequency beyond physiologic loading conditions will result in shielding of the test specimen from the full travel and energy absorption experienced at lower, more physiologic frequencies. It is recommended that frequency studies be conducted on TDRs or other viscoelastic medical devices containing viscoelastic materials before increasing the frequency of testing beyond the 2 Hz specification in total disc replacement ASTM standards.

References

[1] Callister, W. D., *Materials Science and Engineering: An Introduction*, Wiley, Hoboken, NJ, 1985.

[2] Higgins, R. A., *Properties of Engineering Materials*, 2nd ed., Industrial Press, Inc., New York, NY, 1994, p. 363.

[3] Ward, I. M. and Sweeney, J., "Dynamic Mechanical Measurements: The Complex Modulus and Complex Compliance," *The Mechanical Properties of Solid Polymers*, 2nd ed., Wiley, Hoboken, NJ, 2004, pp. 70–71.

[4] Costi, J. J., Stokes, I. A., Gardner-Morse, M. G., and Iatridis, J. C., "Frequency-Dependent Behavior of the Intervertebral Disc in Response to Each of Six Degree of Freedom Dynamic Loading; Solid Phase and Fluid Phase Contributions," *Spine*, Vol. 33(16), 2008, pp. 1731–1738.

[5] Vilendrer, K. S., *Mechanical Testing: Accelerated Protocol Development and Advanced System Design*, MD&DI, March 2000.

[6] White, A. A. and Panjabi, N. M., *Clinical Biomechanics of the Spine*, 2nd ed., J. B. Lippincott Company, Philadelphia, PA, 1990, p. 693.

[7] Nachemson, A. L., "Disc Pressure Measurements," *Spine*, Vol. 6(1), 1981, pp 93–97.

[8] Cheung, J. T. M., Zhang, M., and Chow, D. H. K, "Biomechanical Responses of the Intervertebral Joints to Static and Vibrational Loading: A Finite Element Study," *Clin. Biomech.*, Vol. 18, 2003, pp. 790–799.

[9] Li, S., Patwardhan, A. G., Amirouche, F. M. L., Havey, R., and Meade, K.P., "Limitations of the Standard Linear Solid Model of Intervertebral Discs Subject to Prolonged Loading and Low-Frequency Vibration in Axial Compression," *J. Biomech.*, Vol. 28(7), 1995, pp 779–790.

[10] MacDougall, H. G. and Moore, S. T., "Marching to the Beat of the Same Drummer: The Spontaneous Tempo of Human Locomotion," *J. Appl. Physiol.*, Vol. 99, 2005, pp. 1164–1173.

Reprinted from JAI, Vol. 8, No. 5
doi:10.1520/JAI103556
Available online at www.astm.org/JAI

S. A. Rundell,[1,2] *J. S. Day,*[1,2] *J. Isaza,*[3] *R. Siskey,*[1,2]
D. MacDonald,[2] *and S. M. Kurtz*[1,2]

Derivation of Clinically Relevant Boundary Conditions Suitable for Evaluation of Chronic Impingement of Lumbar Total Disk Replacement: Application to Standard Development

ABSTRACT: Currently available standardized methods for evaluating the long-term wear of total disk replacements do not incorporate the effects of potential device impingement. Creation of a standard that incorporates device impingement is difficult without a thorough understanding of the associated biomechanical environment. Arbitrary modification of the currently available wear-test protocols to account for device impingement may add unnecessary cost, and potentially inaccurate, unrealistic results. Finite element models provide the ability to control variation and test for a wide range of parameters without the excessive time and monetary costs associated with cadaveric testing or wear simulations. However, careful validation and verification of these models is required in order to ensure predictability. Retrieved implants can be used to validate the clinical predictability of finite element models (FEMs). The objective of the current study was to quantify the ability of a previously developed FEM of the lumbar spine to predict polyethylene damage modes and impingement in actual clinical scenarios, and extract the loading and boundary conditions for implementation into a new lumbar TDR wear simulation standard. In order to achieve this objective, actual clinical scenarios, associated with retrieved implants, were

Manuscript received November 8, 2010; accepted for publication April 6, 2011; published online May 2011.
[1] Exponent, Inc., Philadelphia, PA 19104.
[2] Drexel University, Philadelphia, PA 19104.
[3] Louisiana State University, Baton Rouge, LA 70803.

Cite as: Rundell, S. A., Day, J. S., Isaza, J., Siskey, R., MacDonald, D. and Kurtz, S. M., "Derivation of Clinically Relevant Boundary Conditions Suitable for Evaluation of Chronic Impingement of Lumbar Total Disk Replacement: Application to Standard Development," *J. ASTM Intl.*, Vol. 8, No. 5. doi:10.1520/JAI103556.

modeledand simulated. We hypothesized that clinical damage modes, including both impingement and non-impingement scenarios, can be predicted using a FEM that incorporates case-specific clinical factors, anterior-posterior shear forces, coupled translations, and facet contact.

KEYWORDS: spine, lumbar, disc replacement wear test

Introduction

Recently, total disk replacement systems (TDRs) have been introduced as an alternative to spinal fusion in the treatment of degenerative disk disease. Currently, there are two lumbar TDRs approved for implantation in the United States, and several more undergoing pre-clinical testing. The approved implants include a mobile (Charite, Depuy Spine) or fixed (Prodisc, Synthes Spine) polyethylene (PE) bearing surface between two cobalt chrome alloy endplates. These devices are intended to restore the disk height, maintain or correct segmental lordosis, and preserve segmental range of motion [1]. Biomechanical studies have documented a reduction in adjacent level effects after TDR when compared with fusion [2,3]. Despite generally positive clinical results, complications have been reported. Specifically, impingement of the devices has been observed clinically [4–6], and excessive wear of the PE and associated osteolysis has been reported in a small number of cases [4,7–10]. These data indicate the importance of understanding the long-term clinical wear performance of lumbar TDRs, especially since they are often indicated for young, active patients [11].

Determining the clinical wear performance of lumbar TDRs utilizing preclinical protocols can be extremely difficult due to the spine's complex loading environment, large variations in patient morphology and tissue properties, and variation in surgical placement. Currently, two different testing protocols exist for spinal wear simulation (ISO/FDIS 18192-1 and ASTM F2423-05), which consist of different loading and boundary conditions. While these protocols may provide reasonable approximation of wear for the majority of implanted devices, they do not account for potential impingement of the device. Serhan et al. (2006) utilized the ASTM standard to evaluate long-term wear characteristics of the Charite III mobile bearing TDR. The authors concluded that, under these loading conditions, wear debris was minimal, and made no reference to implant impingement. A similar computational study [12] evaluated wear of the Charite using the ISO standard. This study indicated preferential articulation at the superior surface of the mobile core, but did not indicate rim loading or device impingement. These studies indicate that current test protocols do not necessarily evaluate worst-case scenarios, such as device impingement, which has been documented clinically for both mobile and fixed core TDRs [6,9].

While several studies have been performed in order to evaluate the biomechanical effects of lumbar disk replacement technologies using a range of different loading modes [2,3,13–20], none have specifically attempted to model device impingement. Device impingement in total hip arthroplasty (THA) has been extensively studied [21,22]. Impingement in THA has been associated with poor clinical outcomes, and can lead to instability, accelerated wear, and unexplained pain. As a result, hip simulator loading and boundary conditions have

been developed in order to account for impingement [23]. Currently, there is no such similar standard available for TDRs. In order to generate such a standard, a better understanding of the biomechanical environment associated with TDR impingement is required.

Both TDR wear simulation standards incorporate applied rotational displacements in concert with axial compression. This set of loading conditions is based on various assumptions that prevent the ability to evaluate device impingement. First, the magnitudes of these rotations are based on physiologic levels of rotation documented in unimplanted, intact spines. Several biomechanical studies have indicated that implantation of a TDR alters the spine's kinematics [13,14,24,25]. Second, these inputs neglect the contribution of intervertebral shearing forces, which have been indicated in activities of daily living, bending, and lifting [26–29], and have been shown to affect wear patterns in TDR [30]. Third, the standards do not indicate applied translational displacements, which are coupled with rotational motions [31]. Finally, the standards do not include a contribution of the facets, which has been shown to effect intervertebral kinematics [32], and are affected by TDR [24].

It is unclear what the effect of altering applied rotations, including shear forces, dictating fixed translations, and adding facet constraint would have on device wear if implemented into the current standards. However, altering the loading and boundary conditions of the currently available wear-test protocols to account for worst-case scenarios, such as impingement, may be necessary to fully understand potential clinical consequences and assess design robustness. Arbitrary modification of the currently available wear-test protocols may add unnecessary cost, and potentially inaccurate, unrealistic results. Finite element models provide the ability to control variation and test for a wide range of parameters without the excessive time and monetary costs associated with cadaveric testing or wear simulations [24,33]. However, careful validation of these models is required to ensure that the results can be interpreted as predictive and indicative of what is happening clinically. Specifically, the outcome measures provided by these analyses must be associated with known physical outcomes to ensure and quantify the level of predictability.

Component retrieval studies can provide a valuable source of validation data for finite element studies. To date, these studies have identified changes in TDR shape due to mechanical deformation (creep), evidence of adhesive-abrasive wear, chronic inflammation in the peri-prosthetic tissue, and even reported cases of osteolysis [4,8,9,34–38]. These studies, however, cannot quantitatively determine the mechanical environment or in situ component level stresses and strain. Combining computational analyses with retrieval data provides a means for validating preclinical test procedures, and can be used to optimize future device and experimental protocol designs [39].

The objective of the current study was to quantify the ability of a previously developed finite element model (FEM) of the lumbar spine to predict PE damage modes and impingement in actual clinical scenarios, and extract the loading and boundary conditions for implementation into a new lumbar TDR wear simulation standard. In order to achieve this objective, actual clinical scenarios, associated with retrieved implants, were modeled and simulated. We

hypothesized that clinical damage modes, including both impingement and non-impingement scenarios, can be predicted using a FEM that incorporates case-specific clinical factors, anterior-posterior shear forces, coupled translations, and facet contact. Contact pressure acting on the PE cores was output from the FEM and compared with wear maps of the retrievals. Resultant forces experienced by the device and facets as well as the resulting sagittal rotation were determined. Additionally, 1st principal and von Mises strain in the core and forces acting on the core were compared to rim penetration, rim penetration rate, and maximum oxidation index.

Methods

The following sections outline the methods utilized to simulate clinical scenarios using a previously developed FEM of a lumbar spine [24,33]. The clinical scenarios were taken from retrieved implants from Drexel University's Implant Retrieval Center. Exclusion criteria (explained below) were applied to the entire collection of retrieved TDRs, which resulted in a total of 10 scenarios appropriate for simulation. Geometric parameters were derived from the available pre-revision radiology and measurements taken directly from the implants. These parameters were used to alter the existing FEM such that it approximated the implanted, pre-revision state. Loading and boundary conditions, consistent with standing were applied in order to achieve a resultant lordotic angle consistent with the available radiology on a case-by-case basis. Various outcomes from the FEM were compared with data for each of the retrieved implants.

Finite Element Model

A three-dimensional FEM of a ligamentous L3-S1 lumbar spine was generated from quantitative computed tomography (QCT) data of a cadaveric spine. The data set was taken from the publicly available Visible Human data set (Visible Human Project®, National Library of Medicine, National Institute of Health). The spinal geometry was reviewed and found to be free of any bony or disk deformities, i.e., osteophytes or herniations. Hounsfield units were used as a surrogate for bone mineral density (BMD).

The methodology used to develop and validated the model has been previously described [24,33], but will be outlined below. A combination of automatic and manual image segmentation techniques (Analyze, AnalyzeDirect, Inc., Overland Park, KS) were used to extract detailed surfaces corresponding to the major bony structures of L3-S1. The software package allowed for automatic segmentation based on thresholding of the QCT grayscale values. These surfaces were imported into the commercial finite element mesh generation program, HyperMesh (Altair Inc., Troy, MI), and were discretized into a combination of tetrahedral elements for the bony structures and hexahedral elements for the intervertebral disks (IVDs). The central portion of the IVDs, approximately 40 % of the volume [40], were designated to be the nucleus pulposus (NP), while the remaining volume was considered the annulus fibrosus. Major spinal ligaments (anterior longitudinal ligament, posterior longitudinal,

intraspinatus, supraspinatus, intratransverse, facet capsule, ligamentum flavum) were implemented in the model using tension-only nonlinear springs. Shell elements were used to plate the exterior surface of the vertebral bodies and represented the cortex and bony endplate.

BMD-dependent orthotropic material properties were assigned to the cancellous bone of the vertebral bodies. Custom software was written to apply the Young's modulus at each of the nodal points based on the density of the bone. Similar methodology has been used to create models with heterogeneous bone properties of the tibia and femur [41,42]. The quantitative relationship between BMD and elastic modulus in cancellous vertebral bone, as reported by Morgan et al. and Ulrich et al., was utilized to define a nonlinear relationship between BMD and orthotropic elastic modulus [43,44]. Elastic moduli within the vertebral body fell within what has been previously reported in the literature [45–47]. The remaining structures were assigned material properties from the literature and are described in Table 1. Frictionless contact was defined between the facets using a penalty-based contact algorithm.

Retrieval Selection

Retrieved TDRs from the Drexel University Implant Retrieval Center were utilized for the current study. The current retrieval collection consists of a total of 55 mobile bearing implants. In order to determine which retrievals were candidates for modeling and simulating, a variety of exclusion criteria were applied. Primarily, the selected subset of implants would have pre-revision radiology in order to create an implanted FEM that is geometrically consistent. This limited the available pool of implants to a total of 22. Additionally, there were some implant complications that were determined to be confounding variables when attempting to evaluate impingement. Specifically, implants that were revised due to subsidence, anterior migration, and osteolysis/endplate loosing were not considered candidates for this analysis. This left a total of 10 available implants for modeling.

In order to determine how representative the subset of 10 implants was to the entire collection, patient (Table 2) and implant (Table 3) data were compared. The subset of implants was generally a fair representation of the entire collection. All of the implants in the subset were from L3-L4 ($n = 1$), L4-L5 ($n = 4$) or L5-S1 ($n = 5$). The average implantation time for the entire collection was 7.6 years, and 7.5 years for the subset. Seven of the 10 implants from the subset exhibited signs of chronic impingement compared to 43 of 55 for the entire collection. The average rim penetration was approximately three times higher for the entire collection compared to the subset indicating that the subset did not incorporate the more severe cases of rim penetration. However, the subset did encompass implants with essentially zero rim penetration as well as those exhibiting rim penetration, allowing for simulation of both scenarios.

Geometric Case-Specific Model Development

Single level models of L4-L5 and L5-S1 were constructed from the L3-S1 model. Mobile core disk replacements were virtually implanted in each model.

TABLE 1—*Summary of element type and material properties used in the FEM.*

Component	Element Type	Thickness (mm)	Young's Modulus	Poisson's Ratio	Reference
Cortical bone	Shell	0.4 mm	12000	0.3	Ref 48
Vertebral endplate	Shell	0.25 mm	1000	0.2	Ref 49
Cancellous bone	Tet	N/A	$4730\rho^{1.56}$/ $1987\rho^{1.56}$/ $1357\rho^{1.56}$	0.2	Refs 43 and 44
Posterior elements	Tet	N/A	3500	0.25	Ref 50
Annulus fibrosus ground substance	Hex	N/A	1.36	0.45	Ref 51
Annulus fibrosus collagen fibers	Fabric	N/A	Stress-strain curve	···	Ref 52
Nucleus pulposus	Hex	N/A	$K = 1666.7$	Incompressible	Ref 48
Ligaments	Spring	N/A	Hyperelastic	···	Refs 53 and 54
Cartilage endplate	8-Noded Hex	N/A	24	0.4	Ref 19

TABLE 2—*Patient data comparison of the subset of implants chosen for modeling with respect to the total retrieval collection.*

	Total Collection		Modeling Subset	
Total number of implants	55		10	
Level				
L2/L3	1		0	
L3/L4	2		1	
L4/L5	26		4	
L5/S1	25		5	
Unknown	1		0	
Surgeon totals				
Dr. VO	35		9	
Dr. R	8		0	
Dr. I	6		1	
Dr. vWdM	1		0	
Dr. P	1		0	
Dr. K	1		0	
Total number of patients	48		10	
Gender				
Female	32	66.67 %	9	90 %
Male	12	25.00 %	1	10 %
Unknown	4	8.33 %	0	
Implant fixation method				
Non Coated	38		4	
Coated	14		3	
Unknown	3		3	
Implantation time (year)				
Average	7.6		7.5	
Min	1.7		2.2	
Max	16.3		13.6	

A combination of pre-revision radiology measurements, retrieval implant size data, and visual approximation were used to generate geometric case-specific models. Specifically, disk height, intervertebral lordotic angle, implant position, implant size, implant orientation, and sagittal orientation relative to vertical were modeled for each scenario.

The retrieved implant size data was used to determine the appropriate geometric attributes of the FEM. Specifically, dome height, footplate size, and footplate angles measured from the retrievals were used. Corresponding CAD geometry was discretized into FEMs for virtual implantation into either L4-L5 or L5-S1. The footplate angles, however, did not always fully account for the preimplantation lordosis (Fig. 1). In order to compensate for this the FEMs of the implants were biased towards extension. The amount of bias was determined by subtracting the preimplantation lordotic angle from the implant

TABLE 3—*Implant data comparison of the subset of implants chosen for modeling with respect to the total retrieval collection.*

	Total Collection	Modeling Subset
Dome wear (mm)		
Average	0.31	0.31
Min	0.06	0.16
Median	0.25	0.28
Max	0.92	0.61
Wear rate (mm/year)		
Average	0.06	0.05
Min	0.02	0.02
Median	0.04	0.04
Max	0.25	0.18
Radial rim cracks		
Yes	28	7
No	26	3
Transverse cracks		
Yes	24	4
No	30	6
Not applicable	1	0
Fractured wire		
Yes	17	2
No	37	8
Unknown	1	0
Intact rim		
Yes	49	10
No	5	0
Not applicable	1	0
Chronic impingement		
Yes	43	7
No	12	3
Rim penetration (mm)		
Average	0.38	0.13
Min	0.00	0.02
Median	0.23	0.06
Max	2.77	0.18
Rim penetration rate (mm/year)		
Average	0.08	0.05
Min	0.00	0.00
Median	0.02	0.01
Max	1.10	0.36

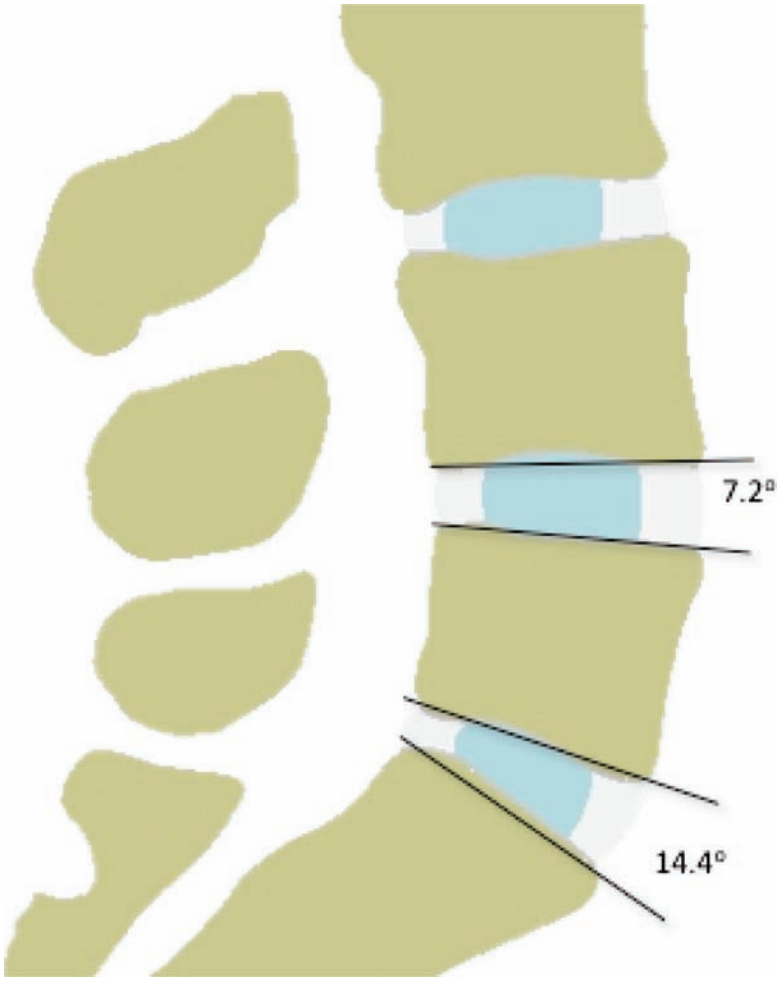

FIG. 1—*Sagittal cutplane of the FEM depicting the lordotic angles of L4-L5 and L5-S1.*

lordotic angle. For example, if two non-angled footplates were used for L4-L5, which had a preimplantation lordosis of 7.2°, then the implants were biased 7.2° towards extension such that they would fit in the disk space, and no alteration to the intact lordotic angle would be required.

Implant size data was used to determine the maximum total inferior-superior dimension of the implanted disk height. The total dome height plus two times the thickness of the metallic footplates at the center of the dome (2.3 mm) equaled the total average post-implantation disk height. Dome heights varied between 8.5 mm and 11.5 mm. Therefore, total post-implantation disk height ranged from 13.1 mm to 16.1 mm. The average preimplantation disk heights were 10.4 mm for L4-L5 and 10.1 mm for L5-S1. Total implantation disk height distraction ranged from 2.7 to 6 mm.

X rays for the subset of implants were imported into the publicly available open source software (OsiriX, v3.6, 32 bit). The angle of the superior endplate of the superior vertebral body at the index level relative to the horizon was measured for each radiograph. The implanted FEMs were then rotated about the medial-lateral axis in order to match these angles. This was done in order to ensure that the shear contribution from vertical upper bodyweight loading would be case-specific.

Loading and Boundary Conditions

The loading paradigm consisted of application of a vertical force simulating upper bodyweight, which was offset anteriorly 30 mm to be at the approximate location of the human upper body center of mass [55]. Additionally, a one dimensional force element was placed between the spinous processes in order to simulate the erector spinae force and restore sagittal balance.

Patient weights were not available for each of the implants within the subset. Therefore, upper bodyweight for a 50th percentile male was chosen. This provided the ability to verify that the loading paradigm resulted in disk pressures consistent with those reported in the literature [56]. Orientation of the spinal segment relative to the vertical upper bodyweight force was determined from the endplate angle radiographic measurements. The force was applied to the upper endplate of the superior-most vertebrae. The erector spinae force was increased from 0 to 300 N for the intact models to determine the point at which the resultant flexion-extension rotation was minimized, i.e., sagittaly balanced in the neutral zone. This loading was then applied to the implanted models. Previous work performed by this laboratory has demonstrated that this loading protocol can produce both impingement and non-impingement for both a mobile and fixed-core device, which suggests that this loading does not bias results towards either outcome. (Rundell et al. 2010, Trans of the Spinal Arthroplasty Society).

Computational application of erector spinae loading was performed iteratively. Specifically, the resulting lordosis from the deformed FEM was compared to the radiographic data to verify that the models were reasonably predicting the final geometric state. The erector spinae force was then increased or decreased in order to result in a more accurate lordosis. Several iterations were performed until the resulting lordotic angle from the FEM closely approximated the angle observed in the pre-revision X rays. In one of the cases spinous process contact prevented the implant from reaching the necessary lordosis. Initial bias of the implant was implemented in this case.

Contour plots of contact stress on the PE core were output for each analysis and compared with the retrieval wear maps. A thorough description of the methods utilized to develop detailed wear maps has been previously described [57]. In order to determine a correlation between the level of impingement exhibited by the retrievals and that predicted by the FEMs, the amount of rim penetration per year was plotted against peak contact stress at the interfaces of the superior and inferior footplate and core versus peak 1st principal strain.

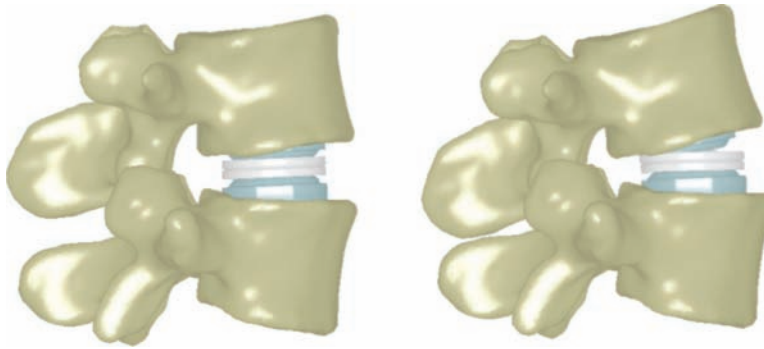

FIG. 2—*Images of the FEM depicting the undeformed state (left) compared to the final, deformed state (right).*

Strain was selected over stress since the PE was modeled using an elastic-plastic model, which results in very small increases in stress after reaching yield. Rim penetration, which reflects the combined effects of creep and wear, was determined by calculating the difference in the measured rim thickness in worn and unworn regions, as previously described [58]. Pearson correlation tests were performed and statistical significance was considered for $p < 0.05$.

Results

All of the models, with the exception of one, resulted in extension rotation as a result of the applied loading (Fig. 2). The average extension rotation was 4.8 degrees with a standard deviation of 3.7°. The average erector spinae force required to reach a lordotic angle consistent with the retrieved radiographs was 284.5 N with a standard deviation of 26.6 N. The intact models experienced extension rotation of 1.5° and 0.4° at 300 N of erector spinae force for L4-L5 and L5-S1, respectively. The resultant anterior-posterior shear force between the superior footplate and PE core was negative for all cases (Table 4). This indicates that the superior vertebra was applying a posterior force relative to the

TABLE 4—*Values of reaction forces generated in the FEMs (negative values for A-P shear indicate posterior force at the superior component; positive values for facet A-P force indicate an anterior directed force applied by the superior vertebra).*

	Average	Standard Deviation
Facet A-P force (*N*)	53.0	31.8
Facet inf-sup (*N*)	56.8	33.5
Facet resultant (*N*)	84.9	44.0
Disk A-P (*N*)	−129.6	69.5
Disk inf-sup (*N*)	467.6	31.4
Disk resultant (*N*)	490.3	28.1

inferior vertebra (posterior shear). All of the FEMs resulted in facet contact forces, which had anterior-posterior and superior-inferior components. The anterior-posterior translation of the superior vertebrae was significantly correlated with rotation in the sagittal plane (Fig. 3(*a*)). Extension rotation was coupled with posterior translation. The resultant facet forces were significantly correlated with anterior-posterior translation of the superior vertebrae (Fig. 3(*b*)).

The average percent difference in the lordotic angle measured from the retrieval X rays compared to the final state of the corresponding FEM was 18.0 % with a standard deviation of 19.4 %. In one case, the FEM substantially underestimated the lordotic angle measured in the retrieval X ray (71.0 %). Detailed review of this scenario indicated two-sided rim impingement for both the retrieval and FEM. The two-sided rim impingement present in the FEM prevented it from being able to fully reach a lordotic angle consistent with the retrieval despite increases in erector spinae force. The greater lordotic angle measured in the retrieval x-ray likely resulted from either subsidence or anterior lift-off of the imlant, which the model was unable to predict. Removal of this case results in an average percent difference between the x-ray measurement and FEM of 12.1 % with a standard deviation of 5.8 %. Lordotic angles ranged from 9.8° to 23.1° for the retrieved implants, and 10.6° to 23.3° degrees for the FEMs.

Qualitatively, contour plots of contact stress appeared similar to the wear maps (Fig. 4). Specifically, areas of contact stress maxima indicated areas of increased inward deformation or wear of the retrieved implants. These areas tended to occur offset from the center of the dome, and in the cases of impingement, somewhere near the rim. Impingement occurred either as one (6/10) or both (2/10) of the metallic footplates contacting the core's rim. Wear maps of the implants indicated wear patterns consistent with both one-sided and two-sided impingement. The model was able to simulate both scenarios.

One-sided rim impingement resulted in bending of the implant core's rim. This was observed by inward deformation on one surface of the rim with outward deformation on the corresponding opposite side (see Br-002 in Fig. 4). This bending was grossly visible in micro computed tomography three-dimensional reconstructions of the retrieved cores. This indicates that the bending experienced *in vivo* was of a great enough magnitude to result in plastic deformation of the core's rim. Evaluation of the EM indicated similar bending in the form of tensile stress generated on the side of the rim being contacted by the metallic footplate (Fig. 5).

Significant correlations were observed between rim penetration rate and loading of the core from the FEM (Table 5). Specifically, the rim penetration rate (mm/year) significantly correlated with peak contact stress at the superior core-footplate interface and peak 1st principal strain. The rim penetration rate did not significantly correlate with inferior peak contact stress at the core-footplate interface.

Discussion

In the current study, we used nonlinear 3-D FEMs of lumbar spinal segments (L4-L5 and L5-S1) to simulate clinical TDR scenarios based on explanted

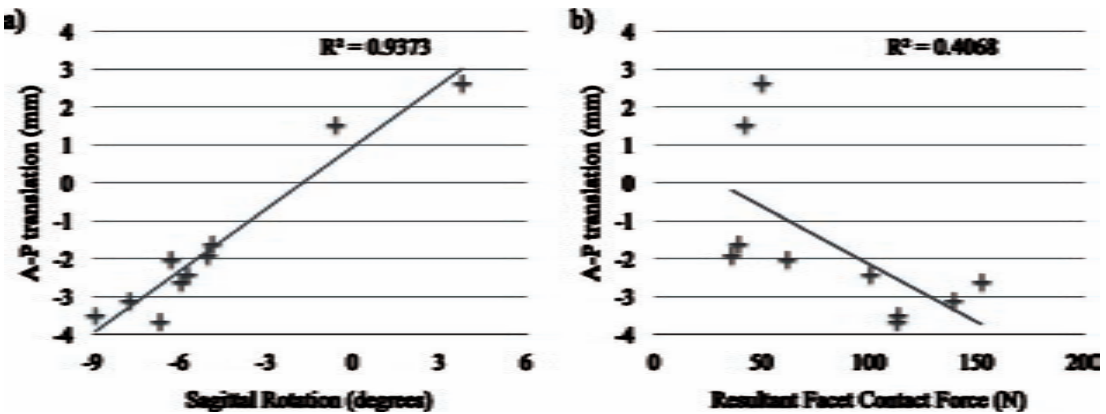

FIG. 3—*Graphs depicting the relationships between anterior-posterior translation and sagittal rotation (negative values correspond to extension) (a) as well as resultant translation and resultant facet contact force (b).*

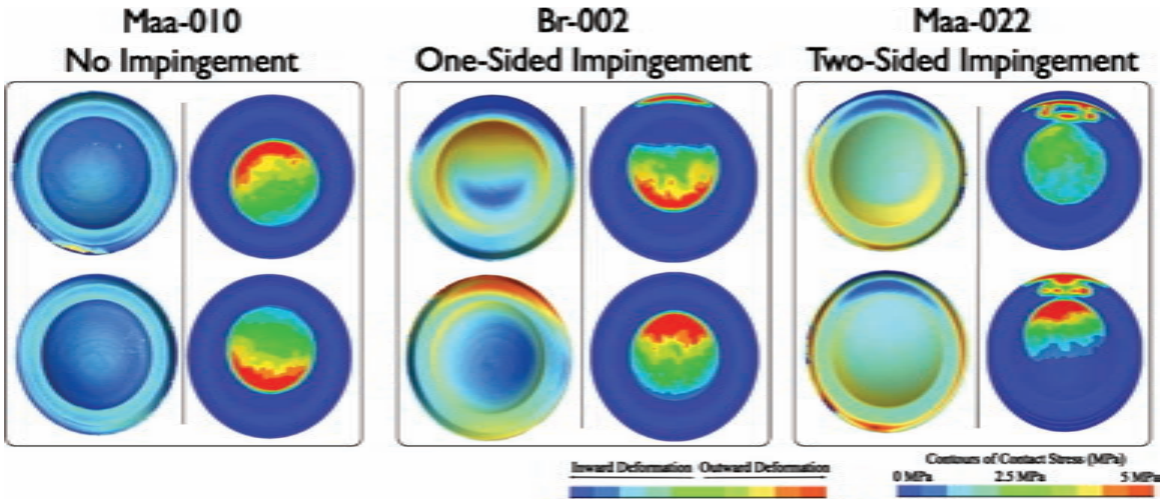

FIG. 4—*Three exemplar side-by-side comparisons of retrieval wear maps (left) with FEM contact stress contour plots (right). The FEM was able to simulate no impingement, one-sided impingement, and two-sided impingement.*

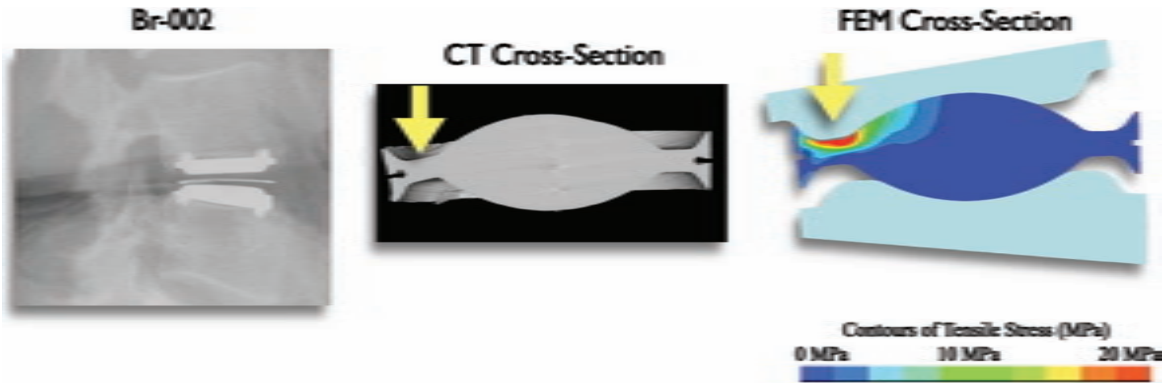

FIG. 5—*Images depicting a sagittal X ray (left), sagittal cross-section of a retrieved implant from a 3D Ct reconstruction, and sagittal cross-section of the FEM with contours of 1st principal stress in the core depicted.*

TABLE 5—*Summary of Pearson correlation test results.*

Correlations	R^2	r	p (One-Sided)	p (Two-Sided)
Peak superior contact stress (MPa) versus rim penetration (mm/year)	0.53	0.72	0.008	0.017
Peak inferior contact stress (MPa) versus rim penetration (mm/year)	0.16	0.40	0.125	0.24
Peak 1st principal strain (mm/mm) versus rim penetration (mm/year)	0.43	0.66	0.019	0.038

retrieval data. The results indicate that the FEM was able to predict both impingement and non-impingement scenarios. Contact stresses on the PE cores were consistent with the wear patterns depicted for the retrieved implants. Peak superior contact stress and peak 1st principal strain in the core from the FEM were significantly correlated with damage of the retrieved implants. These results indicate that the FEM is capable of simulating post-implantation in situ TDR, and predicting PE performance. The model also provided valuable insight into the biomechanical environment associated with both impingement and non-impingement scenarios. The loading and boundary conditions generated in the current study are being utilized to generate a new standard for lumbar TDR wear simulation.

In nine out of the ten simulated cases, loading application resulted in an increase in lordotic angle when compared with the preimplantation state. These results are consistent with previously reported findings of TDR, which have indicated increased potential for extension rotation post-implantation [14,24,59]. A previous in vivo study indicated a significant increase in lumbar lordosis following TDR [60]. The authors of this study suggested a combination of anterior longitudinal ligament transection, an anterior center of rotation, and an increase in disk height with concomitant distraction of the facets as being responsible for the increased lordosis post-TDR. Specifically, they indicated that these factors contributed to an altered biomechanical environment such that static equilibrium of forces and moments occurred at a greater lordotic angle post-TDR. Data from the current study provides a basis for this theoretical suggestion, and indicates that TDR has the ability to alter sagittal balance such that application of standing loads results in initial extension rotation. Data from the current study demonstrates that this initial bias towards extension contributes to posterior device impingement. Inclusion of a simple extension bias in current wear testing standards may provide a cost-effective, initial step towards evaluating device impingement in vitro.

Results from the current study indicated that extension rotation was coupled with posterior translation of the superior vertebra. The posterior translation increased with increasing facet contact force. Loading conditions used in the current study incorporated a vertical load consistent with upper bodyweight. Due to the spine's relative orientation to vertical this resulted in a baseline intervertebral anterior shear force, which acted to engage the facets. Subsequently, extension rotation generated by activation of the erector spinae

caused the facets to articulate and guide the superior vertebra posteriorly. This posterior translation, imparted by facet contact during extension rotation, resulted in intervertebral posterior shear experienced by the TDR. This posterior shear essentially locked the core in place, which allowed for one-sided impingement to cause bending of the rim (Fig. 6). Evidence from the retrieval collection verified the presence of posterior shear in vivo post TDR via downward bending of the posterior rim. A similar phenomenon was observed in several of the other simulations and corresponding retrievals. Moreover, the FEM predicted asymmetric loading of the mobile core's inferior and superior faces that was consistent with the retrieval wear maps. Currently, the available wear test standards do not prescribe a relationship between rotational and translational displacements. Results from the current study suggest that inclusion of the geometrical constraint provided by the facets in addition with a baseline anterior shear consistent with vertical upper body loading can provide the necessary rotation-translation relationship to predict PE deformation patterns in vivo.

Generally, during laboratory testing, the lumbar muscle forces and upper body compressive forces are simulated via a follower load applied at the joint centers, which neglects intervertebral shear. A recent study introduced anterior-posterior shear into the current ISO standard, and observed differences in surface wear patterns for a Prodisc-L, but no significant difference in the overall wear volume [30]. This study applied shearing forces based on previously reported values from the literature, but did not incorporate the geometrical boundary conditions imposed by the facets. As demonstrated in the current study, anterior shear force will engage the facet joints and guide motion during sagittal plane rotation. This will result in a semi-constrained motion pattern, which is necessary to simulate in order to accurately and thoroughly evaluate wear.

A significant correlation was observed between the rim penetration rate and peak superior contact stress. Contact stress is often utilized when evaluating wear performance of PE using computational analyses [61,62]. There was no significant correlation, however, between inferior peak contact stress and rim penetration rate. Closer review of the data indicated that intervertebral shear loading acted to lock the core in place. The superior footplate articulated relative to the locked core, and in many cases contacted the rim. The majority of the simulations that resulted in one-sided impingement (6/10) consisted of contact at the superior footplate-core interface (4/10). These results are consistent with a previous computational and laboratory analyses that have indicated preferential superior relative motion for the Charite device along with evidence of one-sided wear in retrieved implants [12,58].

In conclusion, this is the first study to describe and verify a methodology for evaluating TDR using a FEM with inputs derived from clinical retrieval data. The significant correlations determined in the current study provide the ability to perform future studies that target specific parameters that may influence device wear and impingement. Moreover, the current study provides valuable insight into the biomechanical environment associated with device impingement such that it can be employed in wear simulation. Currently, a work item (WK25942) is focused on taking the results of these analyses and creating a testing guide to simulate impingement in lumbar TDRs. This new standard will

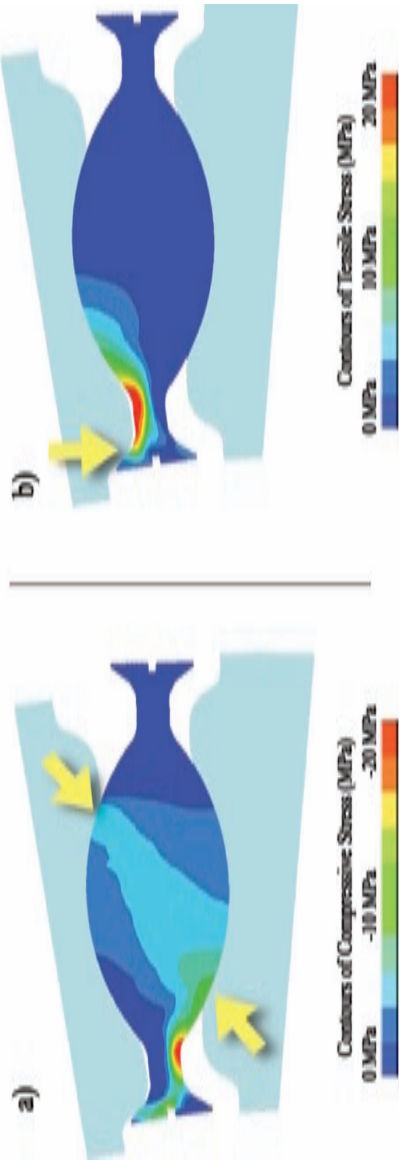

FIG. 6—*Images depicting the core becoming locked (left) resulting in downward bending of the posterior rim as a result of contact between the superior footplate and superior surface of the core (right).*

incorporate the effects of anterior shear from upper bodyweight and translational motions imposed by the geometrical constraint of the facets. The guidelines provided in this new standard will describe an approach for evaluating new designs and design changes to help manufacturers and regulatory agencies make more informed decisions on design choices.

Acknowledgments

This study was funded in part by NIH R01 AR47904, R01 AR056264, and the Food and Drug Administration's Critical Path Initiative. We would also like to thank Jonathan Peck and Genevieve Hill from the FDA for their assistance and support.

References

[1] Mayer, H. M. and Korge, A., "Non-Fusion Technology in Degenerative Lumbar Spinal Disorders: Facts, Questions, Challenges," *Eur. Spine J.*, Vol. 11, Suppl. 2, 2002, pp. S85–S91.

[2] Panjabi, M., Henderson, G., Abjornson, C., and Yue, J., "Multidirectional Testing of One- and Two-Level ProDisc-L Versus Simulated Fusions," *Spine*, Vol. 32, 2007, pp. 1311–1319.

[3] Auerbach, J. D., Wills, B. P., McIntosh, T. C., and Balderston, R. A., "Evaluation of Spinal Kinematics Following Lumbar Total Disc Replacement and Circumferential Fusion Using in Vivo Fluoroscopy," *Spine*, Vol. 32, 2007, pp. 527–536.

[4] Kurtz, S. M., van Ooij, A.,Ross, R., de Waal Malefijt, J., Peloza, J., Ciccarelli, L., and Villarraga, M. L., "Polyethylene Wear and Rim Fracture in Total Disc Arthroplasty," *Spine J.*, Vol. 7, 2007, pp. 12–21.

[5] Choma, T. J., Miranda, J., Siskey, R., Baxter, R., Steinbeck, M. J., and Kurtz, S. M., "Retrieval Analysis of a ProDisc-L Total Disc Replacement," *J. Spinal Disord. Tech.* Vol. 22, 2009, pp. 290–296.

[6] Käfer, W., Clessienne, C. B., Däxle, M., Kocak, T., Reichel, H., Cakir, B., Posterior Component Impingement After Lumbar Total Disc Replacement: A Radiographic Analysis of 66 ProDisc-L Prostheses in 56 Patients," *Spine*, Vol. 33, 2008, pp. 2444–2449.

[7] Kurtz, S. M., Peloza, J., Siskey, R., and Villarraga, M. L., "Analysis of a Retrieved Polyethylene Total Disc Replacement Component," *Spine J.*, Vol. 5, 2005, pp. 344–350.

[8] Punt, I. M., Visser, V. M., van Rhijn, L. W., Kurtz, S. M., Antonis, J., Schurink, G.W. H., and van Ooij, A., "Complications and Reoperations of the SB Charite Lumbar Disc Prosthesis: Experience in 75 Patients," *Eur. Spine J.* Vol. 17, 2008, pp. 36–43.

[9] van Ooij, A., Kurtz, S. M., Stessels, F., Noten, H., and van Rhijn, L., "Polyethylene Wear Debris and Long-Term Clinical Failure of the Charite Disc Prosthesis: A Study of 4 Patients," *Spine*, Vol. 32, 2007, pp. 223–229.

[10] van Ooij, A., Oner, F. C., and Verbout, A. J., "Complications of Artificial Disc Replacement: A Report of 27 Patients with the SB Charite Disc," *J. Spinal Disord. Tech.*, Vol. 16, 2003, pp. 369–383.

[11] Siepe, C. J., Wiechert, K., Khattab, M. F., Korge, A., and Mayer, H. M., "Total Lumbar Disc Replacement in Athletes: Clinical Results, Return to Sport and Athletic Performance," *Eur. Spine J.*, Vol. 16, 2007, pp. 1001–1013.

[12] Goreham-Voss, C. M., Vicars, R., Hall, R. M., and Brown, T. D., "Preferential Superior Surface Motion in Wear Simulations of the Charite Total Disc Replacement," *Eur. Spine J.*, June, 2010.

[13] Cunningham, B. W., Gordon, J. D., Dmitriev, A. E., Hu, N., and McAfee, P. C., "Biomechanical Evaluation of Total Disc Replacement Arthroplasty: An in vitro Human Cadaveric Model," *Spine*, Vol. 28, 2003, pp. S110–S117.

[14] Denoziere, G. and Ku, D. N., "Biomechanical Comparison Between Fusion of Two Vertebrae and Implantation of an Artificial Intervertebral Disc," *J. Biomech.*, Vol. 39, 2006, pp. 766–775.

[15] Huang, R. C., Girardi, F. P., Cammisa, F. P., Jr., and Wright, T. M., "The Implications of Constraint in Lumbar Total Disc Replacement," *J. Spinal Disord. Tech.*, Vol. 16, 2003, pp. 412–417.

[16] Kim, D. H., Ryu, K. S., Kim, M. K., and Park, C. K., "Factors Influencing Segmental Range of Motion After Lumbar Total Disc Replacement Using the ProDisc II Prosthesis," *J. Neurosurg. Spine*, Vol. 7, 2007, pp. 131–138.

[17] Le Huec, J. C., Basso, Y., Aunoble, S., Friesem, T., and Bruno, M. B., "Influence of Facet and Posterior Muscle Degeneration on Clinical Results of Lumbar Total Disc Replacement: Two-Year Follow-Up," *J. Spinal Disord. Tech.*, Vol. 18, 2005, pp. 219–223.

[18] Moumene, M. and Geisler, F. H., "Comparison of Biomechanical Function at Ideal and Varied Surgical Placement for Two Lumbar Artificial Disc Implant Designs: Mobile-Core Versus Fixed-Core," *Spine*, Vol. 32, 2007, pp. 1840–1851.

[19] Noailly, J., Lacroix, D., and Planell, J. A., "Finite Element Study of a Novel Intervertebral Disc Substitute," *Spine*, Vol. 30, 2005, pp. 2257–2264.

[20] Rousseau, M. A., Bradford, D. S., Bertagnoli, R., Hu, S. S., and Lotz, J. C., "Disc Arthroplasty Design Influences Intervertebral Kinematics and Facet Forces," *Spine J.*, Vol. 6, 2006, pp. 258–266.

[21] Brown, T. D. and Callaghan, J. J., "Impingement in Total Hip Replacement: Mechanisms and Consequences," *Curr. Orthop.*, Vol. 22, 2008, pp. 376–391.

[22] Malik, A., Maheshwari, A., and Dorr, L. D., "Impingement With Total Hip Replacement," *J. Bone Jt. Surg., Am. Vol.*, Vol. 89, 2007, pp. 1832–1842.

[23] Holley, K. G., Furman, B. D., Babalola, O. M., Lipman, J. D., Padgett, D. E., and Wright, T. M., "Impingement of Acetabular Cups in a Hip Simulator: Comparison of Highly Cross-Linked and Conventional Polyethylene," *J. Arthroplasty*, Vol. 20, 2005, pp. 77–86.

[24] Rundell, S. A., Auerbach, J. D., Balderston, R. A., and Kurtz, S. M., "Total Disc Replacement Positioning Affects Facet Contact Forces and Vertebral Body Strains," *J Spine*, Vol. 33, 2008, pp. 2510–2517.

[25] O'Leary, P., Nicolakis, M., Lorenz, M. A., Voronov, L. I., Zindrick, M. R., Ghanayem, A., Havey, R. M., Carandang, G., Sartori, M., Gaitanis, I. N., Fronczak, S., and Patwardhan, A. G., "Response of Charite Total Disc Replacement Under Physiologic Loads: Prosthesis Component Motion Patterns," *Spine J.*, Vol. 5, 2005, pp. 590–599.

[26] Schultz, A. B., Andersson, G. B., Haderspeck, K., Ortengren, R., Nordin, M., and Björk, R., "Analysis and Measurement of Lumbar Trunk Loads in Tasks Involving Bends and Twists," *J. Biomech.*, Vol. 15, 1982, pp. 669–675.

[27] Potvin, J. R., Norman, R. W., and Mcgill, S. M., "Reduction in Anterior Shear Forces on the L_4/L_5 Disc by the Lumbar Musculature," *Clin. Biomech. (Bristol, Avon)*, Vol. 6, 1991, pp. 88–96.

[28] Callaghan, J. P., Patla, A. E., and McGill, S. M., "Low Back Three-Dimensional Joint Forces, Kinematics, and Kinetics During Walking," *Clin. Biomech. (Bristol, Avon)*, Vol. 14, 1999, pp. 203–216.

[29] Kingma, I., Staudenmann, D., and van Dieen, J. H., "Trunk Muscle Activation and Associated Lumbar Spine Joint Shear Forces Under Different Levels of External Forward Force Applied to the Trunk," *J. Electromyogr Kinesiol*, Vol. 17, 2007, pp. 14–24.

[30] Vicars, R., Hyde, P. J., Brown, T. D., Tipper, J. L., Ingham, E., Fisher, J., and Hall, R. M., "The Effect of Anterior-Posterior Shear Load on the Wear of ProDisc-L TDR," *Eur. Spine J.*, 2010, pp. 1356–1362.

[31] Li, G., Wang, S., Passias, P., Xia, Q., and Wood, K., "Segmental In Vivo Vertebral Motion During Functional Human Lumbar Spine Activities," *Eur. Spine J.*, Vol. 18, 2009, pp. 1013–1021.

[32] Schmidt, H., Heuer, F., Claes, L., and Wilke, H. J., "The Relation Between the Instantaneous Center of Rotation and Facet Joint Forces—A Finite Element Analysis," *Clin. Biomech. (Bristol, Avon)*, Vol. 23, 2008, pp. 270–278.

[33] Rundell, S. A., Guerin, H. L., Auerbach, J. D., and Kurtz, S. M., "Effect of Nucleus Replacement Device Properties on Lumbar Spine Mechanics," *Spine (Phila Pa 1976)*, Vol. 34, 2009, pp. 2022–2032.

[34] McAfee, P. C., Geisler, F. H., Saiedy, S. S., Moore, S. V., Regan, J. J., Guyer, R. D., Blumenthal, S. L., Fedder, I. L., Tortolani, P. J., and Cunningham, B., "Revisability of the Charite Artificial Disc Replacement: Analysis of 688 Patients Enrolled in the U.S. IDE Study of the Charite Artificial Disc," *Spine (Phila Pa 1976)*, Vol. 31, 2006, pp. 1217–1226.

[35] Pitzen, T., Kettler, A., Drumm, J., Nabhan, A., Steudel, W. I., Claes, L., and Wilke, H. J., "Cervical Spine Disc Prosthesis: Radiographic, Biomechanical and Morphological Post Mortal Findings 12 Weeks After Implantation. A Retrieval Example," *Eur. Spine J.*, Vol. 16, 2007, pp. 1015–1020.

[36] Fraser, R. D., Ross, E. R., Lowery, G. L., Freeman, B. J., and Dolan, M., "AcroFlex Design and Results," *Spine J.*, Vol. 4, 2004, pp. 245S–251S.

[37] Hallab, N., Link, H. D., and McAfee, P. C., "Biomaterial Optimization in Total Disc Arthroplasty," *Spine (Phila Pa 1976)*, Vol. 28, 2003, pp. S139–S152.

[38] Pimenta, L., Diaz, R. C., and Guerrero, L. G., "Charite Lumbar Artificial Disc Retrieval: Use of a Lateral Minimally Invasive Technique," *J. Neurosurg. Spine*, Vol. 5, 2006, pp. 556–561.

[39] Rawlinson, J. J., Furman, B. D., Li, S., Wright, T. M., and Bartel, D. L., "Retrieval, Experimental, and Computational Assessment of the Performance of Total Knee Replacements," *J. Orthop. Res.*, Vol. 24, 2006, pp. 1384–1394.

[40] White, A. A. and Panjabi, M. M., *Clinical Biomechanics of the Spine*, 2nd ed., J.B. Lippincott Company, Philadelphia, Toronto, 1990.

[41] Yosibash, Z., Padan, R., Joskowicz, L., and Milgrom, C., "A CT-Based High-Order Finite Element Analysis of the Human Proximal Femur Compared to In-Vitro Experiments," *J. Biomech. Eng.*, Vol. 129, 2007, pp. 297–309.

[42] Sawatari, T., Tsumura, H., Iesaka, K., Furushiro, Y., and Torisu, T., "Three-Dimensional Finite Element Analysis of Unicompartmental Knee Arthroplasty—The Influence of Tibial Component Inclination," *J. Orthop. Res.*, Vol. 23, 2005, pp. 549–554.

[43] Ulrich, D., van Rietbergen, B., Laib, A., and Ruegsegger, P., "The Ability of Three-Dimensional Structural Indices to Reflect Mechanical Aspects of Trabecular Bone," *Bone*, Vol. 25, 1999, pp. 55–60.

[44] Morgan, E. F., Bayraktar, H. H., and Keaveny, T. M., "Trabecular Bone Modulusdensity Relationships Depend on Anatomic Site," *J. Biomech.*, Vol. 36, 2003, pp. 897–904.

[45] Kopperdahl, D. L. and Keaveny, T. M., "Yield Strain Behavior of Trabecular Bone," *J. Biomech.*, Vol. 31, 1998, pp. 601–608.

[46] Mosekilde, L. and Danielsen, C. C., "Biomechanical Competence of Vertebral Trabecular Bone in Relation to Ash Density and Age in Normal Individuals," *Bone*, Vol. 8, 1987, pp. 79–85.

[47] Hansson, T. H., Keller, T. S., and Panjabi, M. M., "A Study of the Compressive Properties of Lumbar Vertebral Trabeculae: Effects of Tissue Characteristics," *Spine*, Vol. 12, 1987, pp. 56–62.

[48] Kumaresan, S., Yoganandan, N., Pintar, F. A., Maiman, D. J., and Goel, V. K., "Contribution of Disc Degeneration to Osteophyte Formation in the Cervical Spine: A Biomechanical Investigation," *J. Orthop. Res.*, Vol. 19, 2001, pp. 977–984.

[49] Silva, M. J., Keaveny, T. M., and Hayes, W. C., "Load Sharing Between the Shell and Centrum in the Lumbar Vertebral Body," *Spine*, Vol. 22, 1997, pp. 140–150.

[50] Polikeit, A., Nolte, L. P., and Ferguson, S. J., "The Effect of Cement Augmentation on the Load Transfer in an Osteoporotic Functional Spinal Unit: Finite-Element Analysis," *Spine*, Vol. 28, 2003, pp. 991–996.

[51] Schmidt, H., Heuer, F., Simon, U., Kettler, A., Rohlmann, A., Claes, L., and Wilke, H.-J., "Application of a New Calibration Method for a Three-Dimensional Finite Element Model of a Human Lumbar Annulus Fibrosus," *Clin. Biomech. (Bristol, Avon)*, Vol. 21, 2006, pp. 337–344.

[52] Fernström, U., "Arthroplasty with Intercorporal Endoprothesis in Herniated Disc and in Painful Disc," *Acta Chir Scand Suppl*, Vol. 357, 1966, pp. 154–159.

[53] Rohlmann, A., Zander, T., Schmidt, H., Wilke, H. J., and Bergmann, G., "Analysis of the Influence of Disc Degeneration on the Mechanical Behavior of a Lumbar Motion Segment Using the Finite Element Method," *J. Biomech.*, Vol. 39, 2006, pp. 2484–2490.

[54] Schmidt, H., Heuer, F., Drumm, J., Klezl, Z., Claes, L., and Wilke, H.-J., "Application of a Calibration Method Provides More Realistic Results for a Finite Element Model of a Lumbar Spinal Segment," *Clin. Biomech. (Bristol, Avon)*, Vol. 22, 2007, pp. 377–384.

[55] Rohlmann, A., Zander, T., Rao, M., and Bergmann, G., "Applying a Follower Load Delivers Realistic Results for Simulating Standing," *J. Biomech.*, Vol. 42, 2009, pp. 1520–1526.

[56] Wilke, H. J., Neef, P., Caimi, M., Hoogland, T., and Claes, L. E., "New In Vivo Measurements of Pressures in the Intervertebral Disc in Daily Life," *Spine (Phila Pa 1976)*, Vol. 24, 1999, pp. 755–762.

[57] Shkolnikov, Y. P., Bowden, A., MacDonald, D., and Kurtz, S. M., "Wear Pattern Observations from TDR Retrievals Using Autoregistration of Voxel Data," *J. Biomed. Mater. Res., Part B: Appl. Biomater.*, Vol. 94, 2010, pp. 312–317.

[58] Kurtz, S. M., Patwardhan, A., MacDonald, D., Ciccarelli, L., van Ooij, A., Lorenz, M., Zindrick, M., O'Leary, P., Isaza, J., and Ross, R., "What is the Correlation of In Vivo Wear and Damage Patterns with In Vitro TDR Motion Response?," *Spine (Phila Pa 1976)*, Vol. 33, 2008, pp. 481–489.

[59] Dooris, A. P., Goel, V. K., Grosland, N. M., Gilbertson, L. G., and Wilder, D. G., "Load-Sharing Between Anterior and Posterior Elements in a Lumbar Motion Segment Implanted with an Artificial Disc," *Spine*, Vol. 26, 2001, pp. E122–E129.

[60] Cakir, B., Richter, M., Kafer, W., Puhl, W., and Schmidt, R., "The Impact of Total Lumbar Disc Replacement on Segmental and Total Lumbar Lordosis," *Clin. Biomech. (Bristol, Avon)*, Vol. 20, 2005, pp. 357–364.

[61] Brown, T. D. and Bartel, D. L., "What Design Factors Influence Wear Behavior at the Bearing Surfaces in Total Joint Replacements?," *J. Am. Acad. Orthop. Surg.*, Vol. 16, 2008, pp. S101–S106.

[62] Ong, K. L., Rundell, S., Liepins, I., Laurent, R., Markel, D., and Kurtz, S. M., "Biomechanical Modeling of Acetabular Component Polyethylene Stresses, Fracture Risk, and Wear Rate Following Press-Fit Implantation," *J. Orthop. Res.*, Vol. 27, 2009, pp. 1467–1472.

IN VITRO TESTING METHODS

Reprinted from JAI, Vol. 8, No. 9
doi:10.1520/JAI103495
Available online at www.astm.org/JAI

Christina A. Niosi,[1] *Rosemary E. Thompson,*[2] *and Markus Froehlich*[3]

Development of a More Physiological Loading Protocol for Spine In Vitro Flexibility Testing

ABSTRACT: With motion preserving systems, whose behavior is dependent on the loading applied, it is becoming more important to produce a loading environment that better simulates the situation in vivo. Several studies show that the spine experiences high compressive loads that change as a function of position. The purpose of this study was to apply a high compressive dynamic follower load and determine the moment required to produce a physiological range of motion in vitro. Six human specimens (L2-L3) were subjected to a pure moment, in combination with a high compressive dynamic follower load. Appropriate compressive loads were obtained from literature based on in vivo intradiscal pressure measurements. The moments necessary to produce pre-defined angles of rotation in flexion, extension, lateral bending, and axial rotation (in vivo literature values) were recorded. The follower load was attached laterally in flexion-extension and axial rotation and anterior-posteriorly in lateral bending. Tests were also conducted using two traditional loading protocols for comparison: ±10 Nm (no follower load); and ±10 Nm with a 600 N constant follower load, in terms of range of motion (ROM), helical axis of motion (HAM), and flexibility coefficients.The new loading protocol resulting from this study consisted of a compressive follower load of 800 N in the neutral position, a flexion moment of 35 Nm combined with a maximum compressive follower load of 2000 N, an extension moment of 10 Nm combined with 900 N, a moment of ±15 Nm in lateral bending with

Manuscript received October 18, 2010; accepted for publication July 7, 2011; published online August 2011.
[1] MASc, Zimmer GmbH, Winterthur, Switzerland.
[2] PhD, Zimmer GmbH, Winterthur, Switzerland.
[3] MSc, Zimmer GmbH, Winterthur, Switzerland.
Symposium on Static and Dynamic Spinal Implants: Are We Evaluating Them Appropriately? on 16 November 2010 in San Antonio, TX.

Cite as: Niosi, C. A., Thompson, R. E. and Froehlich, M., "Development of a More Physiological Loading Protocol for Spine In Vitro Flexibility Testing," *J. ASTM Intl.*, Vol. 8, No. 9. doi:10.1520/JAI103495.

1100 N, and a moment of ±20 Nm in axial rotation with 1250 N. The anterior-posterior follower load fixation in lateral bending allowed more unrestrained movement. The moments necessary to produce physiological motion under a dynamic compressive follower load are higher than what is currently used and are comparable to calculated in vivo moments.

KEYWORDS: lumbar spine, flexibility testing, load application, non-fusion implants

Introduction

In vitro spine flexibility testing is used primarily to study the behavior of the spine, the function of the various anatomical elements, and for the evaluation of implants. It is a laboratory simplification of the complex forces and moments that the spine experiences in vivo. One goal in the development of protocols for flexibility testing has been to create a test setup that can be performed in the majority of labs, in order to facilitate comparison between studies [1–3]. Historically, in vitro biomechanical testing of implants has been largely focused on spinal devices that aim to eliminate segmental motion, as in fusion. Such implants tend to be rigid in comparison to the flexibility of the anatomical structures of the spine and as such, dominate the biomechanical response to applied loads. The linear, non-time dependent mechanical properties of such implants, in combination with the implant's intention to eliminate motion, renders the test specimen relatively uninfluenced by the loading environment.

With the more recent emergence of dynamic or flexible spinal instrumentation, whose purpose is to achieve spinal stability without fusion or to preserve motion, the mechanical objectives of implants have significantly changed. In addition to controlling motion, these devices are responsible for modifying segmental load transfer.The components of such implants often include polymeric materials, which tend to have non-linear viscoelastic mechanical properties; in contrast to the all-metal implants typical for fusion instrumentation. The behaviour of polymers is dependent upon the loading regime to which they are subjected, which is an important consideration when comparing different implants. The evaluation of the safety and performance of these dynamic devices must therefore involve a load application that replicates the physiological loading environment as closely as possible.

In recent years, there has been some recognition and awareness as to the suitability or unsuitability of traditional implant testing to adequately assess the mechanical objectives of non-fusion instrumentation [4–6]. For example, the helical axis of motion (HAM) is now often reported as a more complete description of the quality and quantity of motion; loading of the posterior elements can be measured, and several other potential technologies for the evaluation of the mechanical performance of spinal instrumentation have been discussed [4–6]. Our paper focuses specifically on the loading protocol for in vitro flexibility testing.

Traditional and generally accepted loading protocols for spine in vitro flexibility testing consist of a pure moment applied to the specimen in each of the

anatomical directions (flexion-extension, lateral bending, and axial rotation) while allowing the spine to move in an unconstrained, three-dimensional fashion [1–3,7]. The magnitude of the continuous pure moment that is normally used for the lumbar spine is around 6 to 10 Nm [3,8–13]. These loads were not intended to represent physiological loads, but were selected because they were sufficient to produce a physiological range of motion in the absence of any axial compression for an intact specimen without damaging the test specimen [1,2,8].

More recently, the concept of a compressive follower load has been introduced in an attempt to simulate the compressive loading that the spinal column experiences in vivo [14]. A follower load follows the contour of the spine so that at each vertebral level, a pure compressive load is applied. Thus, a second commonly used test protocol involves the application of a constant compressive follower load along the flexion-extension center of rotation of the specimen, regardless of the loading direction, in conjunction with the pure moment previously described. The magnitude of the compressive follower load remains constant throughout the test and is typically around 400 N to 600 N for the lumbar spine [3,10,12,13]. The magnitude of these loads tends to be justified by the static weight of the torso superior to the lumbar spine; however, it does not account for the dynamic compression induced by the spinal musculature or motion of the upper torso. Studies measuring intradiscal pressure in the lumbar spine have shown that the spine experiences high compressive loads in vivo and that the compressive loads vary with posture [15–18]. Compressive loads vary from around 800 N in the neutral position to several thousand newtons during certain tasks. Additionally, application of a compressive load has been shown to reduce the flexibility of the specimen [19–22] due to a stiffening effect of the disc [19,20]. Hence, combining a follower load with the aforementioned pure moment is unlikely to result in a physiological range of motion.

The purpose of this study was threefold. The first step was to develop an alternative loading protocol for spine flexibility testing, which includes the application of a dynamic compressive follower load, to better approximate the in vivo loading environment. This type of protocol is particularly important for the testing of non-fusion instrumentation. Second, the moment that was required to produce a physiological range of motion under the dynamic compressive follower load was determined. Finally, the results using this loading protocol were compared with two traditional loading protocols.

Materials and Methods

An existing custom-designed spine testing machine, which has previously been used for spine in vitro flexibility testing, was modified to incorporate a compressive follower load that was of both a higher magnitude and a dynamic nature. The machine applies a continuous pure moment to a spine specimen, while allowing it to move in an unconstrained three-dimensional manner. It consists of a direct current servo motor (Stock Dr. Products, New Hyde Park, NY, USA) connected to a gearbox (Stock Dr. Products, New Hyde Park, NY, USA) and torque load cell (Transducer Techniques, Temecula, CA, USA), which are

supported by a carriage that is free to move in all six degrees of freedom. The motor-gearbox-load cell assembly is attached to the top of the spine specimen, while the bottom of the specimen is attached to a fixed base plate (Fig. 1). Weight compensation is used to offset any additional loads on the specimen due to the carriage and its components. The existing machine also had the capability to apply a static compressive follower load in conjunction with the pure moment.

The proposed new loading protocol incorporates a high magnitude dynamic compressive follower load with pure moment application. The purpose of the dynamic compressive follower load is to simulate the changing compressive load that is present in the human spine in vivo [15–18]. The magnitude of the compressive follower load was chosen based upon in vivo intradiscal pressure measurements that are presented in the literature [16,18]. As a result, the compressive follower load was 800 N in the neutral position. As the specimen moves into flexion, the follower load increases to 2000 N, whereas in extension, the follower load increases to 900 N. Similarly, the follower load increases to 1100 N in lateral bending and to 1250 N in axial rotation.

An electric actuator (Parker Hannifin Ltd, Watford, United Kingdom) was incorporated into the existing machine in order to apply the dynamic

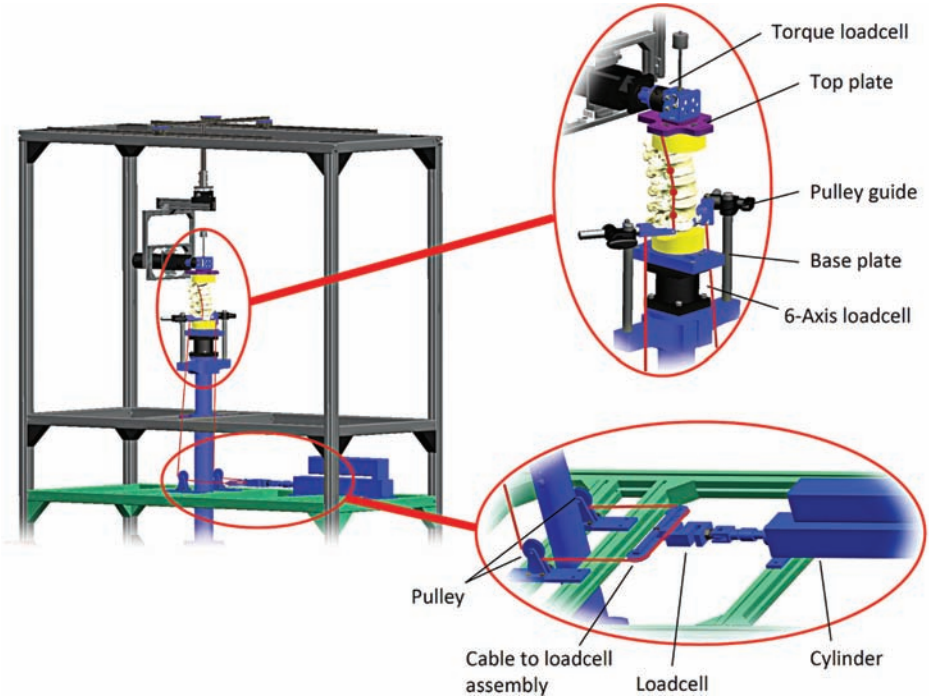

FIG. 1—*Illustration of the custom spine test machine showing the fixation of the specimen to the machine, the pure moment application, and the compressive follower load application in detail.*

compressive load concurrently with the pure moment (Fig. 1). The previous and new loading protocols used in our facility are both depicted graphically in Fig. 2. The link between the pure moment and the compressive follower load application is achieved using a gearing function in LabVIEW (Version 6.0, 2000, National Instruments, Austin, TX, USA). This implies that the actuator operation is directly linked to the application of the pure moment using a specified gearing ratio (N/° or N/Nm) whereby the compressive follower load follows the pure moment using a master-slave relationship.

To measure the compressive load, an s-beam load cell (Omega, Stanford, CT, USA) is connected in series between the electric actuator and the follower load cable. The follower load cable is guided through a pulley system to achieve

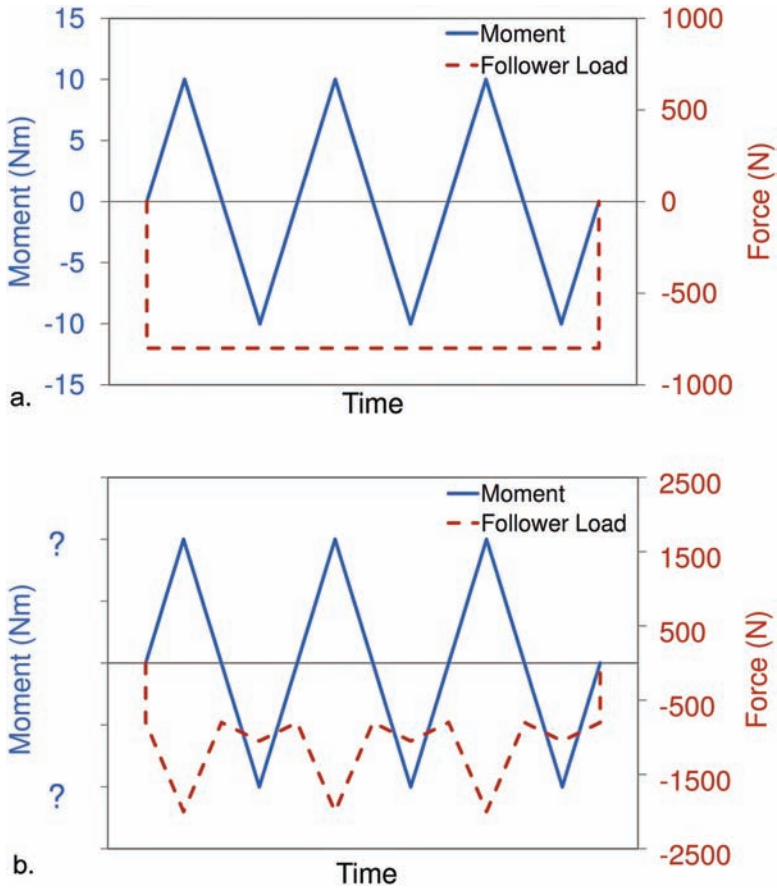

FIG. 2—*Graphical representation of the moment and compressive follower load application. (A) is the traditional load protocol that has been used by our group (Loading Protocol 2) and (B) is the proposed new loading protocol (shown for flexion-extension only). Note that for simplicity, the moment is depicted as being linear with time, but in actuality it is the rotation that is applied linearly with time.*

the desired direction of the applied follower load, then guided along the curvature of the spine using two different positions, and finally attached to a plate on top of the specimen. It is a continuous cable so that theoretically, in the absence of friction, the magnitude of the compressive load is equally applied to both sides of the specimen. In the first follower load position, which is used for testing in both flexion-extension and axial rotation, the cable is guided laterally along the specimen approximately at the flexion-extension center of rotation. In the second position, the cable is guided along the mid-sagittal plane at the anterior and posterior aspects of the specimen. This position is used for testing in lateral bending since it better approximates the lateral bending axis of rotation. In both situations, the position of the follower load is adjusted such that rotation of the specimen due to application of the follower load alone is minimized.

Six fresh frozen human cadaveric lumbar segments (L2-L3) were used in this study. The average specimen age was 63 years (24–80 years) and there were 4 males and 2 females. The specimens were prepared by dissecting the musculature, such that the soft tissues were not damaged. The L2 and L3 vertebrae were then embedded in industrial PMMA with the intervertebral disc horizontal.

The specimens were subjected to flexibility testing using three different loading protocols:

- Loading Protocol 1: Pure moment with a high dynamic compressive follower load (Table 1).
- Loading Protocol 2: Pure moment of ±10 Nm with a static compressive follower load of 600 N.
- Loading Protocol 3: Pure moment of ±10 Nm with no compressive load.

Loading Protocol 1 is the proposed protocol that is thought to represent a more physiological loading environment. Loading Protocols 2 and 3 are representative of the more commonly used traditional loading protocols for lumbar spine flexibility testing [1,2,7]. A continuous moment was applied at a rate of 1.5°/s for three completely reversed cycles in all three directions of loading: flexion-extension, lateral bending, and axial rotation. Three complete pre-tests were conducted in each loading direction to try to minimize viscoelastic effects. The test sequence was not randomized and the order was Loading Protocol 1, 2, and 3.

In order to be able to fully define the new loading protocol (Loading Protocol 1), it was necessary to determine the pure moment required in combination with a high magnitude dynamic compressive follower load to produce a physiological

TABLE 1—*Rotation and compressive follower load for Loading Protocol 1 for each loading direction. The compressive follower load in the neutral position was 800 N.*

Direction	Rotation, °	Follower Load, N
Flexion	10	2000
Extension	3	900
Lateral bending	5.5	1100
Axial rotation	2	1250

range of motion, which is defined as the maximum normal rotation in vivo. The desired amount of rotation was obtained from in vivo measurements found in the literature for the L2-L3 level, and were 10° in flexion, 3° in extension, ±5.5° lateral bending, and ±2° in axial rotation (Table 1) [23]. The maximum allowable pure moment was set to 35 Nm in order to protect the machine and specimen from damage. For the purpose of this study, the compressive follower load application was geared to the angular displacement with a gearing ratio. Normal operation of the system will be the application of a pure moment in displacement control to a specified moment with the magnitude of the compressive follower load geared to the magnitude of the applied moment. This combination is proposed since when implants are incorporated, although the resulting displacement may be different, the loading conditions will remain the same.

One set of four non-collinear infrared light emitting diodes was rigidly attached to each of the two vertebral bodies. The three-dimensional position of the markers was recorded throughout the testing using an optoelectronic camera system (Optotrak 3020, Northern Digital, Waterloo, Canada) with a sampling frequency of 20 Hz. A local coordinate system was created for each of the two vertebrae.

The moment needed to define Loading Protocol 1 was identified as the median moment for the six specimens. For lateral bending and axial rotation, an average was taken of the moments for right and left rotation to generate single value for each specimen.

The behavior of the specimens for the three different loading protocols was compared by looking at the intersegmental motion between L2 and L3. The range of motion (ROM), helical axis of motion (HAM), and flexibility coefficients were calculated for the third loading cycle.

The ROM was calculated as the rotation from the neutral point to the maximum or minimum load. The ROM was separately reported for flexion and extension and as an average of right and left rotation for lateral bending and axial rotation. Only the motion about the primary axis is reported here. Due to the nature of the test, there was no statistical analysis conducted for the ROM (for the development of Loading Protocol 1, a pre-specified rotation was used).

The HAM is the unique axis about which a body rotates and parallel to which it translates [24]. It is an alternative method to represent the complete motion between two bodies and illustrates the entire three-dimensional motion pattern in a clear and concise manner. It is fully defined by six quantities: four that describe the position and orientation of the axis; one defining the amount of rotation about the axis; and one defining the translation along the axis. The HAM in this study was represented by an orientation in two planes and as a point of intersection with either the sagittal, transverse, or coronal plane. The HAM was calculated over the full range of motion (from maximum to minimum rotation), from minimum rotation to the neutral position, and from the neutral position to maximum rotation [24,25]. The location of the HAM was normalized by expressing it as a percentage of the height, width, and anterior-posterior diameter of the L3 vertebral body.

To determine if the HAM was different between the three loading protocols, a statistical analysis was conducted using a repeated measures analysis of

variance (ANOVA), with the load case as the repeated measure and a level of significance of $p < 0.05$. Both the normalized intersection point (two coordinates) and the orientation (three unit vectors) were statistically evaluated for each loading direction. Post hoc analysis was conducted using a Student-Newman-Keuls test.

The flexibility coefficient was calculated as the slope of the best fit line on the load-displacement curve in °/Nm. Due to the non-linear behavior of the spine, flexibility coefficients were calculated in two moment ranges: a low range (0.2–2.0 Nm); and a high range (80–100 % of the maximum applied moment). The high range was specified as a percentage of the maximum applied moment to account for the nature of the different loading protocols, in order to ensure that similar regions of the curves were compared. For axial rotation and lateral bending, the average flexibility coefficient was taken from the right and left rotation to generate a single value.

To determine if the flexibility coefficients were different between the three loading protocols and between ranges, they were statistically compared using a repeated measures ANOVA with one independent factor and a level of significance of $p < 0.05$. The repeated measure was the load case and the independent factor was the flexibility range (low or high). Post hoc analysis was conducted using a Student-Newman-Keuls test.

Results

Based upon Loading Protocol 1, the moment required to produce a physiological range of motion under a high dynamic compressive follower load is shown in Table 2. In flexion, a pure moment of 35 Nm was required, whereas in extension, 10 Nm was needed. In lateral bending and axial rotation, moments of ± 15 and ± 20 Nm, respectively, were required. Typical load-displacement curves are shown for each loading direction in Figs. 3–5.

The ROM for Loading Protocols 2 and 3 are shown alongside that from Loading Protocol 1 in Table 3. It is important to note that for Loading Protocol 1, different moments were applied to each specimen as opposed to Loading Protocols 2 and 3, where the same moment was applied to each specimen. This is also the reason why the standard deviation generally appears smaller for Loading Protocol 1 and why there was no statistical comparison conducted for the ROM.

The HAM is presented only over the full range of motion (maximum to minimum rotation) here, since the differences in the HAM between the loading protocols were generally similar for the three calculation ranges. One specimen was omitted from the HAM analysis for lateral bending since the values were outside a reasonable range. The average HAM (with standard deviation) is shown graphically for each of the loading protocols in Figs. 6–8. For each loading direction, only the graphs showing the position of the intersection point with a particular plane are shown. The graphs displaying the orientation of the HAM are not shown, since there were no significant differences in the orientation of the HAM between the three loading protocols in all directions ($p > 0.07$). Generally, in flexion-extension and lateral bending, the position of the HAM

TABLE 2—*Applied moment and resulting ROM for Loading Protocol 1 for each specimen. The median moment was used to define the loading protocol. Specimen gender and age are specified.*

	Flexion		Extension		Lateral Bending		Axial Rotation	
Specimen	Moment, Nm	ROM, °	Moment, Nm	ROM, °	Moment, Nm	ROM, °	Moment, Nm	ROM, °
Male 80 years	35.0	7.4	3.4	3.0	18.0	5.5	13.0	2.0
Female 68 years	33.0	9.9	5.6	3.0	18.5	5.5	6.0	2.1
Male 24 years	35.0	7.4	6.4	3.0	12.0	5.7	28.9	2.0
Female 59 years	35.0	9.7	18.0	2.3	10.3	5.5	23.3	2.0
Male 76 years	35.0	9.6	12.7	3.0	17.7	5.5	21.2	2.0
Male 69 years	23.1	10.0	25.0	2.5	11.0	5.5	18.0	2.1
Average	32.7	9.0	11.9	2.8	14.6	5.5	18.4	2.0
Std. Dev.	4.8	1.2	8.4	0.3	3.9	0.0	8.0	0.0
Median	35.0	9.6	9.5	3.0	14.8	5.5	19.6	2.0

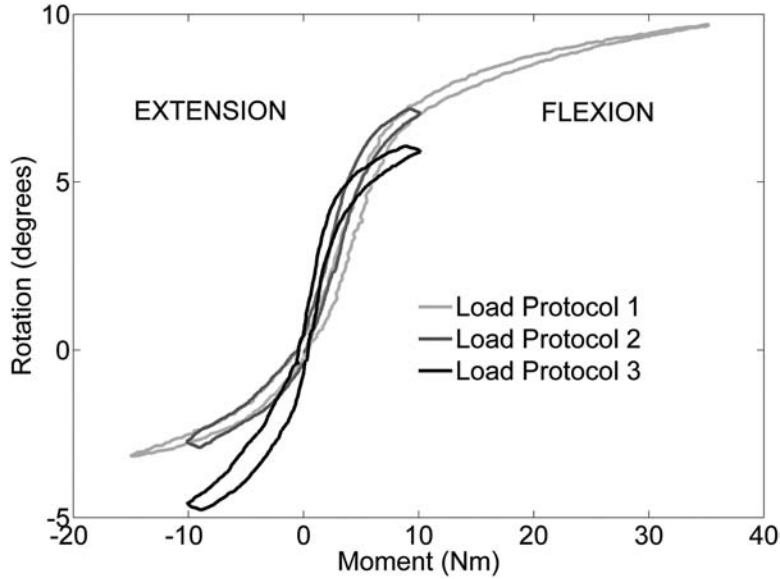

FIG. 3—*Sample flexion-extension moment versus displacement curve, showing the three loading protocols. Loading Protocol 1 is with the dynamic compressive follower load, Loading Protocol 2 is with the static compressive follower load, and Loading Protocol 3 is without a compressive load.*

was close to the center of the L3 vertebral body. In axial rotation, the HAM was located just posterior to the vertebral body and slightly left of center. Statistical analysis revealed that in flexion-extension, there was a significant difference in the position of the HAM between Loading Protocols 1 and 3 ($p < 0.03$) and between Loading Protocols 2 and 3 ($p < 0.04$). In lateral bending, there was no significant difference in the position of the HAM between the three loading protocols ($p > 0.08$). In axial rotation, there was a significant difference in the anterior-posterior position of the HAM between Loading Protocols 1 and 2 ($p < 0.03$) and Loading Protocols 1 and 3 ($p < 0.003$).

The average flexibility coefficients of the load-displacement curves are shown in Table 4 for each of the three loading protocols. The first point of consideration was whether or not the low and high flexibility coefficients were different from one another for a specific loading protocol. The general trend for all loading protocols and directions was that the segments were stiffer at the higher moment range compared to at the lower moment range. Statistical analysis showed that for Loading Protocols 2 and 3, there was almost always a significant difference between the low and high range flexibility coefficients ($p < 0.05$) (except in axial rotation). For Loading Protocol 1, there was a significant difference between the low and high range flexibility coefficients only in flexion and extension ($p < 0.03$). The second question was whether or not the flexibility coefficients were different between loading protocols. Between Loading Protocols 1 and 3 and between Loading Protocols 2 and 3, there was a significant difference

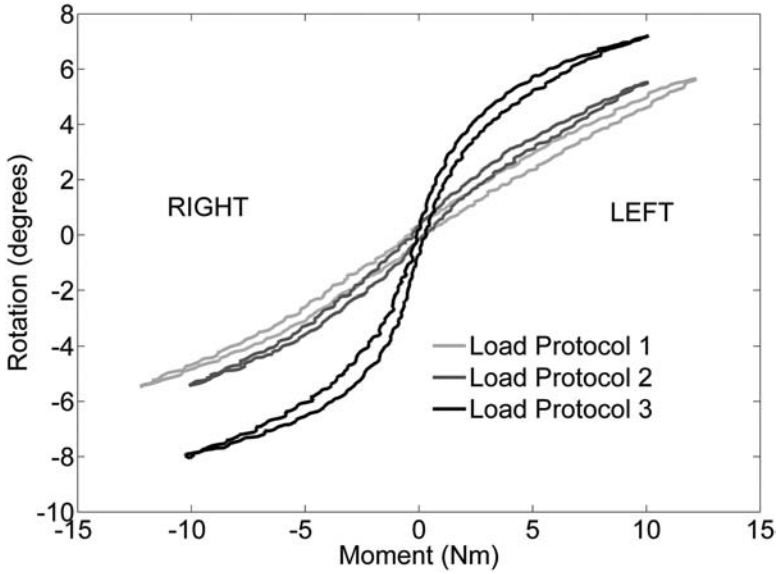

FIG. 4—*Sample lateral bending moment versus displacement curve, showing the three loading protocols. Loading Protocol 1 is with the dynamic compressive follower load, Loading Protocol 2 is with the static compressive follower load, and Loading Protocol 3 is without a compressive load.*

in the low range flexibility coefficient in all loading directions ($p < 0.005$). In the low range, Loading Protocols 1 and 2 resulted in a stiffer segment compared to Loading Protocol 3. Between Loading Protocols 1 and 2, there was only a significant difference in the low range flexibility coefficient in flexion ($p < 0.04$). There was not a significant difference in the high range flexibility coefficient between all three loading protocols ($p > 0.50$).

Discussion

The loading environment is important for testing spinal implants that consist of polymeric components and also for implants that are designed for motion preservation and load sharing or that provide some degree of stabilization without fusion. Traditional loading protocols for spine flexibility testing neglect to include a high magnitude dynamic compressive load that has been shown to be present in the spine in vivo, which may be important for better analysis of nonfusion implantation. This study had the combined purpose to begin defining a new loading protocol by determining the moment required to produce a physiological range of motion under a high dynamic compressive follower load and then to compare the results of the new loading protocol directly with two traditional loading protocols.

The new loading protocol resulting from this study consisted of a compressive follower load of 800 N in the neutral position, a flexion moment of 35 Nm

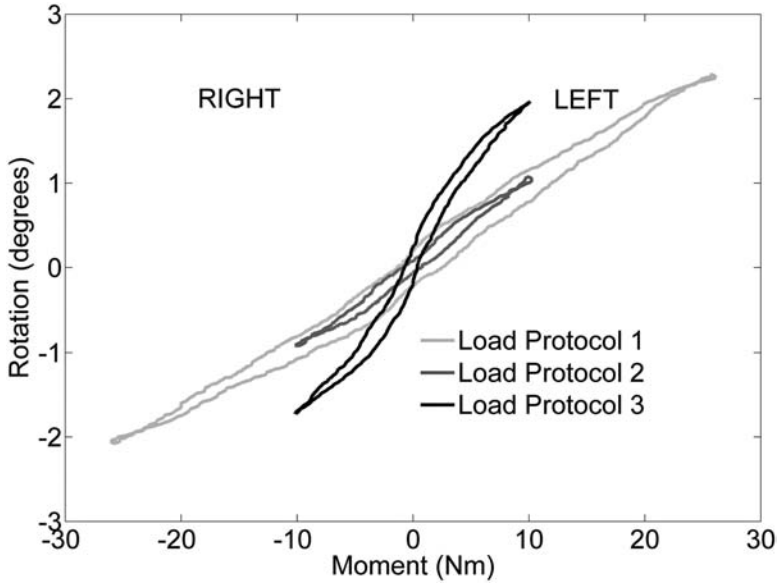

FIG. 5—*Sample axial rotation moment versus displacement curve, showing the three loading protocols. Loading Protocol 1 is with the dynamic compressive follower load, Loading Protocol 2 is with the static compressive follower load, and Loading Protocol 3 is without a compressive load.*

combined with a maximum compressive follower load of 2000 N, an extension moment of 10 Nm combined with 900 N, a moment of ±15 Nm in lateral bending with 1100 N, and a moment of ±20 Nm in axial rotation with 1250 N.

The follower load was dynamic and increased from a minimum in the neutral position to a maximum at the maximum moment. In contrast to the proposed new loading protocol, traditional loading protocols typically apply around 6 to 10 Nm in all loading directions with or without a compressive follower load in the range of 400 N to 600 N [3,8–13].

In this study, the moments that were determined to be necessary to produce a physiological range of motion under a high compressive dynamic follower load were comparable to moments for the ligamentous spine that have been presented in the literature. Potvin et al. have reported a peak moment of 43 Nm in the ligamentous spine of L4-L5 in a stooping position, with a peak compressive load of 3130 N [26]. McGill has likewise predicted a moment of 42 Nm in the ligaments and disc of L4-L5 under 10° of flexion [27].

Some in vitro studies in the literature have applied a similar principle of increasing compressive load [28,29], to which the results of the present study are comparable. Freudiger et al. performed in vitro testing using cables and pulleys on a dynamic neutralisation system for the lumbar spine [28]. They applied an average flexion moment of 18.3 ± 7.5 Nm with a compressive load of 2296 ± 159 N and an anterior-posterior load of 458 ± 99 N, producing an average of 9.6 ± 1.7° of

TABLE 3—*Comparison of ROM for the three loading protocols for each specimen. Specimen gender and age are specified. Note that for Loading Protocol 1, the applied moment was not the same for each specimen. Loading Protocol 1 is with the dynamic compressive follower load, Loading Protocol 2 is with the static compressive follower load, and Loading Protocol 3 is without a compressive load.*

	Flexion			Extension			Lateral Bending			Axial Rotation		
Specimen	Load 1, °	Load 2, °	Load 3, °	Load 1, °	Load 2, °	Load 3, °	Load 1, °	Load 2, °	Load 3, °	Load 1, °	Load 2, °	Load 3, °
Male 80 years	7.4	4.9	7.1	3.0	5.0	6.9	5.5	3.6	8.5	2.0	2.0	3.4
Female 68 years	9.9	7.8	6.8	3.0	3.9	6.1	5.5	3.8	8.0	2.1	3.8	5.3
Male 24 years	7.4	5.2	5.8	3.0	3.7	3.9	5.7	5.5	7.6	2.0	0.7	1.2
Female 59 years	9.7	6.9	6.3	2.3	2.0	3.9	5.5	6.1	8.2	2.0	1.0	1.9
Male 76 years	9.6	7.2	6.3	3.0	2.9	4.5	5.5	4.6	6.5	2.0	1.3	2.1
Male 69 years	10.0	7.8	5.8	2.5	1.7	5.0	5.5	6.1	7.9	2.1	1.5	2.6
Average	9.0	6.6	6.4	2.8	3.2	5.1	5.5	4.9	7.8	2.0	1.7	2.7
Std. Dev.	1.2	1.3	0.5	0.3	1.3	1.2	0.0	1.1	0.7	0.0	1.1	1.5
Median	9.6	7.1	6.3	3.0	3.3	4.8	5.5	5.0	7.9	2.0	1.4	2.4

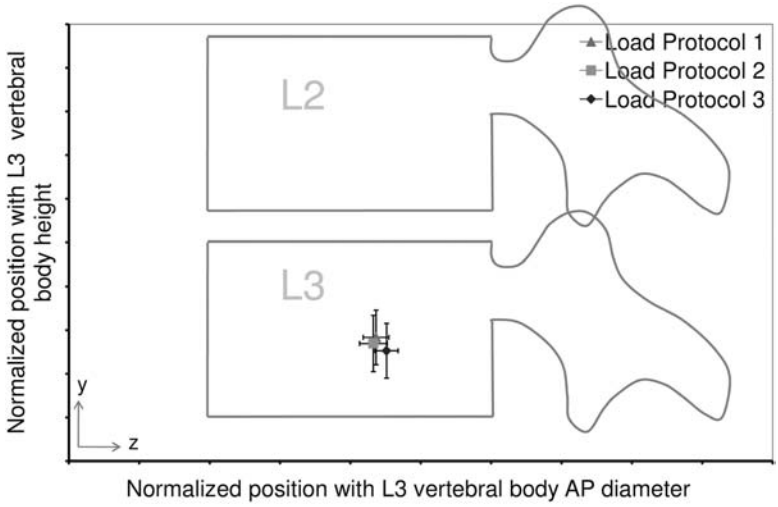

FIG. 6—*Average position of the helical axis of motion (HAM) in flexion-extension normalized by the height, width, and anterior-posterior diameter of the L3 vertebral body. Loading Protocol 1 is with the dynamic compressive follower load, Loading Protocol 2 is with the static compressive follower load, and Loading Protocol 3 is without a compressive load.*

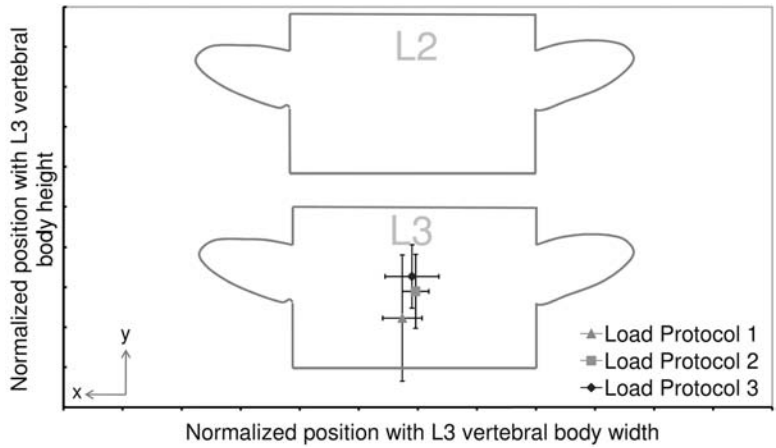

FIG. 7—*Average position of the helical axis of motion (HAM) in lateral bending normalized by the height, width, and anterior-posterior diameter of the L3 vertebral body. Loading Protocol 1 is with the dynamic compressive follower load, Loading Protocol 2 is with the static compressive follower load, and Loading Protocol 3 is without a compressive load.*

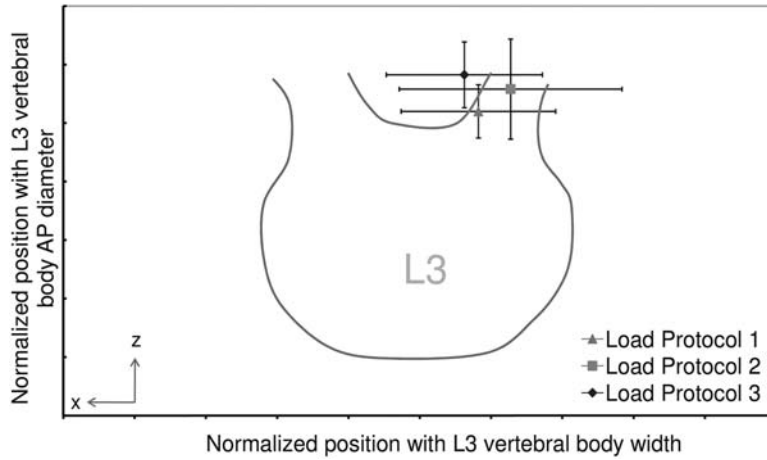

FIG. 8—*Average position of the helical axis of motion (HAM) in axial rotation normalized by the height, width, and anterior-posterior diameter of the L3 vertebral body. Loading Protocol 1 is with the dynamic compressive follower load, Loading Protocol 2 is with the static compressive follower load, and Loading Protocol 3 is without a compressive load.*

flexion at L4-L5. In extension, an average of 12.5 ± 6.2 Nm with a compressive load of 667 ± 21 N and an anterior-posterior shear load of 74 ± 59 N was applied and generated an average rotation of 2.1 ± 1.0°. Adams et al. has also performed cadaveric testing that incorporated an increasing compressive load [29]. In that study, an average of 57 ± 23 Nm was required to move the L2-L3 segment an average of 8 ± 1° in flexion under a high compressive load. However, both of these studies were not using pure moments and in the latter study, specimens were loaded to their elastic limit.

The new loading protocol was designed to generate a physiological ROM. In this study the magnitude of the applied moment was different for each specimen and as such, it was not possible to perform a reliable comparison of the ROM to the two traditional loading protocols. Under normal use, the machine will be operated until a maximum moment is reached and then it will be possible to compare the resulting ROM to traditional loading protocols. The ROM in flexion was an average of 6.6 and 6.4° for testing with a static compressive follower load (Loading Protocol 2) and without a compressive follower load (Loading Protocol 3), respectively, which is substantially lower than the 10° expected in vivo rotation in flexion that is presented in the literature for L2-L3 [23]. It is also worth noting that in extension, lateral bending, and axial rotation, the application of a static compressive follower load (Loading Protocol 2) reduced the amount of rotation compared to without a compressive follower load (Loading Protocol 3). This is consistent with data presented in the literature that has shown that the application of a compressive load or follower load decreases the ROM of the spine [19–22,29,30].

TABLE 4—*Average flexibility coefficients with standard deviation for each of the three loading protocols. The low and high stiffness ranges were 0.2–2.0 Nm and 80–100 % of the maximum applied moment, respectively. Loading Protocol 1 is with the dynamic compressive follower load, Loading Protocol 2 is with the static compressive follower load, and Loading Protocol 3 is without a compressive load.*

	Flexion		Extension		Lateral Bending		Axial Rotation	
Range	Low, °/Nm	High, °/Nm	Low, °/Nm	High, °/Nm	Low, °/Nm	High, °/Nm	Low, °/Nm	High, °/Nm
Load 1	0.64 ± 0.35	0.09 ± 0.04	0.61 ± 0.32	0.29 ± 0.26	0.60 ± 0.24	0.33 ± 0.06	0.19 ± 0.13	0.14 ± 0.07
Load 2	1.04 ± 0.50	0.27 ± 0.08	0.63 ± 0.35	0.17 ± 0.06	0.73 ± 0.26	0.39 ± 0.04	0.24 ± 0.24	0.13 ± 0.03
Load 3	2.08 ± 0.76	0.20 ± 0.04	1.06 ± 0.47	0.22 ± 0.08	2.39 ± 0.68	0.34 ± 0.17	0.58 ± 0.44	0.14 ± 0.03

Overall, the differences in the HAM between the three loading protocols were relatively small and in terms of comparing the new loading protocol to the traditional ones, the HAM did not appear to be a key area of focus. The position of the HAM reported in this study correlates reasonably well to data presented in the literature [10,31–35]. However, in flexion-extension, the HAM has often been reported to lie close to the superior endplate of the caudal vertebral body [10,31,32,35] and less frequently within the caudal vertebral body [34,36]. In the present study, the position of the HAM in both flexion-extension and lateral bending was located approximately in the center of the caudal vertebral body. An explanation for this may lie in the fact that only single spinal segments were tested here, whereas most studies include multiple segments in flexibility testing. In addition, Gerztbein et al. showed that the position of the centrode moves inferiorly when some degree of disc degeneration is present [37]. Although care was taken to select relatively healthy spine specimens in the present study, a detailed analysis of disc degeneration was not performed.

In the literature, it is common to see the neutral zone (NZ) measured and reported in flexibility testing [9–11,13,38]. The NZ is the region of low stiffness of the spine, characterized by the displacement between the neutral position and the initial point of spinal resistance to physiological motion [39]. There is some controversy over the existence and definition of the NZ and the method with which it is quantified [40]. Often the NZ is incorrectly reported as a measure of hysteresis of the loading-unloading curve. This means that with implantation of a device whose function is to stabilize the spine, the NZ often is reported as larger than that for the intact condition due to the polymeric nature of the implant components, which increase the hysteresis of the loading-unloading curve. Due to the lack of clarity surrounding the measurement of the NZ and its relevance, it was decided to report flexibility coefficients here rather than NZ as a measure of the motion segment's response to an applied load.

Application of either a static or dynamic compressive follower load typically resulted in a decreased flexibility coefficient or increased stiffness in the lower moment range compared to testing without a follower load. Qualitatively, the increased stiffness can be seen by the more linear load-displacement curve that resulted when a follower load was used. This effect was most pronounced in lateral bending and axial rotation. Although there is a large variability in the magnitude of the flexibility coefficients presented in the literature [21,39,41,42], the literature also shows a stiffening of specimens when a follower load is used [21,22]. This effect is likely attributed to a stiffening of the disc that occurs due to an increased hydrostatic pressure in the disc under a compressive load, increasing the internal and external bulge of the annulus, thus increasing the resistance to deformation [19]. There were, however, no differences in the flexibility coefficients between the tests with a static and dynamic compressive follower load (except the low range coefficient in flexion), suggesting that the stiffness of an intact specimen was not largely affected by the high magnitude and dynamic nature of the follower load. A correlation between in vivo and in vitro flexibility of the spine is difficult, given the presence of muscles and other supporting structures in vivo that are absent in in vitro testing.

In summary, notable differences in behavior resulting from the new loading protocol compared to the two traditional loading protocols seemed to be in the ROM and the flexibility coefficients (compared to testing without a compressive load). We hypothesize that if there are large differences to be seen, they will become more evident when conducting tests that incorporate implants with polymeric components that aim to preserve motion and share the load or stabilize the spine without fusion.

This study was preliminary in nature and had some limitations that should be recognized. The moment values that were determined to define the more physiological loading protocol were based on testing of a single functional spinal unit. Some additional work has since indicated that the magnitude of the moment might not be directly applicable for flexibility testing of more than one functional spinal unit. Further investigation is required to confirm the appropriateness of this protocol or to assess the requirements for flexibility testing of multiple functional spinal units.

The maximum allowable moment was set to 35 Nm in this study. The reason for this restriction was that we had little experience testing at extremely high moments and thus wanted to prevent damage to the testing machine and specimens. For two specimens in flexion, the maximum moment of 35 Nm was reached at approximately 7.5° instead of the desired 10°. The median moment in flexion was 35 Nm and was the magnitude selected to define the protocol. We feel that 35 Nm in flexion was appropriate for a single functional spinal unit, since the variability of the stiffness of individual specimens should also be taken into account. In the future, further investigation would be beneficial to clarify this point.

This study did not incorporate intradiscal pressure measurements, which would have provided valuable data to compare the compressive loading induced across the disc space experimentally to that which has been reported in the literature from in vivo investigations. Further studies that build on this loading protocol will benefit from the inclusion of intradiscal pressure measurements.

As part of the development of a more physiological loading protocol for spine flexibility testing, the position of the follower load cable was modified for testing in lateral bending. Traditionally, the follower load cable is positioned or guided along the flexion-extension center of rotation at each vertebral level [14], which is a logical choice for testing in flexion-extension because the center of rotation is the point where, theoretically, there is no movement. However, this position is not feasible for applying a compressive load in lateral bending since additional forces and moments are created that change the loading environment and increase the friction in the system, thus producing a large hysteresis artefact that may mask relevant experimental measures.

In this study for testing in lateral bending, the follower load was positioned approximately along the lateral bending center of rotation at the anterior and posterior aspects of the specimen. The loading curves (Fig. 4) show little hysteresis in the resulting motion, suggesting that this follower load position induced minimal experimental artefacts. For testing in axial rotation, the lateral (traditional) positioning of the follower load cable was used, since it is not possible to position the cable along the axial rotation center of rotation and apply a compressive load.

Although an in vitro model that incorporates shear loading or simulation of muscle forces may lead to an even more physiological loading environment, the level of complexity with such models is much greater and there is still a lot of work that needs to be performed to fully understand the in vivo relationship of all of the muscle groups. There is some value gained by using the traditional approach to flexibility testing, which is to try to keep the loading environment relatively simple to facilitate comparison between laboratories. We believe that with the modifications to the traditional loading protocols as discussed in this paper, the loading protocol is still relatively uncomplicated, but much more physiological, which is a necessity for the evaluation of non-fusion implants. It is not suggested that the results of this testing form a finalized protocol, but the intent is that these results are useful in further refining a loading protocol that incorporates a dynamic compressive load.

Conclusion

A cadaveric study was performed to define and present a new loading protocol for spine flexibility testing that is more physiological compared to traditional loading protocols. The proposed loading protocol attempts to replicate the dynamic compressive load that is present in the spine in vivo and combine that with pure moment application. This preliminary testing provides a good basis from which to continue working and further refine the loading protocol.

The moments necessary to produce physiological motion under a dynamic compressive follower load are higher than what is currently used and are comparable to calculated in vivo moments. It is particularly important to use a more physiological loading protocol for the testing of non-fusion spinal implants and those that consist of polymeric components, since the mechanical objectives and the behavior of the materials themselves depend upon the loads to which the devices are subjected.

Acknowledgments

The authors wish to disclose that they are employees of Zimmer, GmbH, Winterthur, Switzerland.

References

[1] Panjabi, M. M., "Biomechanical Evaluation of Spinal Fixation Devices: I. A Conceptual Framework," *Spine*, Vol. 13, No. 10, 1988, pp. 1129–1134.

[2] Wilke, H.-J., Wenger, K., and Claes, L., "Testing Criteria for Spinal Implants: Recommendations for the Standardization of In Vitro Stability Testing of Spinal Implants," *Eur. Spine J.*, Vol. 7, No. 2, 1998, pp. 148–154.

[3] Goel, V. K., Panjabi, M. M., Patwardhan, A. G., Dooris, A. P., and Serhan, H., "Test Protocols for Evaluation of Spinal Implants," *J. Bone Joint Surg. Am.*, Vol. 88, 2006, pp. 103–109.

[4] McNally, D. S., "The Objectives for the Mechanical Evaluation of Spinal Instrumentation Have Changed," *Eur. Spine J.*, Vol. 11, No. 2, 2002, pp. S179–S185.

[5] Wilke, H.-J., Kettler, A., and Claes, L., "Range of Motion or Finite Helical Axis? Comparison of Different Methods to Describe Spinal Segmental Motion In Vitro," *Roundtables in Spine Surgery. Spine Biomechanics: Evaluation of Motion Preservation Devices and Relevant Terminology*, Vol. 1, No. 1, 2005, pp. 13–21.

[6] Cripton, P. A., Oxland, T. R., and Zhu, Q., "The Use of Helical Axis of Motion and Facet Joint Load Information in the Evaluation of Nonfusion Spinal Implants: Concept and Preliminary Results," Roundtables in Spine Surgery. *Spine Biomechanics: Evaluation of Motion Preservation Devices and Relevant Terminology*, Vol. 1, No. 1, 2005, pp. 22–30.

[7] Panjabi, M. M., Abumi, K., Duranceau, J., and Crisco, J. J., "Biomechanical Evaluation of Spinal Fixation Devices: II. Stability Provided by Eight Internal Fixation Devices," *Spine*, Vol. 13, No. 10, 1988, pp. 1135–1140.

[8] Yamamoto, I., Panjabi, M. M., Crisco, T., and Oxland, T., "Three-Dimensional Movements of the Whole Lumbar Spine and Lumbosacral Joint," *Spine*, Vol. 14, No. 11, 1989, pp. 1256–1260.

[9] Schmoelz, W., Huber, J. F., Nydegger, T., Claes, L., and Wilke, H. J., "Dynamic Stabilization of the Lumbar Spine and its Effects on Adjacent Segments: An In Vitro Experiment," *J. Spinal Disord. Tech.*, Vol. 16, No. 4, 2003, pp. 418–423.

[10] Niosi, C. A., Zhu, Q. A., Wilson, D. C., Keynan, O., Wilson, D. R., and Oxland, T. R., "Biomechanical Characterization of the Three-Dimensional Kinematic Behavior of the Dynesys Dynamic Stabilization System: An In Vitro Study," *Eur. Spine. J.*, Vol. 15, No. 6, 2006, pp. 913–922.

[11] Wilke, H.-J., Schmidt, H., Werner, K., Schmölz, W., and Drumm, J., "Biomechanical Evaluation of a New Total Posterior-Element Replacement System," *Spine*, Vol. 31, No. 24, 2006, pp. 2790–2796.

[12] Panjabi, M. M., Henderson, G., James, Y., and Timm, J. P., "StabilimaxNZ Versus Simulated Fusion: Evaluation of Adjacent-Level Effects," *Eur. Spine J.*, Vol. 16, No. 12, 2007, pp. 2159–2165.

[13] Gédet, P., Haschtmann, D., Thistlethwaite, P. A., and Ferguson, S. J., "Comparative Biomechanical Investigation of a Modular Dynamic Lumbar Stabilization System and the Dynesys System," *Eur. Spine J.*, Vol. 18, No. 10, 2009, pp. 1504–1511.

[14] Patwardhan, A. G., Havey, R. M., Meade, K. P., Lee, B., and Dunlap, B., "A Follower Load Increases the Load-Carrying Capacity of the Lumbar Spine in Compression," *Spine*, Vol. 24, No. 10, 1999, pp. 1003–1009.

[15] Nachemson, A. "The Load on Lumbar Disks in Different Positions of the Body," *Clin. Orthop. Relat. Res.*, Vol. 45, 1966, pp. 107–122.

[16] Sato, K., Kikuchi, S., and Yonezawa, T., "In Vivo Intradiscal Pressure Measurement in Healthy Individuals and in Patients with Ongoing Back Problems," *Spine*, Vol. 24, No. 23, 1999, pp. 2468–2474.

[17] Wilke, H.-J., Neef, P., Caimi, M., Hoogland, T., and Claes, L. E., "New In Vivo Measurements of Pressures in the Intervertebral Disc in Daily Life," *Spine*, Vol. 24, No. 8, 1999, pp. 755–762.

[18] Wilke, H.-J., Neef, P., Hinz, B., Seidel, H., and Claes, L., "Intradiscal Pressure Together with Anthropometric Data – A Data Set for the Validation of Models," *Clin. Biomech.*, Vol. 16, Suppl. 1, 2001, pp. S111–S126.

[19] Janevic, J., Ashton-Miller, J. A., and Schultz, A. B., "Large Compressive Preloads Decrease Lumbar Motion Segment Flexibility," *J. Orthop. Res.*, Vol. 9, No. 2, 1991, pp. 228–236.

[20] Cripton, P. A., Bruehlmann, S. B., Orr, T. E., Oxland, T. R., and Nolte, L.-P., "In Vitro Axial Preload Application During Spine Flexibility Testing: Towards Reduced Apparatus-Related Artefacts," *J. Biomech.*, Vol. 33, No. 12, 2000, pp. 1559–1568.

[21] Patwardhan, A. G., Havey, R. M., Carandang, G., Simonds, J., Voronov, L. I., Ghanayem, A. J., Meade, K. P., Gavin, T. M., and Paxinos, O., "Effect of Compressive Follower Preload on the Flexion-Extension Response of the Human Lumbar Spine," *J. Orthop. Res.*, Vol. 21, 2003, pp. 540–546.

[22] Tawackoli, W., Marco, R., and Liebschner, M. A. K., "The Effect of Compressive Axial Preload on the Flexibility of the Thoracolumbar Spine," *Spine*, Vol. 29, No. 9, 2004, pp. 988–993.

[23] Pearcy, M. J., "Stereo Radiography of Lumbar Spine Motion," *Acta Orthop. Scand.*, Vol. 56, Suppl. 212, 1985, pp. 1–45.

[24] Panjabi, M. M., Krag, M. H., and Goel, V. K., "A Technique for Measurement and Description of Three-Dimensional Six Degree-of-Freedom Motion of a Body Joint with an Application to the Human Spine," *J. Biomech.*, Vol. 14, No. 7, 1981, pp. 447–460.

[25] Spoor, C. W. and Veldpaus, F. E., "Rigid Body Motion Calculated from Spatial Coordinates of Markers," *J. Biomech.*, Vol. 13, No. 4, 1980, pp. 391–393.

[26] Potvin, J. R., McGill, S. M., and Norman, R. W., "Trunk Muscle and Lumbar Ligament Contributions to Dynamic Lifts with Varying Degrees of Trunk Flexion," *Spine*, Vol. 16, No. 9, 1991, pp. 1099–1107.

[27] McGill, S. M., "Estimation of Force and Extensor Moment Contributions of the Disc and Ligaments at L4-L5," *Spine*, Vol. 13, No. 12, 1988, pp. 1395–1402.

[28] Freudiger, S., Dubois, G., and Lorrain, M., "Dynamic Neutralisation of the Lumbar Spine Confirmed on a New Lumbar Spine Simulator In Vitro," *Arch. Orthop. Trauma Surg.*, Vol. 119, 1999, pp. 127–132.

[29] Adams, M. A. and Dolan, P., "A Technique for Quantifying the Bending Moment Acting on the Lumbar Spine In Vivo," *J. Biomech.*, Vol. 24, No. 2, 1991, pp. 117–126.

[30] Renner, S. M., Natarajan, R. N., Patwardhan, A. G., Havey, R. M., Voronov, L. I., Guo, B. Y., Andersson, G. B. J., and An, H. S., "Novel Model to Analyze the Effect of Large Compressive Follower Pre-Load on Range of Motions in a Lumbar Spine," *J. Biomech.*, Vol. 40, No. 6, 2007, pp. 1326–1332.

[31] Panjabi, M. M., Yamamoto, I., Oxland, T. R., and Crisco, J. J., "Helical Axes of Motion Change with Lumbar Vertebral Level," *Trans. Annu. Meet. – Orthop. Res. Soc.*, Anaheim, California, 1991.

[32] Pearcy, M. J. and Bogduk, N., "Instantaneous Axes of Rotation of the Lumbar Interverteberal Joints," *Spine*, Vol. 13, No. 9, 1988, pp. 1033–1041.

[33] Haberl, H., Cripton, P. A., Orr, T.-E., Beutler, T., Frei, H., Lanksch, W. R., and Nolte, L.-P., "Kinematic Response of Lumbar Functional Spinal Units to Axial Torsion With and Without Superimposed Compression and Flexion/Extension," *Eur. Spine J.*, Vol. 13, No. 6, 2004, pp. 560–566.

[34] Kettler, A., Marin, F., Sattelmayer, G., Mohr, M., Mannel, H., Dürselen, L., Claes, L., and Wilke, H. J., "Finite Helical Axes of Motion are a Useful Tool to Describe the Three-Dimensional In Vitro Kinematics of the Intact, Injured, and Stabilized Spine," *Eur. Spine J.*, Vol. 13, No. 6, 2004, pp. 553–559.

[35] Yoshioka, T., Tsuji, H., Hirano, N., and Sainoh, S., "Motion Characteristic of the Normal Lumbar Spine in Young Adults: Instantaneous Axis of Rotation and Vertebral Center of Motion Analyses," *J. Spinal Disord.*, Vol. 3, No. 2, 1990, pp. 103–113.

[36] Zhao, F., Pollintine, P., Hole, B. D., Dolan, P., and Adams, M. A., "Discogenic Origins of Spinal Instability," *Spine*, Vol. 30, No. 23, 2005, pp. 2621–2630.

[37] Gertzbein, S. D., Seligman, J., Holtby, R., Chan, K. H., Kapasouri, A., Tile, M., and Cruickshank, B., "Centrode Patterns and Segmental Instability in Degenerative Disc Disease," *Spine*, Vol. 10, No. 3, 1985, pp. 257–261.

[38] Schmoelz, W., Onder, U., Martin, A., and von Strempel, A., "Non-Fusion Instrumentation of the Lumbar Spine with a Hinged Pedicle Screw Rod System: An In Vitro Experiment," *Eur. Spine J.*, Vol. 18, No. 10, 2009, pp. 1478–1485.

[39] White, A. A. and Panjabi, M.M., *Clinical Biomechanics of the Spine*, 2nd ed., J.B. Lippincott Company, Philadelphia, PA, 1990, pp. 46–49.

[40] Thompson, R. E., Barker, T. M., and Pearcy, M. J., "Defining the Neutral Zone of Sheep Intervertebral Joints During Dynamic Motions: An In Vitro Study," *Clin. Biomech.*, Vol. 18, 2003, pp. 89–98.

[41] Guan, Y., Yoganandan, N., Moore, J., Pintar, F. A., Zhang, J., Maiman, D. J., and Laud, P., "Moment-Rotation Responses of the Human Lumbosacral Spinal Column," *J. Biomech.*, Vol. 40, 2007, pp. 1975–1980.

[42] Busscher, I., van Dieën, J. H., Kingma, I., van der Veen, A. J., Verkerke, G. J., and Veldhuizen, A. G., "Biomechanical Characteristics of Different Regions of the Human Spine – An In Vitro Study on Multilevel Spinal Segments," *Spine*, Vol. 34, No. 26, 2009, pp. 2858–2864.

Reprinted from JAI, Vol. 8, No. 10
doi:10.1520/JAI103562
Available online at www.astm.org/JAI

R. E. Thompson,[1] *O. Schwarzenbach,*[2] *J. Seebeck,*[3] *and M. Fröhlich*[3]

Primary Stability of a Dynamic Artificial Disc Tested in a Human Cadaveric Model

ABSTRACT: Sufficient anchorage of an interbody device will allow osseointegration and avoid implant migration. Shear forces in the lumbar spine are transferred across the bone/implant interface, resulting in relative motion between the implant and bone. Relative motion greater than 150 μm will have a detrimental effect on the osseointegration of titanium (Ti) implants. This study developed an in vitro, primary stability testing protocol to assess a total disc replacement (TDR). Testing was performed on seven human cadaveric L4 and L5 vertebrae. Cyclic shear loading of the prepared implant/bone interface was applied for 20 cycles in the anterior and posterior directions to $\pm$350 N under an axial compressive load of 600 N. The relative motion was measured and the average of the last five cycles analysed. The shear force necessary to cause complete anterior migration of the TDR was also measured. The averaged cyclic motion for the last five cycles in both the anterior and posterior directions was below 85 μm for all specimens. The average yield force for complete anterior implant migration was 522.2 N ($\pm$105.9 N) and the failure force was 605.1 N ($\pm$118.4 N). A primary stability testing protocol was developed and employed to assess a TDR in human cadaveric bone. The measured relative motion for this TDR for each loading cycle was below 150 μm, which is favourable for osseointegration with the vertebral body endplates.

KEYWORDS: lumbar total disc replacement, primary stability, shear

Manuscript received November 10, 2010; accepted for publication July 7, 2011; published online October 2011.
[1] Ph.D., Zimmer GmbH, Winterthur, Switzerland.
[2] M.D., Das Rückenzentrum, Thun, Switzerland.
[3] M.Sc., Zimmer GmbH, Winterthur, Switzerland.
Symposium on Static and Dynamic Spinal Implants: Are We Evaluating Them Appropriately?

Cite as: Thompson, R. E., Schwarzenbach, O., Seebeck, J., and Fröhlich, M., "Primary Stability of a Dynamic Artificial Disc Tested in a Human Cadaveric Model," *J. ASTM Intl.*, Vol. 8, No. 10. doi:10.1520/JAI103562.

Introduction

Disc degeneration has been indicated as a contributor to low back pain and interbody implants such as cages and total disc replacements (TDR) have been developed in an attempt to alleviate the pain by removal of the disc tissue and restoration of the disc height. The most frequently operated lumbar levels are L4/L5 and L5/S1. The lower lumbar levels experience the highest loading in the spinal canal due to a combination of the lordotic positioning of the vertebrae and moments caused by the torso's centre of mass and lifting objects with the arms. Forces in the anterior direction up to 350 N are expected to be distributed over the passive lower lumbar segments in an upright position when holding up to 20 kg in the arms [1].

For an interbody device, part of this anterior force is transferred from vertebrae to vertebrae as a shear force between the implant endplate and the vertebral body endplate. In the absence of mechanical fasteners, such as screws to the bone, the interface between the implant and bone has to provide sufficient resistance to this shear force immediately after the surgery to ensure stability of the implant. This resistance is called primary stability and one goal of an interbody device is to provide sufficient primary stability to achieve a strong secondary stability through osseointegration.

Kienapfel et al. [2] describe four implant requirements for osseointegration. These are:

1. Biocompatibility.
2. Implant surface geometry characteristic—optimal surface conditions for osseointegration include an open pore structure in the range of 100–400 μm.
3. Implant/bone interface distance—direct contact between the bone and implant improves the chance of osseointegration. It is also generally accepted that implant contact to bleeding bone is superior to nonbleeding bone.
4. Micromotion—It has been found that small amounts of relative motion at the interface between the bone and implant do not have a deleterious effect on osseointegration. Up to a threshold, relative motion does not result in separation of the implant endplate with the newly connected bone, but rather produces an elastic strain loading on the tissue, which potentially stimulates more bone growth. However, above this threshold, motion damages the cellular connection and results in fibrous tissue encapsulation rather than osseointegration. This upper limit depends on the surface structure of the implant [3]. For bioinert surfaces such as titanium (Ti), this limit exists in the range of 50–150 μm [3,4]. In orthopaedic biomechanics, 150 μm has been used as the "rule of thumb" maximum allowable relative motion between an implant and bone, whereas in dental biomechanics, a more conservative value of 100 μm has been assumed [5].

The DYNARDI dynamic articulating disc is a first generation TDR that is CE-marked, but not available in the United States. It aims to treat low back pain indicated by intervertebral disc degeneration by replacing the disc tissue with two cobalt-chromium-molybdenum (CoCrMo) endplates and an intervening

FIG. 1—*The DYNARDI total disc replacement (Ti, titanium; PE, polyethylene; CoCrMo, cobalt–chromium–molybdenum).*

polyethylene insert (Fig. 1). The ranges of motion of the DYNARDI are 20° in flexion, −10° in extension, ±15° in lateral bending and unconstrained in axial rotation. The medio-lateral and anterio-posterior translations are both ±1.3 mm. All elements of the DYNARDI are sterilised through a gamma radiation sterilisation process. The surface of the CoCrMo endplate in contact with the bone is vacuum plasma sprayed (VPS) with Ti to improve osseointegration. Ti is a biocompatible material that allows the bone growth at the interface to be contact osteogenesis (i.e., the osteoblasts are seeded at the interface and the bone growth front moves away from the interface toward the old bone) [6]. Also, the VPS procedure produces a porous Ti surface that is favourable for oseointegration. The surgical technique for implanting the DYNARDI includes reaming the surface of the vertebral body bone to seat the insertion channel and dome of the DYNARDI endplate. Hence, the instruments ensure that at least the portion of the implant positioned in the reamed space is in direct contact to bloody bone. These features are favourable for osseointegration. However, it is unknown if the relative motion between the DYNARDI endplate and the vertebral body bone under physiological loading conditions is below the recommended threshold.

This study aims to develop an in vitro, primary stability testing protocol involving cyclic shear loading of the implant/bone interface in the anterior and posterior shear directions to ±350 N under an axial load of 600 N representing the neutral position [1]. The primary stability of the DYNARDI TDR will then be assessed under these conditions.

Materials and Methods

Specimens

Four, whole lumbar spines from deceased persons with no history of back pain were included in this study. Ethical approval was obtained through the

Kantonale Ethikkommission Zürich, Switzerland (Ref No. 02/2006). Specimens were stored at −20°C until required for implantation and testing.

Prior to implantation, the specimens were thawed and excess soft tissue removed. For all specimens, the L4/L5 level was implanted with an appropriately sized DYNARDI by a trained spine surgeon according to the surgical technique. Each implantation produced two test specimens (the L4 inferior endplate and the L5 superior endplate). Details of the specimens and implant sizes are given in Table 1.

After implantation, the L4 and L5 vertebrae were isolated from the lumbar spine and stored with their respective DYNARDI endplate at −20°C until required for testing. Prior to testing, the vertebrae and endplates were thawed and all soft tissue and the posterior elements removed such that only the vertebral body was remaining. To facilitate attachment to the testing machine, the vertebral body and DYNARDI endplate were embedded in separate polymethylmethacrylate (PMMA) blocks (Beracryl, Troller-Kunststoffe AG, Fulenbach, Switzerland) using a custom jig that ensured correct alignment.

Test Setup

Testing was performed on a Zwick 1456-60 materials testing machine (Zwick, Ulm, Germany) combined with a custom-made apparatus incorporating two linear bearings, an actuator and load cell (Fig. 2). The potted vertebral body was attached to a horizontal linear bearing such that the longitudinal axis of the vertebral body was aligned with the horizontal axis of the bearing (similar to supine positioning of the spine). A vertical linear bearing provided an attachment point for the embedded DYNARDI endplate to the Zwick machine. In this configuration, the DYNARDI endplate was oriented in the vertical plane such that it mated with the prepared vertebral body endplate. The anterior direction of the vertebral body and endplate was always aligned with an upward movement of the Zwick crosshead.

A constant, axial, compressive load normal to the interface between the vertebral body and DYNARDI endplate was provided by a pneumatic actuator. The magnitude of this axial force was measured by a load cell attached to the actuator. Shear displacement and loading of the interface between the vertebral body

TABLE 1—*Test specimen details.*

Test ID	Level	Age, Years	Sex	Cause of Death	Implant Size
Spec 1	L5	76	M	Liposarkoma	Endplate: 3
Spec 2	L4				Inlay: 3S
Spec 3	L4	68	F	Mesenterial infarct	Endplate: 3
Spec 4	L5				Inlay: 3S
Spec 5	L5	24	M	Subdural bleeding	Endplate: 4
Spec 6	L4				Inlay: 4S
Spec 7	L4	77	M	KHK cancer	Endplate: 3
Spec 8	L5				Inlay: 3S

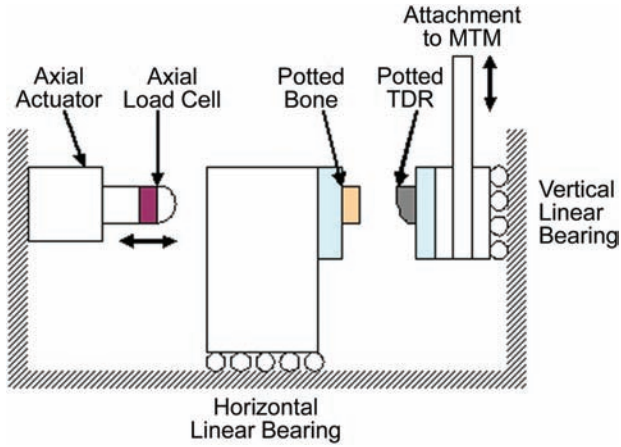

FIG. 2—*Schematic of the testing jig (TDR, total disc replacement; MTM, materials testing machine).*

and endplate was controlled by the vertical actuator and load cell of the Zwick machine. Relative motion between the PMMA block containing the DYNARDI endplate and the PMMA block containing the vertebral body bone was measured with a high-resolution extensometer (M-DVRT-3, Microstrain, VT).

Test Parameters

A static axial compressive load of 600 N was applied by the pneumatic actuator normal to the bone/implant interface for 30 min before the testing began to allow for application of the extensometer to the consolidated specimen. This axial load was held constant throughout the entire test to represent the compressive loading in the spinal column in a neutral standing position [1]. All tests were performed in air at room temperature.

The testing involved performing an anterior cyclic shear test, a posterior cyclic shear test, and finally an anterior shear failure test for each specimen. Testing began with either an anterior or posterior test, the order of which was alternated from specimen to specimen to reduce any influence of test order. Before the anterior and posterior cyclic tests commenced, five cycles from 0 N to either +200 or −200 N, respectively, were applied to precondition the specimen for loading in each direction. The shear cyclic tests were performed in shear force control with a triangular waveform at 50 N/s (0.071 Hz) from 0 to +350 N for the anterior direction and from 0 to −350 N for the posterior direction. Twenty cycles in each direction were performed at 0.7 Hz as pretests showed that this was sufficient to characterise the shear behaviour of the DYNARDI endplate with the vertebral body bone. The relative motion in the anterior and posterior directions between the DYNARDI endplate and the vertebral body was measured with the extensometer. After completion of the cyclic tests, the failure force to cause complete anterior migration of the implant from

the bone was measured by performing a shear displacement controlled test at 1 mm/s for 5 mm.

BMD Measurements

Bone mineral density (BMD) measurements of all specimens were made after testing in one session on a dual-energy X-ray absorptiometry machine. anterior/posterior (AP), lateral and lateral-mid (i.e., not including vertebral endplates or AP cortical walls) measurements were taken and linear regression analysis was used to see if a correlation between the shear properties of the DYNARDI and bone quality exists. Due to the fact that the specimens had no posterior elements and that the cortical bone structure had been disrupted by endplate preparation, insertion of embedding screws and testing, it is only valid to consider the BMD measurements as relative values within the group. It was not possible to determine the absolute bone quality and presence of osteoporosis or osteopenia for these specimens.

Analysis

Shear relative motion data between the implant and bone PMMA blocks and shear force were collected at 35 Hz through the Zwick controller.

Two displacement parameters were determined from the cyclic loading data. These were the micromotion for each cycle to assess the osseointegration potential of the endplate, and the total endplate displacement (TED) to assess the final relative position of the inferior and superior endplates when osseointegration is achieved. The micromotion for each cycle was defined as the relative displacement from the beginning to the end of the loading part of each cycle as measured by the extensometer (see Fig.3). It was analysed by averaging the relative motion of the last five cycles and comparing this average with the threshold value of 150 μm.

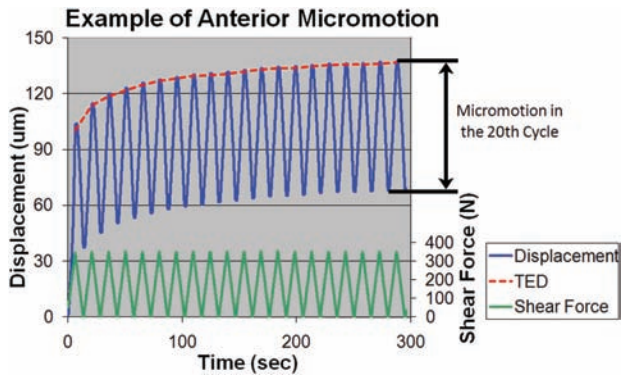

FIG. 3—*Anterior micromotion for a specimen showing the displacement parameters of micromotion andTED.*

The TED was defined as the absolute displacement at the end of each loading cycle from the initial position (see Fig. 3) and was modelled to determine the creeping migration behaviour of the endplate before osseointegration. Given the shape of the time versus total endplate displacement curve, the data could have represented either an exponential or a logarithmic progression. Both curve types were fit to the data using the Curve Fitting Toolbox in Matlab 7.0.0 r14 (The Mathworks Inc, MA) and the most accurate model was determined by observing the standardised residuals. Standardised residuals indicate the variation of the experimental data with the modelled data and should be randomly distributed with a mean of 0 and 95 % of the data points lying between 2 and −2 [7]. To use the logarithmic function, the model needed to be in the positive quadrant. Therefore, to have minimal influence on the characteristics of the raw data, the posterior displacement data were mirrored about the x axis into the positive quadrant by taking the absolute value of the raw data.

The yield shear force could clearly be defined as the first critical point in the force–displacement curve (see Fig. 4). Due to the data acquisition frequency and the trend for the force to continue increasing beyond this critical point to the ultimate failure force, in some cases the calculated derivative of the force–-displacement curve did not reach 0. In all cases; however, the derivative of the force displacement curve reached lower than 2 N/mm. Hence, the yield force was calculated by determining the force in the force–displacement curve, where the slope of the curve dropped below 2 N/mm. The ultimate failure shear force was defined as the maximum shear force measured. Means and standard deviations of these parameters were calculated.

Correlations between the BMD measurements (AP, lateral, and lateral-mid) with micromotion (anterior and posterior) and shear force measurements (yield and ultimate shear force) were made by performing single linear regressions between the variables and determining the coefficient of determination: R^2. Presence of a correlation was investigated when R^2 was greater than 0.8.

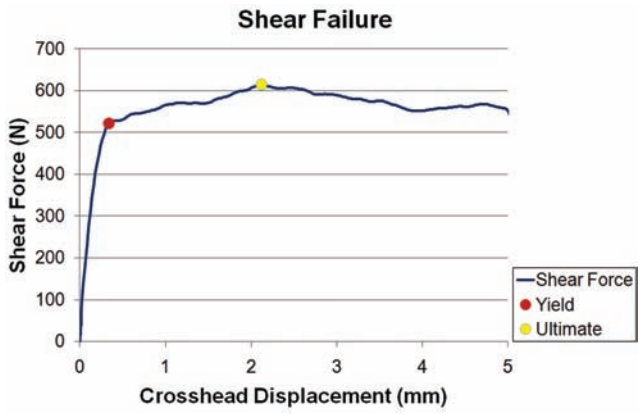

FIG. 4—*Shear force versus crosshead displacement graph for a specimen indicating the yield force and ultimate shear force.*

TABLE 2—*BMD measurement values.*

	BMD Measurements, g/cm^2		
Test ID	AP	Lat	Lat (Mid)
Spec1	0.694	0.824	0.884
Spec2	0.521	0.615	0.662
Spec3	0.460	0.497	0.574
Spec4	0.464	0.608	0.671
Spec5	0.615	0.769	0.912
Spec6	0.599	0.708	0.739
Spec7	0.601	0.636	0.647
Spec8	0.594	0.716	0.725

Results

Spec4 was excluded from the analysis as the bone failed on the first cycle to 350 N. Visual inspection of the vertebral body before testing showed disruptions in the bony endplate and after the test, collapse of the vertebral body was evident. The BMD measurements for Spec4 was in the lower range of the group; however, it was not considerably different to other test specimens (see Table 2).

The average anterior and posterior micromotions, yield force, and ultimate force are shown for each specimen in Table 3. The average anterior and posterior micromotions for each specimen are also compared graphically with the accepted upper maximum allowed relative motion in orthopaedic biomechanics (150 μm) and also the more conservative value accepted in dental biomechanics (100 μm) in Fig. 5.

Analysis of the standardised residuals from the modelled total displacement of the endplate showed that the logarithmic model was a better fit to the

TABLE 3—*Individual specimen results.*

Test ID	Anterior Micromotion (±SD), μm	Posterior Micromotion (±SD), μm	Yield Force, N	Ultimate Force, N
Spec1	84.9 (±1.4)	−55.6 (±1.2)	477.8	550.1
Spec2	70.7 (±2.4)	−77.9 (±1.4)	480.8	480.8
Spec3	74.7 (±0.8)	−70.2 (±0.8)	432.2	456.6
Spec4	…	…	…	…
Spec5	57.9 (±0.2)	−39.2 (±0.5)	527.1	614.9
Spec6	44.0 (±0.7)	−54.4 (±0.7)	450.4	650.9
Spec7	56.2 (±0.3)	−50.7 (±0.7)	541.2	694.1
Spec8	67.7 (±0.2)	−64.0 (±1.3)	745.6	788.0
Mean	…	…	522.2	605.1
SD	…	…	105.9	118.4

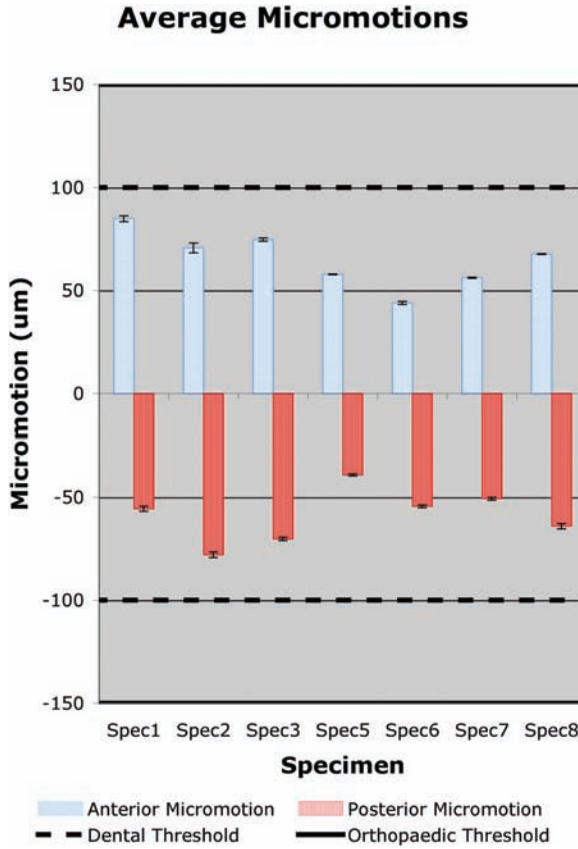

FIG. 5—*Average anterior and posterior micromotion for each specimen.*

maximum cycle displacement data than the exponential model. With the logarithmic model, all residuals were randomly distributed except for Spec7 in the anterior direction and Spec8 in the posterior direction. With the exponential model, the residuals of only half of the displacement curves were randomised. An example of this analysis is shown in Fig. 6.

The logarithmic equation had the form

$$\text{Total endplate displacement} = A\ln(B\text{Time} + C) + D \quad (1)$$

where:

Total endplate displacement = maximum endplate displacement, μm, after a period of continuous cyclic displacement,

A, B, C and D = constants, and

Time = period of time of continuous cyclic loading, s.

The calculated constants for Eq 1 for each specimen are given in Tables 4 and 5 for the anterior and posterior directions, respectively.

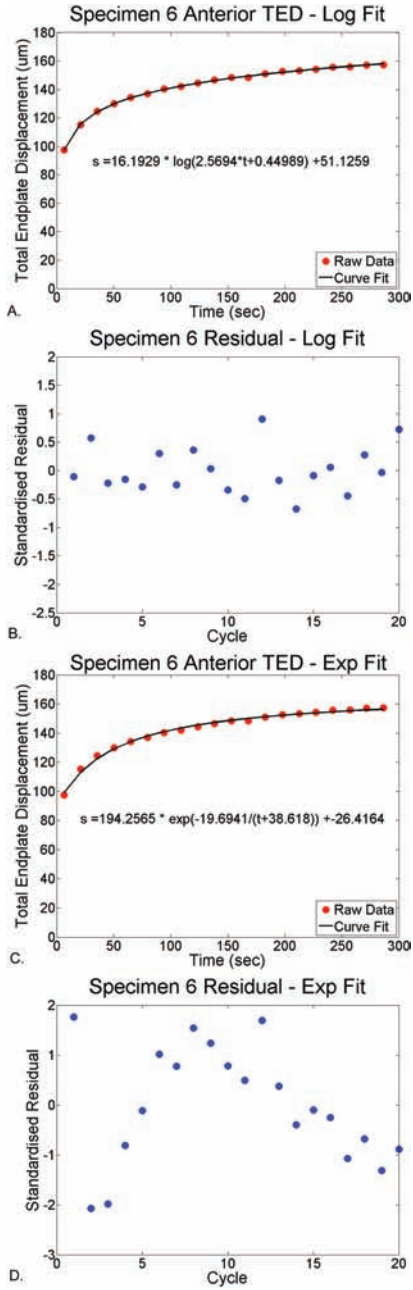

FIG. 6—*Model fitting for the TED in the anterior direction of the DYNARDI endplate for Spec6. (A) Logarithmic curve fit to the raw data, (B) standardised residuals of the logarithmic fit (randomly distributed), (C) exponential curve fit to the raw data, and (D) standardised residuals of the exponential fit (inverted V shape).*

TABLE 4—*Constants for the TED in the anterior direction.*

	Equation 1 Constants			
Test ID	*A*	*B*	*C*	*D*
Spec1	25.6	10.7	24.1	62.7
Spec2	33.1	8.2	44.7	59.6
Spec3	10.4	62.3	−228.8	111.5
Spec4	…	…	…	…
Spec5	7.6	18.4	−79.0	70.9
Spec6	16.2	2.6	0.4	51.1
Spec7	1.0	21.9	−141.9	85.0
Spec8	8.3	15.8	−49.2	67.1

No correlation was found between the BMD measurements and the micromotions or shear force measurements.

Discussion

The developed primary stability test setup aimed to test the interbody device under physiological loading conditions in the neutral position indicative of the environment immediately postsurgery. However, for assessment of a device's safety and effectiveness, testing must be performed under worst case loading regimes. Physiological loading conditions in the lumbar spine consist of an axial compression force and an anterior force that results in a shear force in the disc space. The lowest axial compressive force expected in the lumbar spine is 600 N, coupled with an anterior force of 350 N representing the neutral position [1]. The axial force has been shown to increase during activities such as bending or holding weights in the hands. However, a higher compressive force would increase the frictional resistance of an interbody device with the bone; thus potentially artificially increasing the measured primary stability. Conversely, a

TABLE 5—*Constants for the TED in the posterior direction.*

	Equation 1 Constants			
Test ID	*A*	*B*	*C*	*D*
Spec1	7.6	0.57	3.82	45.9
Spec2	19.4	0.70	15.7	50.7
Spec3	13.6	0.20	3.75	46.8
Spec4	…	…	…	…
Spec5	1.4	35.6	−42.0	34.0
Spec6	11.8	0.81	1.87	37.5
Spec7	13.4	0.22	2.82	43.0
Spec8	16.2	0.61	3.54	41.5

higher compressive force tends to be coupled with a higher anterior force under physiological loading conditions. Potvin et al. found that compressive loads ranging from approximately 3000 to 5000 N could be expected with an anterior force or approximately 500 N when subjects lifted objects ranging in weight from 6 to 32 kg without bending the knees [8]. It is unknown which scenario creates a worst case loading environment for measuring relative motion between an interbody device and the vertebral bone. It may well be that the worst case loading environment is device dependent. Determining the worst case loading environment would be an important starting point for future investigations in this field.

The applied shear force of 350 N represents the anterior force expected in the lower lumbar spine when carrying a weight of 20 kg in the hands [1]. In the intact spine, this force would be resisted by the ligamentous structures and the zygopophysial joints. The load sharing relationship between the ligamentous structures and the zygopophysial joints in shear is unclear. Therefore, it was assumed that 100 % of this anterior force was resisted in the intervertebral disc space and would be transmitted as a shear force across the bone/implant interface.

The applications of the cyclic shear load at the implant/bone interface in the anterior and posterior directions were separated such that only unidirectional load cases were employed. Additionally, these unidirectional load cases were kept separated and not summed together for the assessment of micromotion and TED. This was considered appropriate because throughout the entire range of motion, the AP force on the lower lumbar spine changes in magnitude, but not in direction [9]. This AP load is then transferred to the vertebral bodies as a shear force between the implant and the vertebral endplate. Therefore, assuming that the interbody device acts independently to stabilise the spine in shear, the direction of the shear force depends only on the position of the endplate (for superior endplates, the shear force is posterior and for the inferior endplate, the shear force is anterior).

In the current experiment, it was necessary to define two displacement parameters to fully characterise the motion between the implant endplate and the bone. The micromotion was a measure of the displacement recorded during the loading portion of each cycle. This parameter gives the best indication for osseointegration. Once bone has begun to osseointegrate into an implant surface, the success of the bond will depend on whether relative motion between the implant and bone surfaces preserves or damages the newly formed bone. The threshold for the maximum allowable micromotion to preserve the newly formed bone in orthopaedic biomechanics and dental biomechanics is 150 and 100 μm, respectively. It is difficult to understand why these threshold values differ. Certainly orthopaedic implants are subjected to higher loads, likely resulting in a higher amount of micromotion at the bone/implant interface compared to dental implants. Also, the bone composition of cancellous and cortical bone and the blood supply in the target implantation areas are different. However, the mechanisms governing bone remodelling and osseointegration should be similar in both fields, so it is questionable that the maximum allowable micromotion should be different depending on the implant application. Literature

suggests that the threshold lies in the range of 50–150 μm. Jasty et al. [4] found evidence of bone ingrowth into implants stimulated to 150 μm; however this bone was disconnected to the surrounding host bone through trabecular microfractures. This suggests that even under high relative motions, the initiation of osseointegration is possible. However, the repetitive nature of large cyclic micromotions has a detrimental effect on the healing of the bone at the bone/implant interface. Given that dental implants tend to achieve a higher rate of osseointegration than orthopaedic implants, it may be prudent in future biomechanical assessments to reduce the threshold for the maximum allowable micromotion to 100 μm.

In this study, the cyclic micromotion was not completely recovered on unloading, resulting in a gradual creep of the endplate position from the original, implanted position. This second displacement measure was termed the total endplate displacement. Beyond the first five cycles, the change in the TED was small in comparison to the micromotion measured. As bone is a living tissue and able to adapt to small changes in its environment it is unlikely that the TED will have much influence on whether or not osseointegration occurs. However, it does give an indication on whether the implant will function appropriately in its final position when osseointegration occurs.

The TED measured in this study was found to increase logarithmically with time rather than exponentially. This suggests that the implant will continue to creep from its implanted position until osseointegration occurs. However, the model used to calculate the TED assumes that osseointegration is an instantaneous occurrence and does not take into consideration the gradual stability gained through the osseointegration process. It is possible that, provided the micromotion is below the threshold, the osseointegration process in vivo will result in an exponential behaviour of the TED. However, further investigation is required to support this.

The micromotions of the DYNARDI endplate in the anterior and posterior directions for all specimens in this study were below 85 μm and therefore were consistently below the maximum accepted threshold values for both orthopaedic and dental biomechanics. However, nearly all micromotions measured were higher than the lower threshold limit of 50 μm. Given that osseointegration can be initiated with micromotions as high as 150 μm, it is likely that this will also occur for the DYNARDI endplate. With the initiation of osseointegration, it is anticipated that the resistance to the shear loading will increase, resulting in less cyclic micromotion and further enhancing the possibility of implant osseointegration.

The failure force measured to cause complete anterior migration was approximately 1.7 times higher than the shear force applied in this study. Therefore, it is unlikely that complete anterior migration of the DYNARDI endplate will occur under physiological loading conditions in the neutral position.

BMD measurements of the vertebral bodies did not provide a clinical, predictive measure for the primary stability performance of the DYNARDI endplate. It appears that the shear interaction of the DYNARDI endplate with the vertebral body endplate is independent of the overall bone mass of the vertebral body. However, pathological irregularities in the vertebral body endplate in

combination with the endplate preparation may have a detrimental effect on performance of the DYNARDI, as seen with Spec4.

The use of cadaveric material to assess primary stability is essential as the frictional properties between the implant and bone are of vital importance. However, testing with cadaveric material has inherent limitations. To reduce the influence of the small sample size and large interspecimen variability, each specimen in this study was used to assess the primary stability in both the anterior and posterior directions even though, as described previously, only unidirectional loading would be expected in vivo. With a larger sample size, this would not have been necessary. The employed testing conditions also do not attempt to mimic the in vivo environment as testing was performed at room temperature in the absence of a humidity chamber. As this testing was only concerned with the metal endplate in contact with the cortical bone, it is unlikely that this had an effect on the measured primary stability parameters. The inability of cadaveric tissue to remodel and osseointegrate is also a limitation of this study. While this would have had a minimal effect on the measured micromotion, the TED is strongly influenced by the ability of live tissue to bond with the endplate, as described previously. Nevertheless, the developed primary stability testing protocol could give an indication of the positional safety immediately after surgery and the likelihood that osseointegration would occur for the tested TDR.

Conclusions

In this study, a primary stability testing protocol to assess interbody devices in the neutral position was developed. This protocol required that motion of the device relative to human, cadaveric endplate bone be less that 150 μm when subjected to a constant, axial compressive load of 600 N and cyclic shear loading up to $\pm$350 N in the anterior and posterior directions. Under these loading conditions, relative motion of the DYNARDI endplate was consistently below 150 μm, indicating that osseointegration of the endplates is likely.

Acknowledgments

The authors are either employees of the device manufacturer or receive financial benefit from the tested device.

References

[1] Shirazi-Adl, A., El-Rich, M., Pop, D. G., and Parnianpour, M., "Spinal Muscle Forces, Internal Loads and Stability in Standing under Various Postures and Loads—Application of Kinematics-Based Algorithm," *Eur. Spine J.*, Vol. 14, 2005, pp. 381–392.

[2] Kienapfel, H., Sprey, C., Wilke, A., and Griss, P., "Implant Fixation by Bone Ingrowth," *J. Arthroplasty*, Vol. 14, 1999, pp. 355–368.

[3] Szmukler-Moncler, S., Salama, H., Reingewirtz, Y., and Dubruille, J. H., "Timing of Loading and Effect of Micromotion on Bone-Dental Implant Interface: Review of Experimental Literature," *J.Biomed. Mater. Res.*, Vol. 43, 1998, pp. 192–203.

[4] Jasty, M., Bragdon, C., Burke, D., O'Connor, D., Lowenstein, J., and Harris, W. H., "In Vivo Skeletal Responses to Porous-Surfaced Implants Subjected to Small Induced Motions," *J. Bone Joint Surg. Am.*, Vol. 79, 1997, pp. 707–714.

[5] Brunski, J. B., "Avoid Pitfalls of Overloading and Micromotion of Intraosseous Implants," *Dent. Implantol. Update*, Vol. 4, 1993, pp. 77–81.

[6] Osborn, J. F., "Biowerkstoffe und ihre. Anwendung bei Implantation [Biomaterials and Their Application to Implantation]," *SSO. Schweiz Monatsschr. Zahnheilkd.*, Vol. 89, 1979, pp. 1138–1139.

[7] Ross, S. M., *Introduction to Probability and Statistics for Engineers and Scientists*, Wiley, New York, 1987, pp. 264–266.

[8] Potvin, J. R., McGill, S. M., and Norman, R.W., "Trunk Muscle and Lumbar Ligament Contributions to Dynamic Lifts with Varying Degrees of Trunk Flexion," *Spine*, Vol. 16, 1991, pp. 1099–1107.

[9] Daggfeldt, K., and Thorstensson, A., "The Mechanics of Back-Extensor Torque Production about the Lumbar Spine," *J. Biomech.*, Vol. 36, 2003, pp. 815–825.

Reprinted from JAI, Vol. 9, No. 2
doi:10.1520/JAI103537
Available online at www.astm.org/JAI

C. Schilling,[1] *S. Krüger,*[2] *J. Beger,*[2] *and C. Wing*[3]

Rationale of a Test Setup with a Defined COR for Extra-Discal Motion-Preserving Implants with a Low Implant Stiffness

ABSTRACT: In the current version of ASTM F2624, the center of rotation (COR) is not specified. Potentially, each device can be tested using a different COR, which subsequently makes a direct design comparison of results difficult. Four posterior dynamic stabilization (PDS) devices (Dynesys, DYN, Zimmer; DSS, Paradigm Spine; and two Aesculap implant concepts) were tested in comparison to a rigid-fixation device and to the native situation of the lumbar spine on fresh-frozen human lumbar spines (L3–L5). The instrumented level was L4–L5. The PDS systems have axial compressive stiffness values ranging from 10 N/mm to 230 N/mm and were all made compatible to connect with the pedicle-screw system. The specimens were loaded in a spinal simulator, applying pure moments for flexion/extension, lateral bending and axial rotation (+/−7.5 Nm) with a defined velocity. The COR was analyzed based on the data measured with a 3-dimensional (3D) motion-analysis system. The effect of the PDS on the location of the COR is most pronounced in the sagittal plane. In general, the higher the implant stiffness, the more the COR shifted in a posterior direction. The DYN had a similar COR to the rigid fixator. However, the PDS systems with low axial compressive stiffness values (range: 10–70 N/mm) showed very similar results on CORs, which are located in the region of the posterior border of the intervertebral disc. In the frontal and transversal plane, the COR was found to be close to the native

Manuscript received November 13, 2010; accepted for publication December 14, 2011; published online February 2012.

[1] M.Sc., Aesculap AG, Research and Development, Biomechanical Research, Am Aesculap Platz, 78532 Tuttlingen, Germany; and Julius Wolff Institute and Berlin-Brandenburg Center for Regenerative Therapies, Charité – Universitätsmedizin Berlin, Berlin, Germany (Corresponding author), e-mail: christoph.schilling@aesculap.de
[2] Aesculap AG, Research and Development, 78532 Tuttlingen, Germany.
[3] Aesculap Implant Systems, Research and Development, Center Valley, PA 18034.

Cite as: Schilling, C., Krüger, S., Beger, J. and Wing, C., "Rationale of a Test Setup with a Defined COR for Extra-Discal Motion-Preserving Implants with a Low Implant Stiffness," *J. ASTM Intl.*, Vol. 9, No. 2. doi:10.1520/JAI103537.

situation for each system. Therefore, for PDS devices with low implant stiffness, the location of the COR varies only marginally and can be specified for a test setup. An initial proposal that will allow side-by-side comparison for these kinds of PDS systems is given and the feasibility of the new test setup could be proven for all three loading conditions.

KEYWORDS: dynamic pedicle-screw system, kinematics, center of rotation, biomechanics, spine

Introduction

Posterior dynamic stabilization (PDS) systems offer an alternative to fusion for the surgical treatment of mild degeneration of the spine. The hypothesis is that the ideal PDS will allow stabilization of an unstable degenerated disc by acting as an internal brace, while at the same time ideally permitting a physiological range of motion. Previous work has shown that some flexible rods (e.g., Dynesys, Zimmer) show comparable stabilization characteristics to solid titanium constructs in flexion, extension, and lateral bending [1–6]. From a clinical standpoint, an overly stiff construct will either lead to fusion or cause screw loosening, breakage, or pull out, as well as limited clinical benefit for pathologies of the affected and adjacent segment disc [7–10]. The ability of the PDS rod to allow axial compression and extension was shown to be vital to enable a more physiological or true dynamic performance [6,11–13].

Preclinical testing of such pedicle-screw-based PDS systems is, however, challenging. The main problem is to find a synthetic model, which takes an appropriate loading of the devices into account to estimate the mechanical performance of the devices *in vivo*. Currently, two standards are available for the preclinical testing of dynamic extra-discal spinal-motion-preserving implants: ISO 12189 and ASTM F2624. Whereas the ISO rationalizes an anterior-load support to mimic a load sharing, the ASTM F2624 follows a kinematic attempt to address loading in the three main motion planes: flexion/extension, lateral bending, and axial rotation. For a direct comparison of different implant designs, both standards have limitations. With the ISO 12189, the loading of the device is dependent on the stiffness of the device itself. Higher implant stiffness causes higher stresses in the implant, but by decreasing the axial stiffness, the main load is increasingly born by the anterior (intra-discal) support. As such, an implant with a low axial stiffness will likely not fail under such a test, even though it may actually well be inadequate in terms of fatigue strength to withstand a true physiological load regimen. The implant performance is also dependent on the test setup and a comparison of different designs is not possible or could be possibly underestimated. ASTM F2624 also has its limitations. Although this test method causes displacements that result in significant loads being applied to less axially stiff implant designs, the center of rotation (COR) is not defined because the COR will vary in accordance with device design and intended use. But there only a rationale for the COR is mentioned, based on an *in vitro* test with non-instrumented functional spinal units (FSU) [14]. In fact,

there is no published data to date on the position of the COR with different PDS systems. The result is that during development and pre-clinical testing, the COR of the particular device must be determined by specification of the expected *in vivo* COR. This requires time-consuming *in vitro* flexibility testing for each device. Also, preclinical testing at independent laboratories or even in the same laboratories on different PDS devices will be performed with a different COR and a direct comparison of different designs is not given. Besides, for the execution of ASTM F2624, a bi-axial testing machine is required for the moment application in the recommended test setup, leading to statically over-determined conditions at the force/moment sensor. In addition, the maximum test frequency will be low for moment application with a torsional cylinder (not more than 2 Hz based on our experience), which leads to time-consuming testing for a recommended endurance limit of 10×10^6 cycles, e.g., 58 test days for one run-out specimen tested at 2 Hz.

The objective of our study was to examine the influence of the location of the COR with respect to the different implant-design characteristics or axial and bending stiffness. For this we performed an *in vitro* flexibility test series to investigate the kinematic behavior of human FSU after stabilization with a diverse range of pedicle-screw-based PDS systems. On the basis of our findings, a proposal for a test setup with specific pivot point for standardized fatigue testing of dedicated PDS devices has been made, considering the use of a uni-axial testing machine.

Materials and Methods

Specimens

Six fresh-frozen human lumbar spines (L3–L5) with a mean age of 67 years (range: 55–77) that had been kept at −21°C in triple-sealed bags were thawed overnight at 6°C before the test. CT scans did not reveal any fractures, osteophytes, or signs of severe disc degeneration. Soft tissue was removed, leaving the ligaments, capsules, and supporting structures intact. To fix the specimens firmly in place on the simulator, the cranial and caudal vertebrae (L3 and L5) were embedded with a casting resin (Ureol FC 53, Vantico GmbH, Wehr, Germany) in the test fixtures so that segmental motion was not restricted in any way and the L3–L4 disc was oriented in the horizontal plane.

Instrumentation

Four devices, "DYN" (Dynesys - Zimmer GmbH Switzerland), "DSS" (Paradigm Spine, Wurmlingen, Germany), and two prototype dynamic rods, "LSC" with a leaf spring , and "STC" with a compression spring (Aesculap AG, Tuttlingen, Germany), were tested in comparison to a rigid-fixation device, S^4 (Aesculap AG, Tuttlingen, Germany) "RIG" (Fig. 1), to the native situation "NAT" and to a defect situation "DEF" of the lumbar spine. The segment condition DEF represents a standardized undercutting decompression, as described by Schulte et al. [5]. The instrumented level was L4–L5.

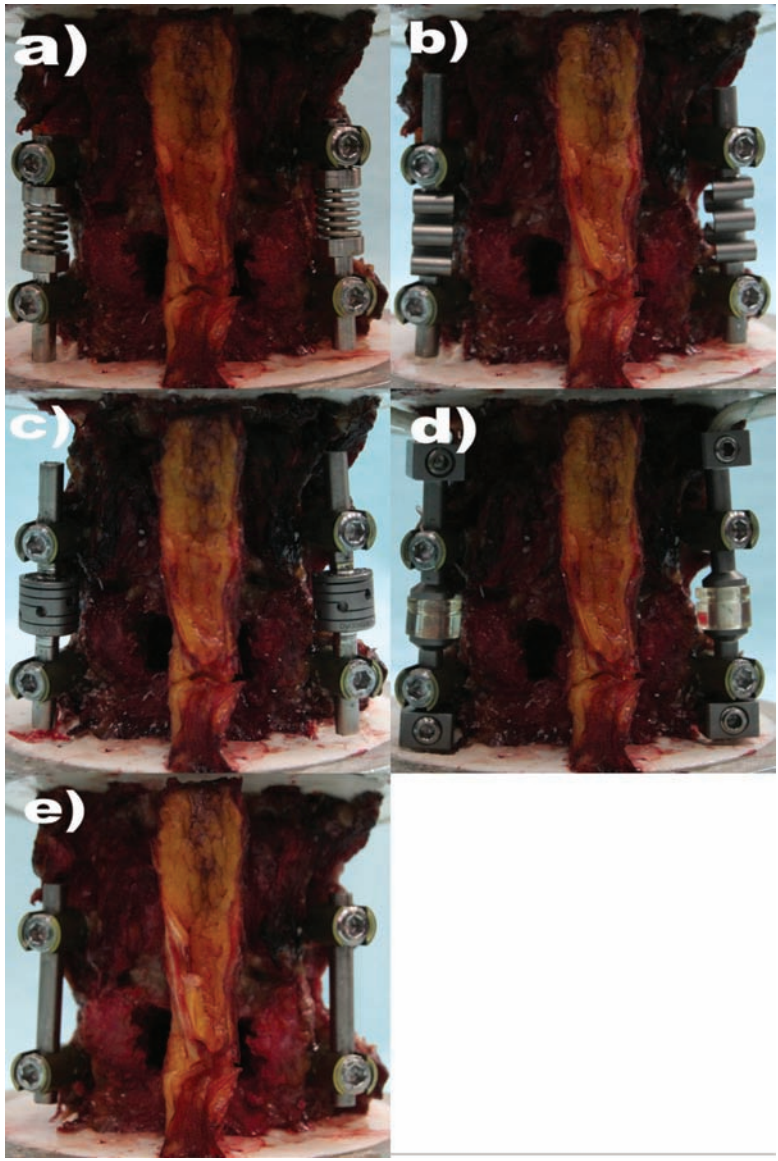

FIG. 1—*Specimens with different instrumentation: (a) spring tube concept (STC); (b) leaf spring concept (LSC); (c) DSS (DSS); (d) Dynesys (DYN); and (e) rigid fixation (RIG).*

Stiffness

The axial stiffness of all devices has been evaluated in a pure axial compression test. The stiffness was determined in the first linear range between 0.1 mm and 1 mm of deformation, which was assumed to be a clinically relevant deformation. The devices (one single rod) have the following axial compressive

stiffnesses: STC: 10 N/mm, LSC: 70 N/mm, DSS: 50 N/mm, DYN: 230 N/mm (dry, room temperature), and RIG: 65,000 N/mm, and the following bending stiffnesses: STC: 15 N/mm, LSC: 3 N/mm, DSS: 5 N/mm, DYN: 6 N/mm, and RIG: 270 N/mm. The latter was measured in a simple pretest with a sample size of $n = 5$. One end of the rod was clamped, the other end subjected to a perpendicular load with a defined lever arm of 30 mm linearly until reaching a displacement of 1.5 mm at the load-application point. The measured results showed a high reproducibility with a standard deviation of less than 2 % of the mean value.

Pedicle-Screw Adaptation of DSS and DYN

The devices were adapted to allow connection with the RIG pedicle-screw system. The DSSs connecting elements on the coupler were replaced by the standard Ø 5.5-mm titanium rod used in the RIG system. The DYN was adapted using a tubular member that fits into the RIG screw and has the same cord-locking and PCU spacer mechanism as for the original device. The goal was to achieve the same primary clamping stability with the adapted devices as for the original. Subassembly testing of axial rod grip and flexion bending was conducted according to ASTM F1798-97 (2003) and brought comparable results. Furthermore, previous synthetic model tests [15] had shown that the adaptation with the Ø 5.5-mm-rod end pieces had not altered the original range of motion of the systems.

Pedicle-Screw Adaptation of STC and LSC

The STC consists of two parts. The basic part comprises a Ø 5.5-mm lower rod and a much smaller upper rod acting as a telescopic arm. Its upper counterpart is a Ø 5.5-mm bi-conical tube on which the telescoping arm, allowing both translational and bending movements, is mounted. A spring connects these two parts. In contrast to the STC, the LSC is a one-piece design. Both ends are solid Ø 5.5-mm rods with a leaf spring in between. This design allows very linear axial and bending stiffness.

The adaptation of all the dynamic rods onto a standard pedicle screw made it possible to insert the pedicle screws in the vertebrae using a cement augmentation technique. This way only the rods needed to be replaced at every instrumentation step (Fig. 2), and the risk of any pedicle-screw loosening during testing was greatly reduced. This procedure allows a side-by-side comparison of the instrumentation techniques as designated in Table 1. The sequence of the instrumentation steps (4)–(7) was randomized for each specimen. The rigid instrumentation was always measured as the first (3) and the last step (8) to quantify the effect, if any, of screw loosening or specimen weakening during the whole test period. This also enabled visualization of any specimen weakening by calculating the mean RIG out of RIG_1 and RIG_2; RIG = mean of steps (3) and (8). This value (e.g., COR of RIG) could then be reasonably compared with the values for each of the randomized steps (4)–(7).

The test method used complies with the testing criteria for spinal implants [16]. The specimens were loaded at room temperature into a spinal simulator

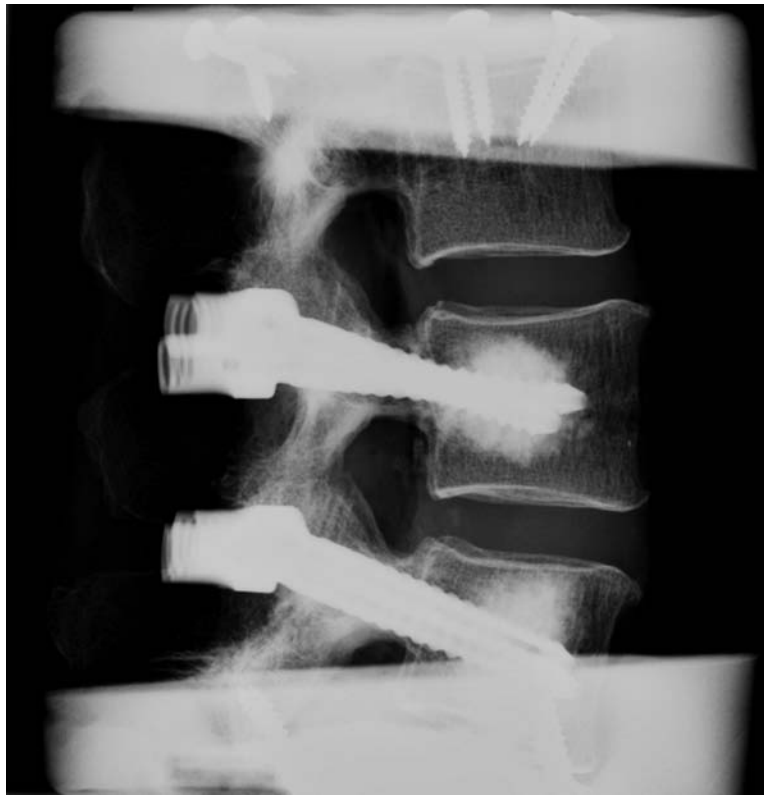

FIG. 2—*X ray of a bi-segmental test specimen (L3–L5) with cemented pedicle screws as a base platform for the consecutive instrumentation of the different dynamic rod systems.*

TABLE 1—*Testing order, segment condition, and identifier of the used systems.*

Testing Order	Segment Condition	Identifier
(1) First	Native	NAT
(2) Second	Defect	DEF
(3) Third	Rigid instrumentation	RIG_1
(4) Random	Spring tube concept	STC
(5) Random	Leaf spring concept	LSC
(6) Random	DSS	DSS
(7) Random	Dynesys	DYN
(8) Last	Rigid instrumentation	RIG_2
Mean of (3) and (8)		RIG

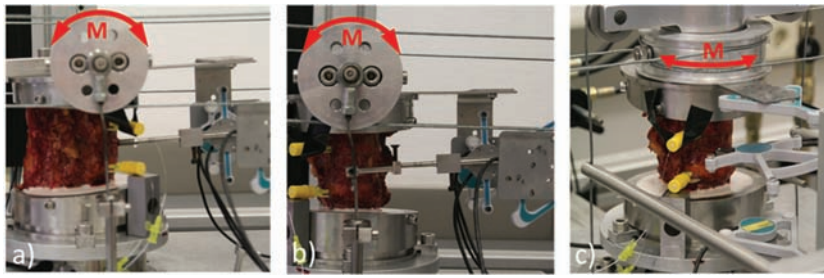

FIG. 3—*Specimen with load application for: (a) flexion–extension; (b) lateral bending; and (c) axial rotation.*

based on the principles of Crawford et al. [17], applying pure moments (+/−7.5 Nm) with a velocity of 3°/s for flexion/extension (FE), lateral bending (LB) and axial rotation (AR) (Fig. 3). The translation vectors and angles in the six degrees of freedom according to Panjabi et al. [18] were measured with a 3D ultrasonic motion analysis system (Zebris, Isny, Germany) for the instrumented segment (L4–L5).

COR Method

The instantaneous COR was calculated using the velocity pole method based on the eulerian velocity equation from the 3D data taken from the third loading cycle. The developed COR algorithm allows the evaluation of the instantaneous centers of rotation during a complete cycle of motion in the three tested principal motion planes. To localize the calculated COR in relation to the tested FSU, two reference points were set on the anterior border of the intervertebral disc (IVD) (Fig. 4). The accuracy of the developed COR algorithm for the determination of an instantaneous COR was ±1 mm^2 in the planar view. This applies to

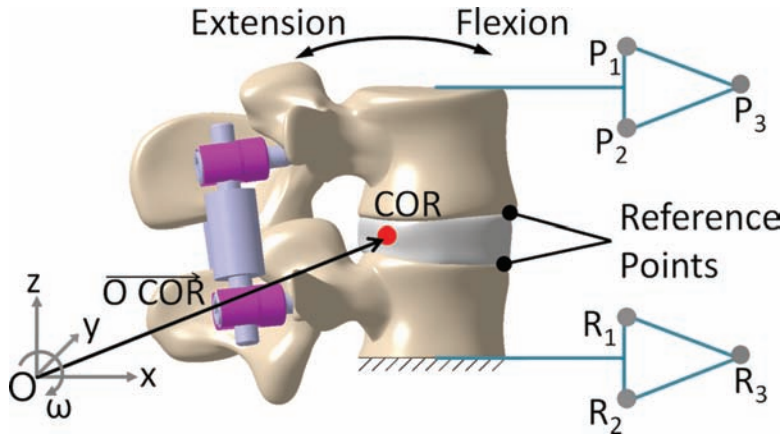

FIG. 4—*Schematic drawing for the COR evaluation.*

both the data acquisition and the test setup used here. In addition, so as to take into account the different dimensions of the individual tested specimens, the X–Y–Z dimensions of each tested IVD were measured and used to normalize the COR results (Figs. 5–7). The pedicle-screw distance in the cranial–caudal direction was also quantified.

Statistics

The effect of segment condition on COR as absolute values was assessed using repeated measures analysis of variance with a significance level of $p = 0.05$. Prior to analysis, the normal distribution of the data was verified with the Kolmogorov-Smirnov test. Least-squares difference test for *post hoc* analysis was used to determine the differences between specific segment conditions. Additionally, a *post hoc* power analysis for the obtained COR results was carried out. All statistical analyses were performed with Statistica 8.0 (StatSoft, Inc.).

Derivation of Test Setup

After analyzing the specific COR results of the different PDS systems, the distance between rod axis and the normalized location of the COR was determined. The distance from the systems rod axis to the posterior border of the IVD was measured from the specimen X-ray photographs. Using both the distance measurement and the COR location enabled the definition of a lever arm for a representative pivot point in a preclinical test setup.

Results

Specimen Dimensions

The mean IVD dimensions for the tested specimens were 43.5 mm ± 4.6 mm in the x direction (anterior–posterior), 57.9 mm ± 4.4 mm in the y direction (medial–lateral), and 14.5 mm ± 1.5 mm in the z direction (cranial–caudal). The mean pedicle-screw distance was 33.3 mm ± 3.5 mm.

COR Results for Flexion Extension

The COR results in the anterior–posterior direction, COR(X), for all tested systems were generally located in the region of the dorsal border of the IVD. There, the center of rotation for the NAT is located in the dorsal third in the anterior–posterior direction and centered in the cranial–caudal direction, COR(Z), of the IVD. The DEF situation does not lead to an alteration of the COR compared to NAT ($p = 0.8446$). The RIG and the PDS system with the highest axial stiffness (DYN) shifted the COR(X) significantly toward the dorsal structures when compared with the NAT (RIG: $p = 0.0188$; DYN: $p = 0.0235$). The DYN was found to be not significantly different from the RIG segment condition ($p = 0.9252$). The COR(X) of the other PDS systems with a lower implant stiffness (STC, LSC, DSS) was located in between the NAT and RIG without significant difference to NAT ($p > 0.05$). However, the PDS systems with low implant stiffness show also

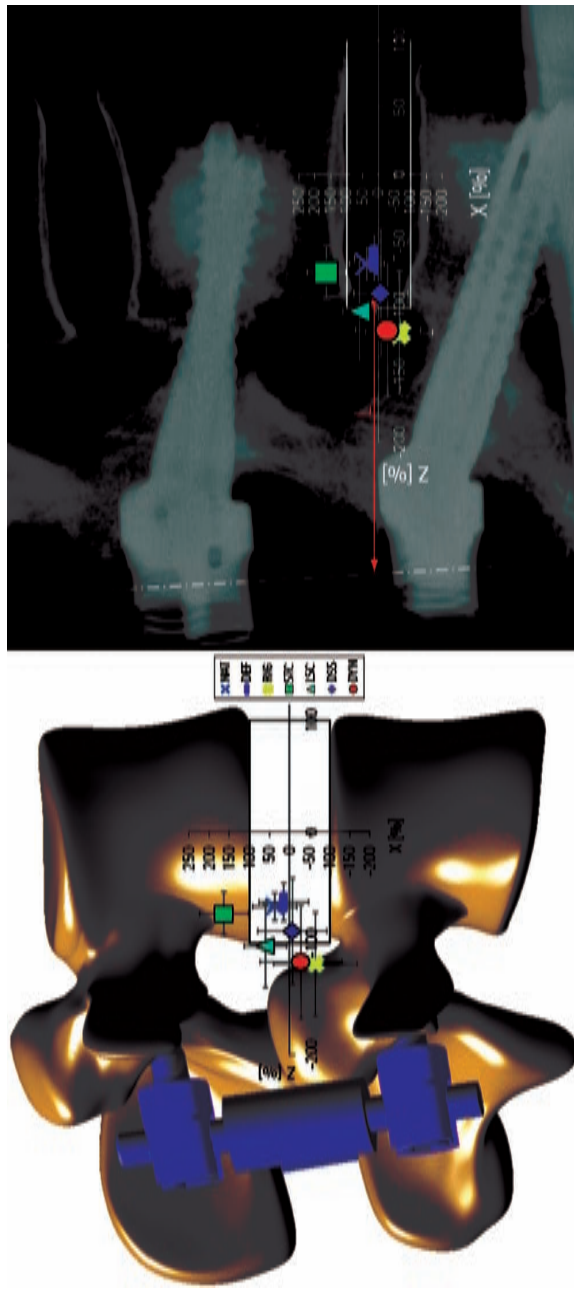

FIG. 5—*COR results as mean ± standard deviation of the different systems in flexion–extension normalized to disc dimensions.*

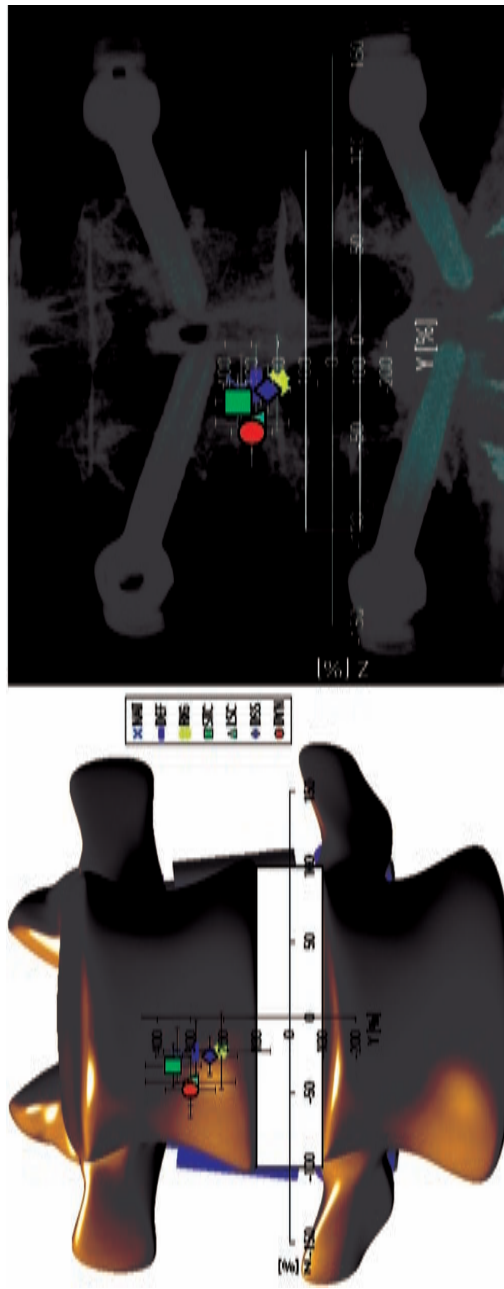

FIG. 6—*COR results as mean ± standard deviation of the different systems in lateral bending normalized to disc dimensions.*

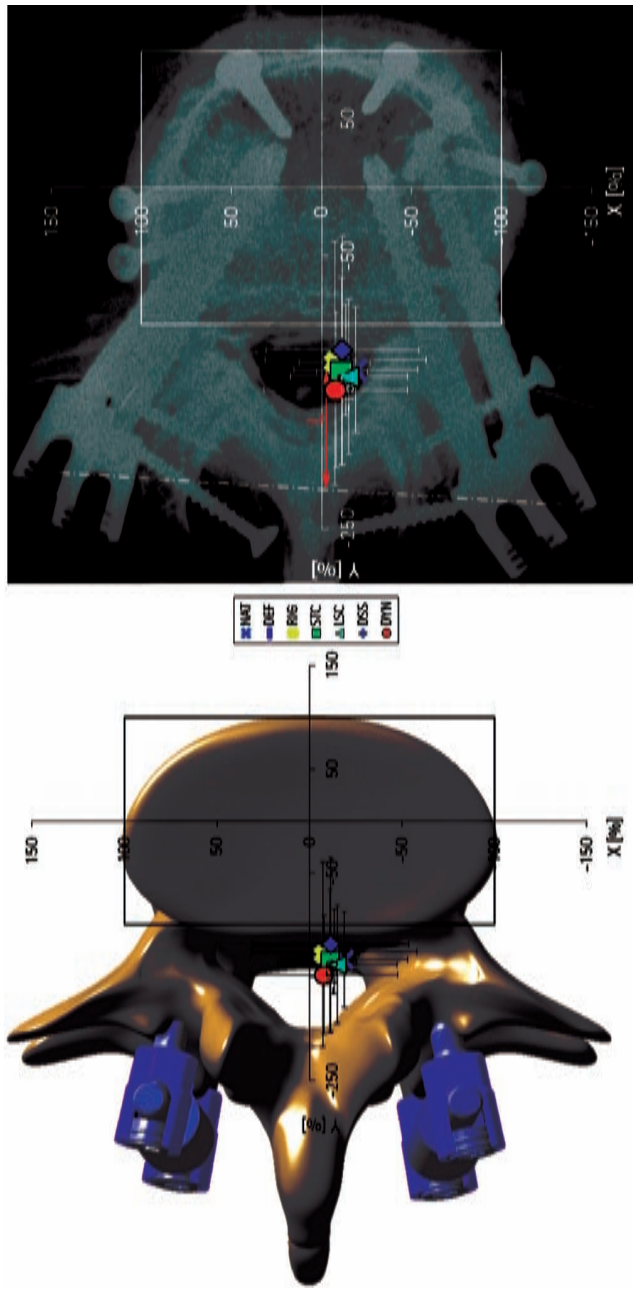

FIG. 7—*COR results as mean ± standard deviation of the different systems in axial rotation normalized to disc dimensions.*

no significant difference in COR(X) to DYN and RIG with the exception of STC (STC to DYN: $p = 0.0462$; STC to RIG: $p = 0.0375$) (Fig. 5, Table 2).

In the cranial–caudal direction, only the asymmetrical designed STC system shifted the COR(Z) significantly in the cranial direction ($p < 0.01$), whereas all the other systems stayed centered within the IVD without significant difference to the NAT segment condition ($p > 0.05$).

From the performed *post hoc* power analysis a statistical power for COR(X) of 0.65 and for COR(Z) of 0.88 was evaluated.

TABLE 2—*COR results (mean ± standard deviation) normalized to disc dimensions for the different segment conditions and loading directions.*

Loading Direction	Segment Condition	COR(X) (%) mean ± standard deviation	COR(Z) (%) mean ± standard deviation
Flexion–extension	NAT	−67.3 (±12.3)	37.3 (±54.9)
	DEF	−63.2 (±17.1)	14.7 (±61.5)
	STC	−73.6 (±19.3)	163.9 (±60.8)
	LSC	−102.7 (±37.5)	60.7 (±52.2)
	DSS	−89.2 (±47.6)	−6.6 (±85.7)
	DYN	−116.8 (±50.5)	−27.6 (±102.1)
	RIG	−118.8 (±46.4)	−63.9 (±104.7)
		COR(Y) (%) mean ± standard deviation	COR(Z) (%) mean ± standard deviation
Lateral bending	NAT	−25.8 (±18.0)	341.1 (±65.6)
	DEF	−23.0 (±20.5)	284.4 (±98.1)
	STC	−32.4 (±14.0)	352.9 (±83.9)
	LSC	−43.3 (±15.9)	300.6 (±136.0)
	DSS	−26.0 (±12.4)	241.9 (±83.6)
	DYN	−48.3 (±18.3)	300.7 (±76.5)
	RIG	−22.6 (±25.1)	207.3 (±148.3)
		COR(X) (%) mean ± standard deviation	COR(Y) (%) mean ± standard deviation
Axial rotation	NAT	−133.7 (±46.3)	−18.8 (±34.2)
	DEF	−126.2 (±40.8)	−13.3 (±44.7)
	STC	−135.1 (±68.9)	−11.0 (±14.2)
	LSC	−138.6 (±56.7)	−14.9 (±32.4)
	DSS	−119.1 (±83.7)	−11.4 (±42.3)
	DYN	−148.5 (±56.9)	−7.8 (±39.9)
	RIG	−128.6 (±89.2)	−7.1 (±19.6)

COR Results for Lateral Bending

In the frontal plane, the COR results for all segment conditions were very similar without any significance ($p > 0.05$) and were all located in the middle of the upper vertebra and close to the sagittal axis (Fig. 6, Table 2). The statistical power was COR(Y): 0.59 and COR(Z): 0.5.

COR Results for Axial Rotation

Also in the transversal plane, the COR results for all segment conditions were very close together without any significance ($p > 0.05$) and located behind the dorsal border of the IVD in the region of the spinal canal, fairly close to the sagittal axis (Fig. 7, Table 2). The statistical power was COR(X): 0.1 and COR(Z): 0.1.

Derivation of Pivot Point for the Test Setup

The determined COR results show that the location of the COR is only marginally influenced by the tested PDS systems at least for the PDS with low implant stiffness (STC, LSC, DSS) in all three principal motion planes FE, LB, and AR.

For this diverse range of PDS systems with different implant stiffnesses and designs, the COR results stay nearly constant. Therefore, the idea to implement one defined pivot axis in a test setup for each motion plane would appear to be logical.

The distance from the rod axis of the dorsal instrumentation to the posterior border of the IVD was 32.2 mm ± 3.7 mm. In FE, the mean COR(X) for STC, LSC, and DSS is located at −88.5 % from the origin of the IVD, which means 2.5 mm ± 2 mm anteriorly to the dorsal border. This leads to a distance from rod axis to pivot point of 34.7 mm ± 5.7 mm. For our proposed FE test setup, the lever arm (distance from the rod axis to the pivot point) was specified as 36 mm, whereas the cranial–caudal position was specified as centered in between the two pedicle screws (Fig. 8).

For LB, a symmetrical position of the pivot point was specified for both medial–lateral and cranial–caudal positions (Fig. 9).

In AR, the mean COR(X) for STC, LSC, and DSS is located at −131.6 % from the origin of the IVD, which means 6.85 mm ± 3 mm posteriorly to the dorsal border of the IVD. This leads to a distance from rod axis to pivot point of 25.35 mm ± 6.7 mm. For our AR test setup, the pivot point was defined with a lever arm (rod axis to pivot point) of 24 mm and specified as symmetrical in the medial–lateral direction (Fig. 10).

After the definition of pivot points based on the *in vitro* results, a test setup was designed considering the use of a uni-axial testing machine with a statically non-over-determined load application (Figs. 8–10).

Following the *in vitro* results, there is one test setup for each main loading direction FE, LB, and AR. Basically, the ASTM test blocks were used but with a decreased cranial–caudal distance between the pedicle screws of 40 mm. The upper and the lower test blocks can rotate about a fixed axis of rotation, which is located at the determined pivot point.

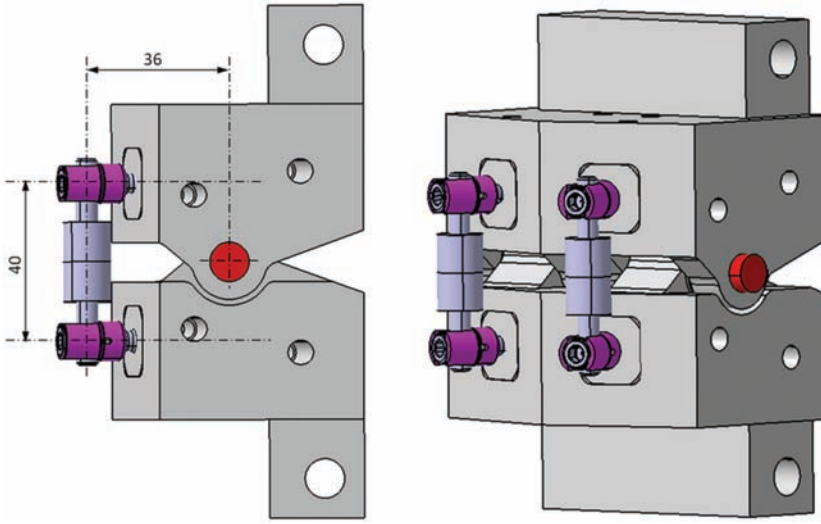

FIG. 8—*Derived test setup for flexion–extension.*

Discussion

In the current version of ASTM F2624, the COR is not defined because the COR can vary in accordance with device design and intended use. Potentially, each dynamic device can be tested using a different COR. Therefore, each system has to be evaluated regarding its COR prior to testing, which is time consuming for

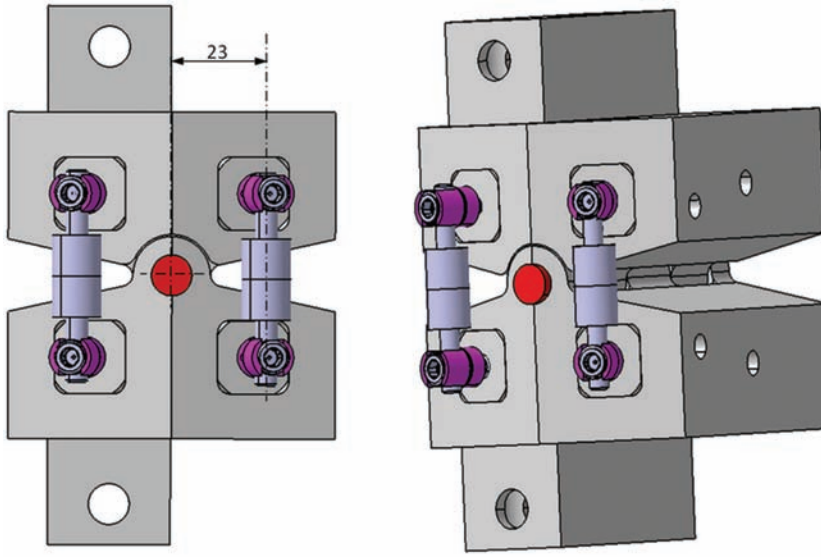

FIG. 9—*Derived test setup for lateral bending.*

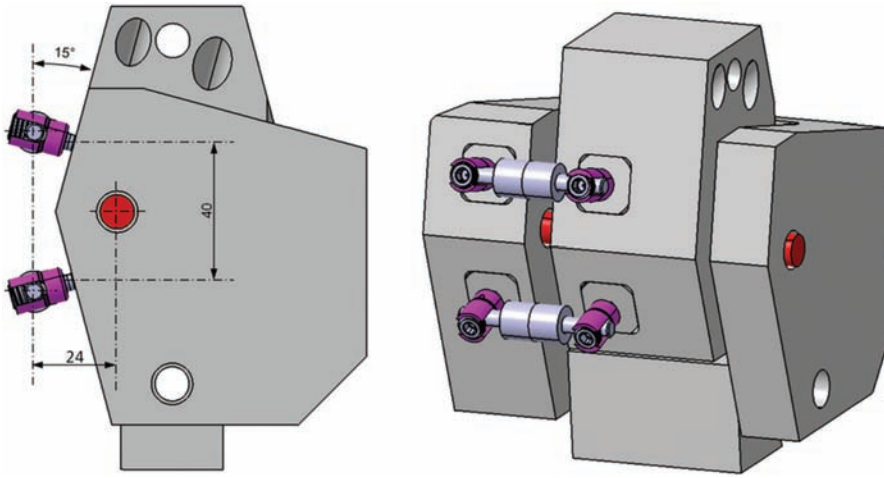

FIG. 10—*Derived test setup for axial rotation.*

those involved. Alternatively, the COR has to be determined based on theoretical assumptions. Furthermore, no biomechanical data exists that shows how the PDS design parameters, such as implant stiffness, influence the location of its COR. To our knowledge, the current *in vitro* flexibility study is the first investigating the influence of different PDS systems, comprising a diverse design range, on the location of their specific COR. Based on this data, a proposal for a test setup with specific pivot point for standardized fatigue testing of dedicated PDS devices has been made.

Six lumbar spine specimens were tested in the spinal simulator in the three main principal motion planes (FE, LB, and AR) following the recommendations for *in vitro* testing of spinal implants [16]. Seven different segment conditions (NAT, DEF, STC, LSC, DSS, DYN, and RIG) were examined, and the COR in the treated segment was analyzed based on the eulerian velocity equation from the measured 3D data. Furthermore, the location of the normalized COR for each segment condition was quantified in relation to the dimension of the tested specimens and to the dorsal instrumentation.

The COR results show that the influence of the different axial stiffnesses and implant designs on the resulting COR is low. This was most pronounced in LB and AR, where the location of each COR for the different PDS designs is very close together and has also been found to be indifferent to the NAT, DEF, and RIG segment conditions. For FE, the location of the COR is governed by the axial stiffness and the design of the dorsal instrumentation. The system with the highest implant stiffness, the RIG, shifted the COR most significantly toward the dorsal structures. Also, the PDS device with the highest stiffness (DYN) showed similar behavior to the RIG. In an anterior–posterior direction (X), all of the other investigated PDS systems, with lower axial stiffnesses than DYN (STC, LSC, DSS), had COR locations in between the segment conditions NAT and RIG near the dorsal border of the IVD.

In the Z direction, all of the segment conditions show a similar COR result with the exception of the STC, which is significantly shifted in the cranial direction. This is considered to be a result of the asymmetric device design.

The used specimens were from fairly old donors, bringing the risk of degeneration, especially of the IVD. Prior to testing, they were CT scanned and visually inspected for signs of severe disc degeneration and excluded if such were found. We were aware that the age of the specimens and the accompanied age-related disc degeneration was not ideal to collect reliable data. But we did not think it would have a significant impact on the kinematic response. The PDS systems are generally implanted in younger patients, but they are intended to treat and correct problems caused by disc degeneration. In addition, previous studies have shown that degeneration of the IVD has only a minimal effect on the range of motion [19] and may even result in a decrease in a severe case [20]. In addition, our already published data regarding the kinematic parameters range of motion and neutral zone [6], which was part of the current study, showed a high consistency to other published data of the DYN [1,3,5] and the DSS [12].

The COR results reported here for the DYN all correspond well with the findings of Niosi et al. [1], who investigated the kinematical behavior of the DYN. There the COR for the NAT and DEF situation were located central in the IVD space for FE without significant difference, similar to our findings. Furthermore, after implantation of the DYN in FE they reported a significant dorsal shift of COR compared to NAT, which was located posteriorly to the dorsal border of the IVD, independent of the used spacer length. However, only a qualitative comparison could be made because of the absence of real data values presented.

Despite the loading with pure moments and a superimposed follower load is more physiological, we decided only to report the COR data for the load case with pure moments following the "testing criteria for spinal implants: recommendations for the standardization of in vitro stability testing of spinal implants" [16]. However, we implemented this load case in our *in vitro* testing protocol, and the results showed a similar response by trend.

In several comparable *in vitro* studies, the use of monosegmental, bisegmental, or three-segmental FSU for the kinematical analysis have been reported [1–5,11,12]. There, the instrumented level, which is usually monosegmental, was evaluated regarding the kinematic response. In our point of view, the use of a bisegmental FSU is sufficient to evaluate the COR, because the COR of the instrumented level is of interest and will be discretely analyzed.

The standard deviation of the COR results are relatively large for the instrumented conditions. It seems that there is a negative correlation between standard deviation and segment mobility in the treated level as a result of the eulerian velocity equation. For NAT, DEF, and the PDS with the lowest stiffness (STC), causing the largest intersegmental movement, the lowest standard deviation was found in FE. And for axial rotation, where the range of motion is generally low, the standard deviations of all segment conditions are large. However, the *post hoc* power analysis of the COR results (means of segment conditions and pooled standard deviations) gives a medium to high power for the COR

data in FE and LB (0.5–0.88), whereas the power for AR was found to be low (0.1).

The assumption in the ASTM F2624 that different PDS devices have different CORs would appear to contradict the COR results for a diverse range of PDS devices obtained here. Taking these results, a test setup for PDS devices with low axial implant stiffness could be defined using one pivot point axis for FE, LB, and AR.

The mean distance from rod axis to the posterior border of the IVD was determined using X-ray photographs to be 32.2 mm ± 3.7 mm. Combining this measured distance with the information on the location of the CORs from the *in vitro* test results enables us to define the pivot points. The determined locations of the CORs for all of the evaluated PDS devices vary little in all three loading directions. The highest variation could be seen in FE loading. There, an increase of the axial stiffness results in a shift of the COR in a posterior direction. In general, however, the CORs could be found to be located in the area of the posterior border of the IVD with the mean position being located slightly anterior of this border. Thus, the anterior–posterior distance from the pivot point to the rod axis was defined to be 36 mm, representing the mean COR for the devices with low axial implant stiffness (STC, LSC, DSS). The CORs of all segment conditions in LB are approximately centered in the medial–lateral direction. Referring to the dimensions of the test blocks specified in ASTM F2624, the lever arm from the pivot point to the rod axis is 23 mm. This results from the defined distance of 40 mm for the pedicle-screw entry points on the test block. For AR loading, the CORs of all segment conditions are basically located posterior to the IVD in the area of the spinal canal and are centered in the medial–lateral direction. This leads to a lever arm of 24 mm, representing the mean COR for the devices with low axial implant stiffness (STC, LSC, DSS).

In the proposed test setup, a symmetrical position of the pivot points was defined. This means that for FE and LB test setups, the cranial–caudal coordinates, and for the AR test setup, the medial–lateral coordinates of the defined pivot points were centered between the screws. This is in consistence with our evaluated results (Figs. 5–7). There, the COR(Z) in the cranial–caudal direction is located at IVD level for FE and above the IVD for LB, which is both in between the cranial and caudal pedicle screws. These findings are in contradiction to the rationale cited in ASTM 2624, where an asymmetrical COR is reported. But the COR only have been evaluated on non-instrumented FSU. A possible reason for the discrepancy of the results could be the type of load application in the study of Zhao et al. [14]. Therefore, the determination of a COR for PDS devices based on this is debatable. However, some PDS devices with an asymmetrical design may have a pivot point, which is not located in the center plane as could be seen for the STC in FE loading (Fig. 5). In such a case, assembling the PDS device with an axial offset can move the system's pivot point into the center plane.

The proposed test setup is a modification of the test setup defined in the ASTM F2624. Basically, the ASTM test blocks were used with a 40 mm distance between the pedicle-screw entry points in the medial–lateral direction and a 15° chamfer on the posterior aspect (e.g., Fig. 8). In the ASTM F2624, the distance

between the simulated endplates (that is, the simulated disc space height) is set to 20 mm. The suggested cranial–caudal distance between the screws, including the dimensions of the test blocks, is 52 mm. For mono-segmental treatment, this distance will be too long for some available dynamic systems. The mean distance between the axis of the pedicle screws measured in the *in vitro* test was 33.3 mm ± 3.5 mm. Hence, to ensure that all dynamic systems fit in between the screws and to offer the possibility to assemble a PDS device with an axial offset, the distance was set to 40 mm. Because the lever arm for the moment application (distance rod axis to pivot point) stays constant, it should not be affected by the defined pedicle-screw distance.

Compared to the ASTM F2624, where a test machine is required with an axial and torsional actuator, the newly developed test setup is based on a uniaxial load application. Therefore, the test frequency could be significantly increased, which makes preclinical testing more effective.

Because of the fixed hinge, the implant motion is defined during testing. However, the COR locations determined using the *in vitro* tests suggest that a fixed hinge can be a good approximation to the physiological kinematics for a selected group of PDS devices.

During testing, the effective lateral lever arm changes as a result of the rotation of the test blocks. This deviation depends on the ratio of the axial and the lateral distances from the load application point to the pivot point. Thus, if the load ratio at the load application point is −1, the resulting load ratio at the implant will be $\neq -1$. This has to be considered when the implant loads are defined. In the current proposed test setup, for an assumed value of the range of motion of $+5^\circ$ or -5°, for example, the deviation of the effective lateral lever arm is 9.9 % in flexion and −11.3 % in extension, respectively. In LB, the corresponding values for $\pm 5^\circ$ of motion are +15.9 % and -16.1 % and in AR + 13.4 % and −13.6 %. However, for a physiological implant load, a ratio $\neq -1$ may be more realistic.

For comparative testing of different PDS systems, the axial and bending stiffnesses of the implants have to be considered. Theoretically, only implants with the same stiffness parameters can be compared directly because they will be subjected to the same loading situation *in vivo*. However, our findings show that, for at least a selected group of PDS systems with low implant stiffnesses, a fair comparison with a specified COR can indeed be taken into account. Features of the implant designs also need to be considered during testing. Such parameters might include, for example, non-linear stiffness characteristics such as utilized by systems exhibiting a positive stop mechanism or with specific material specifications.

Conclusion

From the *in vitro* study, the center of rotation for a diverse range of PDS devices have been investigated. The results show that, for the here-tested PDS systems with low axial stiffnesses (range: 10–70 N/mm), the COR varies only marginally. The definition of pivot points for all three main loading directions FE, LB, and

AR could be derived, and enables the testing of selected PDS devices without dedicated *in vitro* evaluation of the device-specific CORs.

The newly developed and proposed test setup offers the possibility of using testing machines with a single axial actuator. Additionally, the test frequency could be increased because of the more feasible uni-axial load application of the test setup. This makes the preclinical testing of PDS devices more effective, in particular when considering the required endurance limit of 10×10^6 cycles.

References

[1] Niosi, C. A., Zhu, Q. A., Wilson, D. C., Keynan, O., Wilson, D. R., and Oxland, T. R., "Biomechanical Characterization of the Three-Dimensional Kinematic Behaviour of the Dynesys Dynamic Stabilization System: An in Vitro Study," *Eur. Spine J*,, Vol. 15(6), 2006, pp. 913–922.

[2] Niosi, C. A., Wilson, D. C., Zhu, Q., Keynan, O., Wilson, D. R., and Oxland, T. R., "The Effect of Dynamic Posterior Stabilization on Facet Joint Contact Forces: An in Vitro Investigation," *Spine*, Vol. 33(1), 2008, pp. 19–26.

[3] Schmoelz, W., Huber, J. F., Nydegger, T., Dipl, I., Claes, L., and Wilke, H. J., "Dynamic Stabilization of the Lumbar Spine and Its Effects on Adjacent Segments: An in Vitro Experiment," *J. Spinal Disord. Tech.*, Vol. 16(4), 2003, pp. 418–423.

[4] Schmoelz, W., Huber, J. F., Nydegger, T., Claes, L., and Wilke, H. J., "Influence of a Dynamic Stabilisation System on Load Bearing of a Bridged Disc: An in Vitro Study of Intradiscal Pressure," *Eur. Spine J.*, Vol. 15(8), 2006, pp. 1276–1285.

[5] Schulte, T. L., Hurschler, C., Haversath, M., Liljenqvist, U., Bullmann, V., Filler, T. J., Osada, N., Fallenberg, E. M., and Hackenberg, L., "The Effect of Dynamic, Semi-Rigid Implants on the Range of Motion of Lumbar Motion Segments After Decompression," *Eur. Spine J.*, Vol. 17(8), 2008, pp. 1057–1065.

[6] Schilling, C., Krüger, S., Grupp, T. M., Duda, G. N., Blömer, W., and Rohlmann, A., "The Effect of Design Parameters of Dynamic Pedicle Screw Systems on Kinematics and Load Bearing—An in Vitro Study," *Eur. Spine J.*, Vol. 20(2), 2011, pp. 297–307.

[7] Grob, D., Benini, A., Junge, A., and Mannion, A. F., "Clinical Experience with the Dynesys Semirigid Fixation System for the Lumbar Spine: Surgical and Patient-Oriented Outcome in 50 Cases After an Average of 2 Years," *Spine*, Vol. 30(3), 2005, pp. 324–331.

[8] Putzier, M., Schneider, S. V., Funk, J., and Perka, C., "Die Anwendung eines dynamischen Pedikelschraubensystems (DYNESYS) bei lumbalen Segmentdegenerationen: ein Vergleich klinischer und radiologischer Ergebnisse bei unterschiedlichen Indikationen [Application of a Dynamic Pedicle Screw System (DYNESYS) for Lumbar Segmental Degenerations: Comparison of Clinical and Radiological Results for Different Indications]," *Z. Orthop.*, Vol. 142(2), pp. 166–173, 2004 (in German).

[9] Putzier, M., Schneider, S. V., Funk, J. F., Tohtz, S. W., and Perka, C., "The Surgical Treatment of the Lumbar Disc Prolapse: Nucleotomy with Additional Transpedicular Dynamic Stabilization Versus Nucleotomy Alone," *Spine*, Vol. 30(5), 2005, pp. E109–E114.

[10] Wurgler-Hauri, C. C., Kalbarczyk, A., Wiesli, M., Landolt, H., and Fandino, J., "Dynamic Neutralization of the Lumbar Spine After Microsurgical Decompression in Acquired Lumbar Spinal Stenosis and Segmental Instability," *Spine*, Vol. 33(3), 2008, pp. E66–E72.

[11] Schmidt, H., Heuer, F., and Wilke, H. J., "Which Axial and Bending Stiffnesses of Posterior Implants Are Required to Design a Flexible Lumbar Stabilization System?" *J. Biomech.*, Vol. 42(1), 2009, pp. 48–54.

[12] Wilke, H. J., Heuer, F., and Schmidt, H., "Prospective Design Delineation and Subsequent in Vitro Evaluation of a New Posterior Dynamic Stabilization System," *Spine*, Vol. 34(3), 2009, pp. 255–261.

[13] Rohlmann, A., Burra, N. K., Zander, T., and Bergmann, G., "Comparison of the Effects of Bilateral Posterior Dynamic and Rigid Fixation Devices on the Loads in the Lumbar Spine: A Finite Element Analysis," *Eur. Spine J.*, Vol. 16(8), 2007, pp. 1223–1231.

[14] Zhao, F., Pollintine, P., Hole, B., Dolan, P., and Adams, M. A., "Discogenic Origins of Spinal Instability," *Spine*, Vol. 30(23), 2005, pp. 2621–2630.

[15] Schilling, C., Vieweg, U., Grupp, T. M., and Bloemer, W., "A Synthetic in Vitro Model for a Standardized Comparison of Dynamic Stabilization Devices," *J. Biomech.*, Vol. 41(S1), 2008, p. 1.

[16] Wilke, H. J., Wenger, K., and Claes, L., "Testing Criteria for Spinal Implants: Recommendations for the Standardization of in Vitro Stability Testing of Spinal Implants," *Eur. Spine J.*, Vol. 7(2), 1998, pp. 148–154.

[17] Crawford, N. R., Brantley, A. G., Dickman, C. A., and Koeneman, E. J., "An Apparatus for Applying Pure Nonconstraining Moments to Spine Segments in Vitro," *Spine*, Vol. 20(19), 1995, pp. 2097–2100.

[18] Panjabi, M. M., Oxland, T. R., Yamamoto, I., and Crisco, J. J., "Mechanical Behavior of the Human Lumbar and Lumbosacral Spine Shown by Three-Dimensional Load-Displacement Curves," *J. Bone Jt. Surg., Am. Vol.*, Vol. 76(3), 1994, pp. 413–424.

[19] Mimura, M., Panjabi, M. M., Oxland, T. R., Crisco, J. J., Yamamoto, I., and Vasavada, A., "Disc Degeneration Affects the Multidirectional Flexibility of the Lumbar Spine," *Spine*, 19(12), 1994, pp. 1371–1380.

[20] Fujiwara, A., Lim, T. H., An, H. S., Tanaka, N., Jeon, C. H., Andersson, G. B., and Haughton, V. M., "The Effect of Disc Degeneration and Facet Joint Osteoarthritis on the Segmental Flexibility of the Lumbar Spine," *Spine*, 25(23), 2000, pp. 3036–3044.

Reprinted from JAI, Vol. 8, No. 7
doi:10.1520/JAI103408
Available online at www.astm.org/JAI

Boyle C. Cheng,[1] *Daniel J. Cook,*[2] *Mathieu Cuchanski,*[3] *Stephen M. Pirris,*[4] *and William C. Welch*[5]

Biomechanical Cyclical Loading on Cadaveric Cervical Spines in a Corpectomy Model

ABSTRACT: Approved posterior cervical spinal fixation systems have been submitted to the U.S. Food and Drug Administration with results from standardized test protocols from the ASTM. The bench top mechanical studies are designed to minimize biologic and laboratory variability. However, for implant tests such as ASTM F1717 to be more clinically relevant, anatomical and physiologic considerations must be understood. The specific aim of this study was to determine if a human cadaveric cervical spine with a corpectomy and posterior fixation was effective in maintaining stability prior to and following cyclical loading. Six fresh frozen cadaveric human cervical specimens were harvested and prepared. A C5 corpectomy was performed. Posterior cervical instrumentation was implanted from C3 and C7 spanning across the C4–C6 defect. Each specimen followed an established pure moment test protocol to characterize the instrumented spine in flexion extension, lateral bending, and axial torsion at $\pm$2.5 N m and axial compressive loading to 150 N. Subsequently, each specimen was subjected to 10 000 flexion extension cycles. Following the cyclical loading, each specimen was characterized a second time via the same test protocol. Statistical analyses were then performed on the third cycle data between the two pure moment tests. The mean FE bending range of motion (ROM) was 18.0° $\pm$ 10.7° prior to the 10 000 cyclical

Manuscript received September 27, 2010; accepted for publication May 16, 2011; published online July 2011.

[1] Ph.D., Dept. of Bioengineering and Dept. of Neurological Surgery, Univ. of Pittsburgh, Pittsburgh, PA 15212. (Corresponding author), e-mail: boylecheng@yahoo.com
[2] M.S., Dept. of Bioengineering, Univ. of Pittsburgh, Pittsburgh, PA 15212.
[3] Dept. of Neurological Surgery, Univ. of Pittsburgh, Pittsburgh, PA 15212.
[4] M.D., Dept. of Neurological Surgery, Univ. of Pittsburgh, Pittsburgh, PA 15212.
[5] M.D., F.A.C.S., F.I.C.S., Dept. of Neurosurgery, Univ. of Pennsylvania, Philadelphia, PA 19106.

Cite as: Cheng, B. C., Cook, D. J., Cuchanski, M., Pirris, S. M. and Welch, W. C., "Biomechanical Cyclical Loading on Cadaveric Cervical Spines in a Corpectomy Model," *J. ASTM Intl.*, Vol. 8, No. 7. doi:10.1520/JAI103408.

bending protocol. Following cyclical loading, the mean ROM measured 22.0° ± 19.9°. In axial compression, the mean ROM was 4.1 mm ± 1.9 mm prior to cycling and 4.2 mm ± 1.4 mm post-cycling. A statistically significant difference was detected only in the axial torsion mode of loading ($p = 0.030$). Although the ASTM standard provides consistent test methodologies, biomechanical cadaveric testing remains an important step in the validation of all spinal instrumentation. The pure moment biomechanical cadaveric test protocol for the same construct was capable of detecting significant changes pre- and post-flexion extension fatigue cycling only in the axial torsion mode of loading.

KEYWORDS: biomechanical study, cyclical loading, corpectomy, ASTM, flexibility protocol, posterior cervical fixation, bone screw interface, lateral mass bone screw

Introduction

Expulsion or migration of an anterior cervical corpectomy graft in combination with failure of any other anterior fixation instrumentation would leave a patient highly dependent on the posterior constructs for structural stability following cervical corpectomy procedures requiring both anterior and posterior instrumentation. Although rare, such catastrophic failures of the anterior column place considerable stress on the posterior cervical instrumentation. To a lesser extent, conditions from the immediate post-operative state and the short term follow-up period in which fusion has not been achieved, places a higher dependence on the posterior instrumentation. Thus, the requirements for posterior cervical instrumentation should consider the worst case scenario and the survival time of the constructs beyond the immediate post-operative condition.

Pathologies that afflict the cervical spine may require surgical intervention through a posterior approach and in some instances, both anterior and posterior approaches may be deemed necessary by the clinician. Due to significant advances in modern posterior cervical screw and rod fixation constructs, patients may be allowed to return to normal or near normal levels of activity within a short time period post-operatively. The American Society for Testing and Materials International (ASTM) provides guidance on testing of spinal fixation devices including a cyclical test designed to simulate a hypothetical worst case clinical scenario for cervical applications, i.e., corpectomy model with implant hardware subjected to cyclical loading. The bench top tests allow for repeatability and validation across independent laboratories specifically for spinal constructs with specific parameters for posterior cervical instrumentation. The schematic shown in Fig. 1 represents the standardized ASTM Standard F1717 protocol that governs such devices [1].

Cunningham et al. proposed static and cyclical analysis of pedicle screw spinal constructs for the lumbar spine [2]. The study involved a null hypothesis in which the authors postulated there would be no difference in the intrinsic stiffness, bending strength, flexibility, or fatigue life among pedicle screw devices available commercially. In order to test the hypothesis, the authors selected

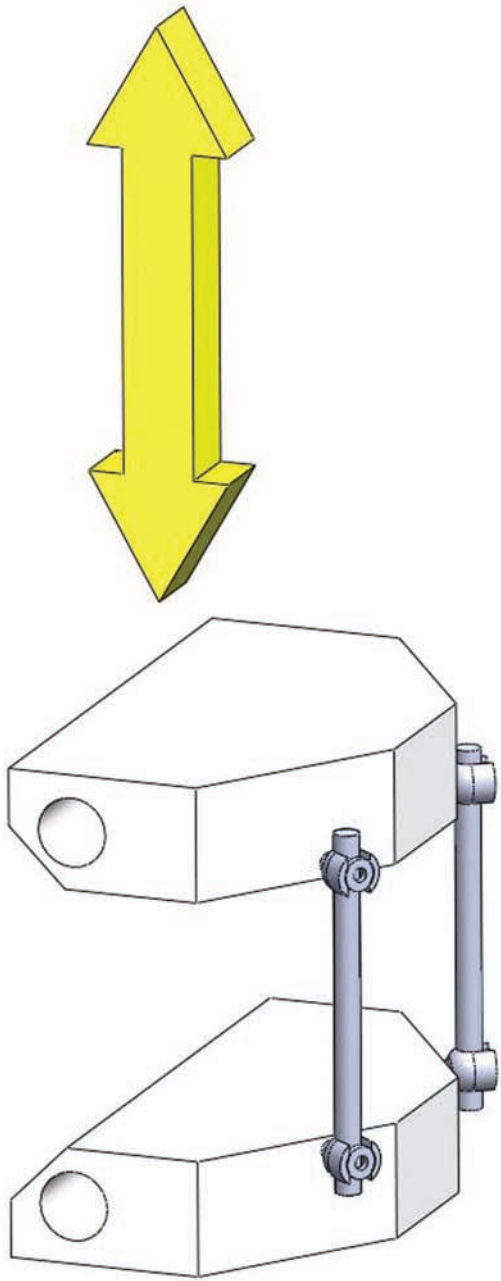

FIG. 1—*ASTM F-1717 test for posterior cervical fixation hardware using simulated polymer vertebral bodies without anterior column support.*

ultrahigh molecular weight polyethylene in order to achieve consistency in fixation for destructive static and fatigue testing of these devices. The value of this original study was the importance of conducting consistent mechanical testing of posterior spinal implants in order to compare and detect the differences between constructs. This methodology is as necessary and relevant now as it was when Cunningham et al. first reported the study. The data not generated from the mechanical test protocols from either screw or hook interfaces with the simulated vertebrae are the implant and host bone environment. This effectively tests the construct itself and not necessarily the screw bone or the hook bone interface. Therefore, in addition to the ASTM standard, interface strength along with viscoelastic properties from cadaveric cervical spine testing may be ascertained through *in vitro* testing on biologic specimens.

In order to better understand the potential clinical ramifications at higher cycles, ASTM standards including F1717-10 help characterize the potential limits of certain fixation devices. Additional metrics, including bone screw interface strength are important in understanding potential clinical complications. Through cyclical loading and comparative pure moment testing, the cadaveric biomechanical information may help clarify potential clinical limitations. Thus, incorporating aspects of the screw bone interface integrity as a function of cyclical loading would establish a more comprehensive performance envelope for such constructs.

Estimates of the number of cyclical bends per year in the cervical spine have been based on the published literature for cervical disc arthroplasty, which in turn references the published work in total hip and knee arthroplasty. The number of cycles has been shown to have been 1.9×10^6 cycles/year [3] in patients with well-functioning total hip arthroplasties and recorded with an accurate two-dimensional accelerometer worn on the ankle. The arthroplasty literature has been used as a reference for standards written for cervical disc replacements and typically approximate 1×10^6 cycles/year as a benchmark. More Recently, Syed et al. proposed a method of empirically deriving the number of cycles in multiple directions for cervical neck motion [4]. In 2008, Sterling et al. published the results of a clinical study [5] from the method described in Syed et al. In the article, Sterling concludes the F2423-05 standard captures the lateral bending and axial rotation sufficiently at 10×10^6 cycles, but underestimates flexion extension bending although the standard reports a higher excursion for this mode of loading [5].

A null hypothesis was formed so that a biomechanical flexibility protocol would not detect significant differences in any mode of loading prior to (pre-) and following (post-) cyclical loading. Additionally, human cadaveric cervical spines were selected as the model in order to accurately represent the acute screw bone interface and associated potential complications. A short duration test, represented by 10 000 cycles, was established as a reasonable cycle count for patients requiring additional treatment and within the limits before the onset of severe biologic tissue breakdown during high frequency fatigue cycling. Tissue degradation at the bone screw interface and remaining osteoligamentous structures would compromise the results of the flexibility test protocol. It may not be readily apparent whether the construct underwent loosening during the

cyclical loading or whether the tissue was no longer structurally competent should a statistical difference be detected pre- and post-cyclical loading.

This study was designed to add additional physiologic parameters to ASTM test standards for posterior cervical systems by testing the instrumented cervical spine before cyclical loading and following cyclical loading. The biomechanical cadaveric testing takes into consideration additional clinical factors, e.g., the bone screw interface, and thereby has the potential to augment existing ASTM bench top mechanical test results with clinically relevant short term construct information.

Methods

Six human cadaveric cervical spines were harvested and stored at −20°C. Each specimen with corresponding donor data has been tabulated in Table 1. The osteoligamentous structures for each spine were meticulously maintained, whereas all other soft tissue was excised. The cervical spine was fixed in polymethylmethacrylate at the superior vertebrae, C1, and the inferior vertebrae, T1. Following a standard C5 corpectomy, the specimen was then mounted on a spine testing machine capable of applying pure moment bending through independently controlled counter-acting torque motors (SmartTest, Bose, Eden Prairie, MN). The spine tester, shown in Fig. 2, depicts the flexion extension motors mounted on the superior and inferior platforms of the tester. The lateral bending motors work in similar fashion in the coronal plane of the platforms. Axial compression and axial torsion are independently controlled from the superior and the inferior aspects of the bending motor platform, respectively.

The ASTM F1717-10 protocol depicted in Fig. 1, requires each construct to sustain 5×10^6 cycles without failure as a minimum endurance life for the hardware. The cadaveric testing, illustrated in Fig. 3, represents cyclical loading under pure moment bending in an environment considered more physiologic than vertebral bodies machined from polyethylene blocks.

The test regimen for each specimen included four modes of loading, flexion extension bending, lateral bending, axial torsion, and axial compression. Flexion extension bending, lateral bending, and axial torsion modes were cycled to ±2.5 N m per recommendations from Goel et al. [6]. In the axial compression mode of loading, a compressive load was applied to the superior vertebrae without a follower load. The axial compression protocol was cycled between 0 and 150 N representing an approximation of two times mean transmitted head weight [7]. All testing was performed under a continuous load control protocol with a sinusoidal waveform corresponding to a period of 200 s/cycle. Also, a 10 N compressive seating pre-load was applied to each spine during the flexibility test protocol following the specified treatment and prior to the onset of all modes of loading. For each mode of loading, three test cycles were under the same actively maintained constant pre-load with the third cycle interpreted for data analysis.

The six degree of freedom kinematic response for each vertebral body in the treated functional spinal unit, was measured through active light emitting diode markers arranged in a noncolinear fashion with four markers on each rigid

TABLE 1—*Specimen donor data.*

Specimen	Age	Height, in.	Weight, lbs.	Sex	DEXA (BMD)	Cause of Death
1	63	63	170	F	0.561	Amyotrophic lateral sclerosis
2	68	65	131	F	0.537	Amyotrophic lateral sclerosis
3	83	70	190	M	0.646	Alzheimer's disease
4	31	Not Available	Not Available	F	0.705	Overdose
5	67	70	210	M	0.718	Chronic obstructive pulmonary disease
6	58	64	230	M	0.426	Pending toxicology

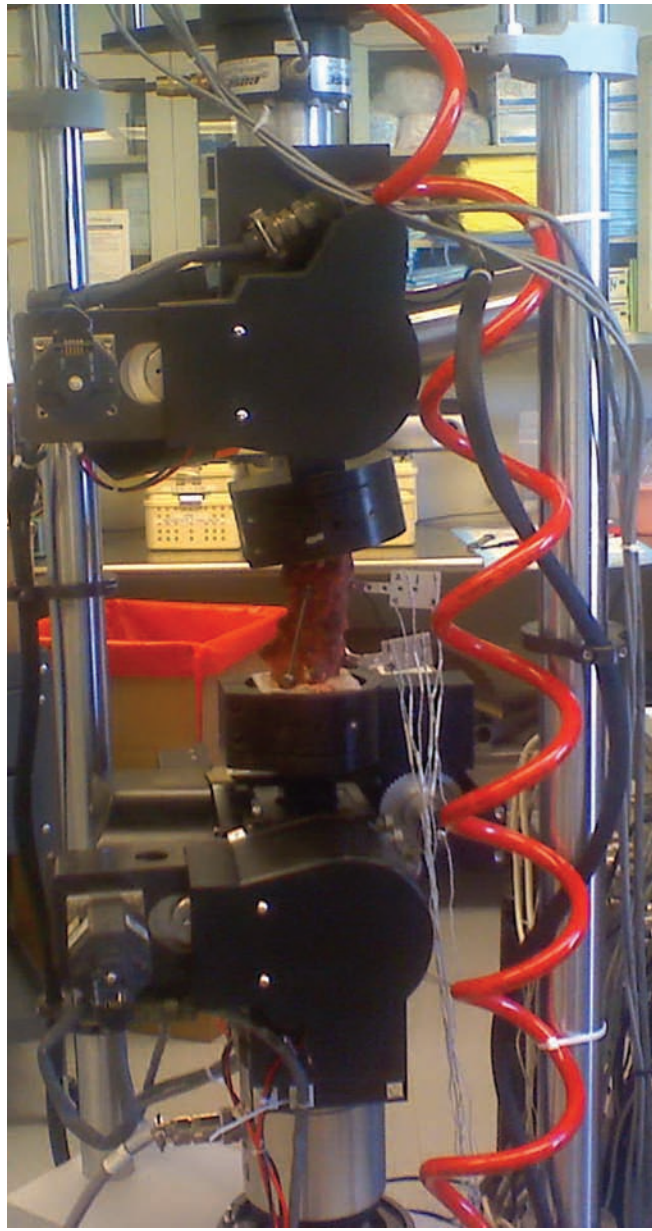

FIG. 2—*Spine tester with electric motors for flexion extension bending on the spine subsystem.*

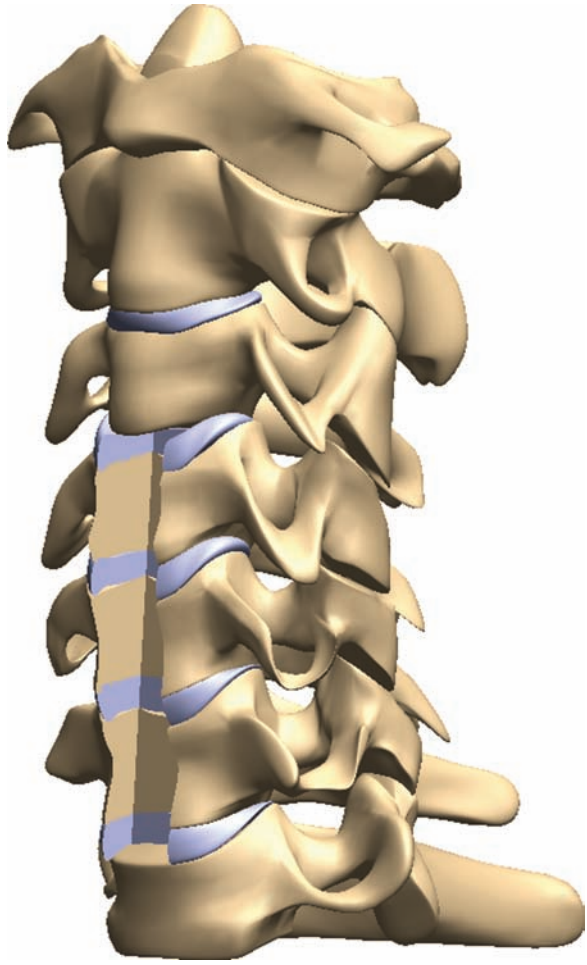

FIG. 3—*C5 corpectomy treatment without anterior column support.*

body flag. Flags were placed on the vertebral bodies of C3 and C7. The kinematic response at C3 was taken relative to C7. All linear and angular measurements were recorded from C3 with C7 as the origin for each mode of loading. The signal emitted from the markers was tracked by an optical electronic measurement system (Optotrak, Northern Digital Instruments, Waterloo, ON, Canada) that utilized a three camera array tracking unit for submillimeter accurate measurements.

Each specimen was subjected to the same corpectomy procedure and biomechanical test regimens. Each specimen underwent the same sequential treatments and biomechanical testing as follows:

1. Intact.
2. C5 corpectomy.

3. Posterior cervical instrumentation from C3 to C7 with screws placed in the lateral mass of the C3 and C7 vertebrae.
4. Pre-cyclical test protocol in four modes of loading.
5. Ten thousand cycle flexion extension bends to ±2.5 N m at 1 Hz.
6. Post-cyclical test protocol in four modes of loading.

A graphical sequential representation of the treatment algorithm is shown in Fig. 4. The first test protocol to include flexibility testing was treatment 4.

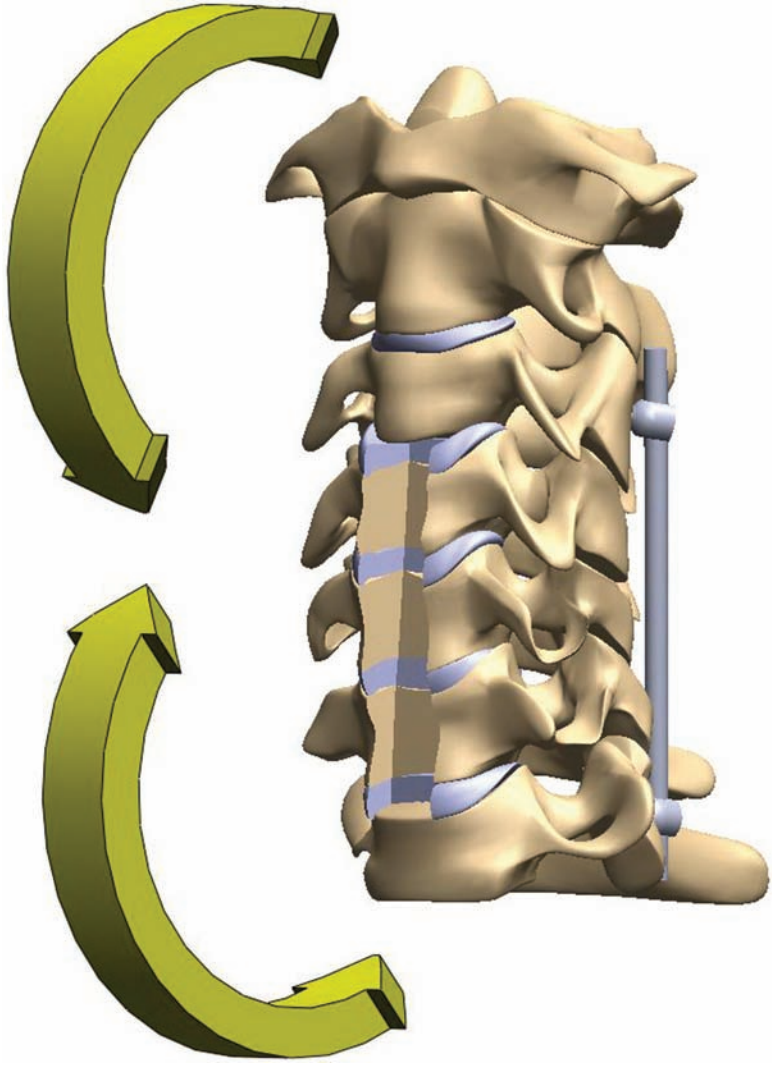

FIG. 4—*Illustrated C3–C7 posterior fixation treatment with pure moment flexion extension bending moments. Each specimen was potted at C1 and T1, although T1 is not depicted here.*

Treatment 6 subjected all specimens to the same test protocol as treatment 4 and the results of the third cycle data were used in the analysis. The actual fatigue cyclical loading occurred in treatment 5 for each specimen with none of the data used for comparison purposes.

The normalized range of motion (ROM) of the specimens was compared via a repeated-measures one-way analysis of variance (ANOVA) model in order to detect differences among the treatment groups. If a significant difference was detected, the least significant difference (LSD) post hoc analysis was used to determine which treatments were significantly different with significance set at the 0.05 level.

Results

The ROM for the vertebral bodies immediately adjacent to the corpectomy, C3–C7, are shown for each specimen in each mode of loading in Table 2. The mean flexion extension bending ROM was 18.0° ± 10.7° prior to the 10 000 cycle bending protocol. Following cyclical loading, the mean ROM measured 22.0° ± 19.9°. The ROM for lateral bending pre- and post-cycling was 5.3° ± 1.8° and 9.7° ± 13.3°, respectively. For axial torsion, the results were 22.9° ± 15.3° prior to cycling compared to 27.5° ± 21.3° post-cycling. Finally, in axial compression the mean ROM was 4.1 ± 1.9 mm prior to cycling and 4.2 ± 1.4 mm post-cycling. Figure 5 graphically displays the mean and standard deviation of the ROM for the flexion extension, lateral bending, and axial torsion modes of loading both pre- and post-cyclical loading.

Although the mean motion increased for flexion extension bending, no statistically significant difference could be detected between the pre-fatigue cycling ROM and the post-fatigue cycling ROM ($p = 0.358$). Likewise for lateral bending, no statistical difference was detected ($p = 0.422$). Similarly, a statistically significant difference in axial compression was not detected ($p = 0.466$) between the pre- and post-cycling flexibility testing. However, a statistically significant difference was detected in the axial torsion mode of loading ($p = 0.030$) between the pre- and post-cycling testing when ROM was used as the comparison metric. If the sample size was increased, it would be reasonable to expect a higher power in detecting differences between pre- and post-cycling ROM in all modes of loading.

Of the six specimens subjected to the biomechanical test protocol, one experienced construct failure via rod slippage on the right side due to set screw loosening. Although each specimen and treatment was prepared in a manner consistent with clinical procedures by the same clinician and according to the

TABLE 2—*Mean ± standard deviation pre- and post-fatigue cycling ROM for C3–C7 in each mode of loading.*

	Flexion Extension, deg	Lateral Bending, deg	Axial Torsion, deg	Axial Compression, mm
Pre-Cycling Mean	18.0 ± 10.7	5.3 ± 1.8	22.9 ± 15.3	4.1 ± 1.9
Post-Cycling Mean	22.0 ± 19.9	9.7 ± 13.3	27.5 ± 21.3	4.1 ± 1.4

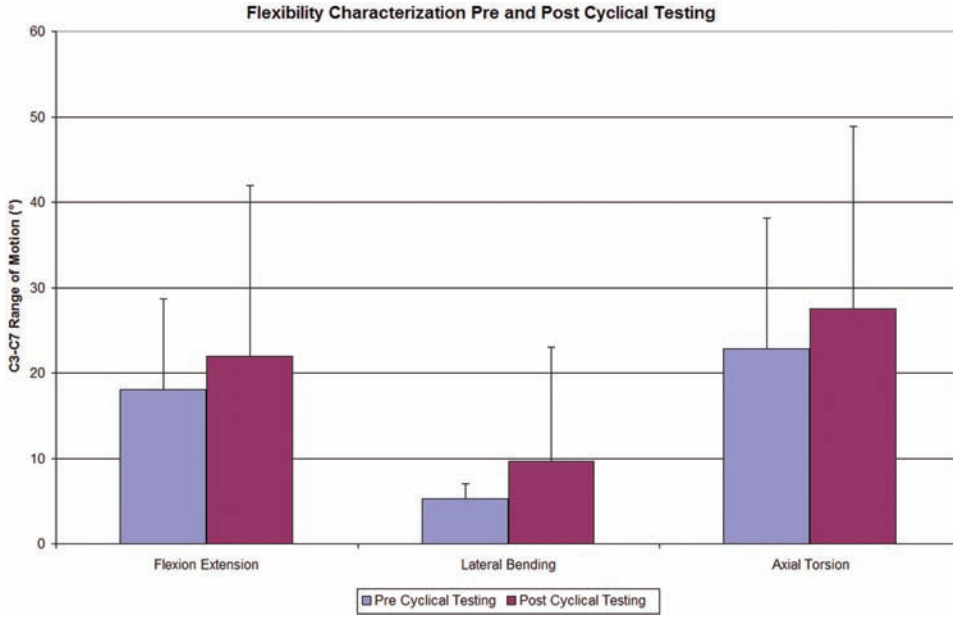

FIG. 5—*Mean ± standard deviation ROM pre- and post-cycling for flexion extension bending, lateral bending, and axial torsion.*

manufacturer's instructions, the set screw loosening was an unforeseen complication. Regardless, the ROM was sufficiently sensitive to detect statistically significant results as indicated in the above-mentioned results for all six treated specimen.

Discussion

The biomechanical tests performed in this study were designed to characterize the ability of a posterior cervical construct to immediately stabilize a corpectomy at C4–C6 with only posterior instrumentation implanted at C3 and C7. Moreover, after 10 000 flexion extension cycles the same biomechanical flexibility protocol was repeated to establish the integrity of the instrumented cervical spine over a short time period simulating the period following failure of all anterior column support or following surgery. From the study, the posterior cervical construct did not exhibit statistically significant differences between the pre-cycled stability and the post-cycled stability in flexion extension, lateral bending, and axial compression as measured by the ROM from C3 to C7, but for all three modes of loading, the mean of the pre- and post-cycling ROM increased. Moreover, in axial torsion, the ROM was statistically significantly increased after cycling compared to pre-cycling stability.

The increase in axial torsion ROM was clinically important given the early time frame that 10 000 cycles would represent in the healing process and the associated loss of stability in the axial plane as opposed to the sagittal bending plane. The 10 000 cycle loading protocol approximates the condition shortly

after the surgical intervention, or following corpectomy graft dislocation with little structural competence from the anterior column. The testing simulated the condition where no fusion had occurred and no fusion construct including allograft struts or corpectomy cages would provide anterior column support, particularly in extension bending. Thus, the clinical analogy was one in which the posterior cervical system was responsible for providing a majority of the stability in the cervical spine. It is important to note the results from this research suggest that patients instrumented with posterior cervical fixation systems should limit activities that involve axial torsion prior to the onset of fusion particularly in compromised or in the absence of anterior column support.

The U.S. Food and Drug Administration (FDA) has cleared a number of upper thoracic screw devices that are commonly used in the cervical spine as posterior stabilization devices at the surgeon's discretion. Screw–rod constructs have been clinically successful [8–10] in the cervical spine due in part to large angle implant versatility and construct stiffness. However, to date there have been no FDA 510(k) cleared polyaxial bone screw and rod constructs for use in the cervical spine. The implant hardware provides surgeons with different screw orientations for the placement of the bone screw implants thereby mitigating risk by allowing alternate bone screw trajectories with known lower complication rates. The combination of stability and intraoperative ease of use has generated increasing popularity for posterior techniques in the cervical spine involving screw–rod constructs. The labeled indications for posterior cervical instrumentation are as temporary adjuncts to fusion, and over time it is commonly accepted that the devices help promote arthrodesis. As the fusion mass becomes weight bearing, the hardware becomes obsolete. In the rare cases that the hardware is integral to long term stability, e.g., pseudoarthrosis or fibular strut graft dislocation, posterior cervical constructs provide stability not only in the condition immediately post-operatively, but also in certain anatomical planes of loading following cyclical loading independent of arthrodesis or anterior column competency as confirmed by this study.

Posterior occiptocervicothoracic spinal fixation systems are traditionally submitted to the FDA with results from the ASTM F1717 test standard [1]. When systems include occipital components that are connected to the cervical and potentially the thoracic spine, the FDA submission would include the test results from the ASTM F2706-08 standard governing occipital-cervical and occipital-cervical-thoracic spinal implant constructs in a vertebrectomy model [11]. The F1717 vertebrectomy test configuration represents a worse case condition and the protocol provides specific guidance for bench top studies that are designed to be independent of biologic and laboratory variability. However, for these types of tests to be more clinically relevant, defined as the correlation between bench top studies and patient outcomes, biomechanical cadaveric studies must associate test results with potential patient complications including bone screw interface effects. The physiologic variables introduced in this study represent a worst case physiologic environment due to the lack of active bone remodeling and other soft tissue degradation. The biomechanical protocols test both the implant and the construct in a cervical spine along with challenges and limitations associated with the surgical environment.

The bone screw interface is critical for immediate stabilization and fixation. The effects of design may not be readily apparent immediately post-operatively. For the period that occurs prior to the onset of arthrodesis, conditions may arise in which patients may rely completely on the hardware. In the test condition, the worst case was approximated through a corpectomy model with no anterior column support. Although standardized protocol testing calls for such constructs in a polyethylene vertebrectomy model without anterior column support, representing a worst case, the bone screw interface is optimized, representing a best case scenario. Protocols for repeatability are designed to test implant constructs and not necessarily the bone screw interface. Consequently, these devices must prove safety and efficacy through comparison of constructs in both bench top and biomechanical protocols. Also, static and dynamic testing is required in the validation and verification of these implants. Physiologic testing provides the opportunity to understand the performance of these constructs, which depends on the host environment as well as the implants. Clearly, bone quality and screw interface are critical for the stability of the construct. Future tests may require longer cadaveric testing ultimately due to higher cycle requirements. However, limitations related to the viability of the tissue in prolonged testing are difficult to overcome.

The advent of bone screws placed with appropriate and safe trajectories has mitigated the complications and challenges associated with cutout from wiring and loosening due to hook–bone interface seating. With the development of screw-plate constructs, clinical outcomes were satisfactory and advances were made with regard to segmental stability [12–14]. The introduction of bone screws for posterior cervical applications originally was a source of concern due to the potential complications from compression or injury to the vertebral artery or neural structures. As the technique became more familiar, the remaining challenge was the constraint of the implants. The posterior plate position was initially dictated by a hole or slot of the implant and then, the remaining screws were constrained by hole spacing. Not only were the insertion points limited, but the screw trajectory was also constrained. Additionally, plate constructs lacked crosslinking capability, which did not allow for the correction of torsional instability [15].

Posterior cervical constructs may potentially present problems ranging from moderate inconveniences to major intraoperative problems. It is important for the clinician to recognize the advantages and disadvantages of each class of implant technology. The multiaxial screw and rod constructs have well documented biomechanical strength advantages that have contributed to the stability of cervical spines for arthrodesis procedures. With the appropriate high risk anatomical landmarks identified, appropriate screw trajectory can mitigate potential hazards associated with bone screw placement. These factors have contributed to the success of multiaxial screw and rod constructs in the cervical spine and have supplanted other posterior cervical implants, but conditions for axial torsional stability in situations lacking sufficient anterior column support should be understood and addressed. Specifically, the construct integrity may be challenged with cyclical loading and the bone implant interface may need further consideration particularly in axial torsion.

Additionally, both the osteoligamentous structures along with the hardware implants will be affected under cyclical test protocols. It is important to recognize these limitations in any experimental setup. These results are meant to predict potential weaknesses for the construct in the *in vivo* condition that are not otherwise obvious in the standard ASTM protocols including ASTM F1717 [1] and F2706 [11]. Other types of testing including direct screw toggle measurement pre- and post-cyclical would provide construct specific information including bone screw interface and should be consideration for future work.

Finally future work should also include other modes of cyclical loading. Flexion extension bending has been shown to be the primary mode of loading in daily activity [5], but this does not address the frequency, amplitude, or the potential for significant damage that may arise in the other modes, particularly during cyclical axial loading or displacement. It has been well established that torsion presents a challenge to any construct and hence the inclusion of a dynamic axial displacement section in F1717. For our initial protocol, it was deemed important to establish a viable test routine including cyclical loading in a cadaveric model to supplement existing construct information provided by standard test methods. Newer protocols should incorporate other modes, particularly axial torsion.

Conclusions

Although the current ASTM guidelines provide consistent methodologies for bench top mechanical testing, biomechanical cadaveric testing remains an important step in the validation of all spinal instrumentation. The biomechanical test regimen for the same constructs detected significant changes pre- and post-fatigue cycling in the axial torsion mode of loading. Significant pre- and post-changes were not detected in flexion extension bending, lateral bending, or axial compression. In a clinical setting, the results of this work would suggest that immediate return to function should be limited to activities that do not include axial torsion particularly in situations where anterior column support is inadequate.

Acknowledgments

The writers wish to acknowledge the sponsor for the research funding that made this study possible. The implant system discussed here is a commercially available 510(k) cleared system with polyaxial bone screws approved for use in the thoracic spine. The surgeon and the research team have chosen to study the screw in an off label indication as deemed clinically appropriate and responsible.

References

[1] ASTM Standard F1717, 2010, "Standard Test Methods for Spinal Implant Constructs in a Vertebrectomy Model," *Annual Book of ASTM Standards*, Vol. 13.01, ASTM International, West Conshohocken, PA, pp. 643–659.

[2] Cunningham, B. W., Sefter, J. C., Shono, Y., and Mcafee, P. C., "Static and Cyclical Biomechanical Analysis of Pedicle Screw Spinal Constructs," *Spine*, Vol. 18, No. 12, 1993, pp. 1677–1688.

[3] Silva, M., Shepherd, E. F., Jackson, W. O., Dorey, F. J., and Schmalzried, T. P., "Average Patient Walking Activity Approaches 2 Million Cycles per Year: Pedometers under-Record Walking Activity," *J. Arthroplasty*, Vol. 17, No. 6, 2002, pp. 693–697.

[4] Syed, F. I., Oza, A. L., Vanderby, R., Heiderscheit, B., and Anderson, P. A., "A Method to Measure Cervical Spine Motion over Extended Periods of Time," *Spine*, Vol. 32, No. 19, 2007, pp. 2092–2098.

[5] Sterling, A. C., Cobian, D. G., Anderson, P. A., and Heiderscheit, B. C., "Annual Frequency and Magnitude of Neck Motion in Healthy Individuals," *Spine*, Vol. 33, No. 17, 2008, pp. 1882–1888.

[6] Goel, V. K., Panjabi, M. M., Patwardhan, A. G., Dooris, A. P., Serhan, H., American Society for Testing and Materials, "Test Protocols for Evaluation of Spinal Implants," *J. Bone Joint Surg., Am. Vol.*, Vol., 88, Suppl 2, 2006, pp. 103–109.

[7] Rapoff, A. J., Conrad, B. P., Johnson, W. M., Cordista, A., and Rechtine, G. R., "Load Sharing in Premier and Zephir Anterior Cervical Plates," *Spine*, Vol. 28, No. 24, 2003, pp. 2648–2650.

[8] Abumi, K., and Kaneda, K., "Pedicle Screw Fixation for Nontraumatic Lesions of the Cervical Spine," *Spine*, Vol. 22, No. 16, 1997, pp. 1853–1863.

[9] Abumi, K., Takada, T., Shono, Y., Kaneda, K., and Fujiya, M., "Posterior Occipitocervical Reconstruction Using Cervical Pedicle Screws and Plate-Rod Systems," *Spine*, Vol. 24, No. 14, 1999, pp. 1425–1434.

[10] Liu, J. K., and Das, K., "Posterior Fusion of the Subaxial Cervical Spine: Indications and Techniques," *Neurosurg. Focus*, Vol. 10, No. 4, 2001, p. E7.

[11] ASTM Standard F2706, 2008, "Standard Test Methods for Occipital-Cervical and Occipital-Cervical-Thoracic Spinal Implant Constructs in a Vertebrectomy Model," *Annual Book of ASTM Standards*, Vol. 13.01, ASTM International, West Conshohocken, PA, pp. 1517–1530.

[12] Ebraheim, N. A., An, H. S., Jackson, W. T., and Brown, J. A., "Internal Fixation of the Unstable Cervical Spine Using Posterior Roy-Camille Plates: Preliminary Report," *J. Orthop. Trauma*, Vol. 3, No. 1, 1989, pp. 23–28.

[13] Levine, A. M., Mazel, C., and Roy-Camille, R., "Management of Fracture Separations of the Articular Mass Using Posterior Cervical Plating," *Spine*, Vol. 17, Suppl. 10, 1992, pp. S447–454.

[14] Roy-Camille, R., Saillant, G., Laville, C., and Benazet, J. P., "Treatment of Lower Cervical Spinal Injuries–C3 to C7," *Spine*, Vol. 17, Suppl. 10, 1992, pp. S442–S446.

[15] Smucker, J. D., and Sasso, R. C., "The Evolution of Spinal Instrumentation for the Management of Occipital Cervical and Cervicothoracic Junctional Injuries," *Spine*, Vol. 31, Suppl. 11, 2006, pp. S44–S52.

LONGITUDINAL SYSTEMS

Reprinted from JAI, Vol. 9, No. 2
doi:10.1520/JAI103505
Available online at www.astm.org/JAI

Laura M. Jensen[1] *and John M. Dawson*[2]

A Method to Test Anterior-Posterior Construct Shear Fatigue Based on the Vertebrectomy Model

ABSTRACT: Dynamic stabilization systems may be subject to anterior-posterior shear loading. However, there is no standard method established for testing a vertebrectomy model in anterior-posterior translation (as may be seen with dynamic spondylolisthesis). A new anterior-posterior shear fatigue test was devised to test one such dynamic stabilization system in anterior-posterior translation. Similar to ASTMF1717 assemblies, constructs were assembled so that screws were placed in ultra high molecular weight polyethylene blocks to attach to the test fixture. The test setup ensures that the entire shear load is transmitted by the implant system. Unlike ASTMF1717 assemblies, the blocks were rotated 180 deg from each other to facilitate loading in the test frame. This configuration is modified from an expected in vivo usage. However, the resultant load vectors are appropriately similar to the shear loads being simulated. The constructs include polymeric components and thus were tested at body temperature in a fluid bath. The blocks were moved ± 5 mm with respect to each other. The constructs were cycled at 2 Hz for a minimum of 5×10^6 cycles. The constructs successfully survived 10×10^6 cycles of anterior-posterior shear displacement. Examination of the constructs demonstrated similarities between components tested via this new method and components retrieved from patients. Comparisons indicate that the shear fatigue test may stress the components as much or perhaps more than what was seen clinically.

KEYWORDS: vertebrectomy, shear, pedicle screw, ASTM F1717, anterior-posterior, fatigue, corpectomy

Manuscript received October 6, 2010; accepted for publication November 30, 2011; published online December 2011.

[1] M.S., Zimmer Spine, Minneapolis, MN 55439.
[2] Ph.D., Zimmer Spine, Minneapolis, MN 55439.

Cite as: Jensen, L. M. and Dawson, J. M., "A Method to Test Anterior-Posterior Construct Shear Fatigue Based on the Vertebrectomy Model," *J. ASTM Intl.*, Vol. 9, No. 2. doi:10.1520/JAI103505.

Introduction

ASTM F1717 [1] provides test methods for spinal implant constructs in a vertebrectomy model. The standard includes test methods for compression bending and axial (tension) compression static and fatigue tests. The standard also provides methods for a static torsion test which can be used as the basis of a torsion fatigue test. There is no standard method established for testing a construct in the anterior-posterior (AP) translation. AP translation is not a primary physiologic motion like flexion/extension, lateral bending, or axial rotation. However, this loading direction may be particularly important for certain pathologies such as dynamic spondylolisthesis, where the usual anatomical structures are compromised or absent. In such cases, the implant system may be required to resist or control shear translation and/or carry shear load. If so, testing should be conducted in anterior-posterior translation to demonstrate that the strength and durability of the implant system is sufficient.

To ensure the fatigue strength of a dynamic stabilization system, an anterior-posterior shear construct fatigue test was devised to test the system construct assemblies in this anterior-posterior translation. The purpose of this paper is to present this test method as an example of how devices could be tested in AP shear. This test method has been used for nearly 10 years to test multiple generations of a dynamic stabilization device but has never before been presented in a public forum. However, with increased interest and discussion about how to test dynamic stabilization devices (e.g., the advent of ASTM F2624-07 [2]), this formerly proprietary test method is submitted to stimulate discussion. Furthermore, data generated from in vivo device retrievals will be discussed to provide context for the results seen in constructs tested with this method.

Objective

The purpose of this investigation was to conduct biomechanical tests to evaluate the cyclic (fatigue) performance of a dynamic stabilization system assembly, interconnections, and components when subjected to motions that simulate vertebral body anterior-posterior translation.

Materials and Methods

Similar to F1717 assemblies, constructs were assembled so that screws were placed in ultra high molecular weight polyethylene (UHMWPE) blocks to attach to the test fixture. The device was constructed between both screws, per the manufacturer's recommendations, such that the entire test load was transmitted through the implant. Unlike F1717 assemblies, the blocks were rotated 180 deg from each other (Fig. 1) to facilitate loading in the test frame. This configuration is modified from an expected in vivo usage because the screws are directed in opposite directions. However, the resultant load vectors are appropriately similar to the shear loads being simulated. This modified orientation of the implant components was implemented for convenience in consideration of

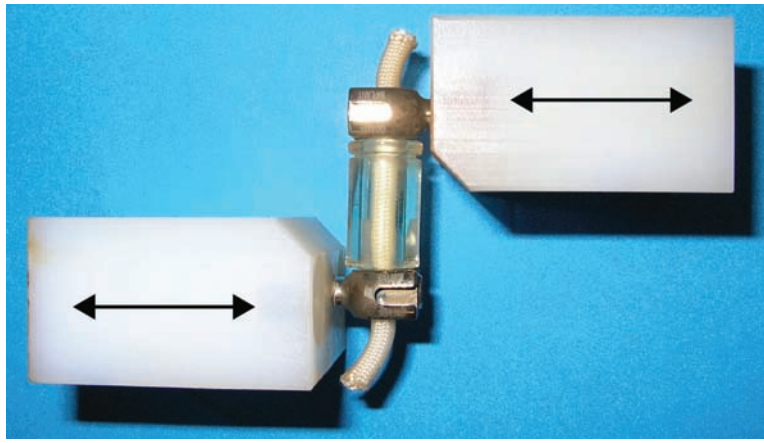

FIG. 1—*A construct assembled for a shear test. The arrows indicate direction of movement.*

the load frame configuration; fixtures could have been designed to conduct the test without modifying the orientation of implant components. The specimen and fixture configuration as well as the test parameters are detailed in the next few sections below.

Test Specimens

This testing was performed on different generations of the *Dynesys* Dynamic Stabilization System family of products (Zimmer GmbH, Winterthur, Switzerland, and Zimmer Spine, Minneapolis, USA.) Generally for each test, multiple constructs were tested simultaneously where each construct consisted of:

- 2 screw anchors (pedicle screws).
- 1 spacer between the 2 screw anchors.
- 1 cord through the spacer and attached to each anchor via.
- 2 set screws (one in each screw to hold the cord).

The implant system's screws are made of titanium metal alloy. The cords are made of polyethylene terephthalate (PET) and the spacers are made of polycarbonate urethane (PCU). Each screw was inserted into its own UHMWPE test block.

Test Fixtures

The test apparatus was configured with two fixture plates, one attached to the test machine actuator and the other was attached to the test machine load cell (see Fig. 2). The load cell was selected where the measured loads were approximately 13 % of the full calibrated range.

A multiplicity of test samples (five or six) was mounted between the fixture plates. Earlier generations of testing generally used five samples (as in Fig. 2),

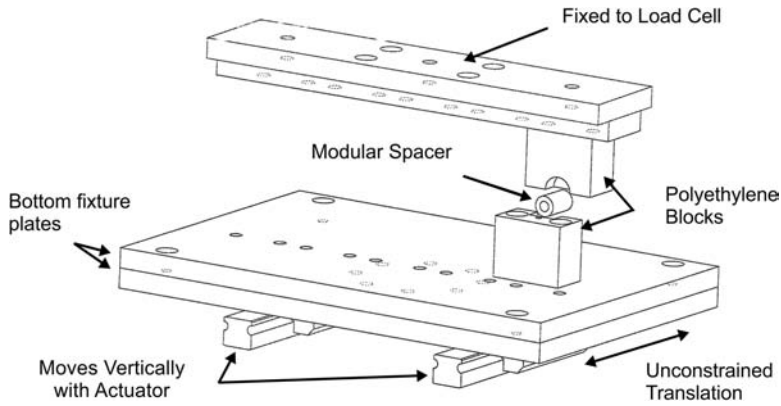

FIG. 2—*Testing configuration showing one assembly. Device cord and screws not shown for clarity; five or six assemblies typically were tested simultaneously; assemblies were immersed in a liquid bath (tank not shown).*

but later generations used six samples as six samples became more widely recognized as a standard minimum [3].

The fixture plates were 1/2-inch thick stainless steel to ensure that the fixtures did not bend during testing and that all samples in a test displaced the same amount. To ensure pure shear loading (as opposed to shear-tension loading), the bottom fixture plate was allowed to glide unconstrained along the perpendicular axis (Fig. 2).

The cords and spacers of the tested system are polymeric components with properties that are temperature dependent. Therefore a tank was attached to the fixture between the bottom fixture plates. The tank was filled with liquid regulated at body temperature (37°C ± 2°C). Different liquid mediums have included distilled water, food-grade soybean oil, saline solution, or Ringer's solution.

Test Methods

Component assembly was performed at room temperature in air. The constructs were assembled per manufacturer's instructs: the cords were tensioned with the cord tensioning instrument designed for the system (approximately 300 N). The set screws were locked into place to secure the cord tension. Consequently the spacers were left in compression after assembly. The cords were cut so they would extend 10 mm beyond the screws.

The constructs were soaked, unloaded, in test medium at body temperature (37°C ± 2°C) for at least 8 h prior to the start of cyclic loading with the exception of those in soybean oil. The lack of soak time for the oil specimens was acceptable because polycarbonate urethane and polyethylene terephthalate (the polymer materials used in tested system) exhibit excellent chemical stability in the presence of lipids, requiring substantial time periods (greater than those used in these tests) for significant absorption and adsorption to occur [4].

After the soak period, the test blocks were attached to the fixture plates. The zero-displacement datum was defined as the position where the longitudinal axis of the specimens was perpendicular to the long axis of the screws (i.e., in the same position as seen in Fig. 1). For the specimens tested herein, it was noted that this zero-displacement datum also coincided with a zero-load condition.

The testing was conducted in sinusoidal displacement control (±5 mm from the zero-displacement datum) at a frequency of 2 Hz to a minimum of 5×10^6 cycles (per the acceptance criteria). However, for all of the specimens reported herein, analysis of the data curves and brief visual inspection of the specimens in the fixtures at 5×10^6 cycles indicated no failure. Therefore, testing was continued for an additional 5×10^6 cycles (for a total of 10×10^6 cycles). Upon completion of testing (10×10^6 cycles), the assemblies were removed from the test fixtures, and all components were individually inspected for mechanical failure. Visible, physical changes were also noted.

Failure Terminology

To assess failure, the constructs and components were examined specifically with the following definitions:

- Failure of the entire construct was defined as any component failure or combination that results in the construct becoming unable to resist load.
- Failure of the spacers would be loss of mechanical integrity as evidenced by cracks visible to the naked eye, rupture of the spacer, or complete parting of the spacer.
- Failure of the screw was defined as breakage of the screw.
- Failure of the cord was defined as parting (complete rupture) of the cord or cord pullout from the pedicle screw.

Rationale for Test Methods

Cycle Count—Construct test standard ASTM F1717 recommends testing to a cycle count of 5×10^6 cycles [1]. The standard suggests that 5×10^6 cycles could represent about 2 years of moderate activity in vivo [1]. Consistent with ASTM F1717, cycle count for this test was also set at 5×10^6 cycles initially for this test. Continuing the test to 10×10^6 cycles was considered acceptable because it represents a more stringent test than 5×10^6.

Translation Amount—A key motivation for this test is to simulate motion as would be similar in a spondylolisthesis patient. Spondylolisthesis is defined in terms of displacement where a grade 1 spondylolisthesis is defined as a displacement of 25 % or less than the depth of the vertebral body. A study measuring the anatomical dimensions of vertebral bodies found that the average endplate depth (anterior-posterior direction) was 35 mm [5]. A grade 1 spondylolisthesis, therefore, would exhibit a maximum vertebral body translation of about 9 mm.

Therefore, the translation in this test was ±5 mm (for a total range of motion equal to 10 mm).

Longitudinal Element Length—In a lumbar vertebrectomy construct for F1717, the active length of the longitudinal element is recommended to be 76.0 mm to simulate a worst case bending situation. While F1717 is not a clinical test and is not directly applicable to clinical situations, the test parameters are informed by clinical anatomy. For example, the 76.0 mm dimensions are based on skeletal measurements of two-level constructs [6].

With a shear test, however, a shorter longitudinal element is a more rigorous test than a longer element. The shorter longitudinal element is more rigorous because the ratio of proportional shear translation to perpendicular translation is higher thus producing greater shear deformations. On the other hand, tests become difficult to fixture and execute for relatively shorter longitudinal elements. For the implant system studied here, a typical length for the longitudinal element (the spacer component) was 22.5 mm. This 22.5 mm length represents the active length in these tests and gives a screw head-to-screw head (center to center) length of 30 mm.

The length of the cord component is determined by the length of the spacer. Per surgical technique, the cord is tensioned and then secured in place by set screws to the pedicle screws. After the cords were tensioned and secured, the cords were cut so that they extended 10 mm past the outside head of the screw.

Results and Discussion

Each time this test was conducted, all five or six constructs survived 10×10^6 cycles of AP shear fatigue (exceeding the 5×10^6 minimum requirement) and were still resisting load at the end of the test. The test medium did not affect the survivability of the constructs: all solutions produced similar and acceptable results.

Construct Integrity

All constructs were able to resist load at the end of 10×10^6 cycles. None of the components failed, and none of the component interconnections failed. Thus the constructs were intact and did not fail according to the definition in *Failure Terminology*.

Resistive Loads During Testing—Figure 2 shows a representative typical plot of resistive load versus cycle count for the duration of the test. The reported loads represent the total resistance for the five or six constructs being tested simultaneously in one testing load frame (i.e., each construct would carry approximately 1/5th or 1/6th of the load). The continuity of the data is evidence that all constructs resisted load throughout the test; there would have been a sudden decrease in the magnitude of the load (of about 1/5th or 1/6th of the load) if one of the five or six specimens were to have failed to resist load. Since all specimens resisted load throughout the test, they all met the acceptance criterion.

The resistive load decreases initially which is a normal response for polymeric materials like the PET cord and the PCU spacer (Fig. 3). Ultimately the curve appears to approach an asymptotic level above zero. This diminishing rate of change implies that the specimens would continue to resist load beyond 5×10^6 (and beyond 10×10^6) cycles. Data for the additional 5×10^6 cycle tests support this assumption where the final resistive loads are slightly less than 90 % (89 % in the same specimens as Fig. 3) compared to the end of the first 5×10^6 cycles.

Physical Examination of Construct—Upon completion of the testing, the specimens were removed from the machines and examined individually and under magnification up to 40x. Notable changes are described below. These changes were typical and consistent for each time the test was run and for all test mediums.

The spacers showed no loss of mechanical integrity. The faces in contact with the heads of the screws were smooth and were burnished. Some conformation to the screw face was noted and described as deformation of the spacer. The spacer deformation patterns are typical and based on the geometry of the screw in contact with the spacer. Spacer components retrieved from patients have exhibited similar deformation patterns [7–9]. Among tested specimens, the deformation pattern of the oil-immersed specimens was located closer to the cord than that of the water-immersed specimens. The location of the

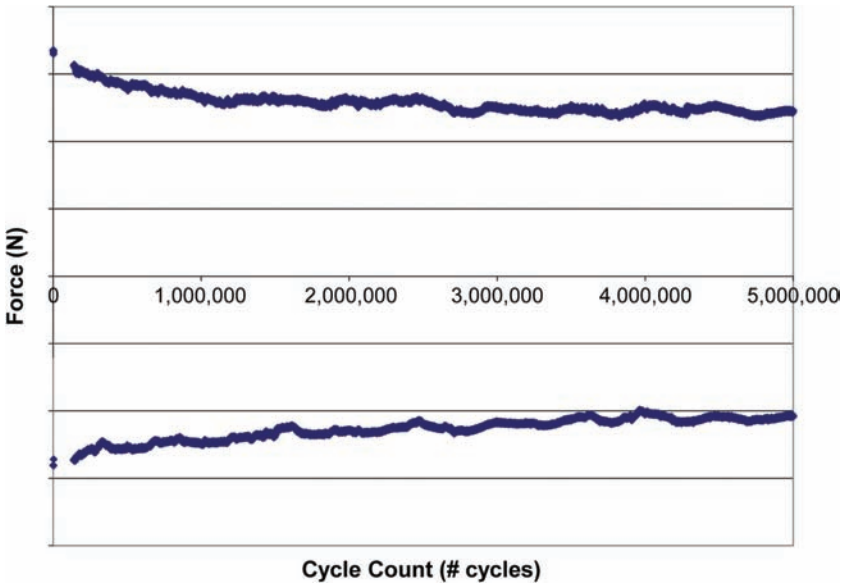

FIG. 3—*Typical plot of resistive peak load versus number of cycles of shear fatigue. Positive load values indicate that the constructs were in tension (i.e., actuator displacement of +5 mm) while negative load values indicate that the constructs were in compression (i.e., –5 mm).*

deformation pattern for the oil-immersed specimens is consistent with greater relative motion between the spacer and the screw compared to the water-immersed specimens, possibly due to the more lubricious nature of oil compared to water.

The screws survived 10×10^6 cycles with no loss of mechanical integrity. In general, the screws looked substantially equivalent to untested screws.

The cord did not rupture, break, or pull out of the pedicle screw. It showed no loss of mechanical integrity. There was superficial breakage of PET fibers on the outer surface of the cord in two areas: (Zone 1) underneath the set screw and (Zone 2) the area of the cord under the junction where the spacer met the screw face. In vivo retrieval studies have not noted significant damage to the cord [7–9]. A study by Trommsdorf and Köttig reports "There were no cases of in vivo fracture of cords or spacers. The retrieved cords typically show minor damage of the outermost fiber-layer in the region of the fixation and no damage elsewhere." [8]. Another study which noted some breakage of outer fibers [9] also noted that it was difficult to find any breakage because the observed area tends to get obscured during implant removal. The implant removal is more difficult in vivo than in the lab and thus damage may be easier to define in the lab specimens. In all of these papers [7–9], the minor damage seen in vivo is consistent with the broken fibers noted in this study in Zone 1 under the set screw. For comparison, assembled but untested specimens were examined and found similar damage. Therefore, this cord deformation seems to be from the initial assembly of the construct but does not appear to worsen during the cyclic testing. The retrieval studies did not note anything correlating to the Zone 2 fibers where the spacer met the screw face. Zone 2 damage suggests that either the shear fatigue test is more rigorous than the in vivo loading environment (i.e., supraphysiologic) or the test induces some nonphysiologic damage.

For all the components, the minor changes did not affect the system integrity and the system remained able to function as intended. None of the changes have ever been implicated as problematic in vivo.

Limitations

This AP shear test method has been shown to be executable and applicable to generate fatigue results that produce implant changes similar to those seen in retrieval studies. However, the test method was never able to produce mechanical failures in the tested system's implants. Ideally a test method would demonstrate failure modes, but these have not been demonstrated yet.

This test method has only been tried on implant components of the *Dynesys* system and has not yet been tried on other types of devices. Other potential types of devices to test include PEEK or metal rods.

This test method was able to test multiple constructs at once because it was tested in displacement control. For other types of devices, a load-controlled test may be more appropriate. In load control, each construct would be tested individually.

The individual resistive loads of each construct could not be measured in this fixture. Instead, one load cell was used to measure the force of all constructs

at once. The loads were assumed to be equally distributed among all the constructs because they had equivalent displacements. A fixture was built to incorporate individual load cells for each construct, and it was tested with a Ringer's solution as the test medium (Fig. 4.) Unfortunately, the load cells (XLS8-100 lb, Load Cell Central, Monroeton, PA) did not survive the fatigue test—probably due to salt corrosion. After more fixture development, a future study could measure the loads of each construct individually.

The material properties of the tested system's components dictated a maximum test rate of 2 Hz to prevent heating of the polymeric components. However, other devices might be able to tolerate increased test rates.

When assessing applicability to other specimens, device geometry should also be considered. For example, this fixture with the rotated blocks may not be appropriate for curved rods. However, curved rods could theoretically be tested in a similar manner if the fixture were altered to accommodate blocks oriented more similarly to ASTM F1717 constructs.

This test method used a symmetrical displacement movement of ±5 mm. For context, it was noted that this 10 mm range is slightly larger than the maximum range of motion of a grade 1 spodylolisthesis for an average patient. However, a clinical spondylolisthesis motion might be assumed to be a movement of 10 mm asymmetrically in one direction. Therefore, a future study might try changing the distribution of the displacements to a 0 to 10 mm range instead of ±5 mm.

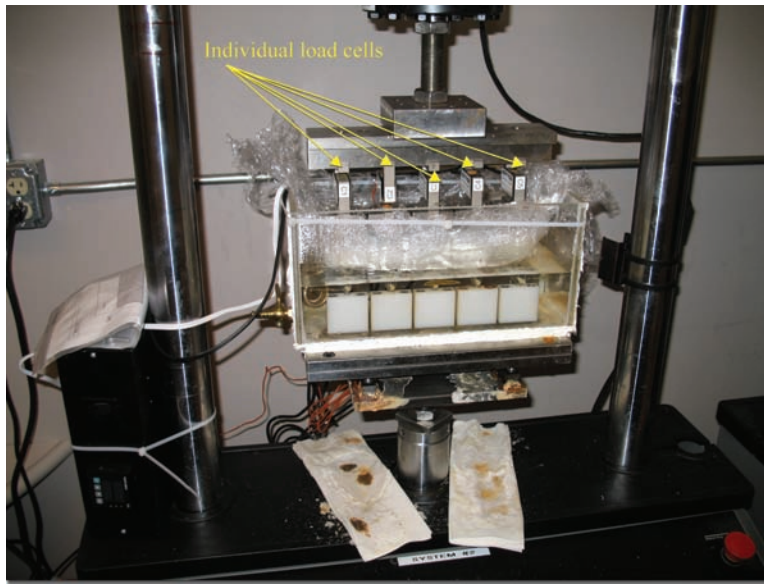

FIG. 4—*An example of a shear test fixture with individual load cells for each specimen construct. Unfortunately, the individual load cells did not survive* 10×10^6 *cycles and the tank developed a leak.*

Conclusions

The fixture and methodology has been established in this study for an anterior-posterior shear fatigue test. This AP shear fatigue test provides a means to test constructs in the anterior-posterior shear translation—a direction previously not tested with current international spine test standards.

Data generated using this shear fatigue test demonstrated that the tested system successfully survived 10×10^6 cycles of AP shear fatigue without failure.

Examination of the constructs demonstrated similarities between components tested via this new method and components retrieved from patients. Comparisons indicate that the shear fatigue test may stress the components as much or perhaps more than what is clinically observed. The similarities between the in vivo components and the test components indicate that the shear fatigue test can be an appropriate method to test dynamic stabilization constructs.

References

[1] ASTM Standard F1717-11a, 2011,"Standard Test Methods for Spinal Implant Constructs in a Vertebrectomy Model," *Annual Book of ASTM Standards*, ASTM International, West Conshohocken, PA.

[2] ASTM Standard F2624-07, 2007, "Standard Test Method for Static, Dynamic, and Wear Assessment of Extra-Discal Spinal Motion Preserving Implants," *Annual Book of ASTM Standards*, ASTM International, West Conshohocken, PA.

[3] *Guidance for Industry FDA Staff, Spinal System 510(k) s*, Document issued on May 3, 2004 by the U.S. Food and Drug Administration, Rockville, MD, 2004.

[4] Tanzi, M. C., Mantovani, D., Petrini, P., Guidoin, R., and Laroche, G., "Chemical Stability of Polyether Urethanes Versus Polycarbonate Urethanes," *J. Biomed. Mater. Res.*, Vol. 36, No. 4, 1997, pp. 550–559.

[5] Panjabi, M. M., Goel, V., Oxland, T., Takata, K., Duranceau, J., Krag, M., and Price, M., "Human Lumbar Vertebrae Quantitative Three-Dimensional Anatomy," *Spine*, Vol. 17, No. 3, 1992, pp. 299–306.

[6] Cunningham, B. W., Sefter, J. O., Shono, Y., and McAfee, P. C., "Static and Cyclical Biomechanical Analysis of Pedicle Screw Spinal Constructs," *Spine*, Vol. 18, No. 12, 1993, pp. 1677–1688.

[7] Trommsdorff, U., Zurbrügg, D., Abt, N. A., Schneider, W., and Rieder, V., "Analysis of Retrieved Components of a Dynamic Stabilization System for the Spine," *Poster, Spine Arthroplast Society Meeting*, 2004.

[8] Trommsdorff, U., and Köttig, P., "Analysis of Retrievals of the Dynesys Dynamic Stabilization System for the Spine," *Poster, Eurospine*, 2005.

[9] Shen, M., Zhang, K., Köttig, P., Welch, W. C., and Dawson, J. M., "In Vivo Biostability of Polymeric Spine Implants: Retrieval Analyses From a United States Investigational Device Exemption Study," *Eur. Spine J.*, Vol. 20, No. 11, 2011, pp. 1837–1849.

Reprinted from JAI, Vol. 9, No. 2
doi:10.1520/JAI103500
Available online at www.astm.org/JAI

Ian Rubín de la Borbolla,[1] *Julien Prevost,*[1] *Christopher Scifert,*[2] *and Joe Turner*[1]

The Use of a Single-Level Construct Model to Evaluate Nonmetallic "Flexible" Rods

ABSTRACT: The current ASTM F1717 standard specifies the static and fatigue testing conditions for extradiscal spinal implant assemblies. For the lumbar region, the standard stipulates a vertebrectomy model for said tests. While this testing setup has proven effective in analyzing overall construct stiffness, yield load, and displacement for rigid constructs, there is a growing segment of products and cases which amendments to the standard might better represent. One opportunity to evolve the current standard is in integrating test parameters which address the greater flexibility of semirigid or flexible systems such as those made from polymeric or metallic-polymeric materials. Since these rods are considerably more flexible when compared to rigid metallic rods, they create unique testing challenges. In addition, the current standard lacks a specification for testing single-level constructs. Considering that the overall dynamics of single-level cases vary greatly from the current vertebrectomy model, a modification or creation of a standard is needed. For the two reasons presented above, a single-level "discectomy" model has been developed to consider these unique testing conditions.

KEYWORDS: ASTM F1717, PEEK rods, load-sharing, single-level constructs, shear, discectomy, polymeric, polymer, flexible rods, semirigid

Introduction

Metallic rods, in association with pedicle screws, have long been used in spinal surgery for stabilizing and facilitating fusion of vertebral bodies. The range of

Manuscript received October 18, 2010; accepted for publication December 5, 2011; published online January 2012.
[1] Spinal and Biologics, Medtronic Inc., Memphis, TN 38132.
[2] Ph.D., Spinal and Biologics, Medtronic Inc., Memphis, TN 38132.

Cite as: Rubín de la Borbolla, I., Prevost, J., Scifert, C. and Turner, J., "The Use of a Single-Level Construct Model to Evaluate Nonmetallic "Flexible" Rods," *J. ASTM Intl.*, Vol. 9, No. 2. doi:10.1520/JAI103500.

pathologies varies from traumatic fracture stabilization to large scale deformity correction to single-segment degenerative stabilization. These corrective procedures are not limited to first-time surgeries and may also encompass iatrogenic corrections. The mechanical requirements for these systems may be quite substantial, and the strength and stiffness of the rods at times must be adequate to withstand extreme pathology. Examples include missing spinal segments, large torsional loads from three-dimensional scoliosis correction, and severe instability. The use of metallic rods for such extreme disorders is well documented from a surgical standpoint; however, flexible rods in the spine are a much younger concept from a clinical standpoint and have had fewer published studies [1].

One standard which was developed to address some of these loading requirements is the ASTM F1717 standard "Standard Test Methods for Spinal Implant Constructs in a Vertebrectomy Model" [2]. The test setup varies between each spinal segment (e.g., vertebral body spacing, test block layout). Specifically focusing on the lumbar region, the standard outlines a vertebrectomy model requirement. This method simulates a scenario wherein the entire central vertebral body has been removed and no unnatural support exists anteriorly. The posterior bilateral construct is assumed to provide any and all stability to the construct. This is an extreme worst case, and truly tests the ability of the system to withstand the harsh conditions which may exist in some patient populations.

It is becoming more common to clinically address less invasive, smaller, and more flexible fixation methods for patients whose pathologies do not require the extremely strong and stiff implant characteristics (e.g. degenerative lumbar disorders, spinal stenosis). In the past few years, spinal device designs have become more pathology specific and tailored to certain types of patients. As surgical options broaden (deformities versus degenerative pathologies), spinal implant designs are diversifying to meet the surgical needs. Other factors of influence for this diversification may include a unique preoperative condition with the patient in addition to adaptations with surgical requirements/techniques.

For these more flexible systems, the aggressive stabilization and load requirements from a biomechanical standpoint are reduced as opposed to an extreme traumatic, degenerative, or deformity case that might require more rigid fixation. Patients in this category typically have fewer involved segments and the degenerative conditions are more stable while containing little to no deformity. A single-level model is desired in part to adhere to surgical techniques outlined for these flexible rod systems (i.e. anchoring at every level), and also to evaluate shear, which will be discussed further.

Due to a greater elasticity in the material, semirigid rods have inherent physical characteristics which allow for increased deflection versus rigid systems. This may be seen as a benefit in an effort to enhance fusion and prevent stress shielding of the anterior graft. This fusion adjunct presents a theoretical advantage by increasing compressive loading to the anterior column of the spine to improve fusion and reducing overall posterior implant stress to reduce implant failure. Semirigid systems have been a highlighted group for posterior dynamic fusions from stenosis and spondylolisthesis to tumor and trauma in

the thoracolumbar region where stability and a more controlled normal motion of the spine is desired. These characteristics will be discussed in depth throughout the article.

The characterizing and assessing of shear is essential due to inherent material differences between polymers and metals; in addition to the need to incorporate it as a guide for design and implant effectiveness. An asymptomatic and healthy spine sustains a natural biomechanical balance of shear (e.g. facets, muscle force, disc). Developments such as facet or disc wear and arthritic conditions can lead to imbalanced shear loading. Over time these imbalances evolve into more degenerative conditions. Depending on the pathology and surgical treatment, a corrective implant may share or sustain all natural shear loading up to the point of spinal fusion. Responsibly addressing the magnitude of this parameter should clarify the importance in improving product evaluation and ensuring design compliance.

Previously, most of these devices were tested under the ASTM F1717 test standard [2]. Figure 1 illustrates the vertebrectomy setup where two UHMWPE blocks represent the vertebral bodies [3]. For the internal setup, the test compared CD Horizon Legacy PEEK rods with its rigid predicate system. When tested to the standard, the semirigid system had historically shown quantitative equivalency to its rigid predicate in static and fatigue loading (e.g., 100 N fatigue load to 5 000 000 cycles). Qualitative equivalency between systems was not always comparable (Figs. 2 and 3) and led to questions regarding yield

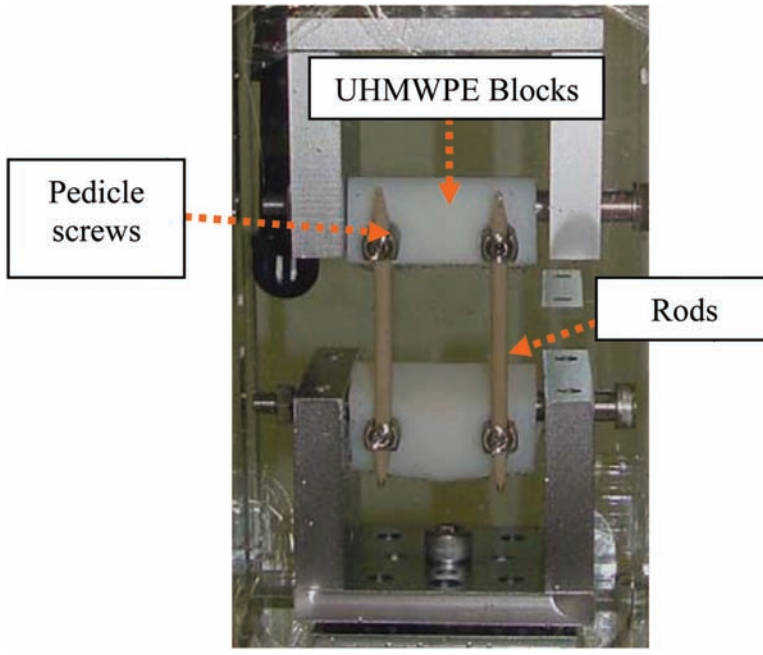

FIG. 1—*Compression fatigue test setup—vertebrectomy model.*

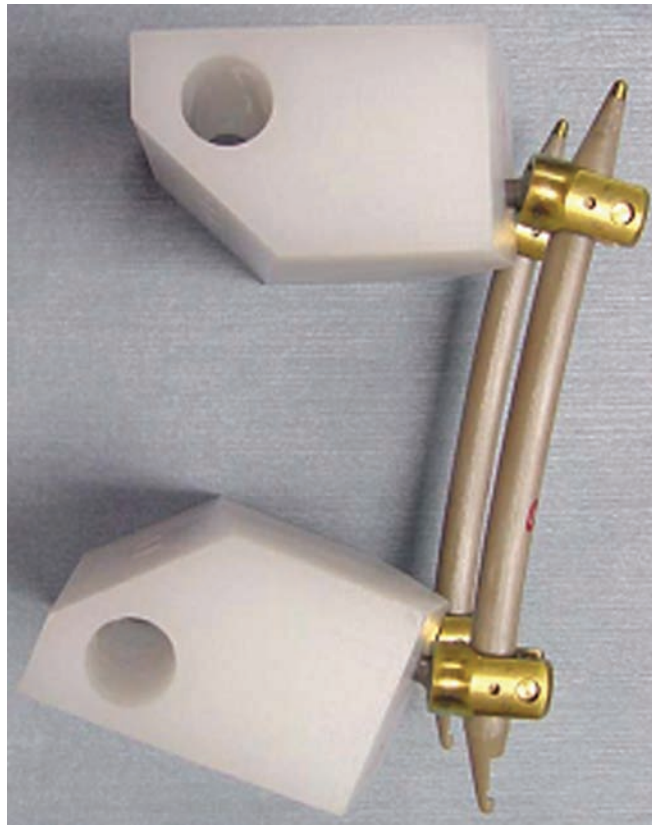

FIG. 2—*Compression fatigue failure at the screw.*

between system components (screws versus rods). (Disclaimer—because load magnitudes in ASTM F1717 testing cannot be correlated to clinical loading, the difference in displacements might be unrealistic when compared to physiological limitations.)

Static semirigid systems showed a 40 % increase in displacement given an equivalent load versus rigid systems. According to Eijkelkamp [4], the mean disc height is 10 mm. In the worst case where there is full disc collapse, the device must not fail. Displacements from synthetic testing were far greater than a more clinically referenced value. Due to the inherently nonphysiologic nature of the displacement resulting from the vertebrectomy test, a more relevant test method may generate more applicable results for situations where the device is used clinically.

For construct fatigue tests, rigid system run-out loads were 35 % lower than the semirigid. Upon closer observation, each system exhibited dissimilar modes of failure; the semirigid system's screws yielded (Fig. 2) and the rigid system's rod failed (Fig. 3). These unequal results could affect the fidelity of more rigid systems' fatigue performance given an equivalent stiffness for both systems.

FIG. 3—*Compression fatigue failure at the rod.*

The presence of shear in the spinal correction (e.g., degenerative disc conditions, pars interarticularis fracture) adds another open variable when evaluating a system against the current ASTM F1717 standard. This loading condition is currently assessed in anterior models (ASTM F2346 standard [5]) (Fig. 4).

In the above configuration, the compressive shear layout consists of an applied resultant force through the superior pushrod with a rigidly attached inferior fixture set at a 45 deg angle. For single-level instrumented cases the current specification may be at times an unrealistic environment in which to test these systems, because of rigid versus semirigid material differences, shear evaluation; in addition to the number of instrumented construct levels. The purpose of this article is to describe a test method for evaluating flexible, semirigid rods in a single-level model.

Methods and Procedures

Single-Level Evaluation

While referencing the current standard, the main focus was to uncover the interpedicular distance of the neutral plane for the proposed single level. Three roads of investigation were evaluated to determine this necessary distance: current single-level literature (to shape an understanding of the indicated level and

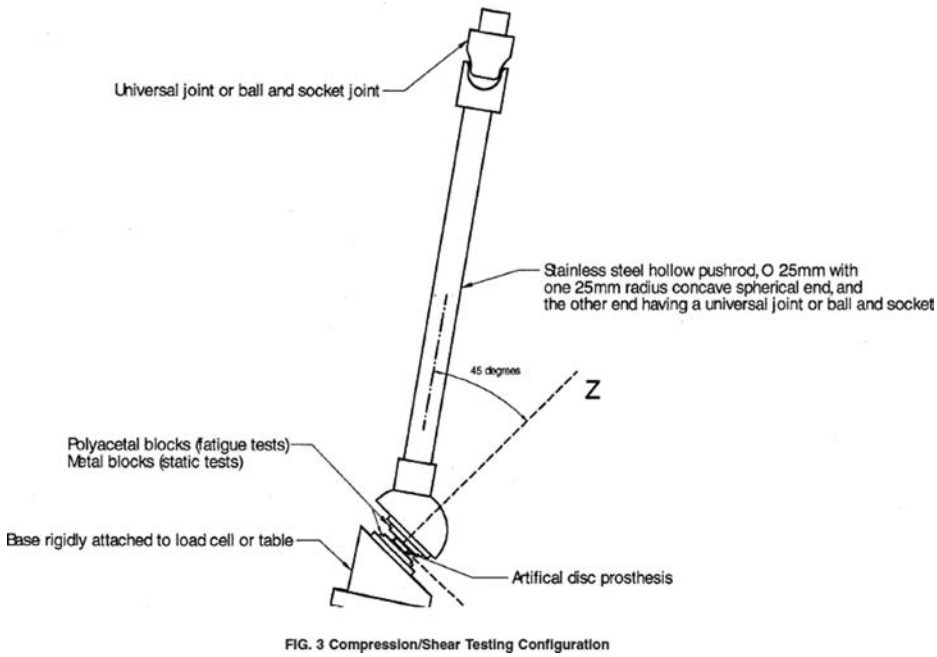

FIG. 4—*ASTM F2346 compression/shear testing configuration.*

pathology), analytical (developing an interpedicular value from the literature's determined level), and empirical (for making a practical in-house method for testing and validating a single-level model).

The following information is divided into both an analytical and experimental format, and focuses on the correlation between each in determining the desired single-level test method. Although data presented is limited to semirigid systems, future side by side comparisons would be needed for rigid systems since predicates of the semirigid vertebrectomy constructs were rigid in origin.

Experimental—Literature Review

To begin, a literature search was generated for cases using flexible instrumentation in the lumbar spine. As mentioned earlier, the search was limited to pathologies which corresponded with the semirigid systems. Search results showed that the implants used to stabilize the lower lumbar spinal segments were predominantly used in single-level or multi-level applications from L3 to S1. These constructs were typically instrumented at every level [1,6–9].

The majority of the cases focused on the following criteria: semirigid systems, degenerative disease, and single-level instrumentation. Highsmith et al. involved three patients with similar diagnoses: all had some form of spinal stenosis with disc bulge and overgrowth, disc degenerative disease, or spondylolisthesis. All patients in this case were instrumented with CD Horizon Legacy PEEK Rod implants (Medtronic Inc., Memphis, TN) [1]. Schaeren et al.'s

primary indication for surgery was due to degenerative spondylolisthesis at L4-L5 (22) versus L3-L4 (4), and evaluated the Dynesys spinal system (Zimmer Spine, Minneapolis, MN) without bone graft [6].

Bothmann et al. involved evaluation of the Dynesys spinal system in 54 clinically evaluated cases. Indications for spinal fusions were 22 degenerative spondylolisthesis (41 %), 9 lumbar disc degenerations (17 %), 6 lumbar disc herniation (11 %), and only 3 segmental instability cases (6 %). Seventy-eight lumbar segments were stabilized and allocated as follows: L1-L2 (2), L2-L3 (5), L3-L4 (22), L4-L5 (36), and L5-S1 (13). Of these, 59 % of the cases were single level [7].

Spinal conditions for Grob et al. were degenerative disc disease where 39 % were located at L4-L5 and L5-S1. This case also utilized the Dynesys spinal system as an implant [8].

Ponnappan et al. compared Expedium PEEK Rods (DePuy Spine, Raynham, MA) with titanium implants through cadaveric testing; however, during these tests instrumentation was focused on L2-L3 and L4-L5. Conclusions from this article included increased anterior column load sharing and a reduction of stress at the bone-to-screw interface for these regions [9].

In the majority of the referenced cases, single instrumentation is used; in addition to some form of semirigid rod placed for posterolateral fusion (PLF). There are variations in pathology and surgical procedure (disc decompression, interbody, bone graft); however, the main focus taken from this clinical data is the indicated use of semirigid rods for degenerative disease in the following region: L3-S1. It is difficult to evaluate the actual loads and resultant forces being subjected pre- and post-operatively; however, it can be concluded from these studies that there is a prevalence of disc and degenerative conditions around the specified region.

Analytical

The next process took into account the above defined spinal segments and evaluated lumbar movement through lateral flexion extension x rays. This method allowed a better understanding of spinal motions and patterns and how each may relate to medical implants fixed to the spine through pedicle screws. Boundary conditions considered included center of rotation, pedicle distance, and neutral position. In establishing these variables for the single-level case, the physiological movement of 50 patients was evaluated. All patients were asymptomatic and healthy at the time of imaging, and a neutral position was calculated referencing each one's flexion and extension positions. The lower lumbar region was tracked (L3-L4, L4-L5, and L5-S1 segments) and geometric pedicle measurements were classified and calculated into the following categories (Fig. 5).

From the figure below, the goal was to measure the distances between vertebral bodies for kinematic evlauation. The equipment used was capable of measuring the changes in interpedicular distance; however, measuring forces would entail more invasive methods and were included for biomechanical reference only.

From the film below (Fig. 6), locations A, B, and C defined the distal vertebral body laterally, and line DE was its corresponding pedicle margin (superior

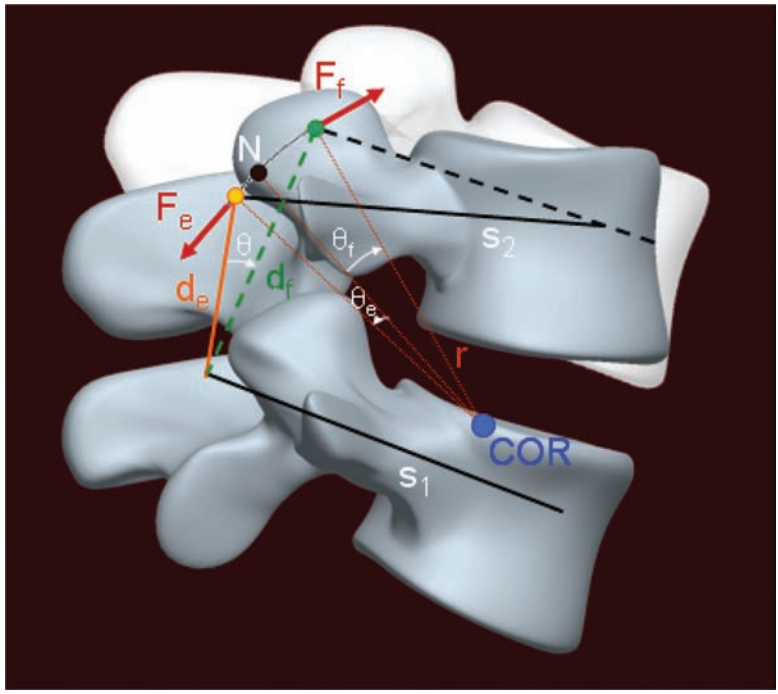

FIG. 5—*Table of terms—single-level analytical analysis.*

to inferior). DE approximated the minimal distance in the pedicle. S1 represented the midpoint reference (M) through DE parallel to AB, as was similar to S2 for the proximal vertebral body. S1 and S2 referenced pedicle screw placements within the vertebral bodies. A focal point F represented the tangency point of the facet joint, and was used to determine the interpedicular distance during extension XY (the line perpendicular to S1 which measured the distance between S1 and S2).

A similar process was used in determining S2′ relative to S1 (Fig. 7) for interpedicular measurement during flexion. The lower vertebral body was frozen between the extension and flexion states, allowing one to view only the change in the upper vertebral components. Keeping X as a reference point from the extension film, line XY' was created by constructing a line perpendicular to S2′. This new line was the defined interpedicular distance during flexion XY'. The angle between XY and XY' was the pedicle flexion-extension angle also defined as the interpedicular angle (range of motion measured in the disc).

To measure the pedicle of the sacrum, it was necessary to track its engagement along the L5 vertebral body (inferior aspect of L5-S1). From this, a theoretical pedicle screw trajectory was determined (Fig. 8).

Referencing Table 1, the study predicted the calculated maximum displacement occurring in the L4-L5 region for extension range of motion with a mean

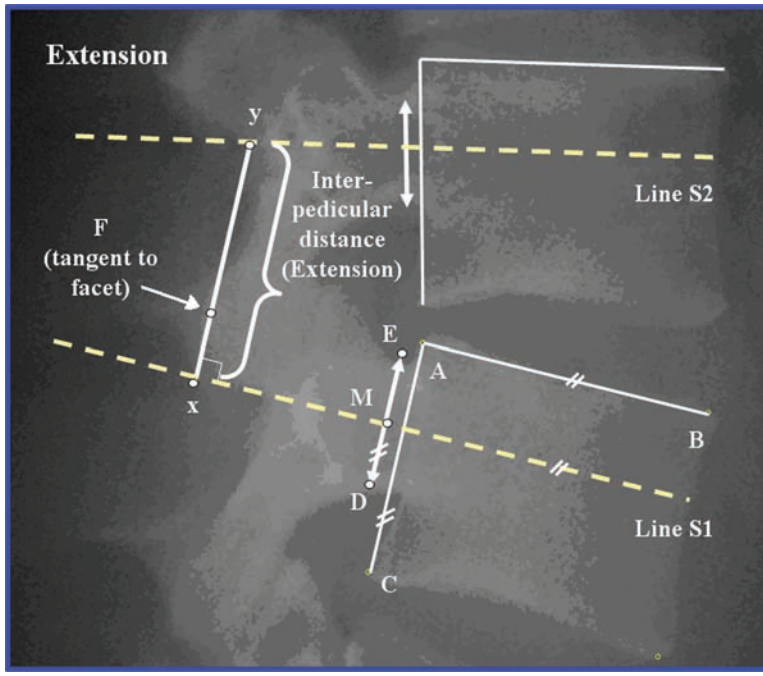

FIG. 6—*Illustrative layout for measurement of interpedicular distance (xy) from an extension film. The location of the interpedicular line was defined as the tangency point to the facet (F).*

difference of 9.2 mm of interpedicular motion. From this, the interpedicular distance was calculated.

The overall dynamics of single-level cases varied from the current ASTM F1717 vertebrectomy model (Fig. 5), both from centroid positioning to interpedicular distance (single versus two level). From the data above, the advised superior-inferior screw-to-screw spacing was calculated at 30 mm. This value was similar in range to Chaynes et al. [11], which measured vertical interpedicular distances at L4-L5 around 30 mm for a 10 sample cadaveric lot. This 30 mm offset represented the previously mentioned "discectomy" distance.

Experimental—Synthetic Model Testing—Current ASTM F1717 Constructs

Citing the aforementioned indicated levels and calculated interpedicular distance rationale, modifications were developed to represent the discectomy testing guidelines based on the current ASTM F1717 standard. Adaptations included an adjustment in interpedicular distance from a vertebrectomy to a discectomy model (30 mm) and the addition of a component for testing in anterior and posterior shear. Unless specified, the remaining setup for ASTM F1717 was adopted (e.g., UHMWPE blocks and attachments [3], load ratio, offset displacement equations [2], rate of testing, tared initial load conditions).

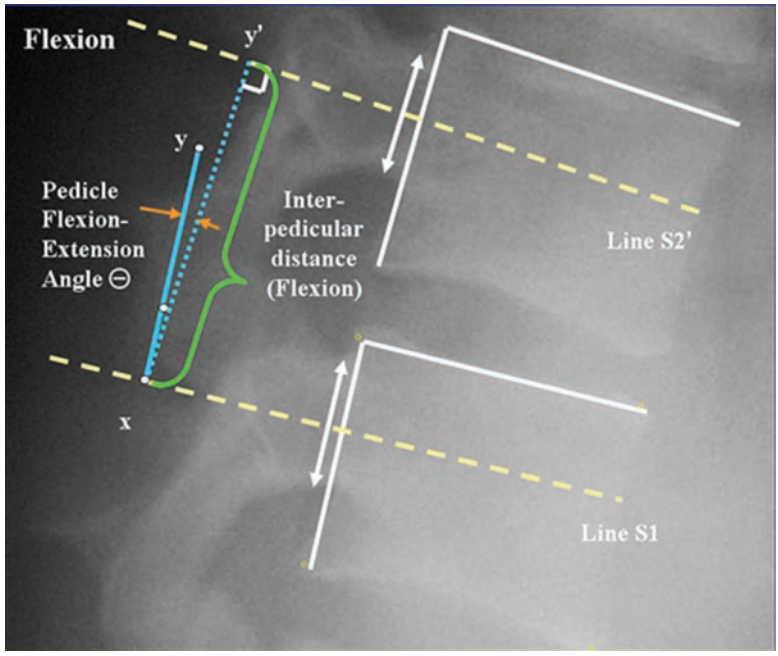

FIG. 7—*Illustrative layout for measurement of interpedicular angle (Θ) from flexion when compared to extension film. Also shown was the measurement for interpedicular distance (xy) for flexion.*

Developed Model for Test Setup

The model developed to represent the discectomy testing arrangement was divided into the following categories: single-level axial torsion, anterior/posterior shear (A/P shear), and axial compression.

Torsion Testing—Single Level

Torsion testing was divided into a static and fatigue discectomy model for testing. Since fatigue testing did not exist within the current ASTM F1717 standard [2], additional test parameters were defined as follows: $R = -1$ and each construct was maintained at 0 N axial load throughout the test.

Internal testing yielded two test construct run-outs to 5×10^6 cycles without any functional failure, as defined in ASTM F1717 for a standard run-out [2]. Since previous standards did not take torsion fatigue into account, data from this study served as a benchmark for comparison alongside future systems.

A/P Shear Testing—Single Level

This failure mode has not historically been a concern with rigid rods, but semi-rigid constructs are more susceptible to such conditions (compare shear strengths/modulus between materials) and should be addressed. For this

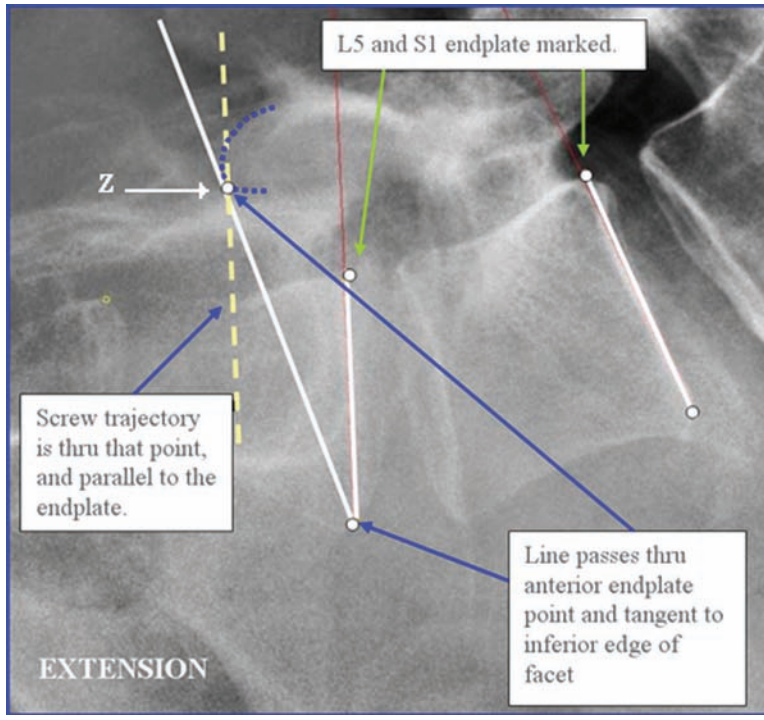

FIG. 8—*The pedicle screw trajectory was parallel to the sacrum endplate passing through point Z.*

section, data were divided into two areas of focus: synthetic model testing and in vivo data taken from a 45 patient abstract. Although the synthetic model and abstract cannot give any direct comparison to equivalent shear loading conditions, they both focus on the evaluation of shear for the exact same device.

For synthetic testing, constructs were assembled with a 30 mm space between the superior and inferior bone screws; however, the manner of affixing the superior and inferior blocks varied from traditional setups. Test blocks were configured such that the inferior test block was rigidly attached directly to the

TABLE 1—*Summary of lateral x-ray data.*

	L3-L4	L4-L5	L5-S1
Interpedicular distance (mm), flexion	36.0	36.1	30.7
Interpedicular distance (mm), extension	27.7	26.9	24.2
Interpedicular motion (mm), Δ	8.3	9.2	6.5
Neutral position gradient calculated from motion [10] (mm)	2.77	3.1	2.17
Calculated interpedicular distance (mm), neutral position	30	29.9	26

stationary test plate, and the superior test block was directly attached to the load cell.

The construct was seated into the test fixture 90 deg rotated, and assumed that the simulated spine was "belly down" and not upright (Fig. 9). This related the actuator's motion with anterior-posterior translation of the blocks. Loading was applied in the z direction until failure occurred or until the construct could no longer withstand loading.

For fatigue single level, testing produced a fully reversed pure anterior-posterior translation of one vertebral body relative to another vertebral body. Fully reversed anterior/posterior shear was meant as a means to compare shear strengths between design iterations. For this iteration it was not intended to simulate physiologic loading magnitudes. Two test constructs achieved run-out to 5×10^6 cycles without any functional failure, as defined in ASTM F1717 for a standard run-out [2].

The A/P shear testing guidelines yielded the following results: for the CD Horizon Legacy PEEK Rod System, at a load of 225 N, there were multiple run-outs at 5 000 000 cycles, as defined in ASTM F1717 for a standard run-out [2]. As mentioned previously, results cannot directly correlate to empirical clinical testing. However, it helps to examine observed clinical results, in part to aid in interpreting and understanding relevant sources.

Referencing empirical clinical testing for A/P shear, the abstract "Surgical Management of Lumbar Spondylolisthesis with Pedicle Based Semi-Rigid Instrumentation and Arthodesis" [12] detailed a 45 patient study regarding the effectiveness of CD Horizon Legacy PEEK Rod System for lumbar spondylolisthesis reduction and stabilization. Patients' pathology was determined as

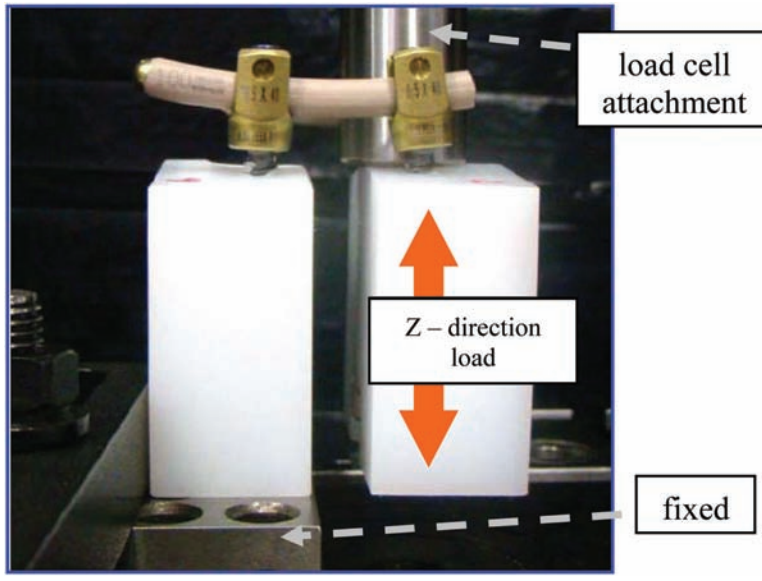

FIG. 9—*A/P shear setup.*

stenosis associated with either a grade I (32 patients) or grade II (13 patients) spondylolisthesis. Following disc decompression and spondylolisthesis reduction, 22 posterolateral only instrumented and 23 circumferentially instrumented fusions were performed. The mean follow-up period was 15 months. Out of the 45 patients, no neurological complication, loss of slip reduction, or instrumentation failure was reported. in vivo conditions are seen as a gold standard for evaluating shear for a device versus synthetic testing, and A/P shear did not present itself as a symptom for this study. Further extensive studies should be performed to correlate the predicted failures versus actual, as this testing layout is meant as a cornerstone for future development.

Compression Testing—Single Level

As stated previously, the characteristic which defines the polymeric properties in the semirigid system also creates challenges if displaced past the vertebral opening of the construct (Fig. 10). Given a great enough load, this may occur with any model (vertebrectomy or discectomy). The phenomenon is magnified with the reduction of space between vertebral bodies; thus increasing the possibility of the blocks touching during compression. The occurrence of false reading from blocks colliding is more likely with this test setup. To limit this possibility, three scenarios were proposed (below); however, for our testing purposes only scenario one was implemented.

The first scenario involves keeping the UHMWPE blocks similar to ASTM F1717 standard geometry [2]. Due to the decreased distance and polymeric material, there exists an increased possibility of the superior and inferior blocks

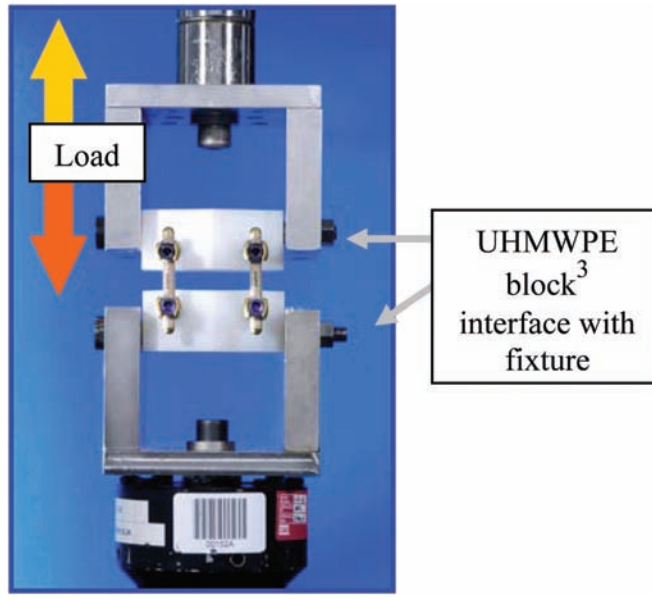

FIG. 10—*Semirigid rod—single-level construct.*

touching during load control for polymeric materials. Results from internal testing may be found in Fig. 12.

Scenario two incorporates a modified UHMWPE block into the testing. Material has been removed form the superior and inferior disc location (Fig. 11). This alternative would allow more distance for the rods to displace. However, for some semirigid materials, the removed geometry might not be adequate to completely negate block collisions.

Scenario three assumes boundary conditions of the UHMWPE blocks with no rotation allowed. This would allow for an equivalent compressive test, and would remove the issue of superior and inferior block contact during load controlled compression. Conversely, this simulation might be more similar to more restrictive approaches (e.g., an interbody bone graft, due to the nature of leaving adjacent segments locked to the vertebral blocks being tested).

The three scenarios above are just suggestions with hypothetical test modes. For the experimental portion, internal tests were performed with scenario one (single level unblocked) in displacement control. Semirigid and rigid systems were compared using the proposed test setup (Fig. 12).

The compression fatigue testing was similar to the static in setup, and an F/N curve was determined (two samples achieving run-out to the 5×10^6 cycle criteria without any functional failure, as defined in ASTM F1717 for a standard run-out).

One existing standard that address similar conditions as the above synthetic testing is ASTM F2624 standard "Standard Test Method for Static, Dynamic, and Wear Assessment of Extra-Discal Spinal Motion Preserving Implants" [13]. Under this standard one can assesses the static and fatigue performance for flexion, extension, and lateral bending; in addition to static torsion and rotational fatigue. ASTM F1717's setup does not take into account the changes in angular rotation which exist between varying implants. ASTM F2624's loading conditions on the construct are represented through a pure angular rotation setup used to create a center of rotation specific to the individual implant for the construct (Fig. 13). Also the standard accounts for simulated intradiscal pressure by inducing a 300 N axial load (or equivalent rationalized load) to the construct in a neutral position.

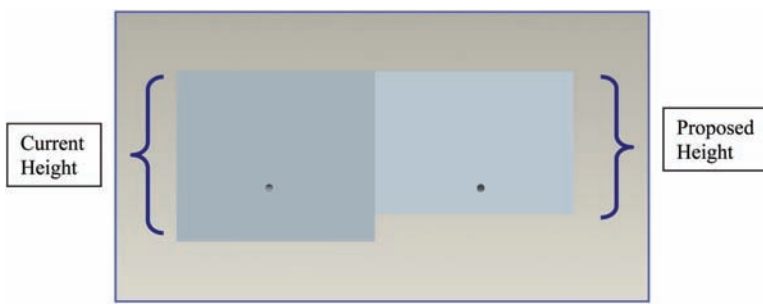

FIG. 11—*Modified UHMWPE block for compression single-level testing (removal of 5 mm of material from block height).*

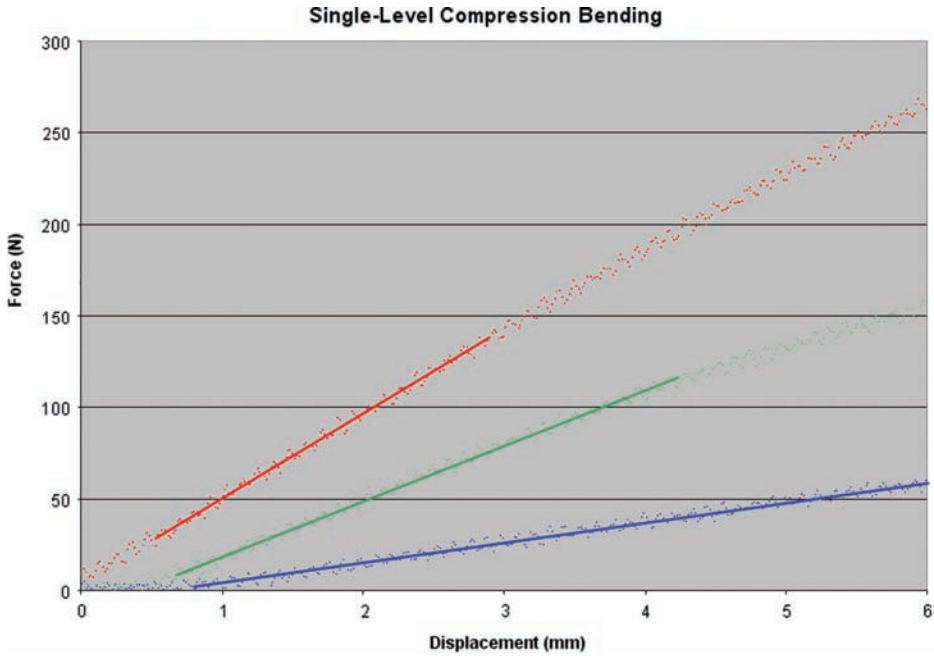

FIG. 12—*Single-level compression bending.*

The intent of ASTM F2624 is the evaluation for conditions where minimal removal of tissue and permitting motion in the spinal segment is priority. Even though the standard mentions its inability of evaluation of the implant in a shear or anterior/ posterior translating condition, it does note the clinical relevance of this type of motion.

The UHMWPE blocks do vary between standards in part due to F2624's option for spinous process evaluation and needed attachment interfaces. Also, the spacing between endplates is set to 20 mm offset, with an option to rationalize the offset. For the proposed standard, the analytical portion of the article rationalizes the 30 mm offset. Other differences include the increase of a run-out from 5×10^6 to 10×10^6 cycles.

Because of the essence of ASTM F1717 being used to address a fusion outcome, the approach did not take into account ASTM F2624. Future developments could incorporate aspects of this standard; however, as each standard does offer possible strengths in understanding implant biomechanical characteristics.

The configurations above are meant as suggested empirical steps toward a single-level offering, while attempting to maintain similarities between the current and proposed standards. These synthetic model layouts attempt to support a biomechanical equivalency in regards to geometry and location; however, one final area for assessment involves outlying differences between the inherent material properties.

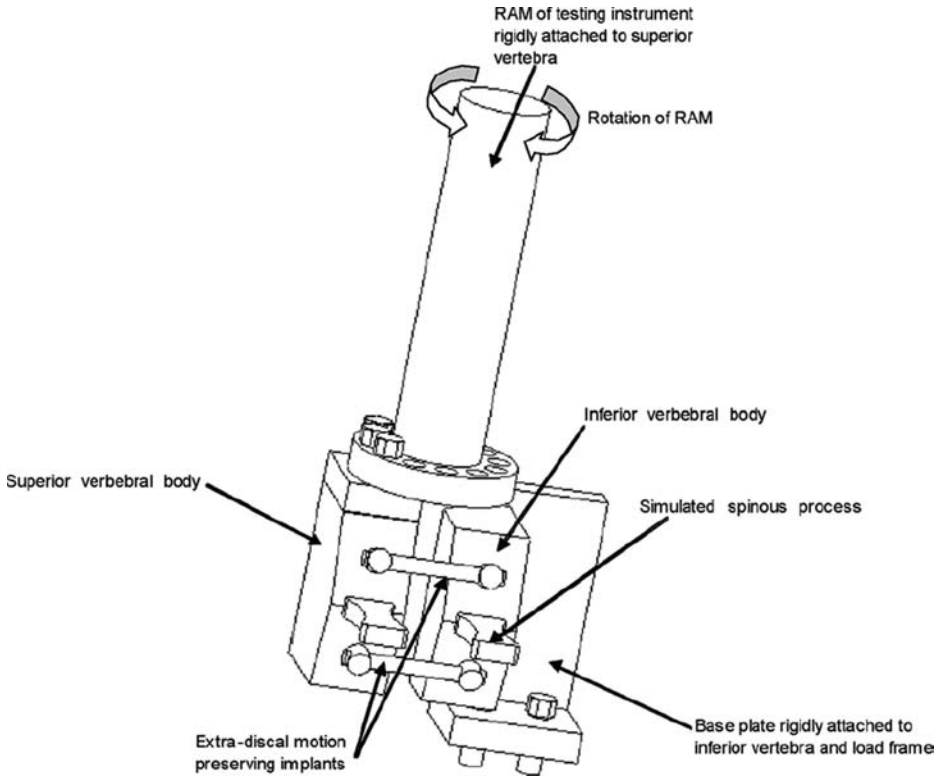

FIG. 13—*ASTM F2624 testing configuration.*

Displacement at 2 % Offset Yield: Rationale

The final portion of the paper's introduction outlines a case where mode of failure (M.O.F.) for stiffness might be equivalent; however, M.O.F. physically showed a dichotomy (rigid—rod fracture; semirigid—screw breakage at equivalent loading conditions). It is well established that these two materials have very different characteristics when reacting in stress and strain (Fig. 14), and more attention is needed regarding each material's analogous and dissimilar characteristics to truly evaluate the phenomena.

The rigid or metal systems act as a more purely elastic material where energy stored during loading is released when the force is removed. This relation may be defined through Hooke's Law where the stress and strain relationship is mainly a proportional relationship.

The semirigid or plastic system acts in a state of viscoelastic behavior, neither acting completely elastic nor viscous (total energy input is absorbed in material and distributed as internal heat). For the viscoelastic system, the energy received is divided into return energy to the system and internal heat generation.

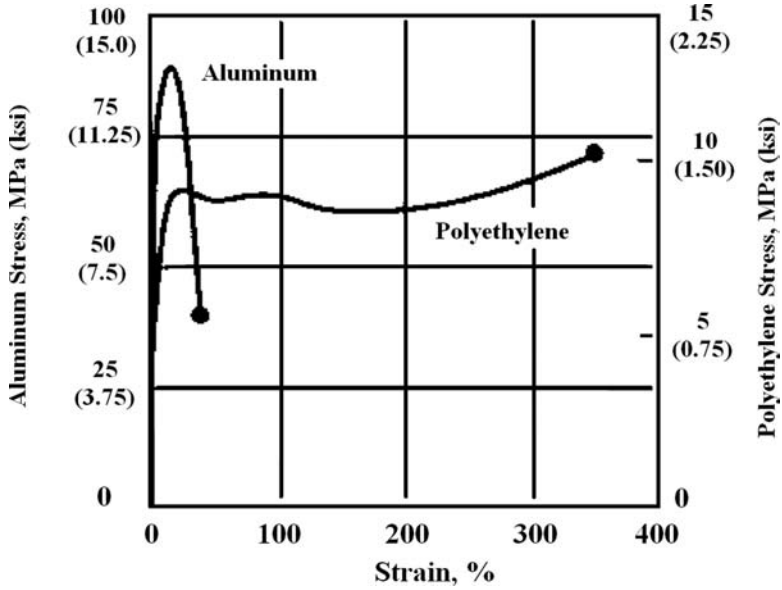

FIG. 14—*Stress-strain curves for aluminum and polyethylene.*

This viscoelastic behavior acts as a natural dampener for given cyclic loads on the material, and is revealed through improved internal fatigue testing versus equivalent-stiffness rigid predicates (rigid run-out loads were 35 % lower compared with semi-rigid systems).

According to the current standard, displacement at 2 % offset yield equates to "a permanent deformation equal to 0.020 times the active length of the longitudinal element" [2]. This elongation element is seen more as an arbitrarily defined value and is known to vary between regions (e.g., United Kingdom adopts a 0.1 and 0.5 % value) [14]. The technique enables one to narrow the yield point or yield strength of materials with a more obscure yield point; however, is not an inherent physical property of the material. Tensile characteristics also are quite different in metals than in plastics, as plastics have a much higher limit of elasticity than metals. Combine with this the unique post-yield phenomena plastics exhibit (Fig. 14), and it leads one to wonder if specifying a simple 2 % offset really incorporates the full yield characteristics of the material.

Conclusion

The article describes a single-level construct accounting for shear, and the authors have attempted to assess it from a well-referenced scientific aspect. Evaluation of the current limitations of the test standards led to a scientific approach to reevaluate the needs of nonmetallic rods with a single-level test construct. Incorporated in this test are considerations for shear behavior analysis, which reflect a responsibly defined need when working with materials of an

anisotropic nature. This shear component is a characteristic evaluated in a single-level test mode in related articles, so each proposal in a way complements the other.

An investigation into clinically relevant literature related to the specified indicated use led to a biomechanical approach, which was employed to assess geometric conditions. The refined information was translated into a realistic synthetic model which shows association to the current standard.

In conclusion, a single-level "discectomy" model has been developed to consider the different use conditions of semirigid rod fixation systems. It has potential as a supplement or alternative to the ASTM F1717 vertebrectomy model for the evaluation of flexible spinal rods. The case is presented from a clinical, empirical, and analytical interpretation. This layout is a simple offering to initiate discussion with the anticipation of future refinements including comparative rigid construct testing.

References

[1] Highsmith, J. M., Tumialán, L. M., and Rodts, G. E., Jr., "Flexible Rods and the Case for Dynamic Stabilization," *Neurosurg. Focus*, Vol. 22, No. 1, 2007, p. E11.

[2] ASTM F1717–04, "Standard Test Methods for Spinal Implant Constructs in a Vertebrectomy Model," *Annual Book of ASTM Standards* Vol. 2005, ASTM International, West Conshohocken, PA, pp. 807–824.

[3] Cunningham, B. W., Sefter, J. C., Shono, Y., and McAfee, P. C., "Static and Cyclical Biomechanical Analysis of Pedicle Screw Spinal Constructs," *Spine*, Vol. 18, No. 12, pp. 1677–1688.

[4] Eijkelkamp, M. F., van Donkelaar, C. C., Veldhuizen, A. G., van Horn, J. R., Huyghe, J. M., and Verkerke, G. J., "Requirements for an Artificial Intervertebral Disc," *Int. J. Artificial Organs*, Vol. 24, 2001, pp. 311–321.

[5] ASTM F2346–05, "Standard Test Methods for Static and Dynamic Characterization of Spinal Artificial Discs," *Annual Book of ASTM Standards* Vol. 2005, ASTM International, West Conshohocken, PA, pp. 1403–1411.

[6] Schaeren, S., Broger, I., and Jeanneret, B., "Minimum Four-Year Follow-up of Spinal Stenosis With Degenerative Spondylolisthesis Treated With Decompression and Dynamic Stabilization," *Spine*, Vol. 33, No. 18, pp. E636–E642.

[7] Bothmann, M., Kast, E., Jens Boldt, G., and Oberle, J., "Dynesys Fixation for Lumbar Spine Degeneration," *Neurosurg Rev.*, Vol. 31, 2008, pp. 189–196.

[8] Grob, D., Benini, A., Junge, A., and Mannion, A. F., "Clinical Experience With the Dynesys Semirigid Fixation System for the Lumbar Spine," *Spine*, Vol. 30, No. 3, 2005, pp. 324–331.

[9] Ponnappan, R. K., Serhan, H., Zarda, B., Patel, R., Albert, T., and Vaccaro, A. R., "Biomechanical Evaluation and Comparison of Polyetheretherketone Rod System to Traditional Titanium Rod Fixation," *Spine J.*, Vol. 9, 2009, pp. 263–267.

[10] Yamamoto, I., Panjabi, M. M., Trey Crisco, and Oxland, T., "Three-Dimensional Movements of the Whole Lumbar Spine and Lumbosacral Joint," *Spine*, Vol. 14, No. 11, 1989, pp. 1256–1260.

[11] Chaynes, P., Sol, J.-C., Vaysse, Ph., Bécue, J., and Lagarrigue, J., "Anatomic Bases of Medical, Radiologic and Surgical Techniques Vertebral Pedicle Anatomy in Relation to Pedicle Screw Fixation: A Cadaver Study," *Surg. Radiol. Anatomy*, Vol. 23, No. 2, 2001, pp. 85–90.

[12] Nockels, R., Bamber, N. I., Hammers, R. L., and Bragg, T. M., "Surgical Management of Lumbar Spondylolisthesis With Pedicle Based Semi-Rigid Instrumentation and Arthodesis," *Paper Presented at 2008 Congress of Neurosurgical Surgeons (CNS) Annual Meeting*, Orlando, FL.

[13] ASTM F2624–05, "Standard Test Method for Static, Dynamic, and Wear Assessment of Extra-Discal Spinal Motion Preserving Implants," *Annual Book of ASTM Standards*, ASTM International, West Conshohocken, PA, 2005, available at: www.astm.org.

[14] Gere, J. M. and Goodno, B. J., *Mechanics of Materials*, 7th ed., Cengage Learning, Toronto, ON, 2009.

Reprinted from JAI, Vol. 9, No. 2
doi:10.1520/JAI103493
Available online at www.astm.org/JAI

J. P. Shorez[1]

Vertebrectomy Model for the Mechanical Assessment of Fusionless Scoliosis Growth Rods

ABSTRACT: Fusionless scoliosis growth rod systems pose many challenges to benchtop biomechanical testing. This study was conducted in order to develop a vertebrectomy model capable of evaluating shear/corrective reduction forces, anterior/posterior load sharing, and long term fatigue properties of these systems. Portions of ASTM F1717 and ISO 12189 were used to develop a custom dynamic construct. Results from the corrective/shear reduction force test demonstrate an expected reduced shear/corrective force at the completion of fatigue testing. Additionally, a bimodal force–displacement curve was demonstrated during confined static compression testing, indicating an anterior/posterior load sharing function of the system. Fatigue testing of the dynamic construct demonstrated the potential to develop a fatigue curve and endurance limit of a growth rod system. Moreover, fatigue testing replicated common in vivo failures. The complexities of scoliosis treatment make the definition of a standardized construct difficult. However, application of the current model can serve as a tool to understand the basic mechanical interactions in these complex systems.

KEYWORDS: growth rods, biomechanical testing, scoliosis

Introduction

Traditional treatment options for scoliosis have included bracing or casting, traction, and fusion surgical treatments [1–3]. Drawbacks to these conventional treatment options include poor outcomes, multiple surgeries, and growth

Manuscript received October 15, 2010; accepted for publication August 31, 2011; published online October 2011.

[1] Senior Research Engineer, Medtronic, 2600 Sofamor Danek Dr., Memphis, TN 38132.

Symposium on Static and Dynamic Spinal Implants: Are We Evaluating Them Appropriately? on 18 May 2010 in St. Louis, MO.

Cite as: Shorez, J. P., "Vertebrectomy Model for the Mechanical Assessment of Fusionless Scoliosis Growth Rods," *J. ASTM Intl.*, Vol. 9, No. 2. doi:10.1520/JAI103493.

restriction of the spine and thorax. Several new fusionless options are becoming available that allow for growth, while providing correction [4]. Typical fusionless scoliosis growth rods rely on the native spinal column to provide structural support with the implant hardware correcting the curvature. Benefits of these systems include reduction in operative treatments and continued growth. As new fusionless options become available, being able to adequately understand the mechanical limitations becomes more important. However, fusionless scoliosis growth rod systems pose many challenges to benchtop biomechanical testing because these systems do not easily fall into any of the standard implant categories. The vertebrectomy standards that are currently used for evaluation of thoraco-lumbar constructs do not sufficiently evaluate the unique attributes of these systems, namely, spinal curvature correction and increased load sharing in the anterior spinal column. For this study a fusionless scoliosis system, currently in development, that guides growth at the proximal and distal regions of the construct was used to evaluate the subject dynamic construct model. To adequately evaluate this bimodal system, components of ISO 12189 and ASTM F1717 have been combined to simulate a dynamic construct [5,6]. The objective of this study was to develop a model that adequately evaluates the unique features of a growth rod system, namely, the shear/corrective force, anterior/posterior load sharing capabilities, and fatigue performance of the system.

Materials and Methods

Ultrahigh molecular weight polyethylene blocks were designed with recessed pockets and extruded studs to contain three die cast springs. Two anterior springs were aligned with the transverse hole used to apply loads. The third posterior spring was located equidistant from the anterior springs as to create an equilateral triangle pattern. Following methods described in ASTM F1717, the modified blocks maintained a 15° medial angulation and 40 mm distance between the pedicle screw insertions. Following methods detailed in ISO 12189, a 76 mm gap between the upper and lower screws was maintained by selecting rectangular die cast springs (ISO 10243 [7] color code Red) with a length of 64 mm and 25 mm outer diameter (spring rate of 123 N/mm). It has been estimated that lumbar stiffness under compression is in the range of 700–2500 N/mm [8–10]. However, these estimates are of adult populations. As such, the cumulative spring stiffness selected for this model, 369 N/mm, was approximately half to be representative of an adolescent population. The fusionless dynamic constructs were assembled with 30° curved sagittal plane rods to represent a corrected lumbar lordotic curvature. Spinal rods were manipulated by hand to the desired angle. Two fixed angle screws and standard break off set screws were inserted into the superior construct block. Two multi-axial screws and modified set screws were inserted into the inferior construct block. See Figs. 1 and 2 for an example of the modified test construct. (Note: Alignment of the inferior and superior construct blocks is achieved by restraining rotation around the transverse loading pins).

The shear/corrective force of the dynamic construct was evaluated by inducing a sagittal reduction force causing the superior and inferior blocks to become

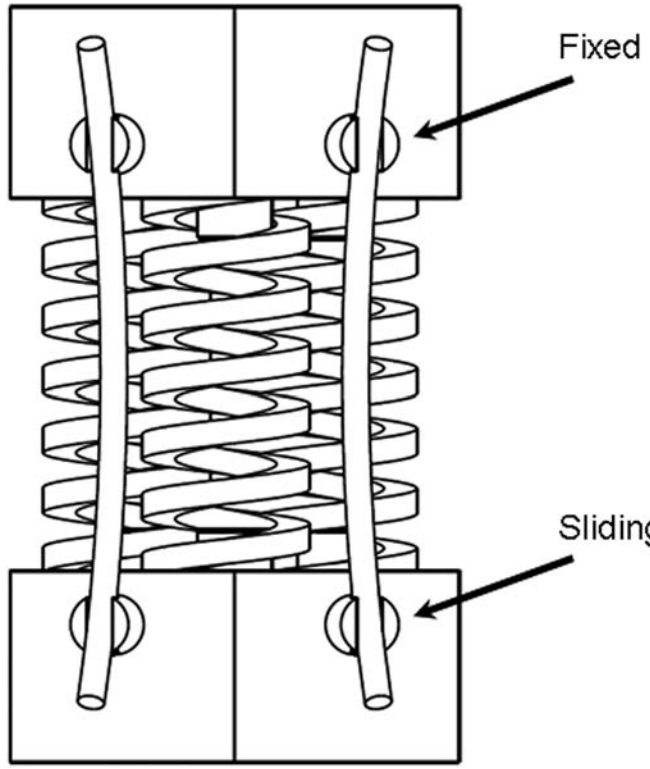

FIG. 1—*Superior fusion level and inferior dynamic level, representative of an ideal growth rod implant configuration with apex fusion.*

aligned by bending and sliding of the spinal rods. The dynamic construct was mounted horizontal to the line of actuation of an MTS (Eden Prairie, MN) electromechanical test frame crosshead. The superior construct block (fixed) was confined in a stainless steel u-block with a custom stainless steel adjustable spacer. The inferior block (sliding) was aligned with an edged push-rod fixture attached to the test frame crosshead (see Fig. 3). A reduction force was applied at constant rate of 10 mm/min until the construct blocks had become aligned. Force and displacement data were collected at a rate of 10 Hz. The peak shear/corrective force was reported. Shear/corrective forces were assessed before and after conducting confined fatigue tests. This strategy allowed for rod deformation and ultimately changes in shear/corrective forces to be evaluated. Had a multi-axis load cell been available, the shear/corrective force would have been monitored throughout the duration of confined fatigue testing.

To assess anterior/posterior load sharing behavior of the dynamic construct, a confined static compression test was conducted. The superior and inferior construct blocks were mounted as described in ASTM F1717 to two stainless steel u-block fixtures affixed to an MTS electromechanical test frame.

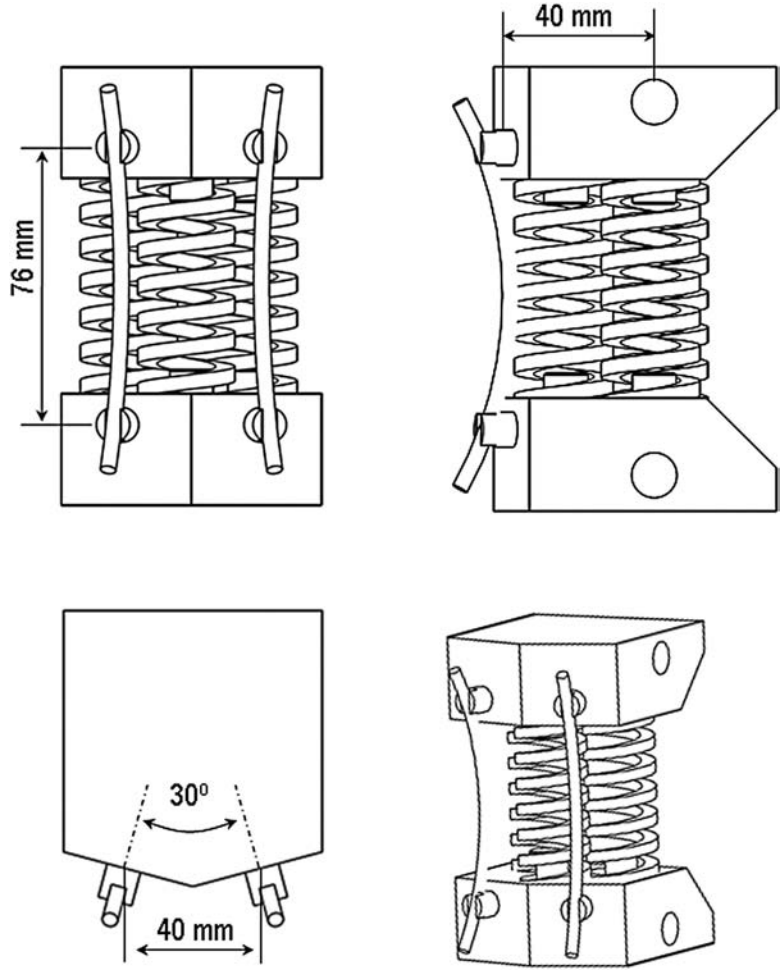

FIG. 2—*Dynamic construct test block configuration (units in millimeters).*

Adjustable spacers were inserted between the construct blocks and u-block test fixture as to align the construct blocks and induce a shear/corrective force due to the curvature of the spinal rods. With only a single axis load cell being used, the shear/corrective force was not measured during testing (see Fig. 4). During alignment of the construct blocks, the axial force was maintained at zero. Static compressive loading was applied at a constant rate of 10 mm/min until 2 mm of displacement was reached. Force and displacement data were recorded at 10 Hz.

Following confined static compression testing, the fatigue performance was evaluated at various loading levels to understand the potential failure modes. The superior and inferior construct blocks were mounted as described in ASTM F1717 to two stainless steel u-block fixtures with adjustable spacers inserted between the construct blocks and u-block test fixture to prevent rotation of the

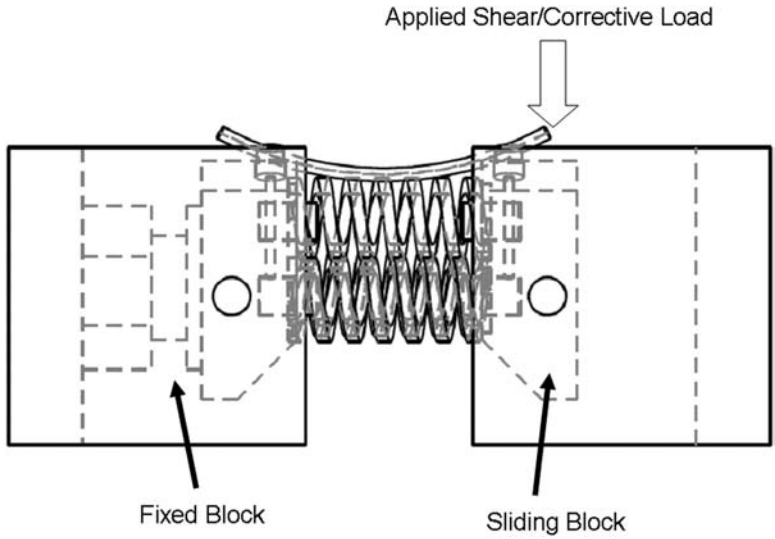

FIG. 3—*Shear/corrective force evaluation in a confined block setup. Loading was applied to the sliding construct block until alignment with the fixed construct block.*

construct blocks around the loading pin. This alignment induced a shear/corrective force due to the curvature of the spinal rods (see Fig. 5). Fatigue testing was conducted using MTS 858 Mini-Bionix servohydraulic test frame at rate of 2 Hz to 5×10^6 cycles. Peak compressive loads ranged from 700 to 1500 N, with a loading ratio of $R = 10$.

Results and Discussion

As expected, a difference in pre- to post-fatigue reduction forces was observed. Pre-fatigue testing demonstrated a reduction force magnitude of 357 N, whereas post-fatigue testing was 230 N, a 55 % decrease. There was no observed permanent deformation to the spinal rods during this reduction maneuver test. Additionally, there was no observed pullout of the pedicle screws from the construct block.

During confined static compression testing a bimodal force–displacement curve was observed. Figure 6 represents a common bimodal force–displacement curve. During the first 0.1 mm of compression, the posterior hardware supported approximately 20 % of the load during a total of 2 mm of compression. There were no observed fractures of the posterior hardware. Rather, sliding of the spinal rods in the multi-axial screw heads was observed as ramped loading was applied. With this testing being conducted with a single axis load cell, the relationship between compressive loading and shear/correction force could not be measured. However, by knowing the reduction forces, it would be assumed that a sagittal corrective force of approximately 350 N was sustained during confined static compression testing.

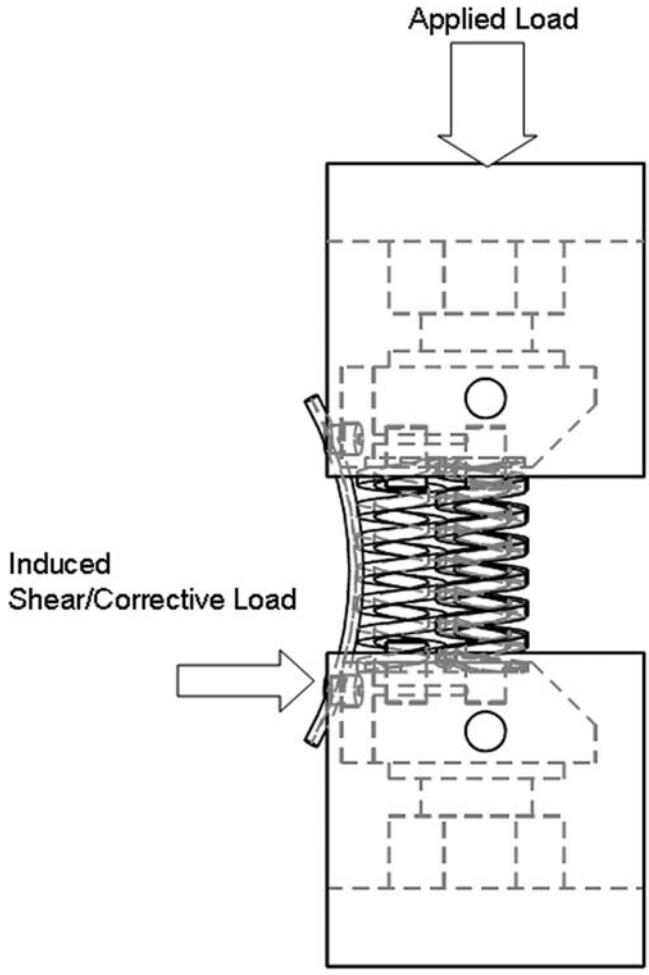

FIG. 4—*Confined static compression test setup. Alignment of the inferior and superior test blocks induces a shear/corrective load due to the curvature of the spinal rod.*

Figure 7 summarizes the fatigue test results of the dynamic construct with anterior support. Four samples reached 5×10^6 cycles without failure (two constructs ran out at the same lower loading condition). Though these samples ran out, wear debris was generated throughout the test. In addition, increasing wear debris was observed with increased load magnitudes. Testing was conducted in air, so no wear debris was collected for analysis. There were two different failure modalities. The first was a fractured spinal rod near the superior construct (fusion level). The second observed failure mode was excessive wear debris resulting in disassembly of the pedicle screw. This sample did not exhibit the traditional sliding motion of the rod. Rather, the multi-axial screw head repetitively rotated about the pedicle screw wearing the screw head junction.

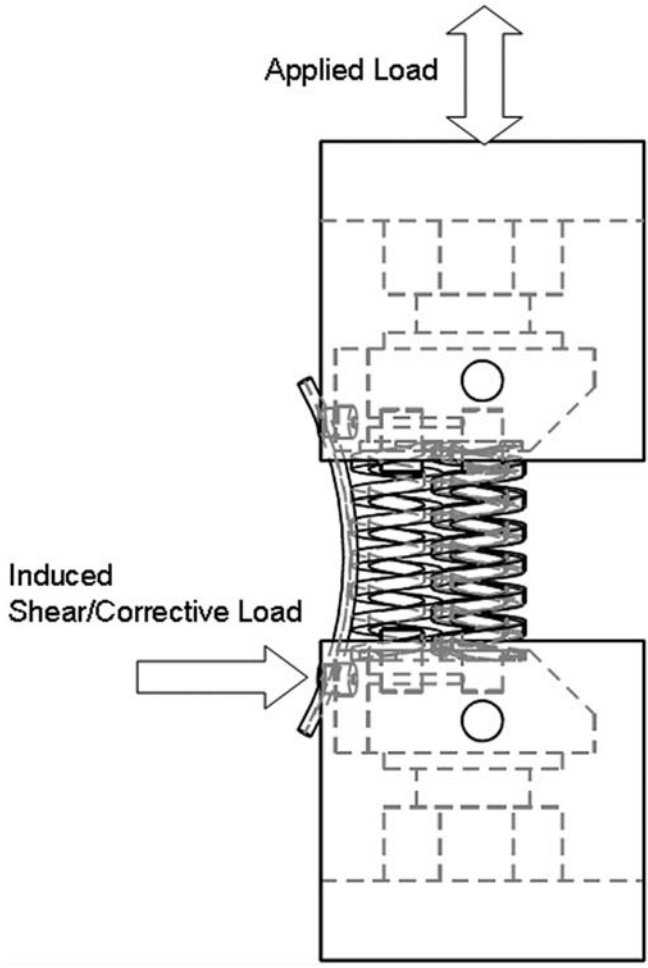

FIG. 5—*Confined fatigue testing setup. Alignment of the inferior and superior test blocks induces a shear/corrective load due to the curvature of the spinal rod.*

The dynamic construct that was assembled for this study represents an ideal clinical scenario. The curvature of the tested rod simulates a normally aligned lumbar curve, where in a clinical application the spinal rod curvature could be drastically different based on the severity of the scoliotic spinal curve and required degree of correction. Additionally, this model only simulates one dynamic level, where in some growth rod applications there may be several dynamic junctions.

Another limitation to this study was the applied load during fatigue testing. Limited knowledge of adolescent spine stiffness and range of motion, limit the ability to capture all loading mechanisms. Even though these are limitations of the current model, previous biomechanical work on growth rod systems has

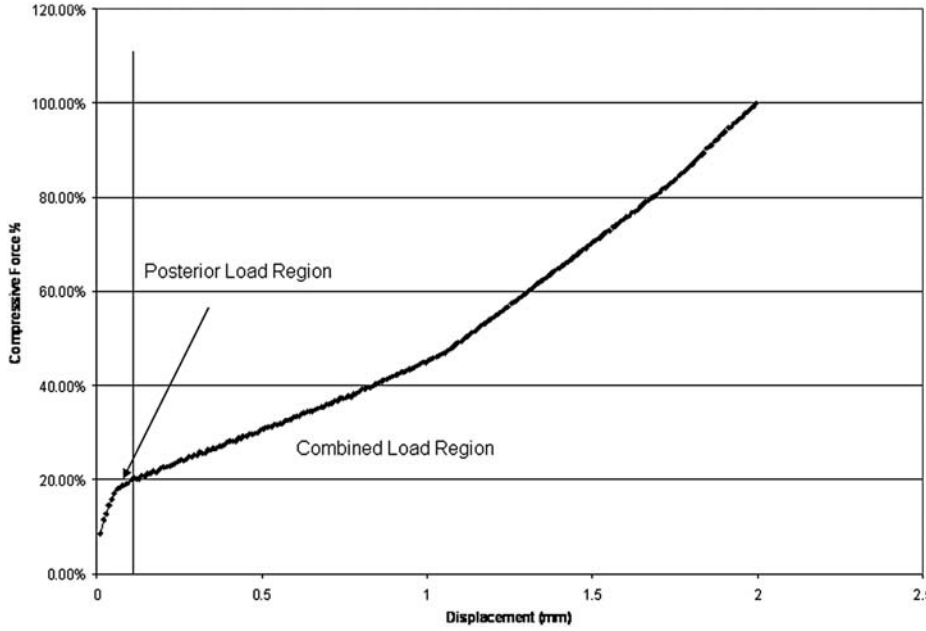

FIG. 6—*Example of force–displacement curve demonstrating bimodal load sharing between the posterior hardware and anterior support.*

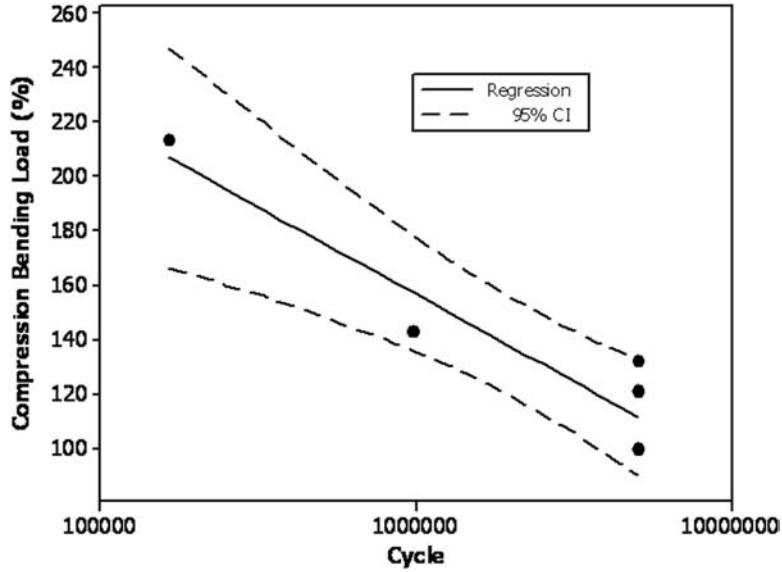

FIG. 7—*Fatigue strength of the fusionless growth rods with anterior support, showing regression fit and 95% confidence interval.*

been limited to cadaveric and animal models [11]. These models provide insight into initial correction capabilities of fusionless options, but do not provide information on the long term corrective capabilities or mechanical failures.

Conclusions

Effectively evaluating fusionless growth rod constructs provides many challenges due to the custom application of the system. Patient size, required curvature correction, and progression of the curvature make defining a standardized construct difficult. The current study evaluated one growth rod system in an anteriorly supported construct. As expected with a growth rod system, the pre- and post-fatigue testing reduction forces were reduced. This finding suggests that the model is sufficiently challenging these specific growth rods, and based on the observed failure modalities in fatigue testing can replicate observed in vivo failures [12]. The utility of this model allows for various growth rod systems to be evaluated in such a manner that does not require the spinal construct to support 100% of the applied load. Additionally, rod curvature can be modeled as induced shear/corrective force. Future evaluations of this model on a multi-plane load cell can elucidate the inherent multi-planer loads induced with a growth rod system. Direct application of this model to other growth rod systems or low stiffness posterior systems may require modifications to the setup due to the custom nature and variation in scoliosis correction hardware. As more understanding of how different factors (i.e., rod curvature, anterior support, etc.) can affect the mechanical performance of growth rod systems, a model based on the current dynamic construct may serve utility in providing a basis for future in vitro evaluations.

References

[1] Charles, Y. P., "Progression Risk of Idiopathic Juvenile Scoliosis During Pubertal Growth," *Spine*, Vol. 31, No. 17, 2006, pp. 1933–1942.

[2] Yang, J., Sponseller, P., Thompson, G. H., Emans, J., McCarthy, R., Salari, P., and Akbarnia, B., "Complications of Expandable Devices in Children with EOS," *Risk Factors for Rod Fractures in Growing Rod Surgery*, ICEOS Meeting, November 2008.

[3] Goldberg, C. J., Moore, D. P., Fogarty, E. E., and Dowling, F. E., "Adolescent Idiopathic Scoliosis: The Effect of Brace Treatment on the Incidence of Surgery," *Spine*, Vol. 26, No. 1, 2001, pp. 42–47.

[4] Torre-Healy, A., and Samdani, A. F., "Newer Technologies for the Treatment of Scoliosis in the Growing Spine," *Neurosurg. Clin. N. Am.*, Vol. 18, No. 4, 2007, pp. 697–705.

[5] ISO 12189, 2008, "Implants for Surgery—Mechanical Testing of Implantable Spinal Devices—Fatigue Test Method for Spinal Implant Assemblies Using an Anterior Support," *International Organization for Standardization*, Geneva, Switzerland.

[6] ASTM F1717, 2010, "Standard Test Methods for Spinal Implant Constructs in a Vertebrectomy Model," *Annual Book of ASTM Standards*, Vol. 13.01, ASTM International, West Conshohocken, PA, pp. 1–18.

[7] ISO 10243, 2010, "Tools for Pressing—Compression Springs with Rectangular Section—Housing Dimensions and Colour Coding," International Organization for Standardization, Geneva, Switzerland, 2010.
[8] White, A. A., and Panjabi, M. M., *Clinical Biomechanics of the Spine*, 2nd ed., Lippincott, Philadelphia, 1990.
[9] Brown, T., Hansen, R. J., and Yorra, A. J., "Some Mechanical Tests on Lumbosacral Spine With Particular Reference to the Intervertebral Discs," *J. Bone Jt. Surg. Am. Vol.*, Vol. 7, No. 5, 1957, pp. 1135–1164.
[10] Shea, M., Takeuchi, T. Y., Wittenberg, R. H., White, A. A., III, and Hayes, W. C., "A Comparison of the Effects on Automated Percutaneous Diskectomy and Conventional Diskectomy on Intradiscal Pressure, Disk Geometry, and Stiffness," *J. Spinal Disord.*, Vol. 7, No. 4, 1994, pp. 317–325.
[11] Mahar, A. T., Bagheri, R., Oka, R., Kostial, P., and Akbarnia, B. A., "Biomechanical Comparison of Different Anchors (Foundations) for the Pediatric Dual Growing Rod Technique," *Spine*, Vol. 8, No. 6, 2008, pp. 933–939.
[12] Maio, F., Dolan, L. A., Luna, V., and Weinstein, S. L., "Posterior Spine Fusion with Moss-Miami Instrumentation for Adolescent Idiopathic Scoliosis: Radiographic, Clinical and Patient-Centered Outcomes," *Iowa Orthop. J.*, Vol. 27, 2007, pp. 28–39.

Reprinted from JAI, Vol. 8, No. 9
doi:10.1520/JAI103492
Available online at www.astm.org/JAI

David Spenciner[1]

Static Evaluation of Pedicle Screw Spinal Constructs to the ASTM Standard: A Comparison of Multiple Test Laboratories

ABSTRACT: Newly acquired mechanical test data along with predicate device data—sometimes from the designer's historical records—are a requisite part of the regulatory submission process for new pedicle screw spinal constructs. Several studies have compared the mechanical properties of various designs of these medical devices, which are commonly inserted during spinal fusion operations. However, a rigorous comparison of the results coming from different laboratories testing the same devices under controlled conditions has not been performed. Six different test labs performed a series of static bending compression and static torsion tests on identically prepared pedicle screw and rod test constructs ($n = 5$ for both tests). Sufficient data were acquired to uncover and understand differential interpretations of the methodology described in the standard test method ASTM F1717. For ultimate displacement in compressive bending, the mean values ranged between 47.64 mm and 71.64 mm, and every single laboratory's data were statistically significantly different from those of every other laboratory. Significant differences in the mean values carried through to the ultimate load data, but this trend did not continue for stiffness, yield displacement, yield load, and elastic displacement. For stiffness in static torsion, the mean values ranged between 0.38 Nm/° and 1.07 Nm/°. There were statistically significant differences among some of the labs for some of the parameters, but no strict patterns emerged. This is likely due to methodological and interpretive differences among the labs, such as the depth of the clevis fixtures and the direction of rotation during torsion testing. These differences in the test labs' methodology have caused the ASTM subcommittees to clarify the standard

Manuscript received October 15, 2010; accepted for publication July 5, 2011; published online August 2011.

[1] DePuy Mitek, Raynham, MA 02767

Cite as: Spenciner, D., "Static Evaluation of Pedicle Screw Spinal Constructs to the ASTM Standard: A Comparison of Multiple Test Laboratories," *J. ASTM Intl.*, Vol. 8, No. 9. doi:10.1520/JAI103492.

so that fewer aspects are open for interpretation, but more work is needed. With appropriate refining of F1717 (and adherence to the new methodology by the test laboratories), test results from different laboratories would likely be more directly comparable than in the current situation.

KEYWORDS: ASTM F1717, spinal construct, fusion, interlaboratory study

Introduction

In the late 1990s, ASTM subcommittee F04.25 drafted and approved F1717, "Standard Test Methods for Spinal Implant Constructs in a Vertebrectomy Model." This standard describes a number of quasi-static and fatigue mechanical tests for spinal constructs typically used in posterior spinal fusion procedures [1]. Test constructs can comprise two parallel rods, four bone screws, and the connectors. These assemblies are rigidly attached to a pair of ultra-high molecular weight polyethylene (UHMWPE) blocks in a configuration that roughly duplicates spinal fusion above and below a complete vertebrectomy. Since its first approval, the standard has undergone multiple improvements and clarifications, and dozens (if not hundreds) of spinal fusion systems have been tested to this standard as part of the mechanical validation process. A U.S. Food and Drug Administration (FDA) guidance document, most recently updated in 2004, specifically calls for manufacturers to test their products to F1717 [2]. Clearly, F1717 is an important part of the regulatory process for these spinal constructs in the United States.

There have been several studies that have compared the mechanical characteristics of multiple fusion constructs using F1717 [3–8], whereas other studies have used the test methods described in this standard to evaluate a single system [9–13]. However, to the best of my knowledge, no previous study has compared the results of multiple laboratories following static testing on identical products. Performing this comparison permits two important results: the calculation of the precision of the standard (which gives test labs, manufacturers, and the FDA an idea for the expected scatter in the results) and the identification of any systematic differences in the current methodology used by different laboratories in their interpretation of the standard. The former has been described in detail previously [1,14], and the resulting precision and bias statement were incorporated into F1717. Therefore, the identification of any systematic differences in the current methodology used by different laboratories in their interpretation of the standard is the focus of the current paper. To the extent possible, the impact of these differences on the data is described.

Methods

The test constructs included rods, polyaxial bone screws, set screws, and, for the quasi-static torsion tests, cross connectors (Table 1), all donated by the manufacturer. From a clinical standpoint, this size of hardware is indicated for fusion in the upper thoracic region of the spine. All hardware was supplied in sterile condition for assembly. In total, 30 complete constructs were prepared

TABLE 1—*Components used to assemble test constructs.*

Description	Size	DePuy Spine Product Code
Summit minipolyaxial screw	3.5 mm × 24 mm	174617724
Set screws		174542200
Rods	3.0 mm	174635000
Cross connectors		174665000

for quasi-static compression bending testing, and 35 constructs were prepared for quasi-static torsion testing (Fig. 1). UHMWPE blocks were sized appropriately for this size of hardware (see Fig. 4 of ASTM F1717); however, the overall length of rods was chosen so as to produce an implant length of 76 mm rather than 35 mm. This deviation from the standard was requested by the donor of the constructs so that data from this study could be compared against their own internal data. In order to maintain the consistency of the test samples, all constructs were assembled by a single engineer over the course of several days. Briefly, the components were assembled in a double-lock vise (Kurt Manufacturing, Minneapolis, MN) with a precision spacer such that the final interblock distance was 66.0 mm. Tightening torque values were 2.5 Nm for the polyaxial screws and 0.2 Nm for the cross connector screws and were applied with a Computorq3 Model 2401CI3 (CDI Torque Products, City of Industry, CA). The heads of the polyaxial screws were spaced 0.5 mm from the UHMWPE blocks with

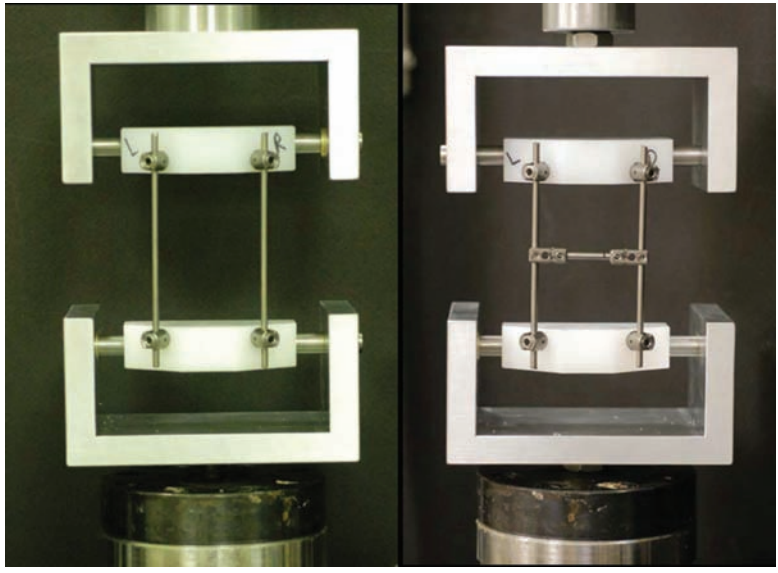

FIG. 1—*Test constructs for quasi-static compression bending tests (left) and quasi-static torsion tests (right).*

TABLE 2—*Participating test laboratories.*

Laboratory Name	Location	Primary/Alternate
Accutek Testing Lab	Cincinnati, OH	Primary
DePuy Spine	Raynham, MA	Primary
Empirical Testing Corp.	Colorado Springs, CO	Primary
Exponent Inc.	Philadelphia, PA	Primary
MarTest Inc.	Cincinnati, OH	Primary
RIH Orthopaedic Foundation	Providence, RI	Primary
MetCut	Cincinnati, OH	Alternate

removable custom spacers. Ten constructs (five of both types) were shipped to various test labs, and the remaining five constructs were held in reserve.

Seven test labs (Table 2) were chosen to participate in this interlaboratory study (ILS). Volunteer testing laboratories were solicited during a regular meeting of the ASTM F04.25 subcommittee and were included as participants on a first-come, first-served basis. As no labs dropped out during the ILS, the alternate lab did not perform any testing. Participating labs were randomly assigned letters between A and F so that the data could be presented in a blinded manner.

Two specific tests described in ASTM F1717 were picked for the ILS: quasi-static compression bending and quasi-static torsion. All of the output metrics required to be reported by the standard for these two tests were included in this study (Table 3).

The test laboratories were asked to submit both their standard test reports and the raw data. Prior to the compilation of summary statistics on the data, the calculation methodology of each metric by the labs was performed. For calculations in which the test laboratory had made an error, the calculation was corrected prior to statistical analysis. However, in cases in which the metric was

TABLE 3—*Listing of output metrics.*

Output Metric	Test
Ultimate displacement (mm)	Quasi-static compression bending
Ultimate load (N)	Quasi-static compression bending
Stiffness (N/mm)	Quasi-static compression bending
Displacement at 2 % offset yield (mm)	Quasi-static compression bending
Yield load (N)	Quasi-static compression bending
Elastic displacement (mm)	Quasi-static compression bending
Stiffness (Nm/°)	Quasi-static torsion
Angular displacement at 2 % offset yield (°)	Quasi-static torsion
Yield torque (Nm)	Quasi-static torsion
Elastic angular displacement (°)	Quasi-static torsion

determined somewhat subjectively (e.g., graphical determination of load versus displacement slope to calculate stiffness), the results supplied by the test labs were not revised. In all cases, the results for the five test specimens from each lab for both tests were combined and a mean and standard deviation calculated. Comparison of these values was performed using a one-way analysis of variance with a Tukey-Kramer post hoc analysis with a significance level of 0.05.

Results

For the static compression bending tests, all of the laboratories successfully completed the tests and had no calculation errors or interpretation discrepancies. For ultimate displacement, the mean values ranged between 47.64 mm and 71.64 mm, and every single laboratory's data were statistically significantly different from those of every other laboratory (Table 4).

This trend of each lab's having different results from the others carried through to the ultimate load data, although due to higher scatter these differences were not all statistically significant (Table 5). The range of mean values was 162.7 N to 229.3 N. Considering that the tests were stopped because the rods were bending rather than following any type of fracture, it is highly likely that this is due to the fact that the various laboratories were compressing their samples by different displacements, and so the rank order is identical except that the lab with the largest displacements had the second-highest loads, and vice versa.

For stiffness (Table 6), the range of mean values was 5.7 N/mm to 7.9 N/mm. There were four labs in the middle (A, D, E, and F), one lab that was significantly higher (B) than the others, and one lab that was significantly lower (C).

There were no significant differences among the labs for displacement at the yield point, and the range of mean values was 11.18 mm to 14.42 mm (Table 7).

For yield load (Table 8), lab C produced significantly higher values than three of the other labs. The range of mean values was 70.7 N to 95.0 N.

The mean values of elastic displacement ranged between 9.66 mm and 13.76 mm (Table 9). Lab C produced higher values than two other labs.

Although all of the labs appeared to produce data with low scatter during bending compression testing (e.g., the standard deviations for their individual data represent only 1 % to 4 % of the mean value for ultimate displacement), there is often a wide range of values for the various parameters. In follow-up discussions with the labs, not only did we discover inconsistency within the

TABLE 4—*Ultimate displacement data (mm) for compression bending tests (n = 5).*

Lab	A	B	C	D	E	F
Mean	68.83	71.64	47.64	63.56	57.42	59.96
SD	0.34	1.00	1.79	0.34	0.42	0.08
$p < 0.05$	B,C,D,E,F	A,C,D,E,F	A,B,D,E,F	A,B,C,E,F	A,B,C,D,F	A,B,C,D,E

TABLE 5—*Ultimate load data (N) for compression bending tests (n = 5).*

Lab	A	B	C	D	E	F
Mean	229.3	206.4	162.7	191.5	178.3	190.7
SD	9.4	8.2	3.9	3.2	7.3	4.2
$p < 0.05$	B,C,D,E,F	A,C,D,E,F	A,B,D,E,F	A,B,C,E	A,B,C,D	A,B,C

TABLE 6—*Stiffness data (N/mm) for compression bending tests (n = 5).*

Lab	A	B	C	D	E	F
Mean	7.1	7.9	5.7	7.0	6.6	7.2
SD	0.5	0.2	0.3	0.2	0.6	0.1
$p < 0.05$	B,C	A,C,D,E	A,D,E,F	B,C	B,C	C

TABLE 7—*Displacement at yield point data (mm) for compression bending tests (n = 5).*

Lab	A	B	C	D	E	F
Mean	13.81	11.18	14.42	12.76	13.62	11.44
SD	3.67	0.43	1.74	0.28	1.02	0.47
$p < 0.05$	No	No	No	No	No	No

TABLE 8—*Yield load data (N) for compression bending tests (n = 5).*

Lab	A	B	C	D	E	F
Mean	85.7	77.5	95.0	78.2	79.2	70.7
SD	17.9	4.7	4.2	1.8	3.5	4.4
$p < 0.05$	No	C	B,D,F	C	No	C

TABLE 9—*Elastic displacement data (mm) for compression bending tests (n = 5).*

Lab	A	B	C	D	E	F
Mean	12.29	9.66	13.76	11.24	12.10	9.94
SD	3.67	0.44	1.67	0.28	1.02	0.46
$p < 0.05$	No	C	B,F	No	No	C

fixture design that allows some labs to test the specimens over a greater actuator displacement, but there was also inconsistency with regard to the choice of when to halt the test. Some labs allowed the polyethylene blocks or fixtures to touch and then looked at the data from immediately prior to this incident, whereas other labs halted the test at some point prior to any touching. Labs with higher mean values for ultimate displacement and ultimate load likely achieved these data by maximizing the actuator displacement during testing (e.g., through a fixture design that does not impinge prior to block-on-block touching or by permitting the blocks/fixtures to actually contact prior to stopping the test).

Given that yield, stiffness, and elastic displacement are calculated well before the end of the test, however, it is unlikely that these parameters were affected by these differences in fixture design and testing protocol. Interestingly, with the exception of lab C, the labs generally succeeded in generating values that were not statistically different than the mean values of other labs. It is not clear why lab C consistently produced data that were so different from many of the other labs.

So far, specific improvements to F1717 that have passed the balloting process include adding the ILS data to the precision and bias statement, fixing the nomenclature so that the various output variables are called by the same name throughout the document, and requiring that the reason for halting the test be reported. These first steps were designed to allow reviewers of test reports to understand more about the laboratory's test methodology. However, a consistent clevis fixture design has not been adopted, and similarly there is not agreement about when the test should be stopped. Based on the data, two key dimensions that should be specified in order to minimize the difference in ultimate loads and displacements between the labs are the length of the side supports and clarification as to whether the 40.0 mm height (e.g., in Fig. 3 of F1717) is between the hole center and the bottom of the clevis support or between the hole center and the top of the clevis support. For now, the ambiguity in F1717 means that there is still inconsistency among laboratories regarding the magnitude of the actuator displacement during compression bending testing.

All of the laboratories except lab A had difficulties with the static torsion testing. Specifically, lab B used the actual rather than the nominal height of construct. This affects the calculation of the aspect ratio, which in turn affects the calculation of the 2 % offset angle. Lab C calculated the elastic angular displacement wrong (they estimated it as 3.5° for all test samples rather than using the formula described in F1717). Additionally, this lab had transcription errors with their transfer of data from the plots to their summary data table. Lab D similarly had errors with the transfer of data from plots to their summary table. Additionally, they used a questionable slope for their stiffness calculation (Fig. 2). Lab E had technical difficulties (fixture slippage) that prevented them from testing the constructs properly. Replacement specimens were tested without cross connectors, and so all static torsion data from this lab were removed from the analysis. Lab F calculated the elastic angular displacement wrong because it used an incorrect value for the active length of the longitudinal element. As described in "Methods," although errors in transcription and calculation were corrected for this analysis, variations in the determination of subjective

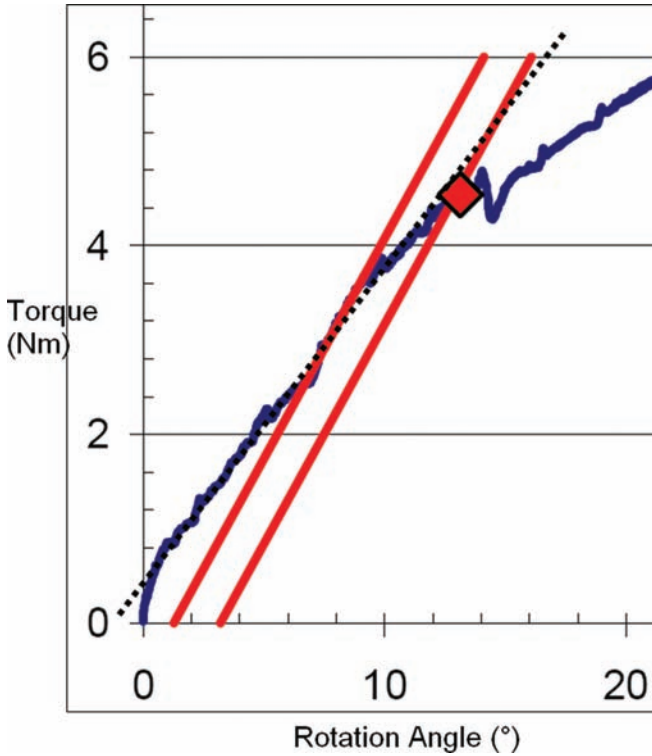

FIG. 2—*Plot of torque versus rotation angle showing raw data, lab D's questionable stiffness and yield lines (solid), and a more typical stiffness line (dotted). The slight dip in torque at 4.4 Nm might represent fixture slippage.*

measurements (such as stiffness) were not changed because the subjectivity of these measurements directly impacts the results.

For stiffness, the range of mean values was 0.38 Nm/° to 1.07 Nm/°, and the labs produced data that were significantly different from most or all other labs (Table 10).

For the 2 % offset yield rotation, the range of mean values was 4.92° to 11.44° (Table 11). There were multiple labs with mean values that differed significantly from those of some of the other labs.

For the yield torque, the range of mean values was 1.86 Nm to 4.14 Nm (Table 12). For this parameter, there were three labs in the middle (B, C, and F),

TABLE 10—*Stiffness data (Nm/°) for torsion tests (n = 5).*

Lab	A	B	C	D	F
Mean	0.38	1.07	0.62	0.48	0.65
SD	0.03	0.06	0.05	0.04	0.09
$p < 0.05$	B,C,F	A,C,D,F	A,B,D	B,C,F	A,B,D

TABLE 11—*2 % offset yield rotation data (°) for torsion tests (n = 5).*

Lab	A	B	C	D	F
Mean	6.92	4.92	7.33	11.44	7.47
SD	0.64	0.26	1.60	1.51	0.97
$p < 0.05$	D	C,D,F	B,D	B,C,F	B,D

one lab that was significantly higher (D) than the others, and one lab that was significantly lower (A).

For the elastic angular displacement, the range of mean values was 3.07° to 9.45° (Table 13). As with the yield torque, there were three labs in the middle (A, C, and F), one lab that was significantly higher (D) than the others, and one lab that was significantly lower (B).

Unfortunately, the large number of errors and methodological differences during static torsion testing confounded the effort to determine the overall test method issues. Clearly, the labs must focus their attention on avoiding fixture slippage during the tests. So far, the only improvement to F1717 specifically related to torsion testing that has passed through the balloting process is a clarification of the language that requires spacer blocks to be used to prevent out-of-plane rotation. This important step ensures that out-of-plane rotation is eliminated for all construct types, as before it was up for interpretation whether some types should allow this rotation. There are several other improvements that should be balloted in the future, including picking a consistent direction to rotate in (acting either to insert the screws more deeply or start to remove them from the blocks), creating a consistent clevis fixture design, adding a maximum requirement for a torsional angle, improving the clarity of the definition of "elastic displacement," and providing pictorial examples of correct and incorrect stiffness calculations. Finally, although the definition of "stiffness" seems to be clear in F1717, users of this standard are cautioned to take a close look at any automated process for determining stiffness. Based on this study, it appears as though blindly recording the output of computer programs designed to calculate this parameter can be problematic if the program does not pick appropriate reference points for determining the slope of the data curve.

Discussion

Despite a variety of quality control practices employed by the participating labs (e.g., certification by the American Association for Laboratory Accreditation,

TABLE 12—*Yield torque data (°) for torsion tests (n = 5).*

Lab	A	B	C	D	F
Mean	1.86	3.38	3.46	4.14	3.53
SD	0.10	0.28	0.32	0.51	0.30
$p < 0.05$	B,C,D,F	A,D	A,D	A,B,D	A

TABLE 13—*Elastic angular displacement data (°) for torsion tests (n = 5).*

Lab	A	B	C	D	F
Mean	4.97	3.07	5.38	9.45	5.52
SD	0.64	0.26	1.60	0.63	0.97
$p < 0.05$	B,D	A,C,D,F	B,D	A,B,C,F	B,D

active involvement in the standards process via attendance at ASTM meetings), one obvious conclusion of this study is that there are significant methodological differences among the laboratories testing spinal constructs that participated in this ILS. It is quite reasonable to suppose that similar issues exist for all laboratories testing spinal constructs. Several steps have been taken to reduce the differences among the laboratories; however, more work is needed in this area.

Although a comparison of the magnitudes of the various output variables with the literature has little relevance due to the differences in construct design, it is interesting to note that the ratio of the standard deviation to the mean value ranges between 2.2 % and 10.3 % for compression bending stiffness and between 2.2 % and 18.8 % for ultimate load in compression bending [3]. Others have found ranges between 1.3 % and 6.9 % for compression bending stiffness and between 1.7 % and 18.6 % for ultimate load in compression bending [4]. These values are the same as or higher than the ranges found within the current study (1.4 % to 9.1 % for compression bending stiffness and 1.7 % to 4.1 % for ultimate load in compression bending). Potential reasons for this difference include the different constructs tested and the earlier state of the test standard during these other studies (in fact, F1717 is based at least partly on the work done by Cunningham et al. [3]).

With four of the six parameters in compression bending (i.e., excepting displacement at yield and elastic displacement), the sample size of five required in the standard was adequate to find significant differences among the labs, with a maximum difference of 10 % in the mean values and a power of 0.8. At the same levels, the sample size of five was not adequate for any of the parameters in the torsion testing. The FDA guidance document calls for a sample size of "six or more" [2] for these tests; however, it is unclear whether increasing the sample size without fixing the methodological and fixture issues first would yield much of an improvement.

There are multiple limitations to this study, including the relatively small sample size, the small number of participating laboratories, and the limited scope of tests performed from F1717. This was necessary due to the difficulty and expense of procuring constructs for testing. The fact that the various laboratories volunteered to participate in this study might have introduced some selection bias—laboratories that send representatives to be present at ASTM subcommittee meetings and volunteer to participate in interlaboratory comparisons might have similar interpretations of F1717 and be more likely to follow this standard exactly. Additionally, whereas the constructs are designed to be used clinically at the upper thoracic levels of the spine, the constructs were

tested as if they were designed for use in the lumbar region. This deviation from the standard was requested by the donor of the constructs so that data from this study could be compared against its own internal data, but it might have affected the results. Because the final tightening was performed prior to the specimens' being sent to the various labs, it is possible that the difference in time between the tightening and testing at the labs varied enough that the stress relaxation of the titanium might have caused some variation in the results. However, this was deemed a reasonable risk because we hoped to eliminate any variability in the tightening torque by having all specimens prepared by a single person. Differences in the construct assembly (alignment jig dimensions, repeatability of torque application in tightening crosslink screws, proximity of screw heads to block, etc.) likely would lead to an increase in the differences in results among the labs. Finally, this study was performed on only a single type of construct, and testing other types (whether from different manufacturers or the same manufacturer) might very well produce different results.

References

[1] ASTM F1717, 2010, "Standard Test Methods for Spinal Implant Constructs in a Vertebrectomy Model," ASTM International, West Conshohocken, PA.

[2] Stevens, T., 2004, "Guidance for Industry and FDA Staff: Spinal Systems 510(k)s," U.S. Department of Health and Human Services, Orthopedic Devices Branch, Silver Spring, MD.

[3] Cunningham, B. W., Sefter, J. C., Shono, Y., and McAfee, P. C., "Static and Cyclical Biomechanical Analysis of Pedicle Screw Spinal Constructs," *Spine*, Vol. 18, No. 12, 1993, pp. 1677–1688.

[4] Stanford, R. E., Loefler, A. H., Stanford, P. M., and Walsh, W. R., "Multiaxial Pedicle Screw Designs: Static and Dynamic Mechanical Testing," *Spine*, Vol. 29, No. 4, 2004, pp. 367–375.

[5] Haher, T. R., Yeung, A. W., Ottaviano, D. M., Merola, A. A., and Caruso, S. A., "The Inverse Effects of Load Transfer and Load Sharing on Axial Compressive Stiffness," *Spine J.*, Vol. 1, No. 5 2001, pp. 324–330.

[6] Lindsey, C., Deviren, V., Xu, Z., Yeh, R. F., and Puttlitz, C. M., "The Effects of Rod Contouring on Spinal Construct Fatigue Strength," *Spine*, Vol. 31, No. 15, 2006, pp. 1680–1687.

[7] Pienkowski, D., Stephens, G. C., Doers, T. M., and Hamilton, D. M., "Multicycle Mechanical Performance of Titanium and Stainless Steel Transpedicular Spine Implants," *Spine*, Vol. 23, No. 7, 1998, pp. 782–788.

[8] Kotani, Y., Cunningham, B. W., Parker, L. M., Kanayama, M., and McAfee, P. C., "Static and Fatigue Biomechanical Properties of Anterior Thoracolumbar Instrumentation Systems: A Synthetic Testing Model," *Spine*, Vol. 24, No. 14, 1999, pp. 1406–1413.

[9] Chen, P. Q., Lin, S. J., Wu, S. S., and So, H., "Mechanical Performance of the New Posterior Spinal Implant: Effect of Materials, Connecting Plate, and Pedicle Screw Design," *Spine*, Vol. 28, No. 9, 2003, pp. 881–887.

[10] Cook, S. D., Salkeld, S. L., Whitecloud, T. S., III, and Barberá, J., "Biomechanical Testing and Clinical Experience with the OMEGA-21 Spinal Fixation System," *Am. J. Orthop.*, Vol. 30, No. 5, 2001, pp. 387–394.

[11] Liu, T., Zheng, W. J., Li, C. Q., Liu, G. D., and Zhou, Y., "Design and Biomechanical Study of a Modified Pedicle Screw," *Chinese Journal of Traumatology*, Vol. 13, No. 4, 2010, pp. 222–228.

[12] Teitelbaum, G. P., Shaolian, S., McDougall, C. G., Preul, M. C., Crawford, N. R., and Sonntag, V. K., "New Percutaneously Inserted Spinal Fixation System," *Spine*, Vol. 29, No. 6, 2004, pp. 703–709.

[13] Mikles, M. R., Asghar, F. A., Frankenburg, E. P., Scott, D. S., and Graziano, G. P., "Biomechanical Study of Lumbar Pedicle Screws in a Corpectomy Model Assessing Significance of Screw Height," *Journal of Spinal Disorders and Techniques*, Vol. 17, No. 4, 2004, pp. 272–276.

[14] Spenciner, D. B., *Interlaboratory Study to Establish Precision Statements for ASTM F1717-09, Spinal Implant Constructs in a Vertebrectomy Model*, ASTM International, West Conshohocken, PA, 2009.

Reprinted from JAI, Vol. 9, No. 3
doi:10.1520/JAI103503
Available online at www.astm.org/JAI

M. C. Anderson[1] *and C. J. Lissy*[2]

ASTM F2624-07—Evaluating an Alternate Fixture for Testing Extra Discal Motion Preserving Implants

ABSTRACT: ASTM F2624-07 prescribes applying flexion/extension, lateral bending, and axial rotation moments to test and evaluate extra discal motion preserving implants (EDMPI). The standard provides a suggested laterally oriented construct (LOC) for conducting flexion/extension (FE) testing. The suggested construct does not have a fixed center of rotation (COR). An alternate set of fixtures to conduct FE testing using a vertically oriented construct (VOC) with a fixed COR is presented. Testing was conducted to quantify the loads applied to an EDMPI using both types of fixtures, quantify shear loading applied to the actuator, determine whether results are frequency dependent, and evaluate whether the fixtures can differentiate between EDMPI using a measure of displacement amplitude. A miniature load cell was mounted to both fixtures to quantify load applied to an EDMPI during testing at several different applied loads or torques and at two testing frequencies (2 Hz and 5 Hz). Lateral actuator shear was measured using a dial indicator. The load cell was replaced with cylindrical test specimens made of stainless steel, titanium, polyether ether ketone, or a polyethylene cable slipped inside a polyurethane tube, and the testing repeated. Results indicated that both fixtures generated similar tensile/compressive loads at an EDMPI. The LOC fixture generated more actuator shear than the VOC. Using a VOC fixture rather than the LOC suggested in ASTM F2624-07 in FE testing may be a reasonable alternative for certain types of devices.

KEYWORDS: ASTM F2624-07, dynamic stabilization, dynamic stiffness, spine implants

Manuscript received October 15, 2010; accepted for publication December 14, 2011; published online March 2012.

[1] Empirical Testing Corp, Colorado Springs, CO 80921 (Corresponding author), e-mail: manderson@empiricaltesting.com
[2] Empirical Testing Corporation, Colorado Springs, CO 80921.

Cite as: Anderson, M. C. and Lissy, C. J., "ASTM F2624-07—Evaluating an Alternate Fixture for Testing Extra Discal Motion Preserving Implants," *J. ASTM Intl.*, Vol. 9, No. 3. doi:10.1520/JAI103503.

Introduction

Extra discal motion preserving implants (EDMPI) have been introduced as a treatment of spinal disorders. The intent of these devices is to provide "dynamic stabilization," i.e., achieving stabilization of the spine and providing pain relief without promoting bony fusion. By preserving the motion of a treated motion segment, these devices also intend to reduce disorders at adjacent segments. At the current time, several EDMPI devices are cleared and in use in the United States under a post market surveillance regimen as prescribed by the FDA. Others are in unrestricted use in international markets.

Innovation in EDMPI design will undoubtedly continue. The medical device testing community should prepare to test and evaluate them in an objective manner. ASTM Standard F2624-07 [1] was developed to evaluate and compare dynamic stabilization devices in a standardized manner. The first version, released in 2007, prescribes a battery of mechanical tests and describes methods to collect and analyze wear debris generated in those tests. The mechanical test battery prescribes applying pure angular rotations around the flexion/extension, lateral bending, and axial rotation axes. A schematic drawing of a fixture for conducting flexion/extension testing by applying torque to a laterally oriented construct (LOC) is provided in that standard. Fixturing for conducting the prescribed lateral bending and axial rotation tests are not provided in the standard.

The LOC lacks a fixed center of rotation (COR). In practical use, this can generate lateral shearing, which damages actuator seals and is a potential and unmeasurable source of error in load cell measurements. The F2624-07 standard allows the user of the test method to determine the COR for the device to be tested. In a study presented at the November, 2010 ASTM F04.25 symposium "Symposium on Static and Dynamic Spinal Implants: Are We Evaluating Them appropriately?" Wing et al. presented cadaver biomechanical testing results which indicated that the COR of a functional spinal unit when instrumented with an EDMPI could be considered fixed [2].

An alternate fixture for evaluating EDMPIs in flexion/extension testing is proposed, which applies compression load to a vertically oriented construct (VOC). With this fixturing, lateral actuator shearing is eliminated, and the COR of the test is fixed at the center of the bearing. At the Nov. 2010 symposium cited earlier, two other studies evaluated similar proposed fixtures for lateral bending and axial rotation testing [3,4].

The F2624-07 standard is relatively new and the LOC fixture untested. The amount of torque that must be applied to the LOC to generate relevant compressive/tensile loads in an EDMPI is not known. The standard prescribes that testing be conducted at frequencies of 2 Hz or less and requires justification from the end user to test at higher frequencies. Finally, the ability to differentiate between and compare devices of different stiffness tested using the LOC has not been proven.

The intent of the experiments described in this manuscript is to compare and evaluate results collected when using the LOC and VOC fixtures. Discussions pertaining to the clinical relevance of modeling spinal motion using a fixed versus non defined COR can be found in other peer reviewed articles. The objectives of this testing were to (1) quantify the applied torque (LOC) or load (VOC) required to

generate an equivalent compressive load in an EDMPI, (2) quantify and compare lateral actuator shear when using the LOC and VOC fixtures, (3) determine whether results are test frequency dependent, and (4) evaluate whether EDMPI devices of different stiffness can be differentiated using the LOC and VOC fixtures.

Methods

Evaluating the F2624-07 LOC

A set of test fixtures complying with the LOC design shown in F2624-07 were manufactured of stainless steel. Instead of a simulated spinous process, ball joint rod ends were mounted to their posterior surfaces, and an 1100 N capacity miniature load cell (LCFD-250, Omega Engineering, Inc., Stamford, CT) was mounted between the rod ends to measure the tensile and compressive forces that would be applied to an EDMPI. The ball joint rod ends prevented shear loads from being applied to the miniature load cell. The distance from the miniature load cell to the COR of the fixtures was 65 mm. The COR of the fixtures was coincident with the COR of the test frame. Fixtures were rigidly mounted to the actuator and base of an Instron 8874 (Instron Corp, Norwood, MA) biaxial testing machine and a series of dynamic tests applying fully reversed ($R = -1$) cyclic torques (7.5, 15, 22.5, 30, 37.5, or 45 N-m) for approximately 150 cycles at frequencies of 2 Hz and 5 Hz were conducted. EDMPI load amplitude was calculated by subtracting load recorded by the miniature load cell at the minimum actuator rotation from load recorded at the maximum actuator rotation at 100 elapsed cycles and dividing by 2. The tip of a dial indicator was placed laterally on the Instron actuator's shaft. Minimum and maximum dial indicator displacements at 100 elapsed cycles during each test were recorded. A photograph of the test setup is shown in Fig. 1.

The miniature load cell was removed and a cylindrical test specimen made of 17-4 ph stainless steel in H900 condition (SS), Commercially Pure Titanium (Ti), polyether ether ketone (PEEK) or a polytheylene cord (PE cord) slipped inside a polyurethane tube, was mounted between the rod ends. Photographs of the cylindrical test specimens and the PE cord test specimen are shown in Fig. 2. The diameter (6.25 mm) and materials of the cylindrical test specimens were selected to be representative of rod based EDMPI systems currently in use. A similar series of dynamic tests applying fully reversed ($R = -1$) cyclic torques (2.5, 5, 7.5, 10, 12.5, 15, 22.5, or 30 N-m) for approximately 150 cycles at frequencies of 2 Hz or 5 Hz were then conducted using each test specimen. LOC rotation amplitude for each test was calculated by subtracting the actuator position at minimum applied torque from the actuator position at maximum applied torque after 100 elapsed cycles. A representative photograph of the test setup is shown in Fig. 3.

Evaluating the Alternate VOC

The VOC applied pure angular rotation about the flexion/extension axis of an EDMPI by applying compressive load through a set of low friction bearings.

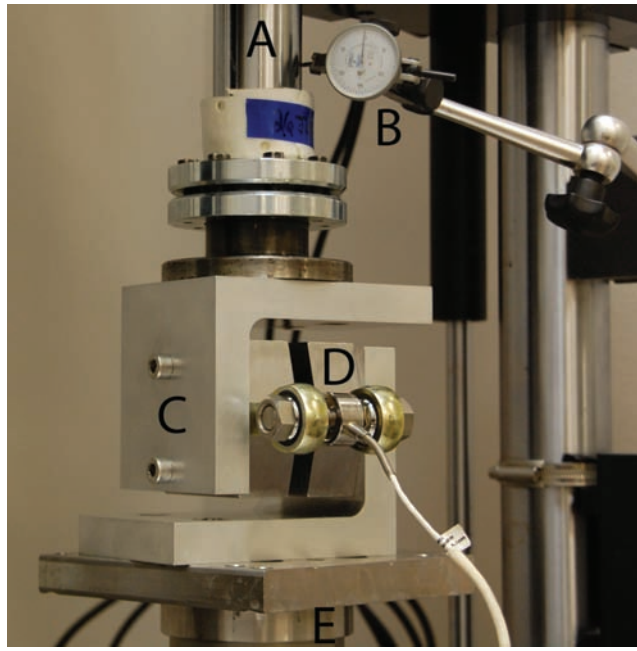

FIG. 1—*Setup for testing with miniature load cell in LOC fixtures. A—actuator shaft, B—dial indicator, C—LOC fixtures, D—miniature load cell, E—torsion load cell.*

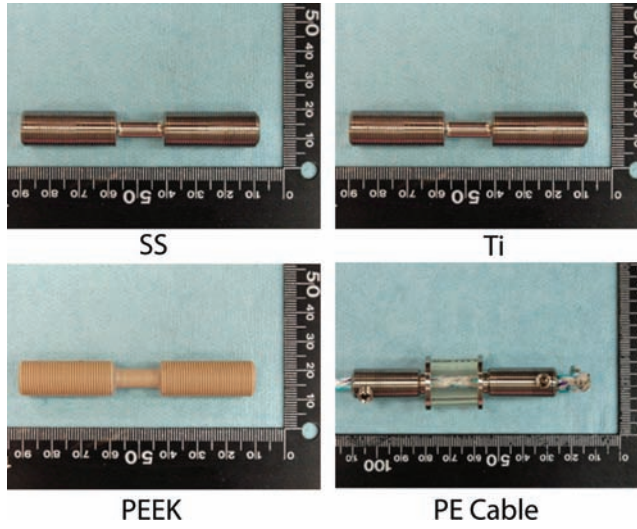

FIG. 2—*Cylindrical test specimens.*

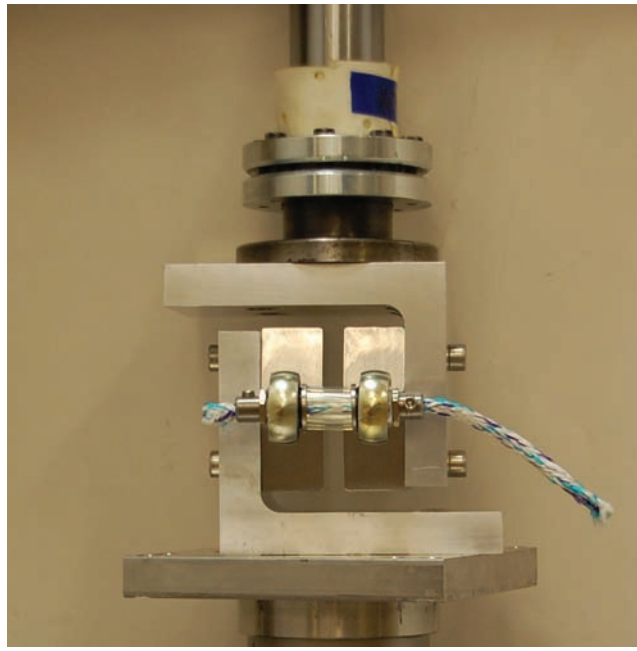

FIG. 3—*Setup for testing with PE cord specimen in LOC fixtures.*

The same set of ball joint rod ends were fitted to the posterior surface of the VOC, and the same miniature load cell mounted between them. The distance from the miniature load cell to the COR of the fixtures was 65 mm. The VOC was mounted to an Instron 8874 biaxial testing machine by passing 3/8 in. diameter pins through C-bracket fixtures. A series of dynamic tests applying compressive/tensile (R = 10) cyclic load (250, 500, 750, 1000, 1250, and 1500 N) at frequencies of 2 Hz or 5 Hz were conducted. EDMPI load amplitude was calculated by subtracting load recorded by the miniature load cell at the minimum actuator displacement from load recorded at the maximum actuator displacement at 100 elapsed cycles and dividing by 2. Lateral actuator shear was recorded during each test using a dial indicator as described previously. A photograph of the test setup is shown in Fig. 4.

The miniature load cell was removed and replaced with the cylindrical test specimens described previously, and a similar set of dynamic tests applying compressive/tensile (R = 10) cyclic load (250, 500, 750, 1000, 1250, 1500 N) at two different frequencies (2 Hz or 5 Hz) were conducted. The PE cord specimen was tested at loads of 250, 375, 500, 625, and 750 N at the same test frequencies. At cyclic loads greater than 750 N the PE cord slipped out of the set screw. VOC displacement amplitude for each test was calculated by subtracting actuator position at the minimum applied load from actuator position at the maximum applied load after 100 elapsed cycles. A representative photograph of the test setup is shown in Fig. 5.

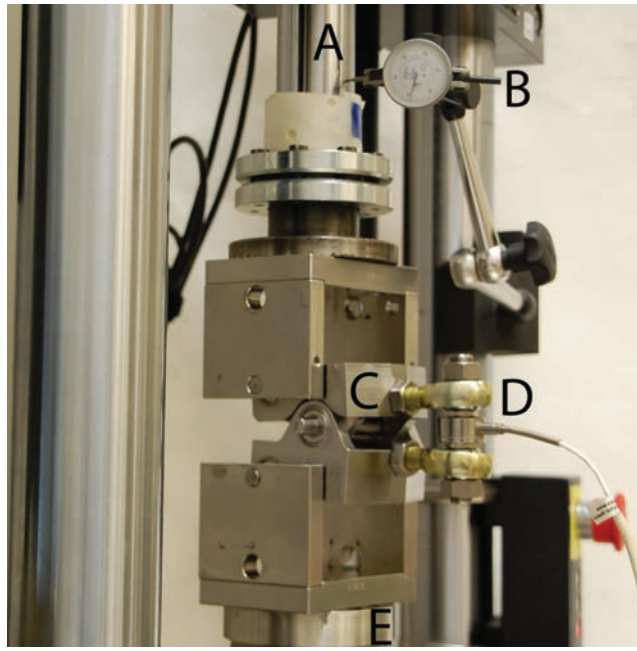

FIG. 4—*Setup for testing with miniature load cell in VOC fixtures. A—actuator shaft, B—dial indicator, C—VOC fixtures, D—miniature load cell, E—compression load cell.*

Results

Forces recorded by the miniature load cell during testing of the LOC and VOC are shown in Figs. 6 and 7. The applied torques and loads were selected to produce EDMPI forces of similar magnitude. Force increased as applied torque or load increased, and was independent of test frequency. Producing 400 N of EDMPI compressive force required the application of approximately 25 N-m of torque in the LOC and 750 N of compressive load in the VOC.

Lateral actuator displacement recorded during testing at 5 Hz is shown in Figs. 8 and 9. Data collected during testing at 2 Hz are not shown, but were similar. During LOC testing, lateral actuator shear increased as applied torque increased. Under an applied torque of 25 N-m, lateral actuator shear was approximately 0.2 mm. During VOC testing, shear was less than the detection threshold of the dial indicator (0.01 mm) at all loads except 1500 N.

Rotation amplitudes when testing the cylindrical and PE cord test specimens with the LOC are shown in Figs. 10 and 11. Amplitudes increased proportionally to increases in applied torque. Differences between the cylindrical test specimens were not easily discernable. Displacement of the PE cord specimen also increased as load was applied, but not at the same rate as the cylindrical test specimens. Results were independent of test frequency.

Displacement amplitudes when testing the cylindrical and PE cord test specimens with the VOC are shown in Figs. 12 and 13. Amplitude increased as

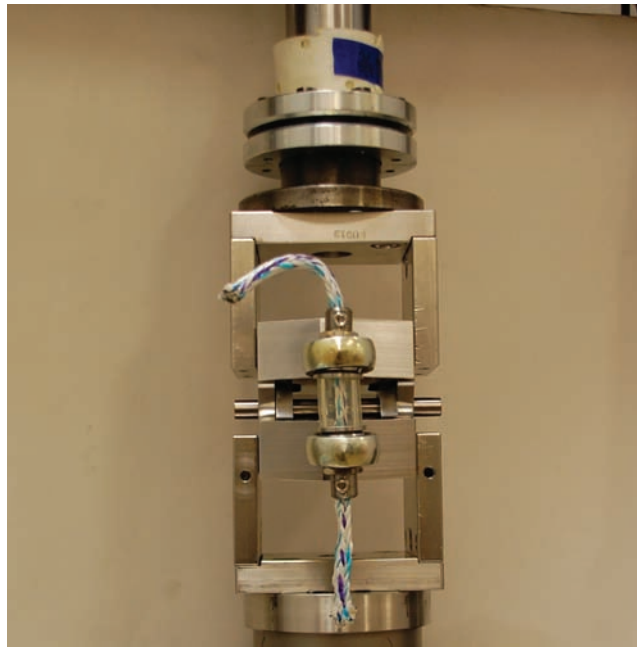

FIG. 5—*Setup for testing with PE cord test specimen in VOC fixtures.*

applied load was increased, but the relationship was not as linear as that recorded with the LOC. Differences in displacement amplitude between the SS, Ti, and PEEK cylinders were discernible at both test frequencies, but were more pronounced at 2 Hz. Displacement of the PE cord specimen again increased as load was applied, but not at the same rate as that of the cylindrical test specimens.

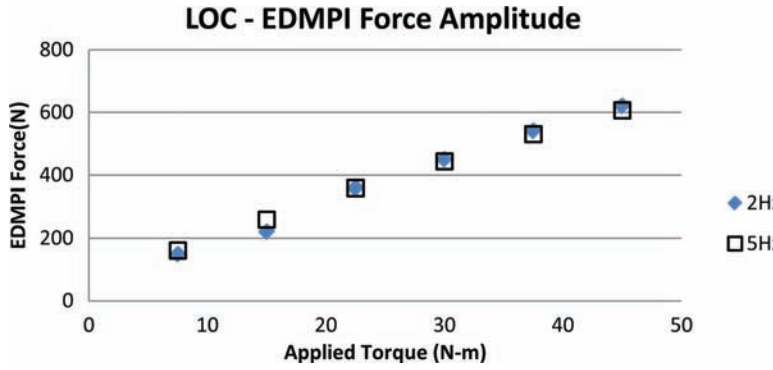

FIG. 6—*Force amplitude recorded by miniature load cell during testing with LOC fixture.*

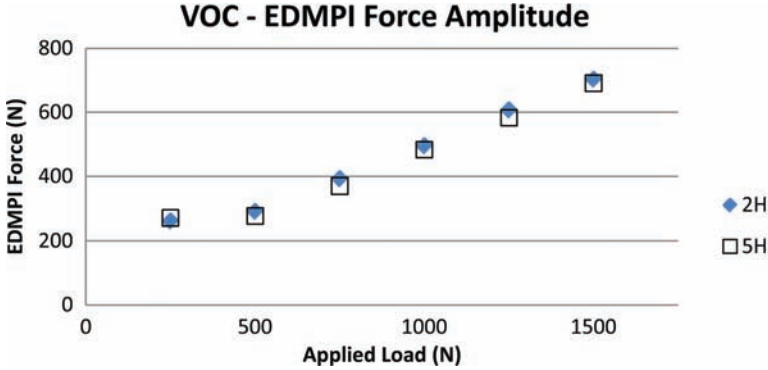

FIG. 7—*Force amplitude recorded by miniature load cell during testing with VOC fixture.*

Discussion

Shepherd et al. [5] reported mean load to fracture of the spinous process in the superior/inferior direction in n = 32 L3 and L4 cadaver vertebrae as 339 N, with 95% confidence intervals at 257 N and 447 N. If a 3× engineering factor of safety is applied, EDMPI force magnitudes recorded in this testing can be considered relevant for the mechanical testing of spinous process based EDMPI devices.

Applying relevant EDMPI forces using the LOC generated more lateral actuator shear than when using the VOC to apply similar levels of EDMPI force. It was hypothesized that due to the lack of a fixed COR, the side opposite the ball joint rod ends of the LOC fixtures (anatomic anterior) displaced laterally as applied torque increased. With increasing applied torque, a part of the resulting increase in angular displacement was due to shear movement rather than an increase in flexion/extension of the test specimen.

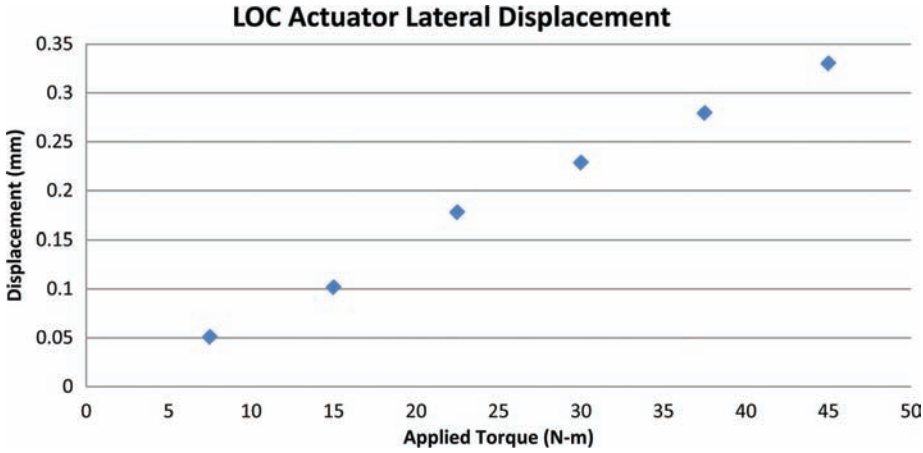

FIG. 8—*Actuator lateral displacement recorded during testing with LOC fixture.*

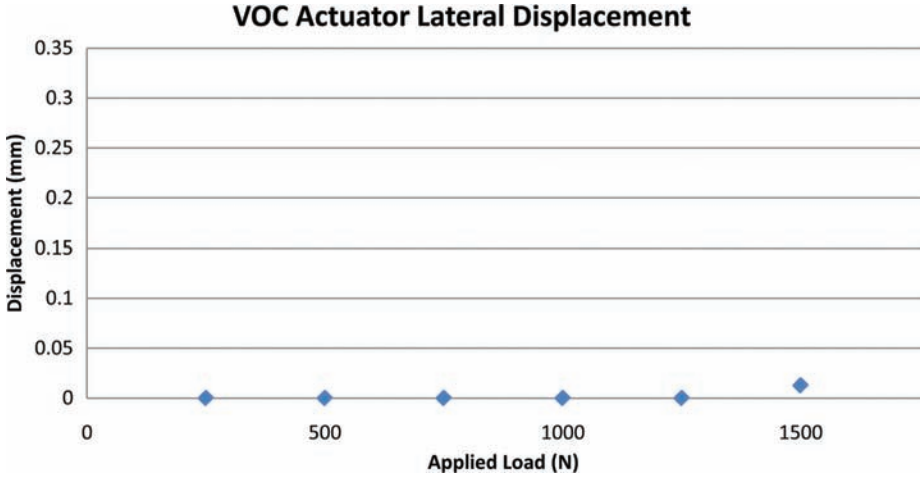

FIG. 9—*Actuator lateral displacement recorded during testing with VOC fixture.*

Rotation and displacement amplitude of cylindrical test specimens increased with increasing levels of applied torque/load with both LOC and VOC fixtures. Differences between the cylindrical test specimens appeared more pronounced with the VOC fixtures than the LOC fixtures, but results also indicate that results when using the VOC fixtures may be frequency dependent. Friction in the bearings of the VOC may be the reason for the difference.

There are several limitations to this study that should be considered. The mechanical test battery prescribed in F2624-07 differentiates between EDMPI devices by constructing a fatigue curve. This entails progressively failing specimens and ultimately determining a device's run out load to 10 000 000 cycles. In

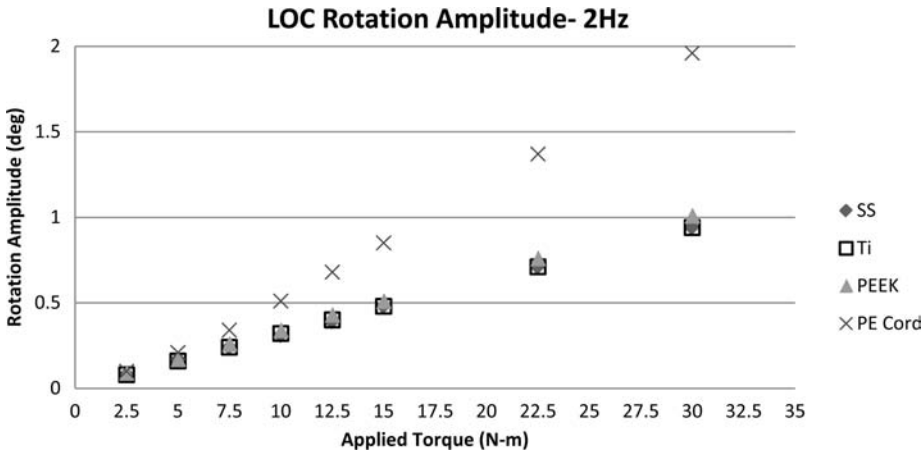

FIG. 10—*Rotation amplitude of test specimens during testing with LOC fixture at a frequency of 2 Hz.*

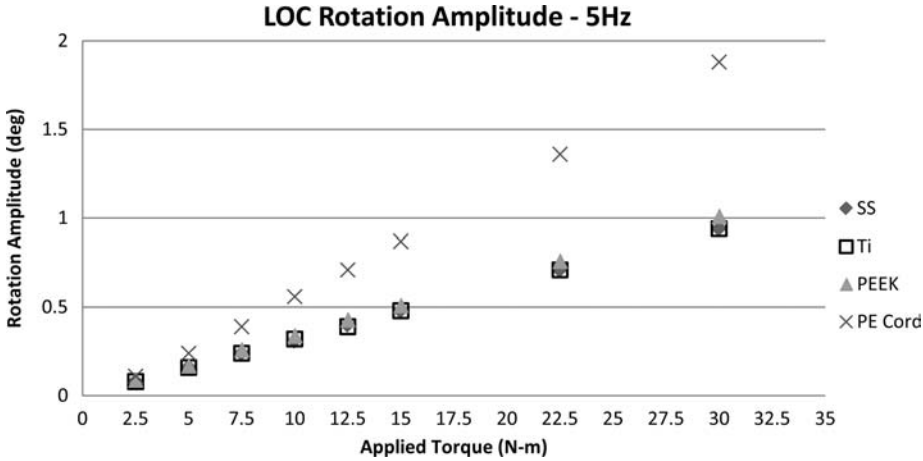

FIG. 11—*Rotation amplitude of test specimens during testing with LOC fixture at a frequency of 5 Hz.*

this experiment, actuator displacement (rotation in the case of the LOC, and linear in the case of the VOC) amplitude after completing 100 cycles was used as a metric to differentiate between EDMPI devices of different stiffness rather than constructing a fatigue curve. After 100 cycles, it was observed that displacement amplitude reached steady state and test specimens had not experienced plastic deformation. Variables such as friction in the VOC bearings and a lack of constraint in the LOC fixtures may have obscured the true stiffness differences between the test specimens. Further experimentation is necessary, including

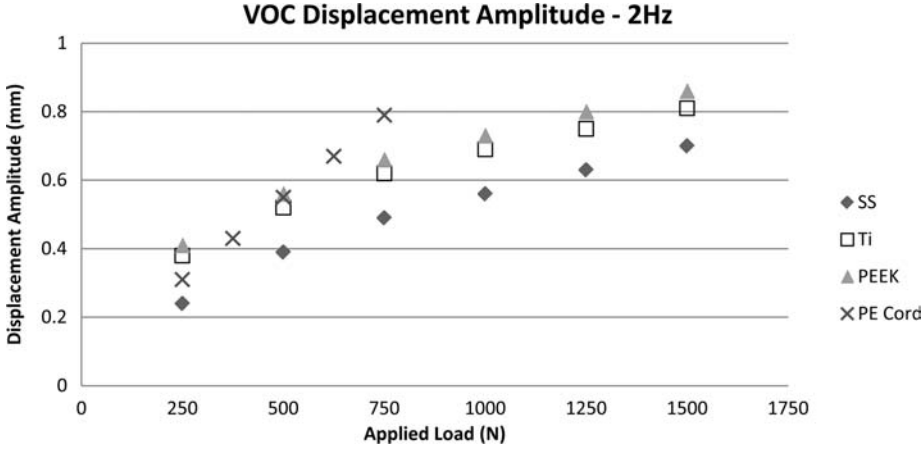

FIG. 12—*Displacement amplitude of test specimens during testing with VOC fixture at a frequency of 2 Hz.*

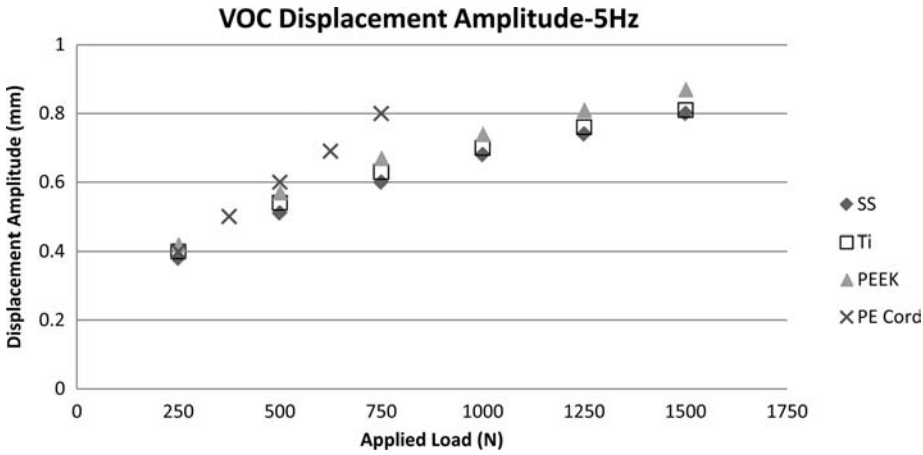

FIG. 13—*Displacement amplitude of test specimens during testing with VOC fixture at a frequency of 5 Hz.*

running specimens to failure, before rotation and displacement amplitude metrics should be used to differentiate between or compare EDMPI devices.

It should be noted that actuator lateral displacement data were collected with a miniature load cell mounted in the fixture, whose stiffness is likely greater than an EDMPI device. The SS and Ti cylindrical test specimens are also likely stiffer than EDMPI devices that would potentially be tested using the F2624-07 standard. They are representative, however, of hardware currently in use to promote fusion in the spine and therefore could be considered a worst case test condition.

In conclusion, both fixtures are capable of applying relevant compressive and tensile loads to EDMPI devices. VOC fixtures generate less actuator lateral displacement than LOC fixtures, extending the life of actuator seals and reducing potential error caused by load cell shear. The use of rotation or displacement amplitude as a metric to differentiate between EDMPI devices of different stiffness was not supported for the specimens tested.

The design and function of EDMPI devices varies widely. Devices are made of metallic, polymeric, or biologic materials, may attach to the spinous process, facets, or pedicles, and permit and restrict motion of the spine using different methods. ASTM F2624-07 attempts to provide guidance and test methods to test any and all of these devices, but the method to be used is ultimately left to the user of the standard to select and justify. The VOC fixture presented in this manuscript presents another option to the user of this standard. The VOC may be more appropriate if the EDMPI device to be evaluated constrains motion to rotation about a fixed COR or minimizes translational (shear) motion.

Acknowledgments

This research was funded exclusively by Empirical Testing Corporation.

References

[1] ASTM F2624-07. 2007, "Standard Test Method for Static, Dynamic, and Wear Assessment of Extra-Discal Spinal Motion Preserving Implants," *Annual Book of ASTM Standards*, ASTM International, West Conshohocken, PA.

[2] Wing, C., Kruger, S., Beger, J., and Schilling, C., "In Vitro Study to Evaluate the Centre Of Rotation (COR) Following Dynamic Stabilization Using Different Pedicle Screw Based Dynamic Posterior Stabilization Systems (PDS)—Recommendation for the Implementation of a Standardized COR in ASTM F2624," *Symposium on Static and Dynamic Spinal Implants: Are We Evaluating Them Appropriately?* San Antonio, TX, November 16, 2010, ASTM International, West Conshohocken, PA, p. 24.

[3] Wing, C., Kruger, S., Beger, J., and Schilling, C., "Dynamic Testing of Pedicle Screw Based Dynamic Posterior Stabilization Systems (PDS) using and Alternative Test Set-up to ASTM F2624," *Symposium on Static and Dynamic Spinal Implants: Are We Evaluating Them Appropriately?* San Antonio, TX, November 16, 2010, ASTM International, West Conshohocken, PA, p. 33.

[4] Anderson, M., and Lissy, D., "ASTM F2624—Evaluating Alternate Fixtures for Flexion/Extension, Lateral Bending, and Axial Rotation Testing of Extra Discal Motion Preserving Implants," *J. ASTM Int.*, Vol. 9, No. 2, 2012.

[5] Shepherd, D. E., *et al.*, "Spinous Process Strength," *Spine*, Vol. 25, No. 3, 2000, pp. 319–323.

Reprinted from JAI, Vol. 9, No. 2
doi:10.1520/JAI103510
Available online at www.astm.org/JAI

M. C. Anderson[1] *and D. A. Lissy*[2]

ASTM F2624—Evaluating Alternate Fixtures for Flexion/Extention, Lateral Bending, and Axial Rotation Testing of Extra Discal Motion Preserving Implants

ABSTRACT: ASTM F2624-07 prescribes applying flexion/extension (FE), lateral bending (LB), and axial rotation (AR) moments to test and evaluate extra discal motion preserving implants (EDMPI), but parameters such as fixture design and load parameters are left to the user to define. A set of fixtures to conduct FE, LB, and AR testing rotation of EDMPI devices about a fixed center of rotation were developed by Aesculap Implant Systems. Their design was shared, and a set of these fixtures were manufactured and evaluated independently at Empirical Testing Corp. Testing was conducted to quantify the loads applied to an EDMPI in the FE and LB fixtures, determine whether results are frequency dependent, and evaluate whether EDMPI of different stiffnesses can be differentiated when using the fixtures. Miniature load cells were mounted to FE and LB fixtures to quantify load applied to an EDMPI during testing at several different applied loads and at two testing frequencies (2 Hz and 5 Hz). The load cells were replaced with cylindrical test specimens made of stainless steel, titanium, polyether ether ketone (PEEK), or a polyethylene cable slipped inside a polyurethane tube and the testing repeated. Results indicated that loads measured during FE testing were similar in magnitude to those recorded during LB testing but 90 degrees out of phase. No frequency effects were observed. Differences in displacement

Manuscript received October 18, 2010; accepted for publication November 14, 2011; published online December 2011.

[1] Empirical Testing Corp., Colorado Springs, CO 80918 (Corresponding author), e-mail: manderson@empiricaltesting.com

[2] Empirical Testing Corp., Colorado Springs, CO 80918.

Symposium on Static and Dynamic Spinal Implants: Are We Evaluating Them Appropriately? on 16 November 2010 in San Antonio, TX.

Cite as: Anderson, M. C. and Lissy, D. A., "ASTM F2624—Evaluating Alternate Fixtures for Flexion/Extention, Lateral Bending, and Axial Rotation Testing of Extra Discal Motion Preserving Implants," *J. ASTM Intl.*, Vol. 9, No. 2. doi:10.1520/JAI103510.

amplitude when testing the stainless steel, titanium, and PEEK specimens in FE and LB testing at both 2 Hz and 5 Hz were not discernable. The displacement amplitude of the polyethylene (PE) cord specimen was different than the other specimens, but no frequency effect was noted. The fixtures developed by Aesculap are a reasonable attempt to conduct EDMPI testing in FE, LB, and AR motions. Potential users of these fixtures should conduct further studies to determine whether their use is appropriate to test their specific EDMPI device.

KEYWORDS: ASTM F2624-07, dynamic stabilization, posterior stabilization

Introduction

Extra discal motion preserving implants (EDMPI) have been introduced for the treatment of spinal disorders. The intent of these devices is to provide "dynamic stabilization," i.e., achieving stabilization of the spine and providing pain relief without promoting bony fusion. By preserving the motion of a treated motion segment, these devices also intend to reduce disorders at adjacent segments. At the current time, several EDMPI devices are cleared for use in the USA under a post market surveillance regimen as prescribed by the FDA. Others are in unrestricted use in international markets.

Innovation in EDMPI design will undoubtedly continue; the medical device testing community should prepare to test and evaluate them in an objective manner. ASTM standard F2624-07 [1] was developed to evaluate and compare dynamic fixation devices. This standard prescribes a battery of mechanical tests and describes methods to collect and analyze wear debris generated in those mechanical tests. The methods for mechanical testing consist of applying pure angular rotations around the flexion/extension (FE), lateral bending (LB), and axial rotation (AR) axes. A schematic drawing of a fixture for conducting FE testing by applying torque to a laterally oriented construct is provided in the standard, but fixtures for conducting LB and AR testing are not described. Their design, and the justification for their use, is left to the user. Justification for testing at frequencies greater than 2 Hz is also not provided.

A set of fixtures to conduct FE, LB, and AR testing of EDMPI devices about fixed centers of rotation were developed by Aesculap Implant Systems. Their development, and results of in vitro testing conducted to evaluate EDMPI systems, were described at the November, 2010, ASTM F04.25 symposium, Symposium on Static and Dynamic Spinal Implants: Are We Evaluating Them Appropriately? [2,3]. Their design was shared, and a set were manufactured and evaluated independently at Empirical Testing Corp. The mechanical test battery prescribed in ASTM F2624-07 [1] differentiates between EDMPI devices by constructing a fatigue curve. This entails progressively failing specimens and ultimately determining a device's run out load to 5 000 000 cycles. For this experiment, an alternate metric that did not require testing specimens to failure was proposed to differentiate between EDMPI devices of different stiffness: displacement amplitudes.

Described in this paper are tests to evaluate the suitability of these fixtures to test and evaluate EDMPI when applying pure angular rotations around fixed

FE, LB, and AR axes. The objectives of this testing were to (1) quantify the applied load required to generate relevant compressive loads in an EDMPI, (2) determine if results are test frequency dependent, and (3) evaluate whether EDMPI devices of different stiffnesses can be differentiated based upon displacement amplitude using these fixtures. Compressive loads in EDMPI were measured only in the FE and LB axes of rotation, while the evaluation of test frequency and the ability to differentiate between EDMPI of different stiffnesses were evaluated in the FE, LB, and AR axes of rotation.

Methods

Photographs of the FE, LB, and AR test fixtures are shown in Fig. 1. Bronze bushings and case hardened steel shafts were used at the articulating joints of each fixture. Ball joint rod ends were mounted bilaterally to the posterior surfaces of the FE and LB fixtures; solid rod ends were mounted bilaterally to the AR fixtures. To quantify loads that would be applied to an EDMPI, two 1100 N capacity miniature load cells (LCFD-250, Omega Engineering, INC., Stamford, CT, USA) were mounted between rod ends of the FE and LB fixtures. The ball joint rod ends prevented shear loads from being applied to the miniature load cells in FE and LB testing, but shear generated during AR testing could not be mitigated by the ball joint rod ends. As shear loading is a potential source of error in load cells, tests to measure forces applied to an EDMPI using the AR

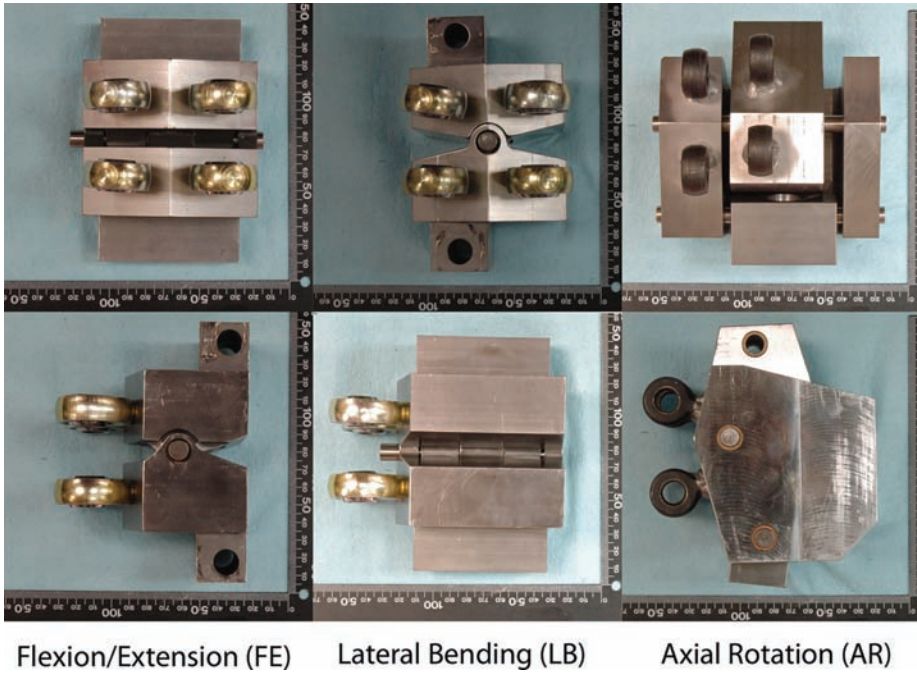

FIG. 1—*Posterior and lateral views of FE, LB, and AR fixtures.*

fixtures were not conducted. As test fixtures were not manufactured of corrosion resistant materials, all testing was conducted in ambient air. Test fixtures were mounted to an INSTRON 8874 (Instron Corp, Norwood, MA, USA) load frame using 3/8 in. diameter pins and F1717 compliant C-bracket fixtures. A series of dynamic tests applying cyclic compressive/tensile ($R = -1$) load (250 N, 500 N, 750 N, 1000 N, 1250 N, and 1500 N) at two different frequencies (2 Hz or 5 Hz) were conducted. The EDMPI load magnitude of each test was calculated by subtracting minimum from maximum loads recorded by both load cells after approximately 500 cycles of testing and dividing by 2. A representative photo of the test setup with load cells in place is shown in Fig. 2.

To determine whether specimens of different stiffness could be differentiated using these fixtures, the miniature load cells were removed and cylindrical specimens made of 17-4 ph stainless steel in H900 condition (SS), Titanium (Ti), polyether ether ketone (PEEK) or a polyethylene cord (PE cord) slipped inside a polyurethane tube were mounted between the bilateral rod ends. Photographs of the cylindrical test specimens and the PE cord test specimen are shown in Fig. 3. The diameter (5.5 mm) and the materials of the cylindrical test specimens were selected to be similar to those of rod based spinal implant systems currently in use. The PE cord specimen was not dimensionally similar to a system currently in use due to constraints of the test fixtures. The same set of cyclic load tests applied to the miniature load cells were then conducted using each cylindrical specimen in the FE, LB, and AR fixtures. Each set of cylindrical test specimens was tested one time in each test fixture. Displacement amplitude for each test was calculated by subtracting actuator position at minimum applied load from actuator position at maximum applied load after approximately 500 cycles. A representative photo of the test setup with cylindrical test specimens in place is shown in Fig. 4.

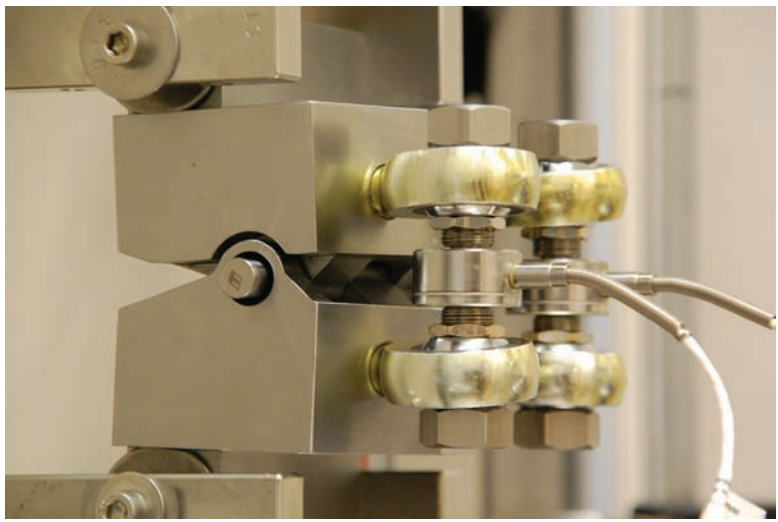

FIG. 2—*FE fixture with EDMPI load cells mounted.*

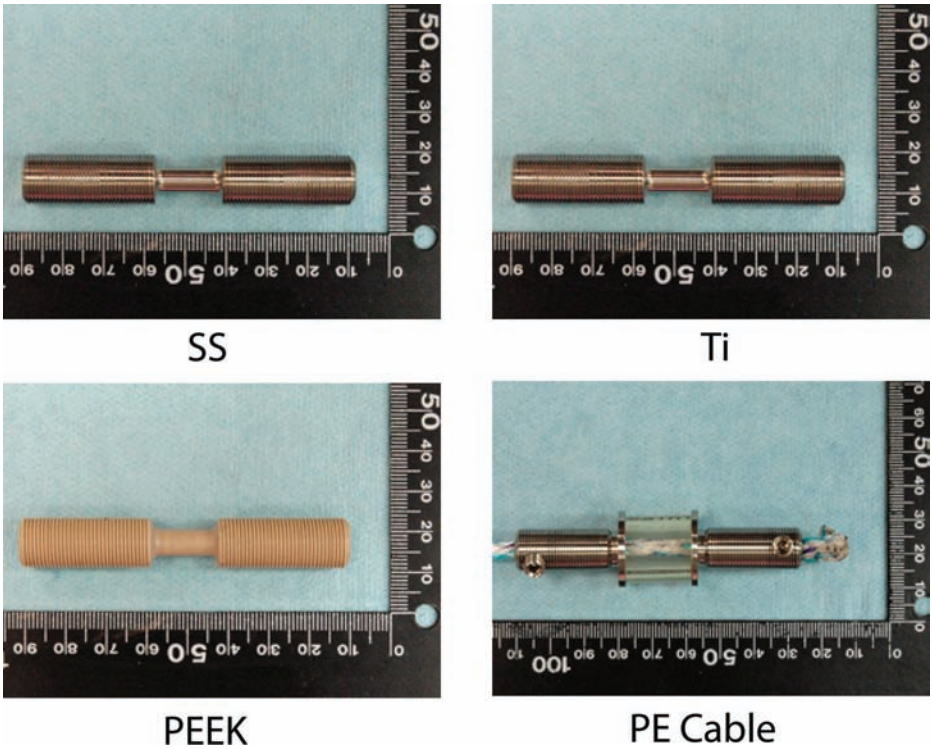

FIG. 3—*SS, Ti, PEEK, and PE cord cylindrical test specimens.*

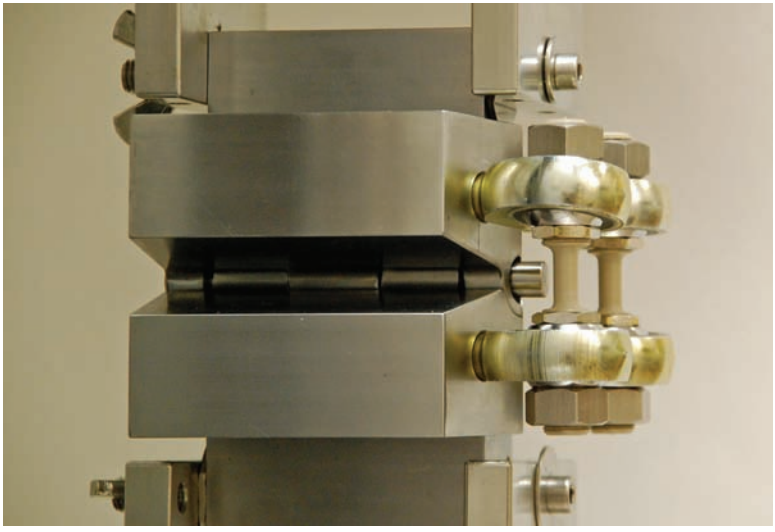

FIG. 4—*LB fixture with PEEK cylindrical test specimens mounted.*

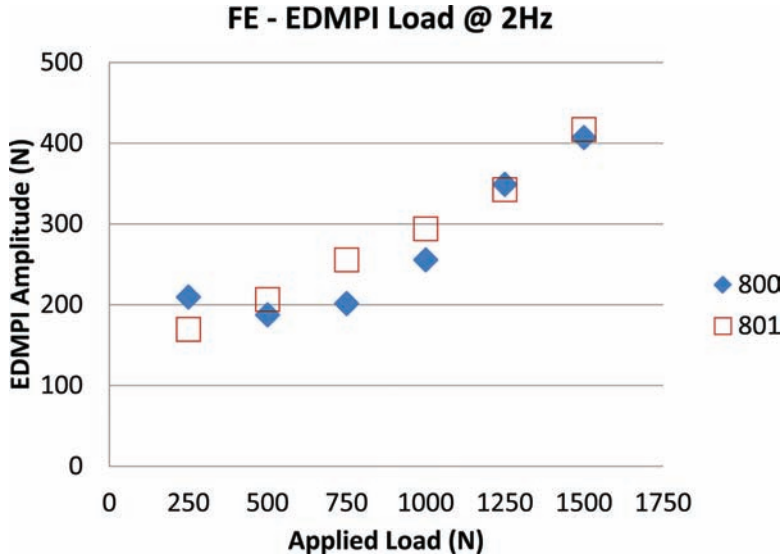

FIG. 5—*Forces recorded by miniature load cells during testing with FE fixture, 2 Hz frequency. 800 and 801 refer to load cell serial numbers.*

Results

Force amplitudes recorded by both EDMPI load cells (labeled by their serial numbers 800 and 801) during testing of the FE and LB fixtures are shown in Figs. 5–8. EDMPI load amplitude increased in both load cells as applied load increased, as expected. EDMPI load magnitudes appeared independent of test frequency in both the FE and LB fixtures.

Displacement amplitudes recorded during testing of the cylindrical and PE cord test specimens in the FE, LB, and AR fixtures are shown in Figs. 9–14. Testing using the PE cord fixtures was not conducted at applied loads greater than 500 N in AR, as the set screw holding the PE cord in place slipped. Testing using PEEK test specimens in AR was halted after a specimen fractured under an applied load of 3500 N. Displacement amplitudes of the SS, Ti, and PEEK cylinders were not differentiable in FE and LB testing, but the PEEK cylinders (at applied loads greater than 500 N) and the PE cord specimens displaced more than the SS and Ti cylinders in AR testing. Displacement amplitudes appeared independent of test frequency.

Conclusions

The proportional increases in EDMPI load measured by load cells in both the FE and LB test fixtures indicate that the fixtures effectively transfer applied load to EDMPI. Load cells in the FE fixtures are simultaneously loaded in the same direction (compression or tension), while those in the LB fixtures are opposite each other (when one is in compression, the other is in tension). EDMPI load

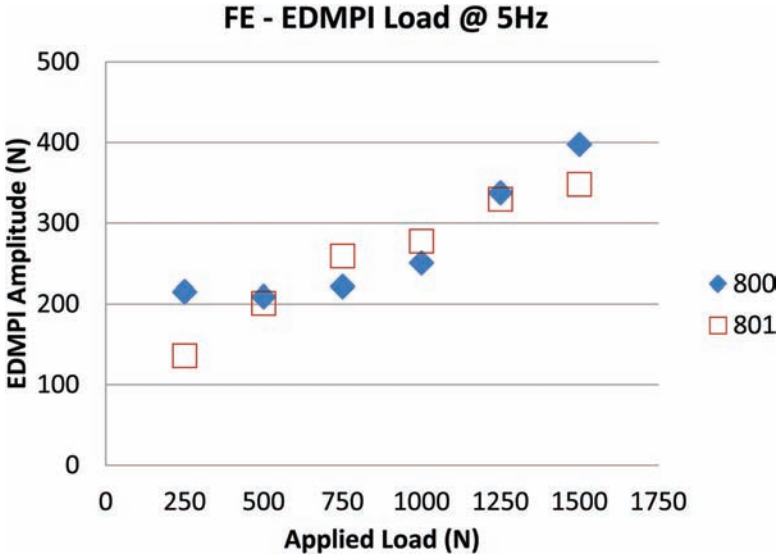

FIG. 6—*Forces recorded by miniature load cells during testing with FE fixture, 5 Hz frequency. 800 and 801 refer to load cell serial numbers.*

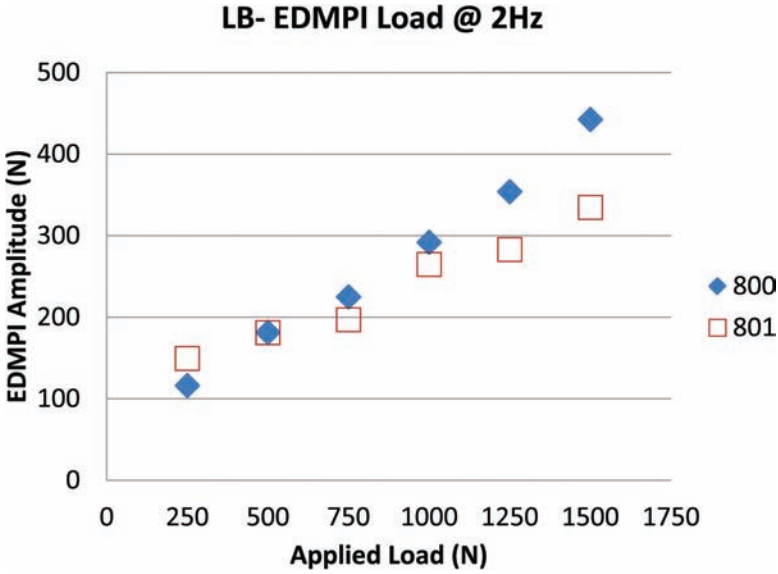

FIG. 7—*Forces recorded by miniature load cells during testing with LB fixture, 2 Hz frequency. 800 and 801 refer to load cell serial numbers.*

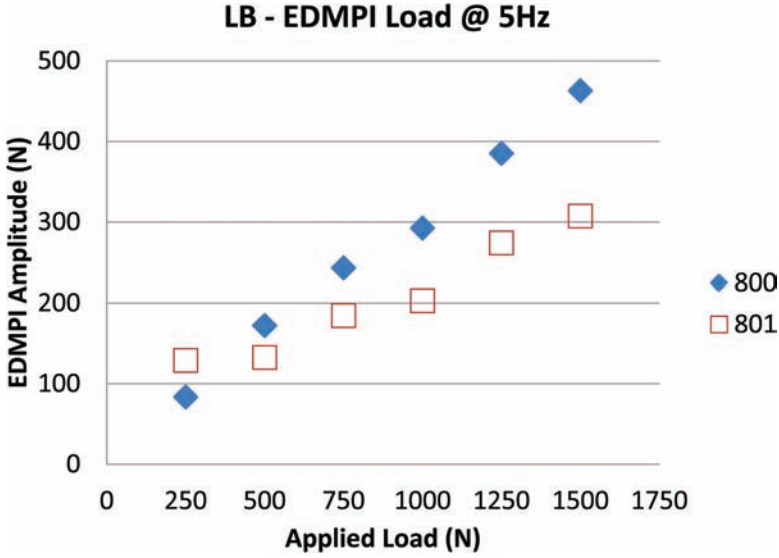

FIG. 8—*Forces recorded by miniature load cells during testing with LB fixture, 5 Hz frequency. 800 and 801 refer to load cell serial numbers.*

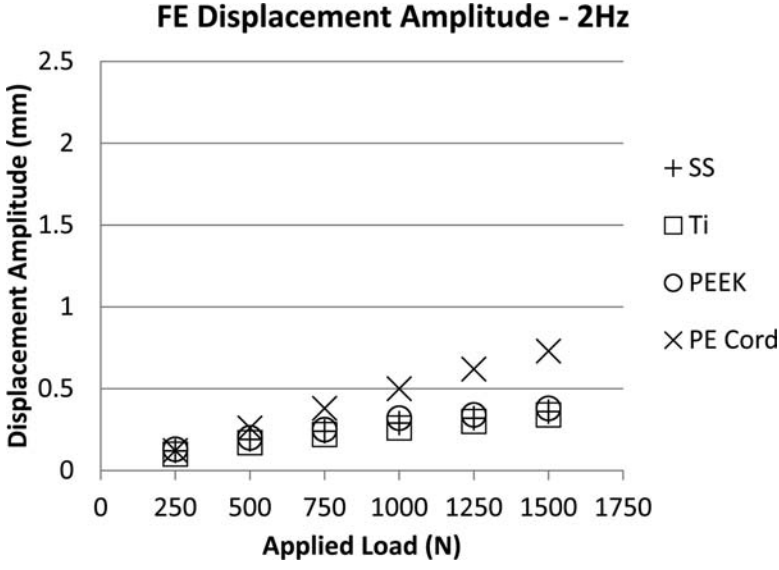

FIG. 9—*Displacement amplitude, FE fixture, 2 Hz frequency.*

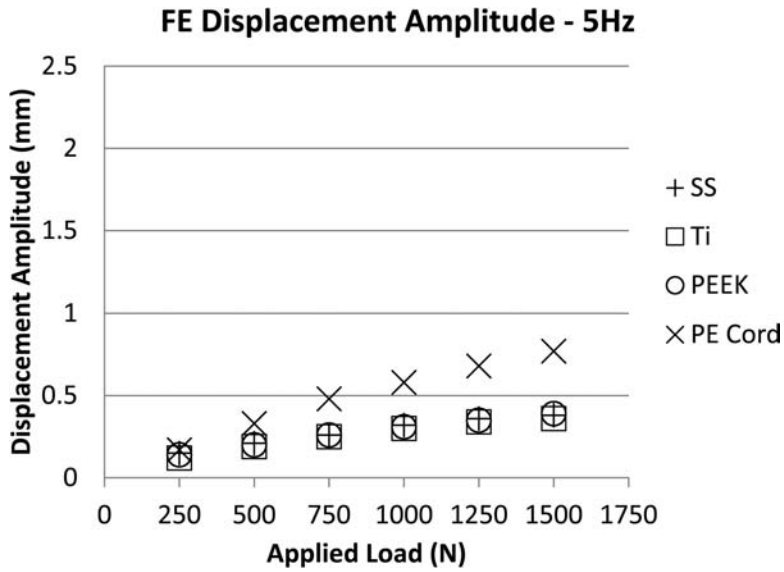

FIG. 10—*Displacement amplitude, FE fixture, 5 Hz frequency.*

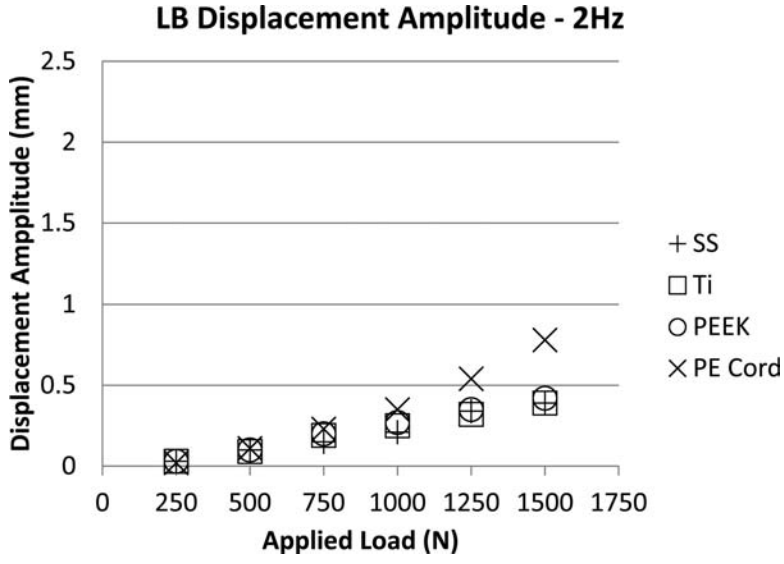

FIG. 11—*Displacement amplitude, LB fixture, 2 Hz frequency.*

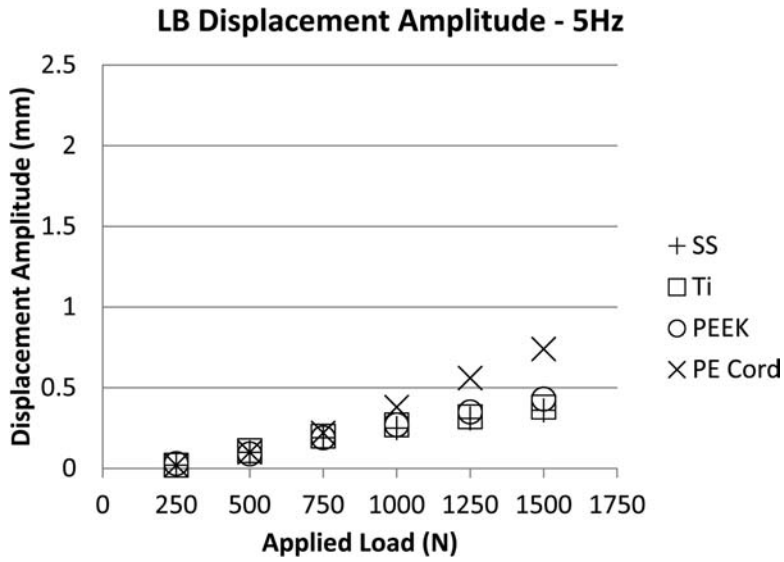

FIG. 12—*Displacement amplitude, LB fixture, 5 Hz frequency.*

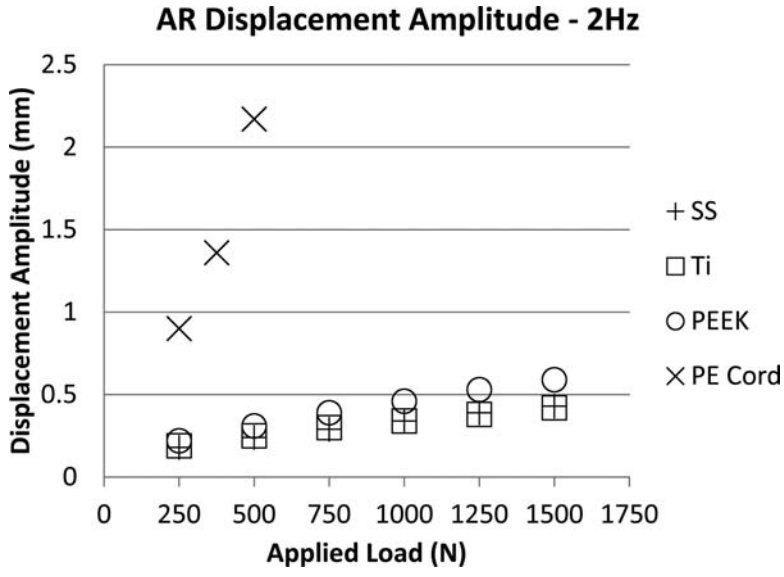

FIG. 13—*Displacement amplitude, AR fixture, 2 Hz frequency.*

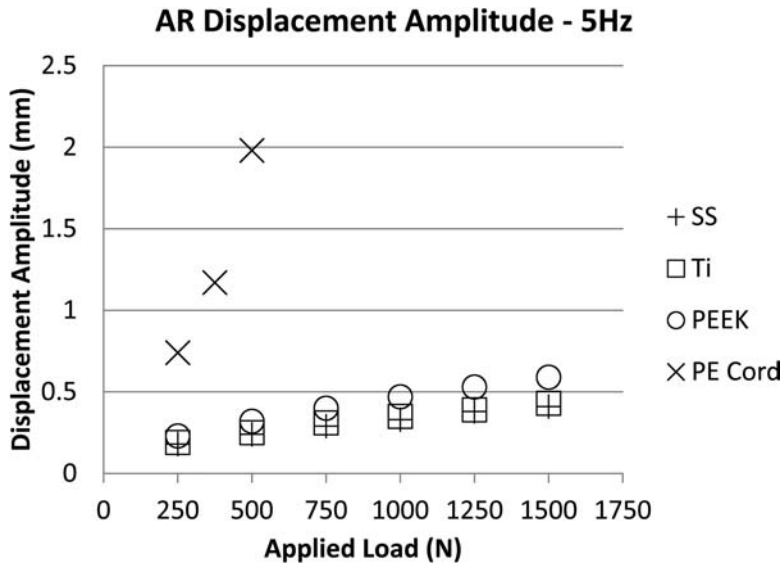

FIG. 14—*Displacement amplitude, AR fixture, 5 Hz frequency.*

magnitudes during FE testing are approximately half of those recorded during testing using a similar vertically oriented construct (VOC) reported at the previously referenced November, 2010, ASTM F04.25 symposium [2]. The halving of load magnitude is expected because applied load is divided between two load cells in this testing, and was recorded using only one load cell in the test referred to.

Load amplitudes recorded by the EDMPI load cells during LB testing were identical to those applied during FE testing, only 180° out of phase with each other. Although LB and FE are different physiologic motions, no measureable differences in EDMPI load magnitude were observed. This result suggests that for anisotropic bilateral pedicle fixation EDMPI devices, LB testing may not be required if FE testing is conducted.

Displacement amplitude was not a suitable metric for differentiating between the cylindrical test specimens, despite their differences in stiffness. However, it should be noted that motion preserving EDMPI devices that would be evaluated with this fixturing will likely be much less stiff than the SS, Ti, and PEEK cylinders tested, more likely on the order of the PE cord specimen. Displacement amplitude of the PE cord specimen was different than the other specimens, particularly in AR testing. Further testing using other flexible test specimens is necessary to identify any trends. When characterizing the durability of an EDMPI device, observations of displacement amplitude are no substitute for constructing a fatigue curve, as prescribed in ASTM F2624-07 [1].

Testing at frequencies greater than the 2 Hz maximum prescribed in the F2624-07 standard [1] using these test fixtures did not have an effect on the load applied to an EDMPI, or the resulting displacement amplitude during testing.

Limitations to this study include the fact that the cylindrical specimens tested were several orders of magnitude stiffer than the devices that will most likely be evaluated using the F2624-07 standard [1]. Only the stiffness of the PE cord specimen could be considered representative of an EDMPI device. Materials for the cylindrical test specimens are, however, representative of materials used for non motion preserving (fusion-promoting) fixation devices, to which EDMPI devices may be compared in regulatory review. Regardless, potential users of these fixtures should conduct additional testing using flexible test specimens to determine their response when loaded. Potential users should also examine the effects of environment, as the set of fixtures manufactured for this testing were not capable of being tested in a heated saline environment.

In conclusion, the fixtures developed by Aesculap represent a reasonable attempt to test EDMPI devices in FE, LB, and AR motions according to the F2624-07 standard [1]. Potential users of these fixtures should review carefully the in vitro testing conducted prior to their development [3,4] to determine whether they are appropriate for evaluating their specific EDMPI design.

Acknowledgments

This research was funded exclusively by Empirical Testing Corp.

References

[1] Anderson, M. C., Lissy, D. A., Lissy, C. J., Wing, C., Kruger, S., Beger, J., and Schilling, C., "ASTM F2624—Evaluating Alternate Fixtures for Flexion/Extention, Lateral Bending, and Axial Rotation Testing of Extra Discal Motion Preserving Implants," in *Symposium on Static and Dynamic Spinal Implants: Are We Evaluating Them Appropriately?* San Antonio, TX, November 16, 2010, ASTM International, West Conshohocken, PA.

[2] Anderson, M. C., Lissy, D. A., and Sandekian, P. J., "ASTM F2624-07—Evaluating an Alternate Fixture for Testing Extra Discal Motion Preserving Implants," in *Symposium on Static and Dynamic Spinal Implants: Are We Evaluating Them Appropriately?* San Antonio, TX, November 16, 2010, ASTM International, West Conshohocken, PA.

[3] Wing, C., Kruger, S., Beger, J., and Schilling, C., "In Vitro Study to Evaluate the Centre of Rotation (COR) Following Dynamic Stabilization Using Different Pedicle Screw Based Dynamic Posterior Stabilization Systems (PDS)—Recommendation for the Implementation of a Standardized COR in ASTM F2624," in *Symposium on Static and Dynamic Spinal Implants: Are We Evaluating Them Appropriately?* San Antonio, TX, November 16, 2010, ASTM International, West Conshohocken, PA.

[4] Schilling, C., Beger, J., Kruger, S., and Wing, C., "Recommendations for Implementation of an Alternative Test Set Up Derived from ASTM F2624 but With a Defined From an in-Vitro Study on Different Posterior Dynamic Stabilization (PDS) Devices," in *Symposium on Static and Dynamic Spinal Implants: Are We Evaluating Them Appropriately?* San Antonio, TX, November 16, 2010, ASTM International, West Conshohocken, PA.

Reprinted from JAI, Vol. 9, No. 2
doi:10.1520/JAI103502
Available online at www.astm.org/JAI

Sasidhar Vadapalli[1] *and Daniel L. Woods*[2]

Symposium on Static and Dynamic Spinal Implants: Are We Evaluating Them Appropriately? Effect of Tightening Torque on ASTM F1798 Axial Gripping Capacity

ABSTRACT: The objective of this study was to investigate how the axial gripping capacity can be affected by varying the tightening torques applied to the set screws in a pedicle screw ASTM F1798 subassembly. Although the current ASTM F1798 standard indicates that all tightening loads to the locking mechanism be applied as specified by the manufacturer, the torque limiting instruments used in the field can have nominal upper and lower torque limits. The interconnection assemblies were assembled using a multi-axial screw, spinal rod, and set screw. Six groups were assembled using different types of spinal rods. Each group was sub-divided into three groups each containing five interconnection assemblies. The three sub-groups of interconnection assemblies were locked to the nominal torque value as indicated by the manufacturer technique, lower limit, and higher limit respectively. Static axial grip testing was performed according to ASTM F1798 guidelines. Axial gripping capacity was influenced by the nominal tightening torque and lower tightening torque and holds true regardless of rod diameter and rod material. There is no significant difference in the axial gripping capacity between the nominal tightening torque and higher tightening torque. These results indicate that the set screw tightening torque has an effect on the gripping capacity and could potentially affect yield load, ultimate load, and failure

Manuscript received October 15, 2010; accepted for publication December 5, 2011; published online January 2012.
[1] Medtronic, 1800 Pyramid Pl., Memphis, TN 38132 (Corresponding author), e-mail: sasi.vadapalli@medtronic.com
[2] Medtronic, 1800 Pyramid Pl., Memphis, TN 38132.
Symposium on Static and Dynamic Spinal Implants: Are We Evaluating Them Appropriately? on 16 November 2010 in San Antonio, TX.

Cite as: Vadapalli, S. and Woods, D. L., "Symposium on Static and Dynamic Spinal Implants: Are We Evaluating Them Appropriately? Effect of Tightening Torque on ASTM F1798 Axial Gripping Capacity," *J. ASTM Intl.*, Vol. 9, No. 2. doi:10.1520/JAI103502.

modes when performing ASTM F1717 compression bending testing. With the wide range of materials used to manufacture pedicle screw systems and the processing techniques that are currently available, e.g., anodization and shot peening, critical thinking should be put into determining if the torque applied to the system represents a worst-case scenario.

KEYWORDS: axial gripping capacity, F1798, F1717, interconnection, spinal implants

Introduction

Spinal fusion is a surgical procedure performed to alleviate pain due to pathologic conditions of the spine and restore segmental stability and alignment. Non-instrumented spinal fusion is achieved using bone graft in the anterior disc space. Instrumented spinal fusion can be achieved by using plate and screw, hooks, cables/wires, pedicle screw with rods, and/or anterior plating systems [1].

A variety of pedicle screw-rod based spinal fusion devices are now available in the market. Pedicle screw fixation systems consist of a combination of anchors (e.g., bolts, hooks, and/or screws); interconnection mechanisms (e.g., nuts, screws, sleeves, or bolts); longitudinal members (e.g., plates, rods, or a combination); and/or transverse connectors. Although these systems are not highly differentiated, the manner in which they are connected to the longitudinal support mechanism varies significantly among the commercially available systems.

Objective and Clinical Relevance

In pedicle screw fixation systems, the longitudinal member is connected to other implant components by one, or a combination, of seven commonly used fundamental types of locking mechanisms: (a) three-point shear clamps; (b) lock screw connectors; (c) circumferential grip connectors; (d) constrained bolt-plate connectors; (e) constrained screw-plate connectors; (f) semi-constrained screw-plate connectors, and (g) semi-constrained component-rod connectors (Fig. 1) [2]. Some component-component interfaces rely mainly on torque or other applied forces; others rely more on friction between components to secure the desired interface integrity [2].

Clinically, a surgeon would use a torque wrench (torque measuring, torque limiting, or a non-torque limiting instrument) in conjunction with an anti-torque wrench instrument to lock the individual components to the longitudinal member. Depending upon the spinal system used, the surgeon would: (1) hand-tighten the component using the non-torque limiting instrument, which could result in a variable tightening torque (Fig. 2); or (2) tighten the component using the torque limiting instrument (Fig. 3). Although the torque limiting instrument is set to a pre-determined torque, the torque applied sometimes could be within $\pm 10\%$ of the set value.

ASTM F1798-03, "Standard Guide for Evaluating the Static and Fatigue Properties of Interconnection Mechanisms and Subassemblies Used in Spinal

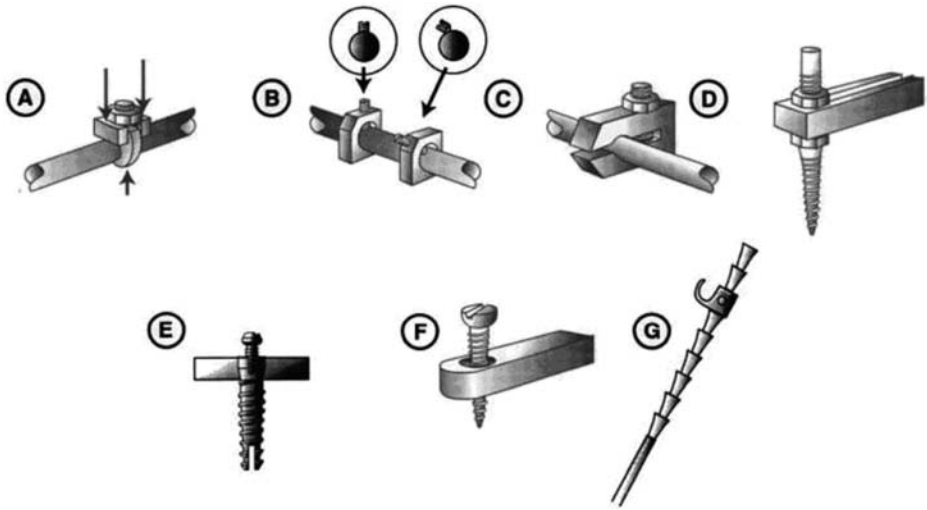

FIG. 1—*The seven fundamental component-component locking mechanisms (Reprinted with permission from Benzel, E.C., "Component-Component Interfaces" in Benzel, E. C. (Ed.), Biomechanics of Spine Stabilization, Thieme, New York, 2001, p. 143).*

Arthrodesis Implants" provides guidelines to measure the uniaxial static and fatigue strength and resistance to loosening of the component interconnection mechanisms of spinal arthrodesis implants [3].

Static testing for the "axial gripping capacity" measures the interconnection's capacity to resist sliding when a load is applied to the longitudinal member (rod/plate). Benzel [2] pointed out that laboratory biomechanical assessments are performed under ideal circumstances and if an appropriate tightening torque (as defined by laboratory studies) is not applied in vivo (as may often be the case), the application of laboratory biomechanical data to the clinical situation is meaningless. Complications involving pedicle screw surgeries can include: screw fracture; screw loosening; rod fracture; disconnection between rod, bolt, nut, or screw; inaccurate screw placement; loss of correction; dural leaks; infection; transient neural injury; and permanent neural injury [4]. More specifically, the disconnection between rod, bolt, nut, or screw is better

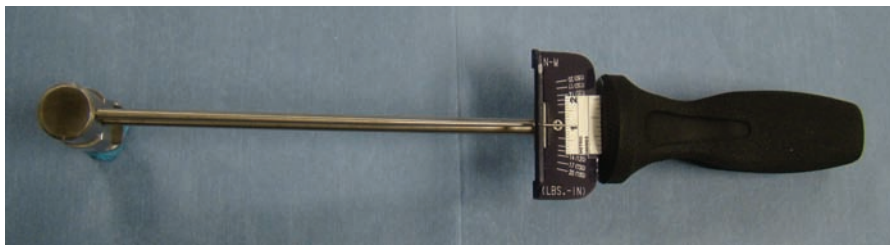

FIG. 2—*Torque measuring torque wrench.*

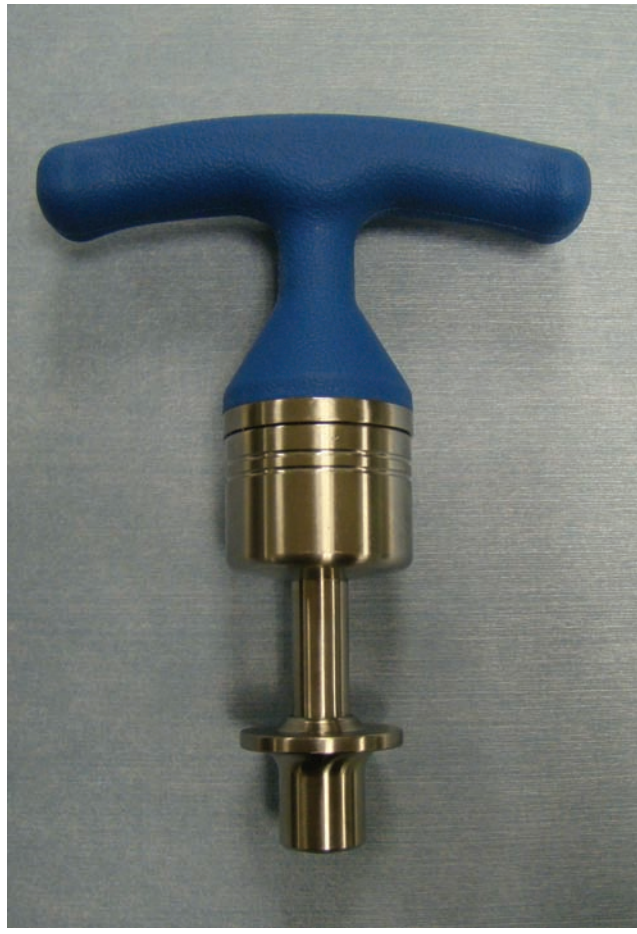

FIG. 3—*Torque-limiting instrument (Reprinted with permission from Medtronic Spinal and Biologics, Memphis, TN).*

understood by the "axial grip" testing indicated in ASTM F1798 as an assessment of the integrity of the assembly.

Thus, the objective of this study was to quantify how the axial gripping capacity is changed by varying the tightening torques applied to the set screws in a pedicle screw-rod ASTM F1798 assembly. We hypothesized that there is a positive relationship between tightening torque and axial grip strength. In addition we hypothesized that axial grip strength would be affected by the rod diameter and type of rod material used in the interconnection assembly.

Materials and Methods

The study was conducted in the Biomechanical Testing Lab at Medtronic Spinal and Biologics, Memphis, TN. The constructs were assembled and tested under

the guidelines of ASTM F1798-97 (2008), "Standard Guide for Evaluating the Static and Fatigue Properties of Interconnection Mechanisms and Subassemblies Used in Spinal Arthrodesis Implants" [3]. The interconnections were assembled using a multi-axial screw (MAS), spinal rod, and set screw. Six interconnection assembly groups were formed using 3 material choices and 2 rod sizes:

1. 3.2 mm diameter cobalt chromium molybdenum rod (3.2 CCM).
2. 3.2 mm diameter cobalt chromium molybdenum plus rod (3.2 CCM+).
3. 3.2 mm diameter Titanium rod (3.2 Ti).
4. 3.5 mm diameter Cobalt chromium molybdenum rod (3.5 CCM).
5. 3.5 mm diameter Cobalt chromium molybdenum plus rod (3.5 CCM+).
6. 3.5 mm diameter Titanium rod (3.5 Ti).

Three locking torques were considered in the assembly process:

1. nominal torque value as indicated by the manufacturer technique.
2. higher torque limit (111.1% of nominal).
3. lower torque limit (88.9% of nominal).

The ±11.1% value was selected instead of ±10% to accommodate a rounded off torque value read out by the electronic torque wrench used for locking the interconnection assembly.

Per the standard, with 5 replicates in each test group, there were a total of 90 interconnection assemblies built and tested: 3 materials (CCM, CCM+, Ti), 2 diameters (3.2 mm, 3.5 mm), 3 torques (nominal ±11.1%), and 5 replicates (Table 1).

Static axial grip testing was performed using an MTS (Eden Prairie, MN) Alliance RT/50 electro-mechanical load frame. The specimen rod was positioned into the axial grip test fixture such that the rod and the test system actuator were parallel. Figure 4 is an image of the test setup. The loading fixture was attached to the actuator and displaced at the rate of 6 mm/min and force versus displacement was recorded at a frequency of 10 Hz. With the connector (MAS) being held rigid, loading was applied axially to the long axis of the spinal rod until 3 mm of displacement was reached. Peak load during 3 mm of displacement and gripping capacity were measured. Per the ASTM F1798, the axial gripping capacity was defined as the maximum applied load during the first 1.5 mm of permanent displacement. Statistical analysis was performed using ANOVA

TABLE 1—*Total interconnection assemblies undergoing axial grip testing.*

	Number of Specimens		
Test Group	Lower Torque Limit	Nominal	Higher Torque Limit
3.2 CCM	5	5	5
3.2 CCM+	5	5	5
3.2 Ti	5	5	5
3.5 CCM	5	5	5
3.5 CCM+	5	5	5
3.5 Ti	5	5	5

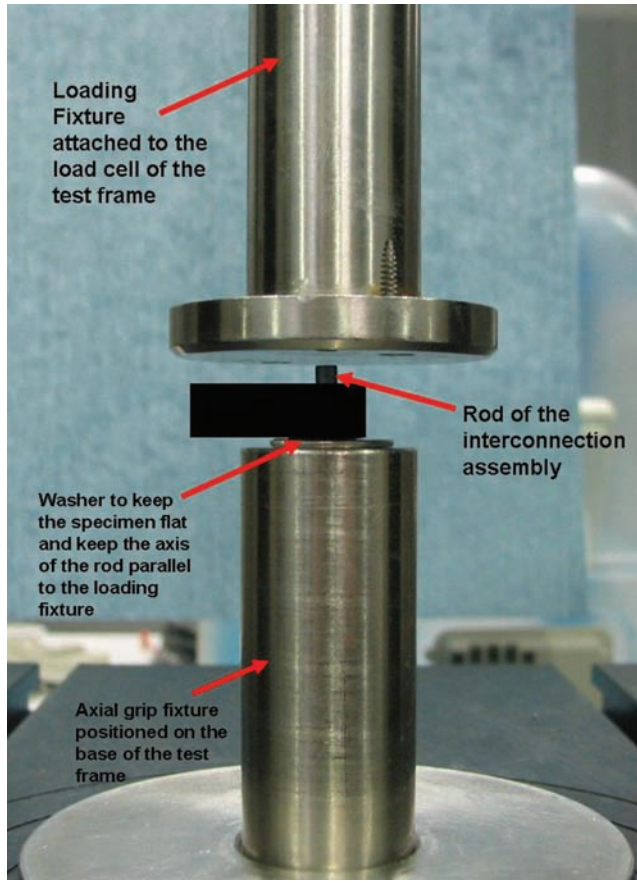

FIG. 4—*Static test setup for the axial gripping strength.*

with Tukey's method for multiple comparisons based on rod material, rod diameter, and tightening torque. A p value of 0.05 was chosen as significant.

Results

In Fig. 5, the axial gripping capacity for each test specimen was normalized by the maximum axial gripping capacity of all 90 interconnection assemblies tested. The maximum value of axial grip was observed for the larger diameter, CCM+ rod at the highest assembly torque. The minimum grip capacity was 70% lower with the smaller diameter, CCM rod at the lowest assembly torque. Statistical differences with high significance ($p < 0.01$) were found for all the following cases:

1. Lower tightening torque versus nominal tightening torque.
2. Lower tightening torque versus higher tightening torque.
3. 3.2 mm diameter rod versus 3. 5 mm diameter rod.

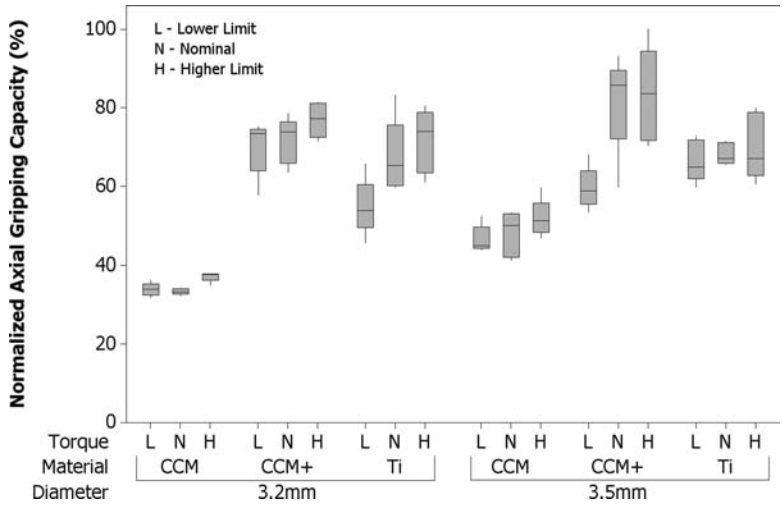

FIG. 5—*Box plot of the normalized gripping capacity for the various assemblies. Data was normalized to the max axial gripping capacity of all 90 interconnections tested. (CCM—cobalt chromium molybdenum; CCM+—cobalt chromium molybdenum plus; Ti—titanium). The boxes represent 25–75 percentiles and the whiskers represent the range of the data.*

4. CCM versus CCM+.
5. CCM versus Ti.
6. CCM+ versus Ti.

No significant differences in the axial gripping capacity were found between the nominal tightening torque and higher tightening torque. A consistent trend was noticed through each group, regardless of the rod diameter and rod material.

Discussion

Axial gripping capacity is dependent not only on the tightening torque but also on the material and size of the rod. The following are some of the limitations of the current study:

1. Only one of the seven fundamental component-component locking mechanisms was used.
2. Even with the single component-component locking mechanism evaluated, there are a variety of pedicle screw fixation systems from other spinal device manufacturers, which could yield different results.
3. Spinal rods commonly used (4.5 mm, 5.5 mm, and 6.0 mm diameter) for thoracic and lumbar surgeries were not evaluated.

Conclusions

Axial gripping capacity is influenced by the nominal tightening torque and lower tightening torque and holds true regardless of rod diameter and rod

material. The tightening torque is not a factor once the nominal value is reached. There is no significant difference in the axial gripping capacity between the nominal tightening torque and higher tightening torque.

The conclusions from this study could be applied to the construct testing performed under ASTM F1717 guidelines, where the interconnections within the constructs are locked to the nominal tightening torque. The authors hypothesize that for the compression bending testing performed under the F1717 guidelines,

1. A functional failure like slip between the pedicle screw-rod/plate interconnection could occur if the interconnection is tightened to a lower tightening torque.
2. The subassembly tightened to a nominal tightening torque might not be a worst-case situation, as the rod/plate component is less stressed compared to an interconnection tightened to the higher torque limit.

Additional testing needs to be conducted to confirm the aforementioned hypothesis of the effects of tightening torque on ASTM F1717 testing.

References

[1] Millennium Research Group, "U. S. Markets for Spinal Implants," *Report No.* RPUS20SP09, Millennium Research Group, Toronto, Ontario, Canada, 2009, www.mrg.net.

[2] Benzel, E. C., *Biomechanics of Spine Stabilization*, Thieme/American Association of Neurological Surgeons, New York, 2001.

[3] ASTM F1798, 1997, 2008, "Standard Guide for Evaluating the Static and Fatigue Properties of Interconnection Mechanisms and Subassemblies Used in Spinal Arthrodesis Implants," *Annual Book of ASTM Standards*, ASTM International, West Conshohocken, PA.

[4] Jensen, M. L., Springer, S. S., Campbell, S. F., and Gray, E., "Interconnection Strength Testing and Its Value in Evaluating Clinical Performance" *Spinal Implants: Are We Evaluating Them Appropriately?, ASTM Spec. Tech Publ.*, Vol. 1431, 2003, pp. 55–62.

Erratum for JAI103502, Symposium on Static and Dynamic Spinal Implants: Are We Evaluating Them Appropriately? Effect of Tightening Torque on ASTM F1798 Axial Gripping Capacity, Vadapalli, Sasidhar, Woods, Daniel L., published in the Journal of ASTM International (JAI), February, 2012, Volume 9, Issue 2, and included in STP1535, Static and Dynamic Spinal Implants: Are We Evaluating Them Appropriately?

The correct title of the article: Effect of Tightening Torque on ASTM F1798 Axial Gripping Capacity.

Reprinted from JAI, Vol. 8, No. 7
doi:10.1520/JAI103499
Available online at www.astm.org/JAI

Regina J. Konz,[1] *Laura M. Jensen,*[2] *and Brian L. Kincaid*[3]

Comparison of Self-Drilling and Self-Tapping Cervical Spine Screws Using ASTM F543-07

ABSTRACT: ASTM F543-07 is used to evaluate insertion load (Annex A4), driving torque (A2), and axial pullout (A3) characteristics of self-tapping metallic medical bone screws. F543-07 was designed to evaluate screws that utilize a pre-drilled pilot hole and was not intended for self-drilling screws. The objectives of this study were to (1) adapt the F543-07 test methods to allow evaluation of both self-drilling and self-tapping screws and (2) quantify differences in performance between the two screw types. For all three tests (A4, A2, A3) appropriately sized pilot holes were pre-drilled into the surrogate test medium for all the self-tapping screw designs per ASTM F543-07. No pilot holes were created for the self-drilling screws. During the insertion load tests (A4), a constant rotation was applied to the screws under an initial, near-zero axial force state. While monitoring axial load, torque, and displacement, the axial load was gradually increased. The maximum load at which there was a marked increase in torque and displacement on the graph was indicative of the force required to engage the self-drilling or the self-tapping feature. To measure driving torque (A2), a constant rotation was applied. To maintain screw driver–screw contact, a constant-force axial pre-load was required. The axial insertion load, determined during the insertion load testing (A4), was used as the preload for the driving torque testing. Axial pullout testing (A3) measured the axial tensile force required to remove a screw from the test medium. Quantifiable differences in mean insertion load, driving torque, and pullout load were found, demonstrating that these methods are able to discern differences in performance between different screw designs.

Manuscript received October 15, 2010; accepted for publication May 8, 2011; published online July 2011.

[1] Ph.D., Zimmer Spine, Minneapolis, MN 55439 (Corresponding author), e-mail: gina.konz@zimmer.com
[2] M.S., Zimmer Spine, Minneapolis, MN 55439.
[3] M.S., Zimmer Inc., Warsaw, IN 46581.

Cite as: Konz, R. J., Jensen, L. M. and Kincaid, B. L., "Comparison of Self-Drilling and Self-Tapping Cervical Spine Screws Using ASTM F543-07," *J. ASTM Intl.*, Vol. 8, No. 7. doi:10.1520/JAI103499.

Finally, this study demonstrated it is possible to adapt the test methods outlined in ASTM F543-07 to evaluate the insertion load, driving torque, and axial pullout performance of self-drilling screws in addition to self-tapping screws.

KEYWORDS: ASTM F543, insertion load, driving torque, axial pullout, bone screws, self-drilling, self-tapping

Introduction

ASTM F543-07 is used to evaluate insertion load (Annex A4), driving torque (A2), and axial pullout (A3) characteristics of metallic medical bone screws. The standard is under the jurisdiction of the ASTM F04.21 Subcommittee (Osteosynthesis) and has been historically associated with the evaluation of bone screws that employ a pre-drilled pilot hole, typical in a trauma application for fracture repair of long bones. It is unclear from F543-07 if the test methods contained within are intended to evaluate performance characteristics of self-drilling screws in addition to screws that require a pre-drilled pilot hole. Additionally, the standard describes dimensions and tolerances for metallic bone screws, but further explains that the test methods may also be applicable to other screws.

Cervical spine screws are designed to anchor plates onto cervical spine vertebrae. Although these screws are not designed to the dimensions and tolerances in ASTM F543-07, the test methods are still applicable. This study used the ASTM F543-07 standard as a basis for developing testing specific to both self-tapping and self-drilling cervical spine screws.

A *self-tapping screw* is defined as a screw that has any number of flutes at its tip that are intended to cut the screw's thread form into the bone upon insertion into a pre-drilled pilot hole, per ASTM F543-07 (section 3.1.21). Additionally, for the purposes of this investigation, a *self-drilling screw* incorporates a special tip to pierce the substrate and drive the screw during screw insertion, thus eliminating the need for drilling a pilot hole.

Objective

The objective of this study was to adapt the ASTM F543-07 test methods to allow evaluation of both self-drilling and self-tapping cervical spine screws.

Materials

To reduce variability often found in cadaveric bone, synthetic rigid, closed-cell polyurethane foam material with properties similar to that of cancellous bone was used as the test medium. Multiple densities of foam media conforming to ASTM F1839 (as recommended in ASTM F543-07) were utilized to simulate differences in cervical bone strength. *Last-o-Foam* FR-3720 (General Plastics, Tacoma, WA), Grade 20 foam with a density of approximately 320.4 kg/m^3, was used to simulate very strong, healthy cancellous bone [1]. This foam was used

to perform the insertion load and driving torque tests, as a stronger bone represents worst case for these tests. FR-3715 foam, Grade 15 foam with a density of approximately 240.3 kg/m^3 was utilized to simulate weaker cancellous bone [1]. This foam was used to perform the axial pullout test as weaker bone represents worst case for this test.

Appropriately sized pilot holes (per manufacturer's recommendations) were drilled into the test media prior to all testing of self-tapping screws. Pilot hole spacing followed the recommendations of ASTM F543-07. Appropriately sized drivers (per manufacturer's recommendations) were used to conduct all testing. A custom fabricated fixture conforming to ASTM F543-07 was used to conduct the axial pullout test.

Sampling Plan and Rationale

To evaluate the performance of different cervical spine screw designs, self-drilling (SD) and self-tapping (ST) screws were tested using three of the methods described in ASTM F543-07. Additionally, in an effort to better quantify the definition of "self-tapping" and "self-drilling," one screw was tested for insertion load and driving torque as both a self-drilling and self-tapping screw (SD 1 and ST 1). This screw was only evaluated as a self-tapping screw in pullout, as a pilot hole was considered to represent worst case for pullout strength (i.e., it is believed that the loss of material from the pilot hole may be indicative of a loss of holding power of the screw in the material).

A sample size of eight was used for each screw design tested, with the exception of one self-drilling screw (SD 5), where availability limited the sample size to five. A sample size of eight provided sufficient power for a one-way ANOVA among groups. See Table 1 for the entire study scope and specimen details. It should be noted that some of the screws tested were available in two variations (ST 1, ST 1a, ST 2, ST 2a, SD 2, SD 2a, SD 3, and SD3a). The screw variations with the larger outer diameters were utilized for the insertion load and driving torque tests, as it was rationalized that these screws represented the worst case for these two tests. The smaller outer diameter screw variations were utilized for the axial pullout tests, as a smaller diameter represents a worst case for pullout testing. For some of the screws tested, only one variation of the screw was available. Therefore, these screws were used for insertion load and driving torque testing as well as pullout.

Methods

Insertion Load Test

Background—The purpose of the insertion load test was to determine the axial compression load (force) required to engage the self-tapping or self-drilling feature of bone screws into a standard test medium. The test was performed per ASTM F543-07 A4 except the test method was utilized for both self-drilling and self-tapping screws. No pilot hole was generated for the self-drilling screws, so that the axial compressive load (force) recorded was indicative of the

TABLE 1—*Study scope and specimen detail.*

Insertion Load (A4) and Driving Torque (A2) Specimen ID	Pullout (A3) Specimen ID	n	Description	Size (mm)[a]	Pilot Hole Diameter, mm
ST 1	…	8	Self-Tapping Design #1	4.4/3.0 D × 15.8	2.5
…	ST 1a	8	Self-Tapping Design #1a	4.0/2.6 D × 15.6	2.5
ST 2	…	8	Self-Tapping Design #2	4.4/2.9 D × 15.8	2.5
…	ST 2a	8	Self-Tapping Design #2a	4.0/2.5 D × 15.6	2.5
ST 3	ST 3	8	Self-Tapping Design #3	4.2/2.3 D × 16.3	2.3
SD 1	…	8	Self-Drilling Design #1	4.4/3.0 D × 15.8	n/a
SD 2	…	8	Self-Drilling Design #2	4.4/2.9 D × 15.8	n/a
…	SD 2a	8	Self-Drilling Design #2a	4.0/2.5 D × 15.6	n/a
SD 3	…	8	Self-Drilling Design #3	4.4/2.9 D × 15.8	n/a
…	SD 3a	8	Self-Drilling Design #3a	4.0/2.5 D × 15.6	n/a
SD 4	SD 4	8	Self-Drilling Design #4	4.2/2.3 D × 16.3	n/a
SD 5	SD 5	5	Self-Drilling Design #5	4.0/3.0 D × 14.2	n/a

[a] Major/minor diameter × overall length.

force required to engage the self-drilling feature of the screw. Upon completion of insertion load testing, the same screws were removed and re-used for driving torque testing.

Test Procedure—Testing was conducted on a modified MTS Model 858 *Mini Bionix II* servohydraulic test machine with *FlexTest* controller (MTS Systems Corporation, Eden Prairie, MN) that allowed continuous, 360° + rotation of the rotary actuator, simultaneously independently applying a varying axial compressive force. The machine was equipped with both load and torque transducers that allowed simultaneous monitoring of the torsional and axial compressive forces applied to the specimen, as well as axial displacement data from the machine's crosshead (Fig. 1). The test medium was clamped to the base of the load frame so that the longitudinal axes of the pilot hole (if applicable) and screw and driver were aligned with the direction of the applied load and torsion. An adequate, yet minimal "preload" was applied to the test

FIG. 1—*Insertion load test setup in Grade 20 polyurethane foam (320 kg/m^3).*

TABLE 2—*Parameters used during the insertion load testing of self-tapping (ST) screws in Grade 20 polyurethane foam (320 kg/m^3).*

Setup Parameter	ST 1	ST 2	ST 3
Preload, N	5–7	7	1
Rate, N/s	0.5	0.5	0.25– 0.5
Sensitivity, N	4	4	<4
Follower load, N	0	0	0

construct (test media-screw-driver) in order to maintain engagement. A constant rotation rate of 30 rpm was applied to the specimen, simultaneously increasing axial compressive load applied at a uniform "rate" until screw engagement was detected. Engagement was defined per the guideline given in ASTM F543-07 and a software algorithm with a "sensitivity" parameter was used to detect the rapid decrease in axial load associated with engagement. After engagement detection, a minimal "follower load" was used to maintain construct engagement as the screw was advanced five complete revolutions. Data were continuously acquired from the axial load, displacement and torsion channels. A load and torque versus axial displacement curve was constructed, and the maximum compressive load achieved at engagement is reported as the insertion load. Test machine parameters are summarized in Tables 2 and 3 and were determined experimentally for each specimen type prior to testing. As no extra setup specimens were available, the first specimen was generally reused until consistency was obtained in the results with the parameters used.

Driving Torque Test

Background—The purpose of this test was to measure the torque required to drive a self-tapping or self-drilling bone screw to a standard depth in a test medium. The test was performed per ASTM F543-07 A2.

Test Procedure—Testing was conducted utilizing a modified Instron Model 1125 electromechanical tension/compression and torsion test machine (Instron Corporation, Norwood, MA). The machine's crosshead was locked in position to prevent movement and a constant axial compressive load was applied to the test

TABLE 3—*Parameters used during the insertion load testing of self-drilling (SD) screws in Grade 20 polyurethane foam (320 kg/m^3).*

Setup Parameter	SD 1	SD 2	SD 3	SD 4	SD 5
Preload, N	60	2–10	2	2	2
Rate, N/s	0.1	0.1	0.1–2	0.5–2	0.5
Sensitivity, N	3	3–5	5–7	4–7	3–4
Follower load, N	20–60	5–20	6	6	6

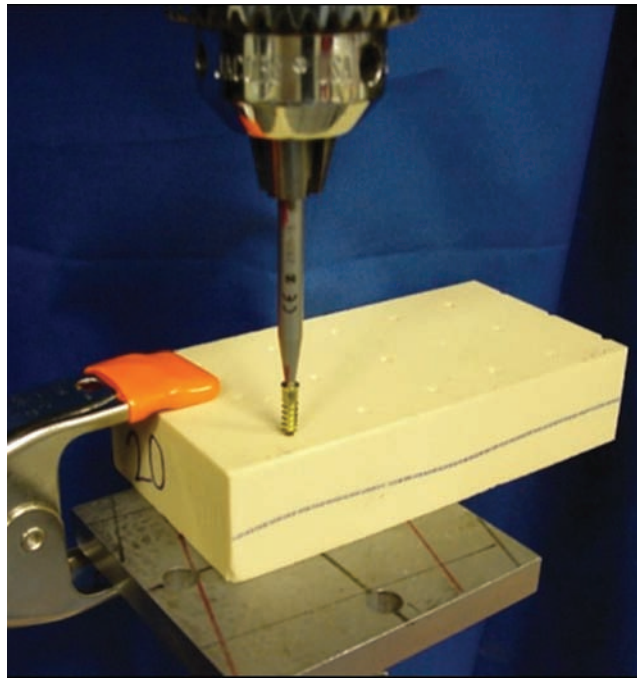

FIG. 2—*Driving torque test setup in Grade 20 polyurethane foam (320 kg/m^3).*

construct (test media-screw-driver) via a spring-loaded platen in order to initiate self-tapping (or self-drilling) and to maintain construct engagement throughout the test (Fig. 2). The insertion load determined previously, in the section entitled "Insertion Load Test," was used to approximate the spring load applied to the specimens. The machine was equipped with a torsional load transducer to continuously record the torsional force applied to the specimen. The test medium was clamped to the base of the load frame so that the longitudinal axes of the pilot hole (if applicable) and screw and driver were aligned with the direction of the applied torsion. The rotary actuator applied torsional displacement to the construct at a constant rate of 2.5 rpm and data were continuously acquired from the rotary displacement and torsion channels. The test specimen was driven four revolutions and a torque versus rotation curve was constructed. The driving torque was reported as the maximum reading recorded during the initial four revolutions, of the screw. An example of the test setup is provided in Fig. 2.

Axial Pullout Strength

Background—The purpose of this test was to measure the axial tensile force required to remove a screw from the test medium. The test was performed per ASTM F543-07 A3 except the screws were inserted into the test medium using a hand-held screw driver.

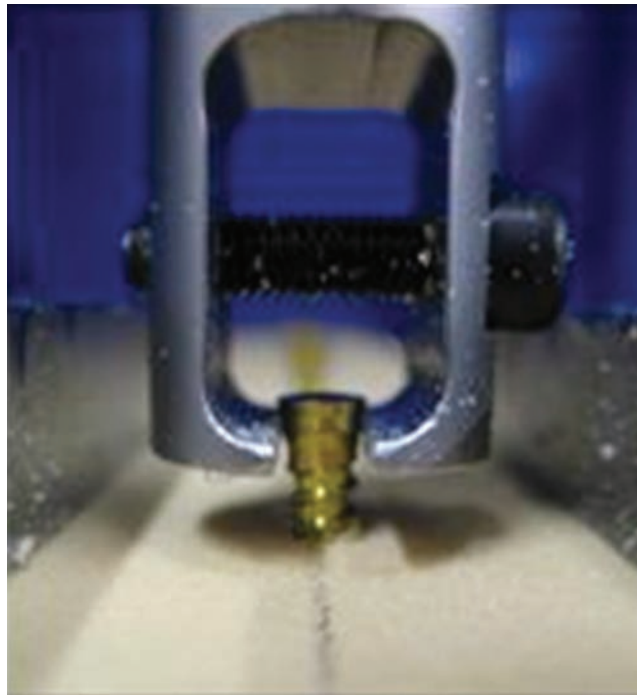

FIG. 3—*Pullout test setup in Grade 15 polyurethane foam (240 kg/m^3).*

Test Procedure—Prior to testing, the test specimens were inserted by hand into the test medium to a specified depth of 60% of the threaded length. Testing was conducted on an *MTS 858 MiniBionx* (MTS Systems Corporation, Eden Prairie, MN) servohydraulic load frame equipped with a bi-axial load-torque transducer.

The test medium was clamped to the base of the load frame so that the longitudinal axis of the screw was aligned with the direction of the applied load. The screw head was placed in the load fixture and a tensile load was applied to the test specimen at a rate of 5 mm/min until the screw fractured or released from the test medium (Fig. 3). Data were continuously acquired from axial displacement and load channels and a load versus displacement curve was constructed. The maximum load required to fracture/remove the screw from the foam was reported as the axial pullout strength.

Results

Insertion Load

The insertion loads correspond to the load recorded at the time of engagement for self-tapping and self-drilling screws, respectively. Data looked similar to Figure A4.2 "Typical Test Method Output" in ASTM F543-07 (Fig. 4). Figure 5

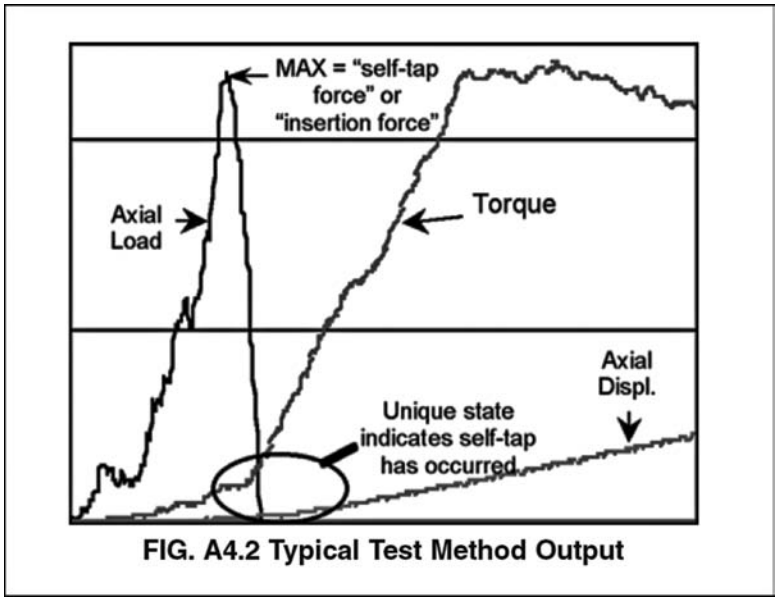

FIG. 4—*Figure A4.2 'Typical Test Method Output' from ASTM F543-07; Reprinted from F543-07, "Standard Specification and Test Methods for Metallic Medical Bone Screws," copyright ASTM International, 100 Barr Harbor Dr., West Conshohocken, PA 19428.*

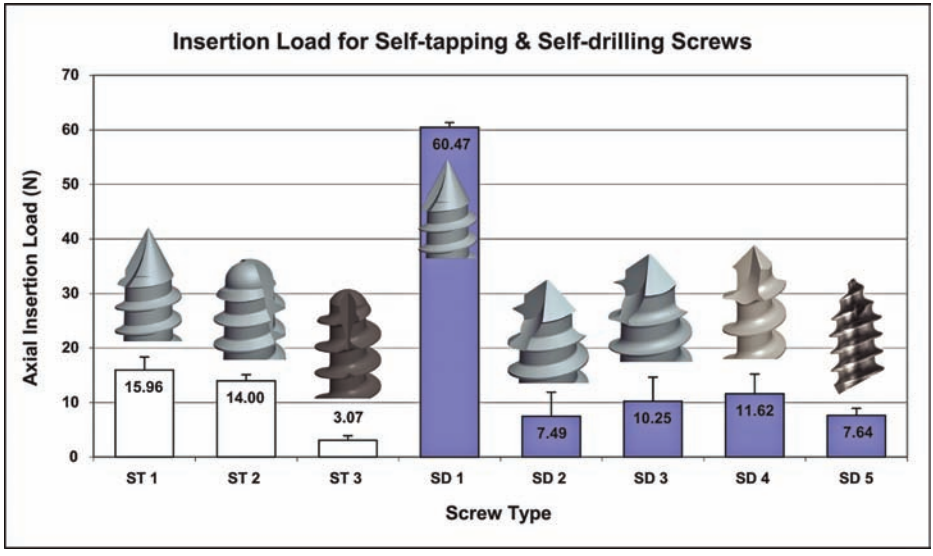

FIG. 5—*Mean insertion loads for the self-tapping (ST) and self-drilling (SD) screw designs evaluated (error bars represent 1 standard deviation).*

TABLE 4—*Screw pairs with significantly different insertion loads.*

Insertion Load	Larger Insertion Loads	Smaller Insertion Loads
Self-tapping versus self-tapping	ST 1	ST 3
	ST 2	ST 3
Self-drilling versus self-drilling	SD 1	SD 2
	SD 1	SD 3
	SD 1	SD 5
Self-drilling versus self-tapping	SD 1	ST 3

summarizes the mean insertion load and 1 standard deviation for all screw designs evaluated.

Prior to repeated measures analysis of variance (ANOVA) analysis, the assumption of normality was checked and the data were found to not follow a normal distribution. Therefore, data were analyzed using Kruskal–Wallis one way ANOVA on ranks (non-parametric analysis). The differences in the mean values among the different screw designs were significant ($P \leq 0.001$). To determine which screw designs significantly differed from the others, multiple cross-comparisons were made using Dunn's method. Table 4 provides a summary of the screw design pairs that were significantly different for insertion load at $P < 0.05$, at 95% confidence level.

The results indicate that the ST 1/SD 1 screw, whether tested as self-tapping or self-drilling, always required significantly greater insertion loads compared to the other self-tapping and self-drilling screws that were tested.

Driving Torque

A representative example of the output for the driving torque test is shown in Fig. 6. Figure 7 summarizes the mean driving torque and 1 standard deviation for all screw designs evaluated. Note that convention on the test machines prints data plots, such as seen in Fig. 6, with the maximum torque as most negative. However, for readability, the absolute value of the output is reported and summarized in the text, tables, and charts (such as seen in Fig. 7).

Prior to ANOVA analysis, the assumption of normality was checked and the data were found to follow a normal distribution. Therefore, a one way ANOVA analysis was performed to determine the significance of differences in the results. The differences in the mean values among the groups were significant ($P \leq 0.001$). To determine which screw designs significantly differed from each other, multiple cross-comparisons were made using the Holm–Sidak method. Table 5 provides a summary of the screw design pairs that were significantly different for driving torque at $P < 0.05$, at 95% confidence level.

The results indicate that the ST 1/SD 1, whether tested as self-tapping or self-drilling, generally required significantly greater driving torques compared to the other self-tapping and self-drilling screws that were tested.

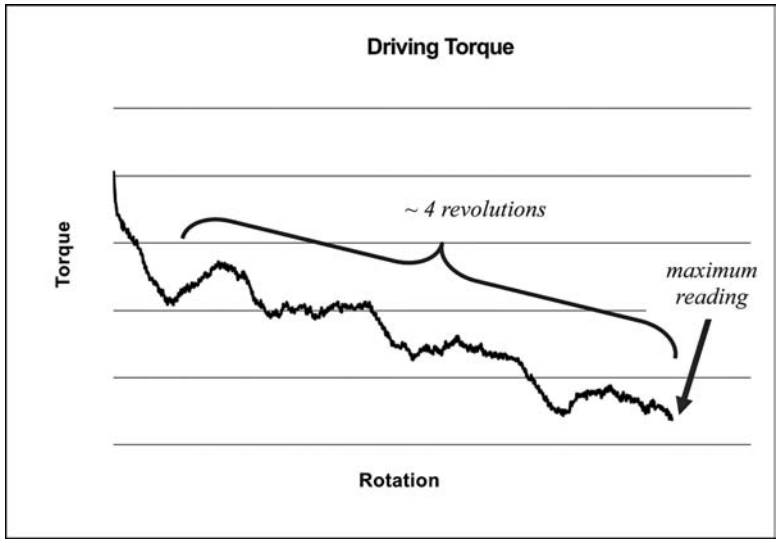

FIG. 6—*Representative driving torque plot for sample 1 for SD 4.*

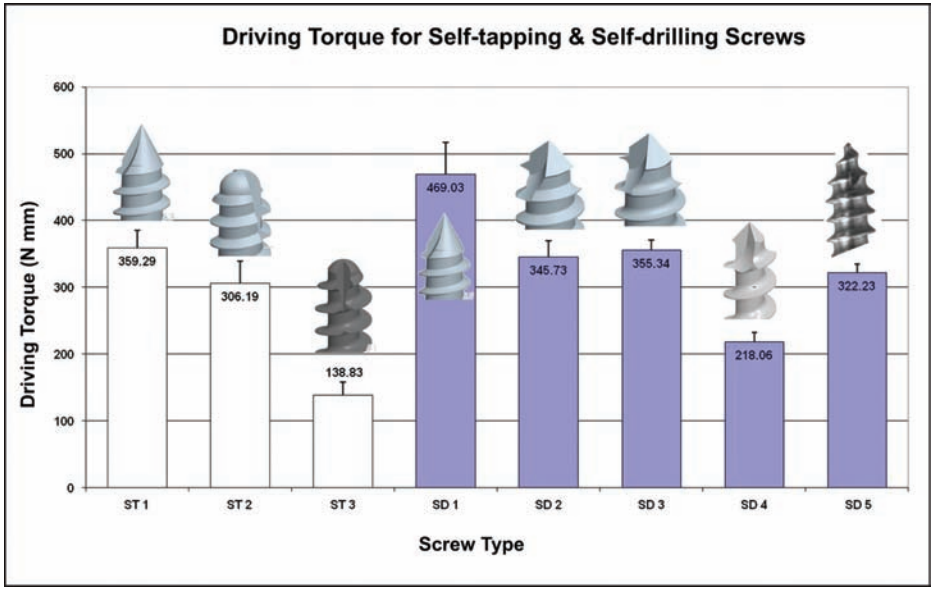

FIG. 7—*Mean driving torque for the self-tapping (ST) and self-drilling (SD) screw designs evaluated (error bars represent 1 standard deviation).*

TABLE 5—*Screw pairs with significantly different driving torques.*

Driving Torque	Larger Driving Torques	Smaller Driving Torques
Self-tapping versus self-tapping	ST 1	ST 2
	ST 1	ST 3
	ST 2	ST 3
Self-drilling versus self-drilling	SD 1	SD 2
	SD 1	SD 3
	SD 1	SD 4
	SD 1	SD 5
	SD 2	SD 4
	SD 3	SD 4
	SD 5	SD 4
Self-drilling versus self-tapping	SD 1	ST 1
	SD 1	ST 2
	SD 1	ST 3
	SD 2	ST 3
	SD 3	ST 3
	SD 4	ST 3
	SD 5	ST 3
	ST 1	SD 4
	ST 2	SD 4
	SD 2	ST 2
	SD 3	ST 2

Axial Pullout Strength

Figure 8 summarizes the mean pullout strength and 1 standard deviation of all screw designs evaluated. Note ST1/SD1 was only evaluated in the worst case condition, as a self-tapping screw with a pilot hole (i.e., tested as ST1 only and not SD1).

Prior to ANOVA analysis, the assumption of normality was checked and the data were found to follow a normal distribution. Therefore, a one way ANOVA was performed to determine the significance of differences in the results. The differences in the mean values among the groups were significant ($P \leq 0.001$). To determine which screw designs significantly differed, multiple cross-comparisons were made using the Holm-Sidak method. Table 6 provides a summary of the screw design pairs that were significantly different for pullout load at $P < 0.05$, at 95% confidence level.

Discussion

The objective of this study was to adapt the ASTM F543-07 test methods to allow evaluation of both self-drilling and self-tapping cervical spine screws. This

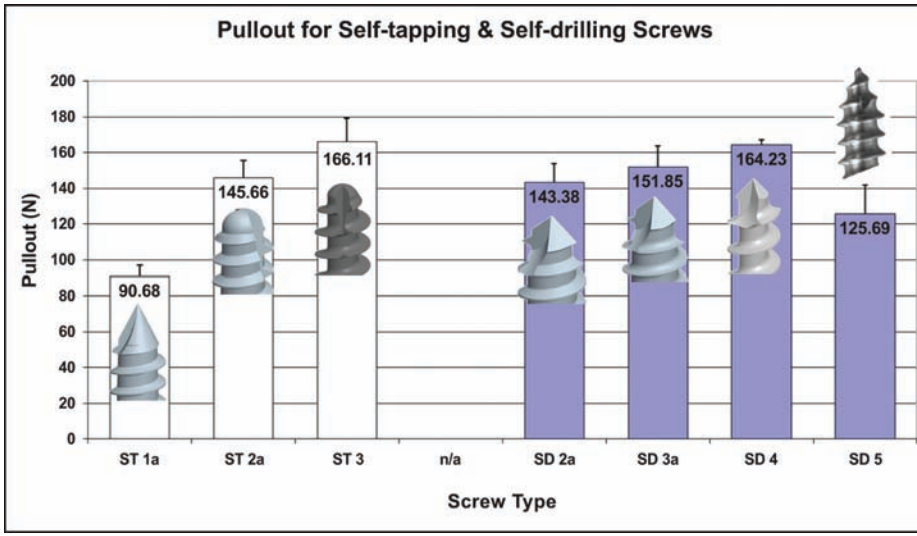

FIG. 8—*Average pullout strength for the self-tapping (left) and self-drilling (right) screw designs that were tested (error bars represent 1 standard deviation).*

study has demonstrated that the methods outlined in ASTM F543-07, with minor modifications, can be adapted for use with self-drilling bone screws in addition to self-tapping screws. Although these investigations all utilized closed-cell foam, as is specified in Annexes 2–4 of ASTM F543-07, it is acknowledged

TABLE 6—*Screw pairs with significantly different pullout loads*.

Pullout	Larger Pullout Loads	Smaller Pullout Loads
Self-tapping versus self-tapping	ST 2	ST 1
	ST 3	ST 1
	ST 3	ST 2
Self-drilling versus self-drilling	SD 3	SD 5
	SD 4	SD 5
	SD 4	SD 2
Self-drilling versus self-tapping	SD 2	ST 1
	SD 3	ST 1
	SD 4	ST 1
	ST 3	SD 2
	ST 3	SD 5
	SD 5	ST 1

Note: The results indicate that the ST 1/SD 1, tested as self-tapping, generally required significantly less force to be pulled out of foam test blocks compared to the other self-tapping and self-drilling screws that were tested.

that this characteristic differs from the open-cell structure of cancellous bone. Therefore, future work may include repeating these investigations using an open-cell foam.

There has been some interest in the literature as to the ideal pilot hole size for minimizing insertion load and driving torque, simultaneously allowing for adequate screw pullout strength. Battula et al. [2] determined that a pilot hole size of less than 71.5% of the screw outer diameter will provide an effective balance between reasonable insertion torques and adequate pull-out strength. In the current investigations, it was verified that the manufacturer's recommended pilot hole sizes were less than 71.5% of the screw outer diameter.

More detailed discussions of the findings from each type of measurement are contained in the following sections. Going beyond the scope of the initial study, additional analysis was performed to quantify differences between self-tapping and self-drilling screws and is discussed in the upcoming section entitled "Driving Torque."

Insertion Load

The insertion load test described in ASTM F543-07 A4 specifically excludes the evaluation of self-drilling screws. Thus, these tests were modified (no pilot holes were drilled when testing the self-drilling screws) to accommodate the testing of self-drilling screws. Due to the novel use of this test with self-drilling screws and the sensitivity of the insertion load test to the screw design differences, data were sometimes difficult to interpret, potentially leading to greater variability in these results.

To better describe this testing, a term "follower load," not defined in ASTM F543-07, was added as seen in Tables 2. This follower load describes the additional axial force needed to keep the screw advancing after the threads first engage the foam. It was found that the follower load was not needed for self-tapping screws but was required for self-drilling screws. Without the follower load, the self-drilling screws had a tendency to cease advancement into the media and "strip out" of the foam.

In addition to defining the follower load, other parameters such as rate and preload also differ from those recommended in the standard. These differences are not surprising given the different (smaller) dimensions and tolerances of these cervical spine screws compared to those typically used in a trauma application. A significant difference from the standard was noted in the experimental loading rate, where a slower rate was required. When the standard rate (2.0 ± 1.0 N/s) was applied, it was observed to be too fast and caused difficulties distinguishing characteristic points in the load versus time chart (Fig. 4). The slower experimental loading rate for these small screws facilitated more robust results and more consistent data interpretation.

Examining the one screw design (ST 1/SD 1) that was tested in both the self-tapping and self-drilling protocols, it was found that when tested as a self-drilling screw, a greater insertion load was required than when tested as a self-tapping screw. This is not surprising given additional work likely required to drill and remove material ahead of the threads during the screw insertion

process. This material was absent when the screw was tested as a self-tapping screw utilizing a pre-drilled pilot hole. It is unknown whether this is true of other screw designs. However, for the screws evaluated in this study, the difference between insertion loads for self-tapping screws and self-drilling screws was generally not large. The ANOVA showed only two screws with statistically significant differences, and those were at the extreme ends—the smallest insertion load for a self-tapping screw and the largest insertion load for the self-drilling screw. Further testing on a variety of screw designs should be performed.

Driving Torque

Some quantifiable differences in driving torque were found among the different self-tapping and self-drilling screws. The ST 3 screw had a driving torque significantly lower than the other self-tapping screws in one analysis and significantly lower than all the self-drilling screws in another analysis. Additionally, comparing the design (ST 1/SD 1) that was tested both as a self-tapping and as a self-drilling screw, the driving torque was higher when it was tested as a self-drilling screw. This is not surprising given the rationale outlined in the previous section: There is more material to resist the screw's rotation and must be displaced in the absence of a pre-drilled pilot hole.

However, from the initial test results alone it was difficult to demonstrate a difference between the self-tapping screws and the self-drilling screws as a group. Therefore, other parameters were examined in more detail in an attempt to better quantify differences between self-tapping versus self-drilling screws. A representative screw from each design was chosen to be examined in more detailed analyses.

These analyses included computation of the initial slope from the load–-displacement curve generated during the data acquisition. An example is provided in Fig. 9. This initial slope is believed to represent a measure of the screw

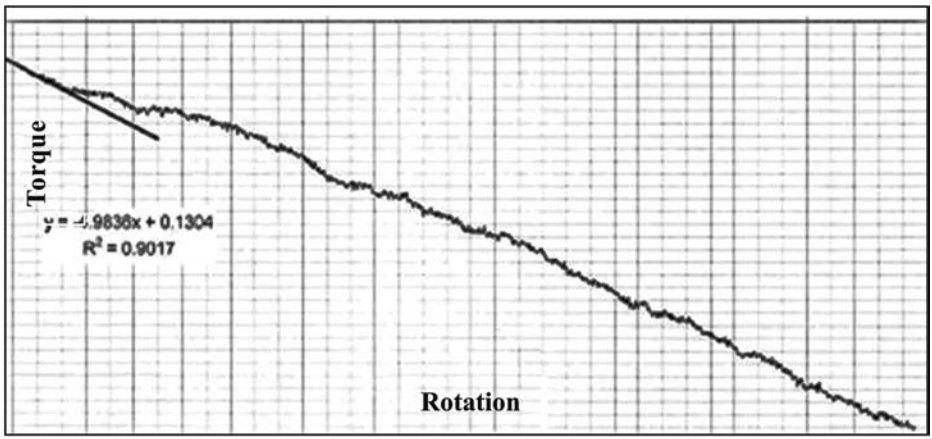

FIG. 9—*Driving torque data from sample 3 of the ST 1/SD 1, when tested as a self-tapping screw.*

TABLE 7—*Initial mean slope of the torque-rotation curve generated during driving torque testing for the three self-tapping screw designs tested.*

Screw	Slope, N mm/deg
ST 1	−0.309
ST 2	−0.204
ST 3	−0.235

tip behavior as it is being inserted into the foam, prior to thread engagement. The three self-tapping screws displayed the same trend—linearity in the force–-displacement curve, and slopes were in relatively good agreement between these three designs. Table 7 depicts the initial slope results for all the self-tapping screw designs tested.

In contrast, all self-drilling screws, with the exception of SD 5, displayed greater initial slopes when compared to all self-tapping designs, as well as exhibited a step-wise increase in the torque–rotation curve (Fig. 10). Typically six steps were seen, each step ranging over 180° of rotation. The SD 5 screw did not have a step-wise pattern and had a much lower initial slope that was much different than the other designs. Table 8 depicts the initial slope results for all the self-drilling screw designs tested.

Although not specifically analyzed in this study, screw diameter (major and minor) and thread geometry likely play a role in the magnitude of the maximum driving torque, as well as how a particular screw behaves relative to the test media. For example, the ST 1/SD 1 driving torque load–displacement curves

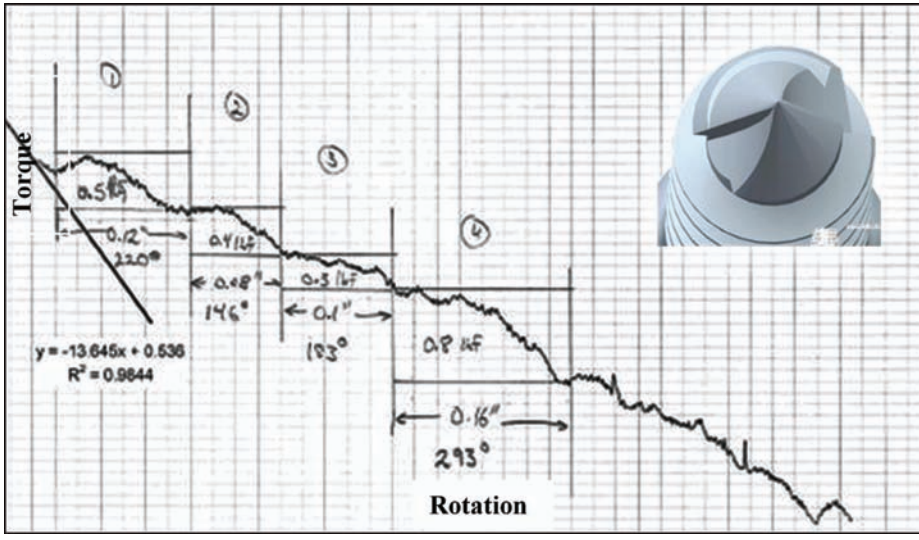

FIG. 10—*Driving torque data from sample 7 of ST 1/SD 1, when tested as a self-drilling screw.*

TABLE 8—*Initial mean slope of the torque–rotation curve generated during driving torque testing for the five self-drilling screw designs tested.*

Screw	Slope, N mm/deg
SD 1	−0.840
SD 2	−0.574
SD 3	−0.896
SD 4	−0.568
SD 5	−0.142

were relatively linear when tested as a self-tapping screw (Fig. 9), yet showed a step-wise pattern when tested as a self-drilling screw (Fig. 10). When tested as a self-tapping screw, the space within the foam created by the pilot hole prevented a portion of the screw tip from interacting with the foam. When tested as a self-drilling screw, the tip geometry interfaced with the foam during the entire test. Similar patterns were seen with the self-tapping screws compared to most of the self-drilling screws. In every self-drilling screw design where the tip is notched approximately 180°, the step-wise load-displacement pattern was observed, potentially indicating a correlation to ease or smoothness of insertion. The SD 5 screw had a different self-drilling screw-tip geometry compared to the other self-drilling screws, potentially explaining the difference in its torque-rotation curve shape.

The results of the present study are in relatively good agreement with an investigation by Su, et al. [3], where insertion torques of self-tapping orthodontic mini-implants were found to be lower than insertion torques of the self-drilling implants tested. In general, this same trend was observed in the current investigations. However, Lim et al. [4] investigated the maximum insertion torque for cylindrical and taper type mini-screws and determined that the maximum insertion torque increased with screw length for both screw types tested. Additionally, their results showed that maximum torque also increased with increasing outer diameter. In the current investigation, longer screws and larger outer diameters were not observed to correlate to larger insertion torques, although the current study was not specifically designed to observe such trends, and therefore did not include great diversity in screw length or diameters.

Axial Pullout Strength

It was originally speculated that the self-tapping screws would, as a group, have a lower pull-out strength than the self-drilling screws. However, the data demonstrated that although there were statistically significant differences among all the screws, the two groups themselves were not different. In fact, the strongest and weakest screws in terms of pullout strength were both in the self-tapping group.

The ST 1/SD 1 screw was tested in pullout only as a self-tapping screw, with a pilot hole as this was thought to be worst case. In the future it would be interesting to test this screw as both a self-tapping and a self-drilling screw (i.e. with

and without a pilot hole) to more directly test if the pilot hole affects the pullout strength.

Conclusions

Quantifiable differences in the mean insertion load, driving torque, and pullout load were found (Figs. 5, 7 and 8), demonstrating that these methods are able to discern differences in performance between different cervical spine screw designs in a surrogate test medium.

The insertion load magnitudes were similar for the self-drilling screw designs when compared to the self-tapping screw designs. However, the one screw (ST 1/SD 1) that was tested as both a self-tapping and self-drilling screw demonstrated higher insertion loads as a self-drilling screw compared to a self-tapping screw. The same screw (ST 1/SD 1) demonstrated lower driving torques as a self-tapping screw compared to a self-drilling screw. However, among all designs, there was not a strong difference in driving torque between the self-tapping designs when compared to the self-drilling designs. No discernable differences in axial pullout performance were noted between the two styles of screws.

This study has demonstrated that it is possible to adapt the test methods outlined in ASTM F543-07 to evaluate the insertion load, driving torque, and axial pullout performance of self-drilling screws in addition to self-tapping screws.

References

[1] Dawson, J., Boschert, P., Macenski, M., and Rand, N., 2003, "Clinical Relevance of Pullout Strength Testing of Pedicle Screws," *Spinal Implants: Are We Evaluating Them Appropriately, ASTM STP 1431*, pp. 68–77.

[2] Battula, S., Schoenfeld, A. J., Sahai, V., Vrabec, G. A., Tank, J., and Njus, G. O., "The Effect of Pilot Hole Size on the Insertion Torque and Pullout Strength of Self-Tapping Cortical Bone Screws in Osteoporotic Bone." *J. Trauma*, Vol. 64, No. 4, 2008, pp. 990–995.

[3] Su, Y. Y., Wilmes, B., Hönscheid, R., and Drescher, D., "Comparison of Self-Tapping and Self-Drilling Orthodontic Mini-Implants: An Animal Study of Insertion Torque and Displacement under Lateral Loading." *Int. J. Oral Maxillofac. Implants*, Vol. 24, No. 3, 2009, pp. 404–411.

[4] Lim, S. A., Cha, J. Y., and Hwang, C. J., "Insertion Torque of Orthodontic Miniscrews According to Changes in Shape, Diameter and Length," *Angle Orthodon.*, Vol. 78, No. 2, 2008, pp. 234–240.

Reprinted from JAI, Vol. 8, No. 7
doi:10.1520/JAI103513
Available online at www.astm.org/JAI

V. G. Shah,[1] *M. C. Anderson,*[2] *D. A. Lissy,*[1] *and C. J. Lissy*[1]

Fixture Variations When Evaluating ASTM F1717 Construct Stiffness: Pin Diameter and Material

ABSTRACT: The ASTM F1717 test standard describes the fixtures to be used when testing spinal implant construct, but leaves some room to interpret. As a result, the same device could be evaluated using different fixturing and it would not be considered a deviation because the standard does not specifically allow or prohibit the method used. Three potential variations in fixturing when conducting F1717 testing were selected for analysis in this study: changes to pin diameter, changes to pin material, and changes to test fixture hole configuration. To evaluate these parameters, a sample F1717 construct was designed and manufactured. Specimens, $N = 6$, were tested in six different configurations of pin diameter, material, and hole configurations. A review of all F1717 test batteries conducted at Empirical Testing Corporation during CY2009 was conducted to provide context for results from the sample F1717 construct. Differences noted in test results for axial compression bending stiffness occurred when sleeves were used to adapt 3/8 in. pins diam for use in 1/2 in. diam holes. Significant differences were noted in torsional stiffness when using a half-hole configuration, and when comparing 3/8 in. diam pins to using 1/2 in. diam pins. The torsional stiffness and compression yield load of the sample lumbar F1717 construct is within the range of F1717 constructs tested during CY2009, but outside the range for compression stiffness and yield torque. Users of the test standard are advised to not use 3/8 in. diam pins (which are prescribed for cervical construct tests) when testing lumbar constructs, and to avoid the use of half holes in torsion testing.

Manuscript received October 18, 2010; accepted for publication May 8, 2011; published online July 2011.

[1] Empirical Testing Corporation, Colorado Springs, CO 80918.
[2] Empirical Testing Corporation, Colorado Springs, CO 80918 (Corresponding author), e-mail: manderson@empiricaltesting.com

Cite as: Shah, V. G., Anderson, M. C., Lissy, D. A. and Lissy, C. J., "Fixture Variations When Evaluating ASTM F1717 Construct Stiffness: Pin Diameter and Material," *J. ASTM Intl.*, Vol. 8, No. 7. doi:10.1520/JAI103513.

KEYWORDS: F1717, F1717 construct stiffness, pin diameter, pin material, F1717 fixture

Introduction

Test methods described in the F1717 test standard [1] facilitate comparisons of spinal implants used to stabilize the spine and promote fusion. The current version of the standard (F1717-10) is the fifth version since its initial release in 1996. The standard describes in general terms the fixtures to be used when testing, but leaves some items for the user to interpret. As a result, the same F1717 test construct could be evaluated several times using different fixtures, and it would not be considered a deviation because the standard does not prohibit the fixtures used. A recent interlaboratory study conducted by ASTM Committee F04.25 noted multiple variations between test labs in fixturing used when testing F1717 test constructs [2]. Such fixture variations may or may not have an effect on stiffness and yield results. The objectives of this study were to examine the effects of three potential fixture variations when conducting F1717 testing: changes to pin size, changes to pin material, and changes to test fixture hole configuration. It was hypothesized that significant differences in stiffness and yield would result due to fixture variations.

Methods and Materials

A sample lumbar F1717 construct was designed and manufactured at Empirical Testing Corp. (ETC). The sample construct consisted of four main components: (1) [1/4] in. × 1-[1/2] in. hex flange lag screws (to simulate pedicle screws), (2) custom built steel connector (to simulate a monoaxial pedicle screw housing), (3) 4140 alloy steel rods (to simulate pedicle screw system rods), and (4) [1/4]-20 × [1/2] in. GR8 hex flange bolts (to simulate set screws). The components were assembled into standard F1717 UHMWPE test blocks with 1/2 or 3/8 in. diam lateral holes as shown in Figs. 1 and 2. Steel connectors were reused multiple times after each set of configuration tests. The test block gap (defined as the distance between connector and test block face) was maintained at approximately 2 mm and the set screws were tightened with a tightening torque of 80 in. lbs. Six sample constructs were tested in each test configuration (see Fig. 3). All testing was performed using an INSTRON 8874 Bi-Axial Table Top Servohydraulic Dynamic Testing System (INSTRON, Norwood, MA) with a 25 kN axial and 100 N m torsional load cell. C-bracket fixtures, shown in Fig. 5, were made of three pieces of 17-4SS with 76 mm width and holes for 3/8 or 1/2 in. lateral pins, and were common across all tests. Lateral pins were made of three different materials: (1) common steel, represented by the use of a Grade 8 SAE bolt, (2) 17-4 stainless steel, and (3) 18-8 stainless steel. In configuration 3, the lateral pin rested on half-hole adapter plates screwed to the top of the C-bracket fixture. For all other test configurations the lateral pin was inserted through the lateral holes of the C-bracket fixture and the UHMWPE test block of the construct. Fixture "sleeves" were used to adapt 3/8 in. diam pins for use in 1/2 in. diam fixture holes. Test pin configurations are shown in Fig. 4. An example of the test

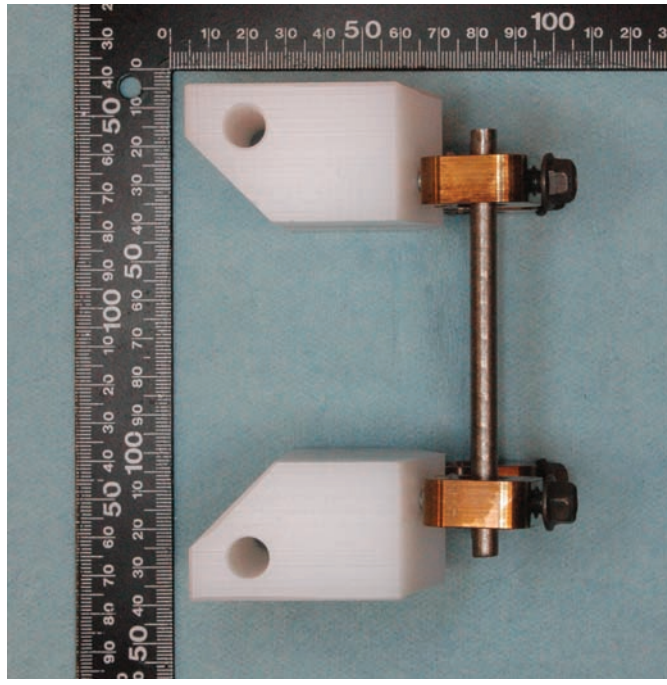

FIG. 1—*Untested sample construct: lateral view.*

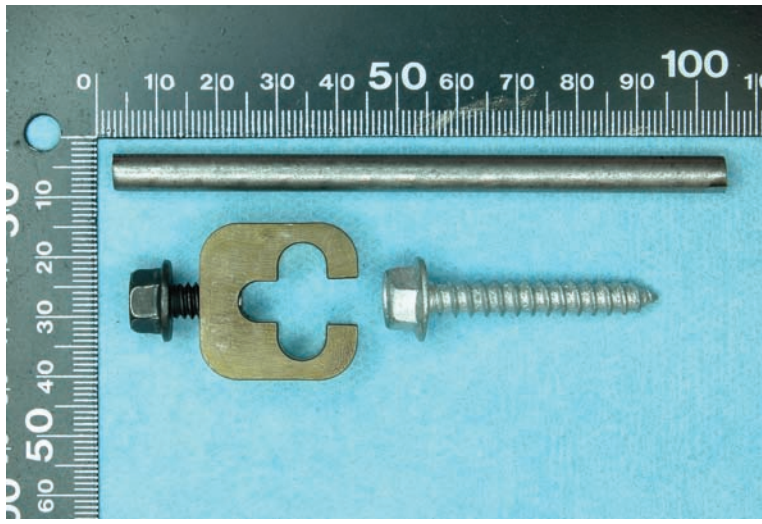

FIG. 2—*Untested sample construct: unassembled parts.*

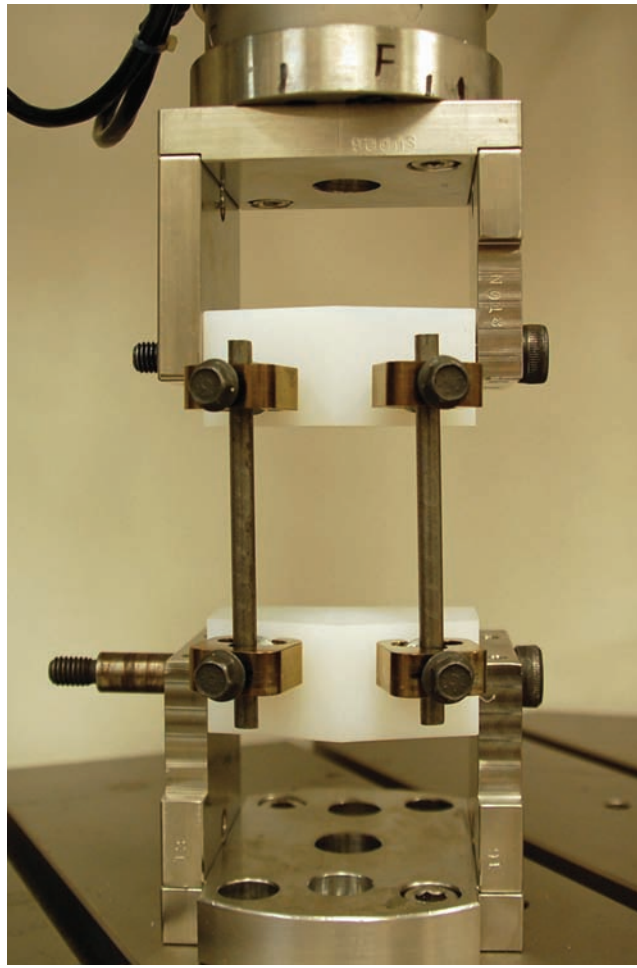

FIG. 3—*Static axial compression bending and static torsion setup.*

configuration is shown in Fig. 5. Table 1 outlines the lateral pin and fixture hole configurations tested.

Static axial compression (AC) bending testing was run in axial displacement control at a rate of 0.2 mm/s. The testing was terminated when gross failure occurred or test blocks touched. Static torsion (TR) testing was run in angular displacement control at a rate of 1°/s with an axial preload of −12 N held in displacement control. Aluminum spacer blocks were not used to constrain sagittal plane rotation; this is a deviation from the F1717-10 standard and is the ETC default test method for F1717 static torsion testing. Testing was terminated when gross failure occurred or the construct interfered with the test blocks. Load versus displacement and torque versus angle data were collected

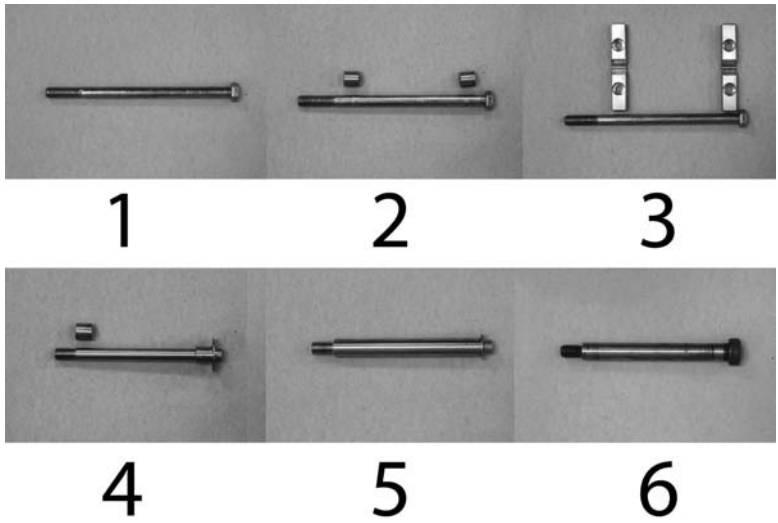

FIG. 4—*Pins used in each test configuration.*

using Instron's Wavemaker software (Version 7.1.0, Instron Corporation, Canton, MA).

Upon completion of testing, all data were analyzed using a least squares linear regression method to find the best fit of the linear (stiffness) region of the data curve. A 2% offset line was then created to determine the yield load or torque, as prescribed in the F1717-10 standard. Two-way single factor repeated measures analysis of variances (ANOVAs) ($\alpha = 0.05$) and two-tailed Student's *t*-tests ($\alpha = 0.05$) with Holm's correction for multiplicity were used post hoc to test for significant differences between test configurations.

To determine whether test results from the sample lumbar F1717 construct were representative of an actual lumbar F1717 construct, a review of results of all F1717 test batteries conducted at ETC during CY2009 was conducted. Inclusion criteria were that the system tested was a bilateral posterior metallic rod based system intended for use in the lumbar spine (76 mm construct length), and that both static compression and static torsion testing with $n = 6$ constructs in each test were conducted.

Results

Six constructs were tested in each of the six test configurations in static axial compression bending and static torsion. Table 2 contains the mean and standard deviation values for the compressive bending stiffness (N/mm) and compressive bending yield load (N) yield torque (N m) and torsional stiffness (N m/deg) calculated for each configuration. Results are also shown graphically in Figs. 6–13.

FIG. 5—*Test configuration 3: C-bracket with half-hole brackets mounted.*

With $p < 0.001$ for the static axial compression bending stiffness ANOVA, and $p = 0.001$ for the static axial compression bending yield load ANOVA, it was concluded that differences were significant. Post hoc tests indicated that configuration 2 (3/8 in. GR8 SAE bolt thru 1/2 in. holes with sleeves) was significantly stiffer than configurations 1, 3, and 6 as shown in Fig. 7, but found no significant differences in yield load, as shown in Fig. 9.

With $p < 0.001$ for the static torsion stiffness and static torsion yield torque ANOVAs, it was concluded that differences were significant. Post hoc tests on the torsional stiffness data indicated that configuration 3 was less stiff than all

TABLE 1—*Descriptions of test configurations.*

Configuration	Pin diameter, in.	Pin material	Fixture hole diameter, in.	Fixture hole adapter
1	3/8	GR8 SAE Bolt	3/8	No Sleeve
2	3/8	GR8 SAE Bolt	1/2	With Sleeve
3	3/8	GR8 SAE Bolt	Half hole	No Sleeve
4	3/8	17-4 SS	1/2	With Sleeve
5	1/2	17-4 SS	1/2	No Sleeve
6	1/2	18-8 SS	1/2	No Sleeve

TABLE 2—*Static axial compression and torsion results.*

Configuration	Comp bending stiffness, N/mm	Comp bending yield load, N	Torsional stiffness, N m/deg	Yield torque, N m
1	67.5 ± 2.512	415.4 ± 5.61	4.4 ± 0.08	23.6 ± 0.87
2	74.2 ± 3.25	437.5 ± 21.41	4.2 ± 0.16	23.8 ± 0.61
3	68.1 ± 1.98	415.2 ± 9.94	3.8 ± 0.11	22.8 ± 0.37
4	70.5 ± 1.63	407.3 ± 7.74	4.5 ± 0.17	23.2 ± 0.49
5	71.4 ± 1.92	407.4 ± 12.22	4.78 ± 0.14	24.4 ± 0.37
6	66.3 ± 3.74	414.5 ± 4.19	4.7 ± 0.20	24.6 ± 0.60

Note: Means are expressed with ±1 standard deviation.

other configurations, configuration 2 was different from configurations 3, 5, and 6, and configuration 1 was less stiff than configurations 5 and 6, as shown in Fig. 11. Post hoc tests on the yield torque data indicated that the yield torque of configuration 3 was less than configurations 5 and 6, and the yield torque of configuration 4 was also less than configurations 5 and 6, as shown in Fig. 13.

Of all the F1717 test batteries conducted at ETC during CY2009, 12 met the inclusion criteria described previously. Four were monoaxial systems and the remaining eight were polyaxial. CY2009 results are shown alongside results testing the sample construct in configuration 5 (ETC's default configuration used

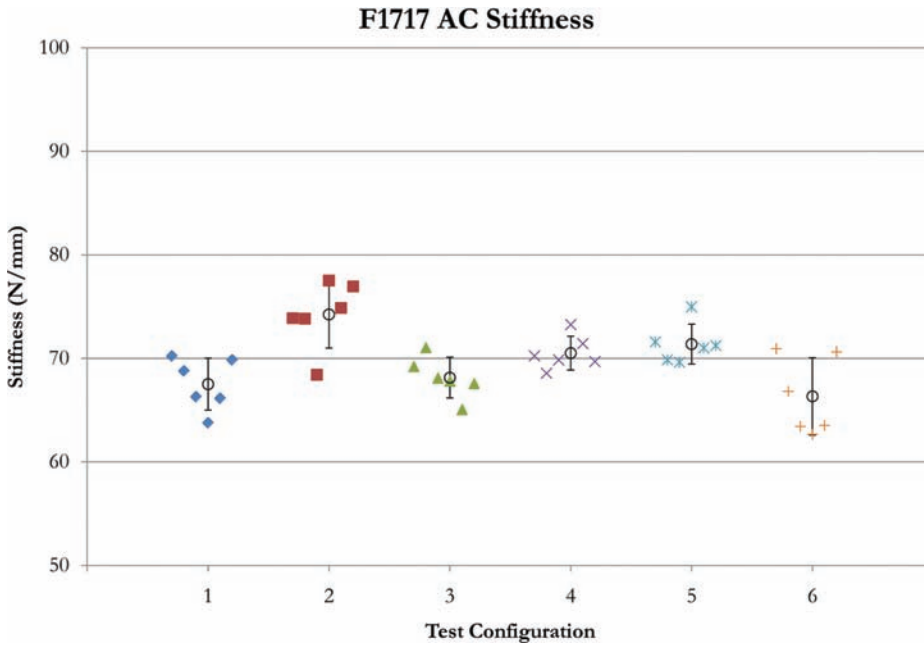

FIG. 6—*F1717 static axial compression bending stiffness results.*

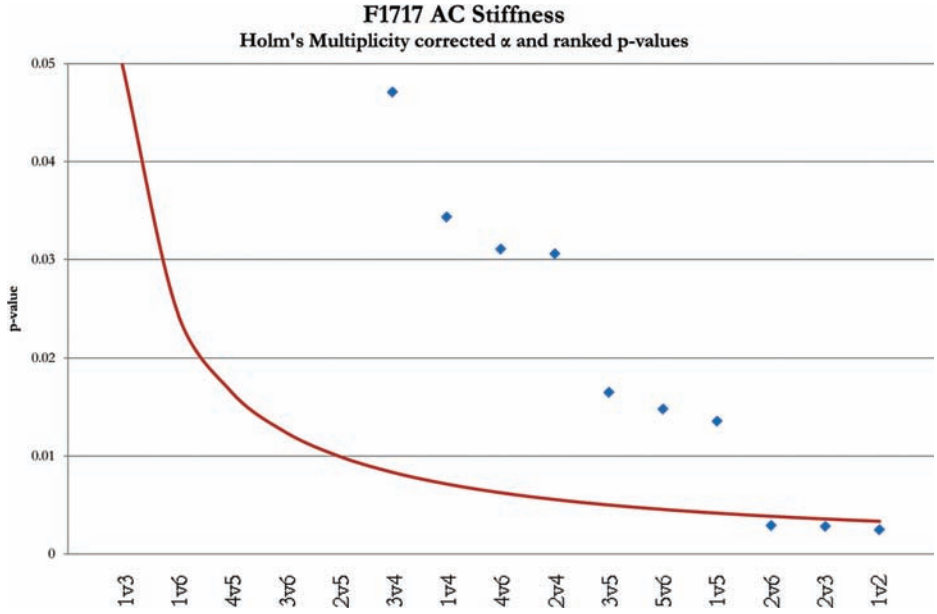

FIG. 7—*Static axial compression bending stiffness post hoc test results. Diamonds are ranked p-values from t-tests, the solid line denotes Holm's corrected α. Comparisons resulting in $p > 0.05$ are not shown. Significant difference is indicated when $p < \alpha$.*

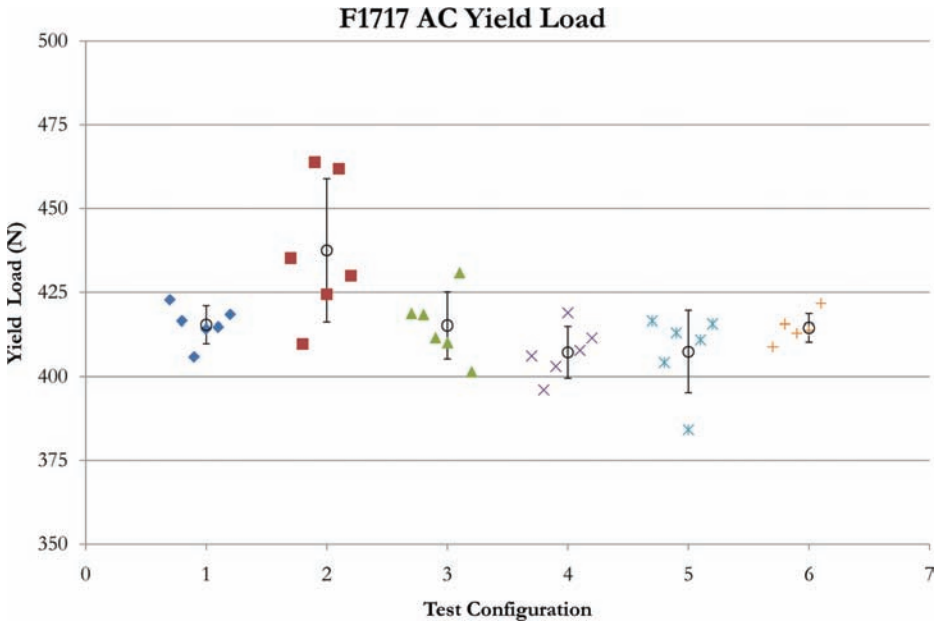

FIG. 8—*F1717 static axial compression bending yield load results.*

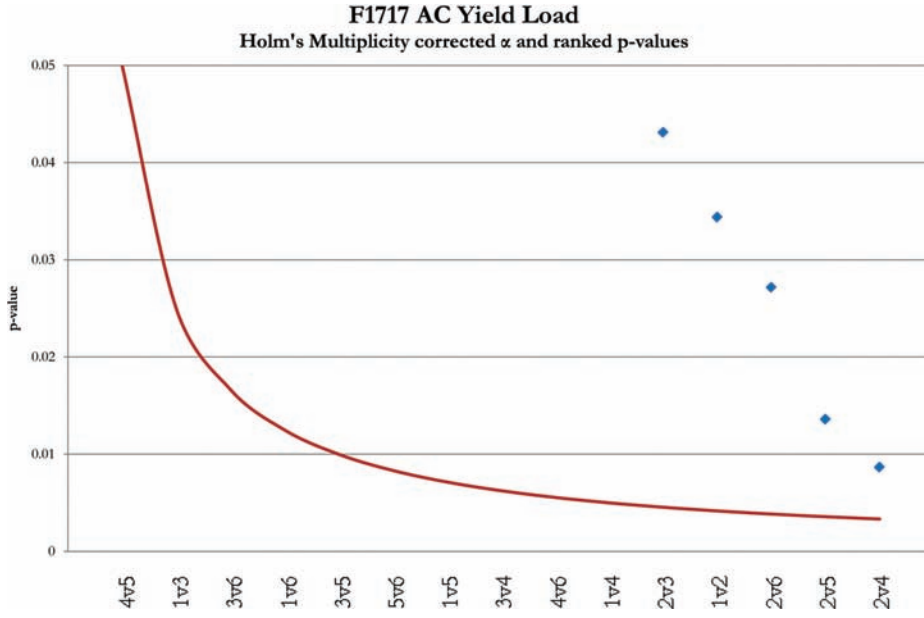

FIG. 9—*Static axial compression yield load post hoc test results. Diamonds are ranked p-values from t-tests, the solid line denotes Holm's corrected α. Comparisons resulting in $p > 0.05$ are not shown. Significant difference is indicated when $p < \alpha$.*

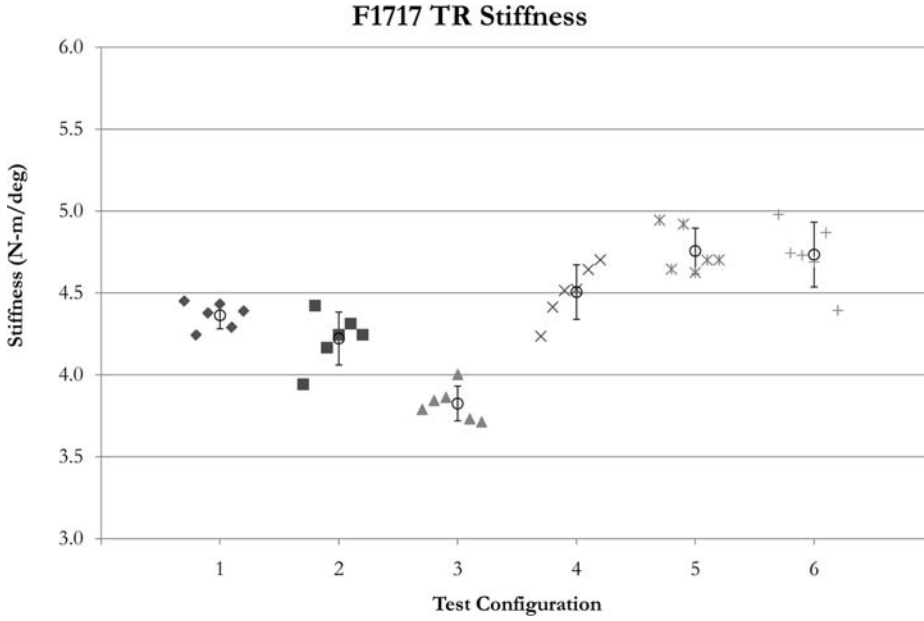

FIG. 10—*F1717 static torsion stiffness results.*

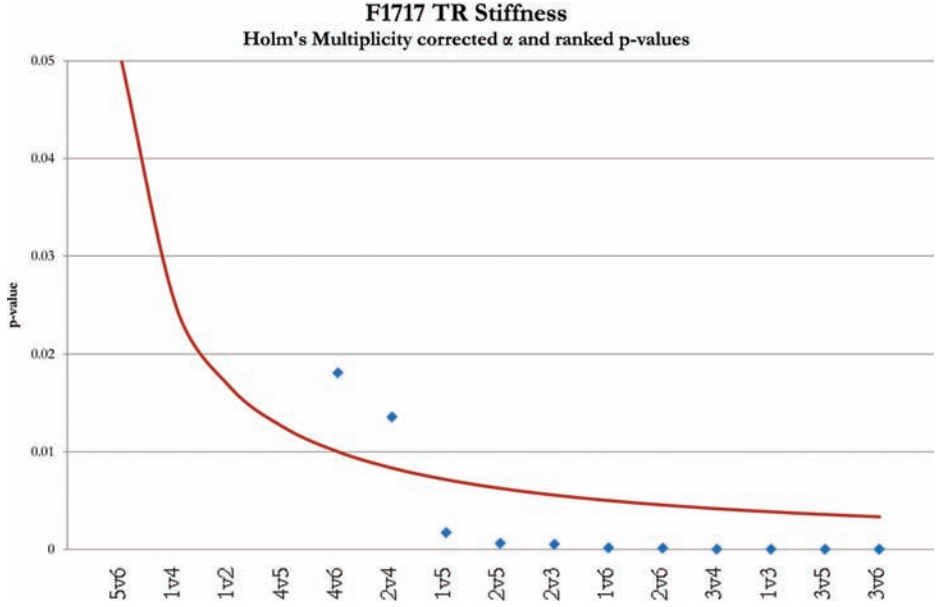

FIG. 11—*Static torsion stiffness post hoc test results. Diamonds are ranked p-values from t-tests, the solid line denotes Holm's corrected α. Comparisons resulting in $p > 0.05$ are not shown. Significant difference is indicated when $p < \alpha$.*

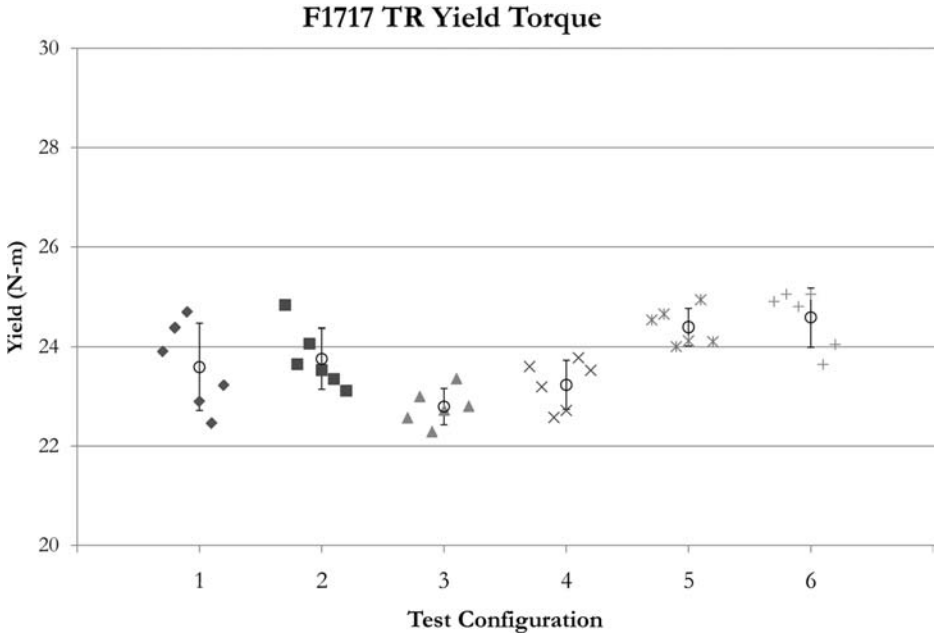

FIG. 12—*F1717 static torsion yield torque results.*

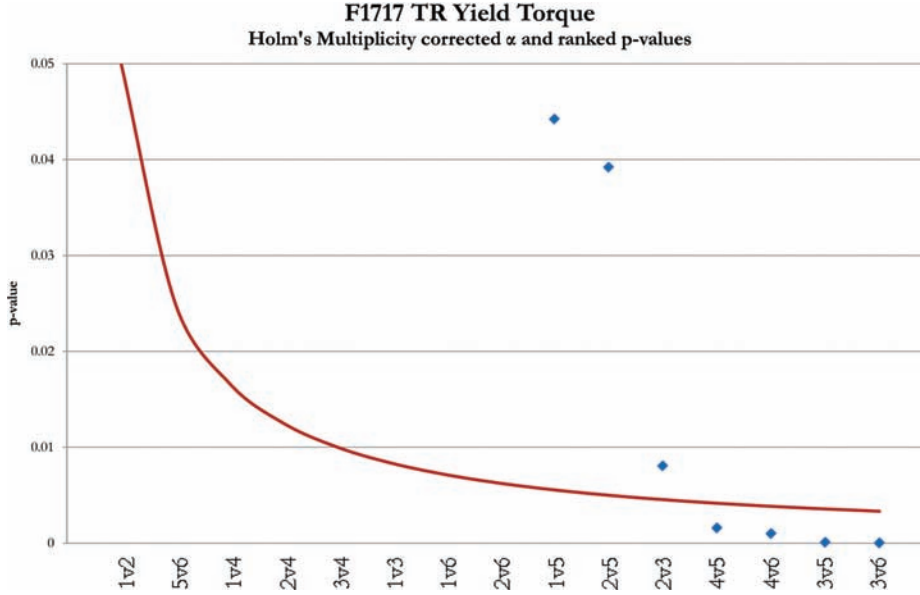

FIG. 13—*Static torsion yield torque post hoc test results.*

during CY2009 testing) in Figs. 14–17. The torsional stiffness and compression yield load of the sample lumbar F1717 construct is within the range of F1717 constructs tested during CY2009, but outside the range for compression stiffness and yield torque.

Conclusions

In axial compression bending, significant differences in stiffness occurred only for configuration 2 (SAE GR8 bolt with sleeves). All other differences were not significant. Configurations 1 and 2 differed only in the use of a sleeve around the pin, yet configuration 2 was significantly stiffer, indicating that the use of a sleeve influenced the stiffness of the system. However, this difference between configuration 2 and the others did not repeat itself in the compression yield data.

In torsion testing, configuration 3 (GR8 SAE bolt in half holes) was significantly less stiff than other configurations, but this result is not unexpected when considering the test setup. The half-hole configuration is used at some test labs for axial compression testing, but it is not practical for torsion testing. It was included in this study for the sake of completeness. The data confirms what is common knowledge: that the half-hole configuration should not be used in static torsion testing.

Configurations 5 and 6 were more torsionally stiff, and resulted in higher yield torques than other configurations, indicating that pin diameter does have an affect on test results. Differences in pin material (configuration 5 used a 17-4 SS

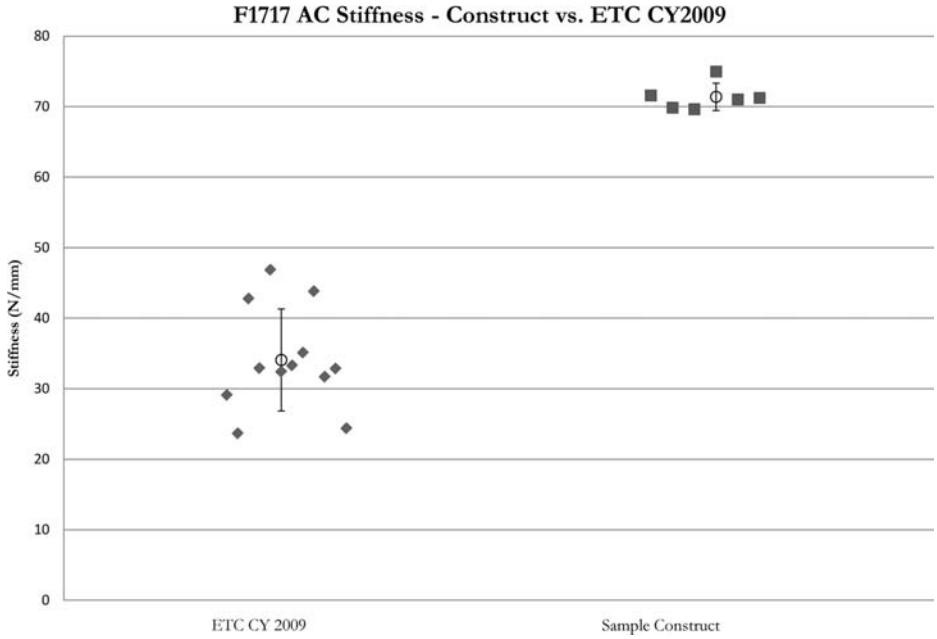

FIG. 14—*F1717 static axial compression bending stiffness results compared to ETC FY2009 results. Sample construct was tested in configuration 5.*

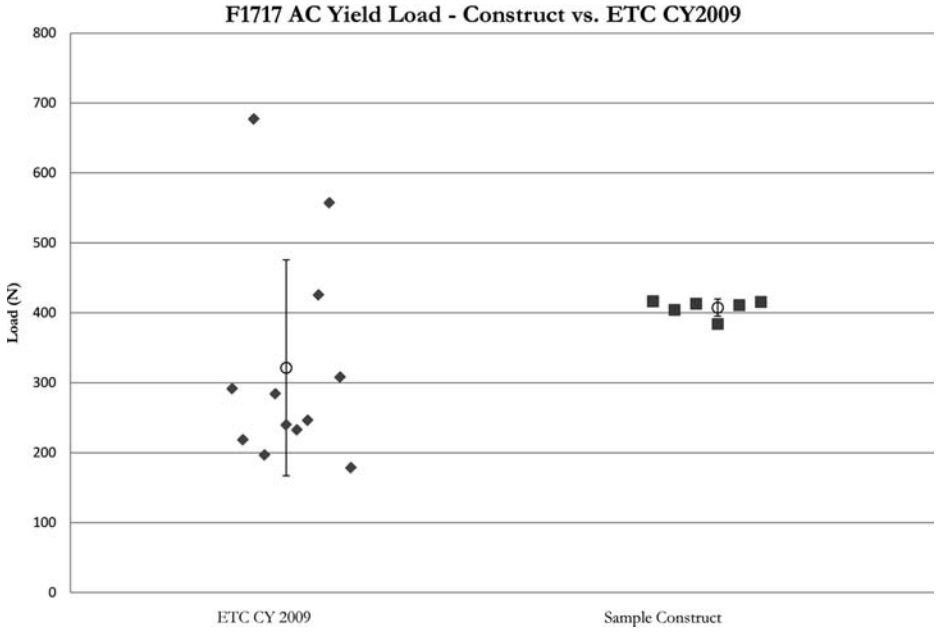

FIG. 15—*F1717 static axial compression bending yield load results compared to ETC FY2009 results. Sample construct was tested in configuration 5.*

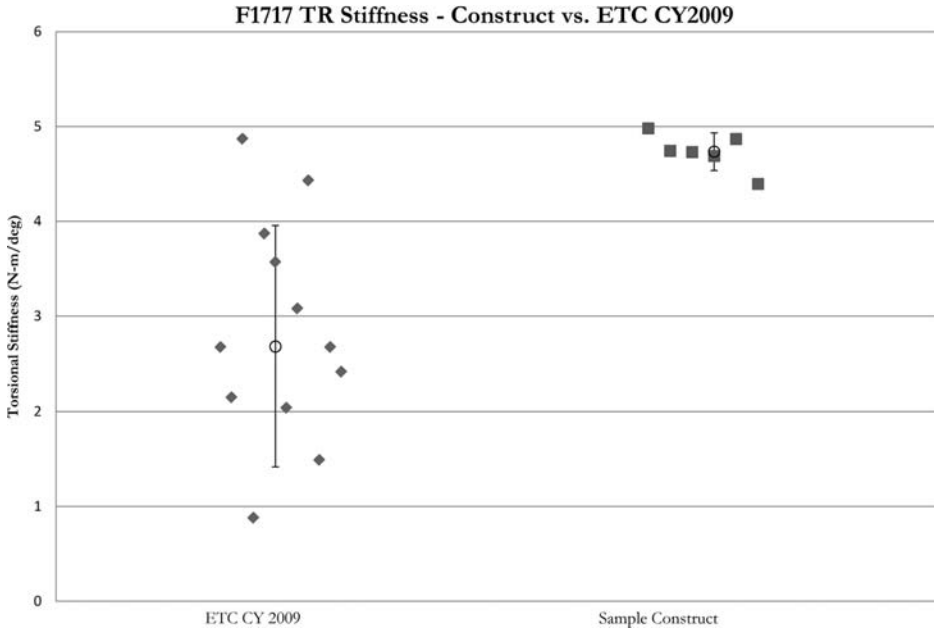

FIG. 16—*F1717 static torsion stiffness results compared to ETC FY2009 results. Sample construct was tested in configuration 5.*

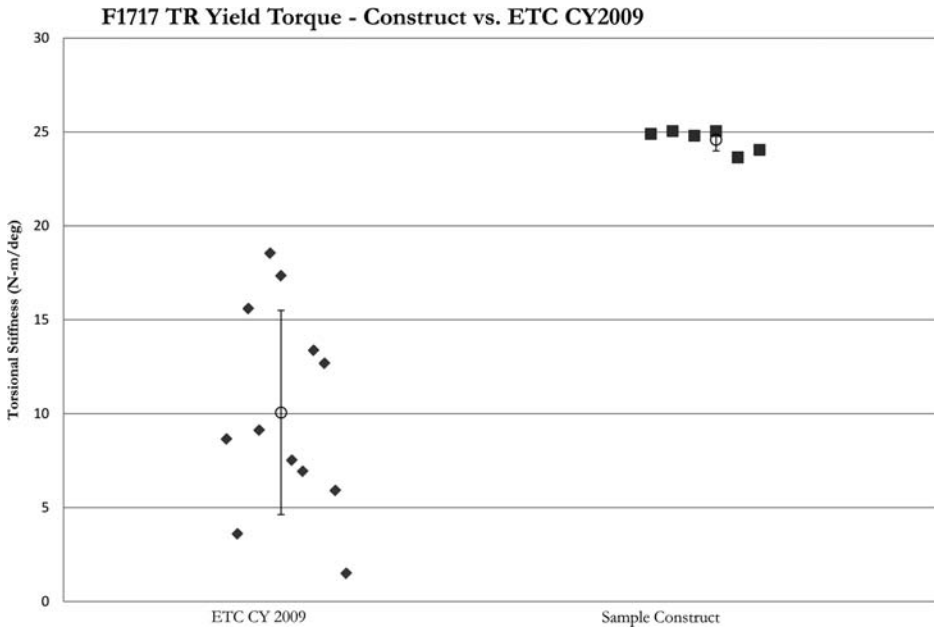

FIG. 17—*F1717 static torsion yield torque results compared to ETC FY2009 results. Sample construct was tested in configuration 5.*

pin, whereas the pin for configuration 6 was made of 18-8SS) did not lead to significant differences in torsional stiffness or yield torque.

The overall performance of the sample construct in static compression bending and static torsion testing can be considered comparable to actual devices. It is not a perfect model for all parameters, but for the purposes of this study, it was considered adequate.

A shortcoming of this study is that the test sample construct used is not an actual pedicle screw system. As shown in the review of CY2009 data, some of the test sample construct's mechanical properties (AC yield load and TR stiffness) are within the range of those measured for pedicle screw systems, but not in others (AC stiffness and TR yield torque). The sample construct hardware was also used in a parallel study that evaluated the effects of changes to torsion test methods upon torsional stiffness and yield torque [3]. A repeatability analysis conducted at the end of that study showed that initial results could not be repeated. Upon further examination, it was determined that the steel connectors were plastically deformed over the course of testing. This observation casts some doubt over the results of this study, as there is no clear indication as to when the deformation occurred. Donation of actual pedicle screw hardware by industry so that these tests can be repeated would be the best possible result of this study. The intent of such a study would be to determine if the F1717 standard should contain specific specimen geometry and fixturing requirements

In conclusion, of the fixturing changes chosen for analysis in this study, pin diameter and the use of half holes were the only ones that resulted in significant differences in stiffness and yield measurements. Users of the test standard are advised to not use 3/8 in. diam pins (which are prescribed for cervical construct tests) when testing lumbar constructs, and to avoid the use of half holes in torsion testing.

Acknowledgments

This research was funded exclusively by Empirical Testing Corp.

References

[1] ASTM F1717-10, 2010, "Spinal Implant Constructs in a Vertebrectomy Model," *Annual Book of ASTM Standards*, ASTM International.

[2] "Interlaboratory Study to Establish Precision Statements for ASTM F1717-09," *Spinal Implant Constructs in a Vertebrectomy Model*, D. B. Spenciner, Ed., ASTM International, West Conshohocken, PA, 2009.

[3] Shah, V., *et al*. "Fixture Variations When Evaluating F1717 Constructs in Torsion: Axial Load, Sagittal Plane Rotation Constraints, and Test direction." in *Symposium: Spinal Implants: Are We Evaluating them Appropriately?* San Antonio, TX, 2011, ASTM International, West Conshohocken, PA.

Author Index

Subject Index

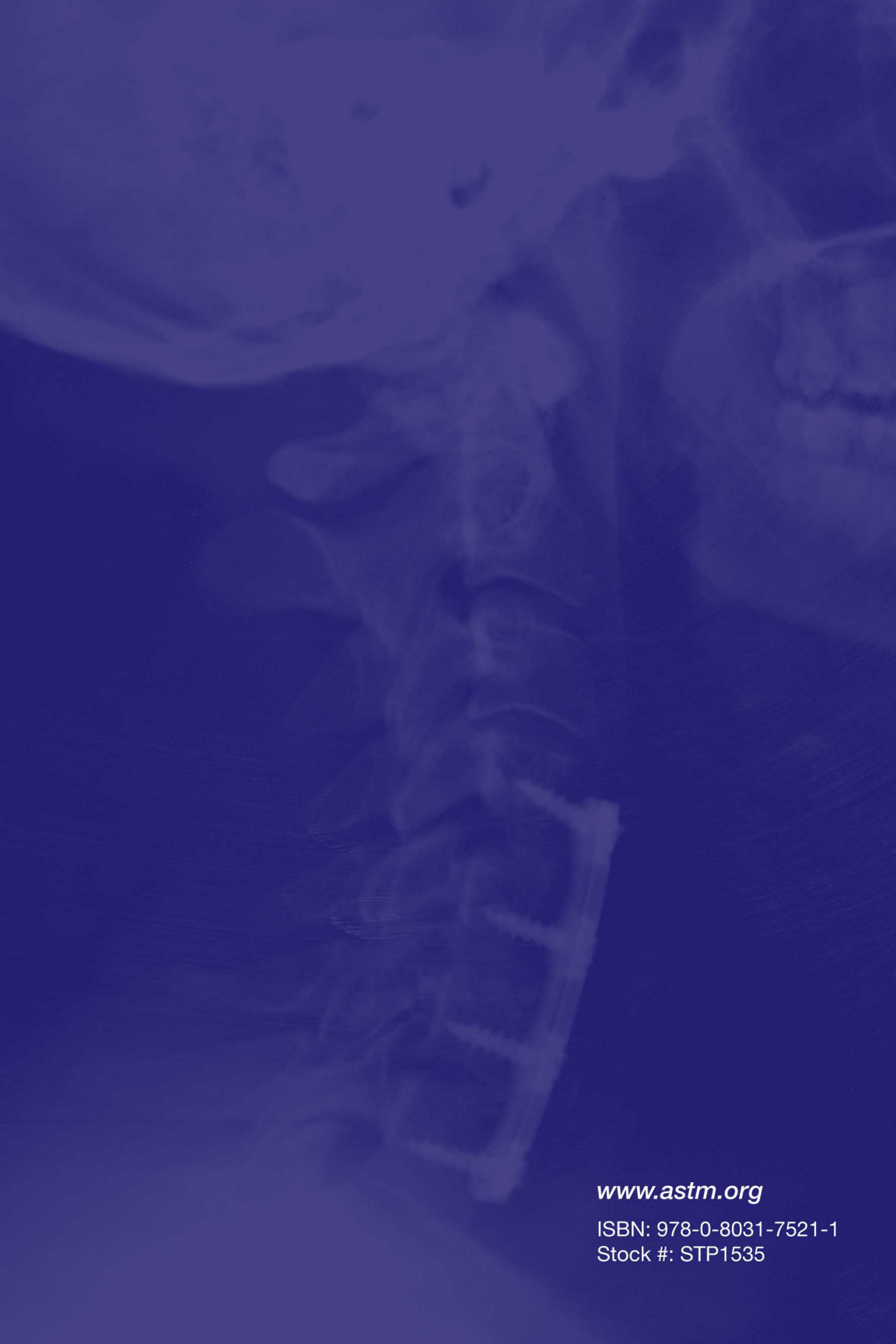

www.astm.org

ISBN: 978-0-8031-7521-1
Stock #: STP1535